A Comparative Study on Homogenization Strategies for Multi-Scale Analysis of Materials

J. M. Ortolano
J.A. Hernández
J. Oliver

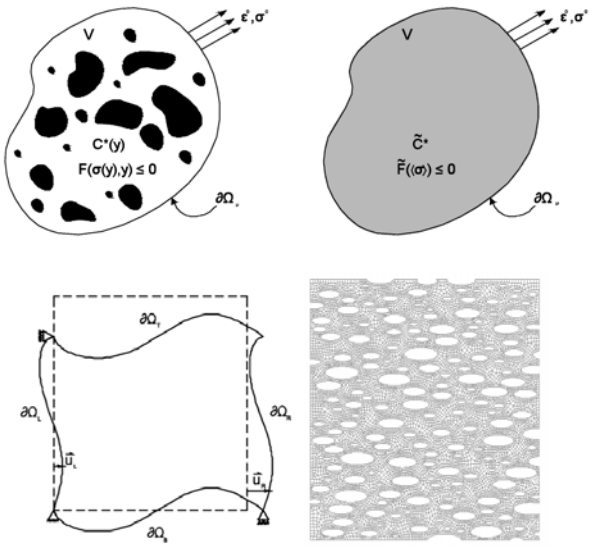

Monograph CIMNE Nº-135, February 2013

A Comparative Study on Homogenization Strategies for Multi-Scale Analysis of Materials

J. M. Ortolano
J.A. Hernández
J. Oliver

Monograph CIMNE Nº-135, February 2013

International Center for Numerical Methods in Engineering
Gran Capitán s/n, 08034 Barcelona, Spain

INTERNATIONAL CENTER FOR NUMERICAL METHODS IN ENGINEERING
Edificio C1, Campus Norte UPC
Gran Capitán s/n
08034 Barcelona, Spain
www.cimne.com

First edition: February 2013

A COMPARATIVE STUDY ON HOMOGENIZATION STRATEGIES FOR MULTI-SCALE ANALYSIS OF MATERIALS
Monograph CIMNE M135

ISBN: 978-84-941004-6-8

Depósito legal: B-6732-2013

Acknowledgements

The European Research Council, on the one hand, and the Spanish Ministry of Economy and Finance, on the other hand, are gratefully acknowledged for their financial support to this research under grants ERC-2012-AdG 320815 COMP-DES-MAT (*"Advanced tools for computational design of engineering materials"*) and BIA2011-24258, respectively.

Abstract

One of the most important engineering tasks over the years has been the design and manufacture of increasingly sophisticated structural materials as a result of the requirements related to the technological progress. In the last decades, the growing needs for improved properties of products have been partially solved through the development of composite materials. A key to the success of many modern structural components is the tailored behavior of the material to given applications. Therefore, research efforts in material science engineering have been focused in the design of new materials either through the creation of new structures at the scale of single atoms and molecules or through the development of structural materials by changing the composition, size, arrangement and topology of the constituents at larger scales: the *microscopic/mesoscopic* level.

The development of new materials has been linked to the development of a new theoretical field within the mechanics of solids. This branch of the mechanical, known as *Continuum Micromechanics*, introduces a series of new concepts that are key to the definition of the macroscopic properties of composite materials on the basis of the definition of the characteristics of its components. Starting from the premise of separation of scales and the concept of Representative Volume Element, defined the so-called *homogenization* methods, whose number has been increasing as the Micromechanics is gone extend over the years. Such methods are many and varied, although especially there have been two that have been used and developed by the majority of authors: the so-called Mean-Homogenization techniques and the multi-scale based on Finite Element Approaches.

Mean-field homogenization schemes are an efficient way to predict the behavior of heterogeneous materials. They range from the simplest hypotheses of the stress or strain sharing among the phases which do not require analytical solution on the associated boundary-value problem to more involved geometric models based on the solution of a boundary-value problem involving a single or composite inclusion embedded in an equivalent homogenized medium whose elastic module become part of the solution procedure. In general, they are based on analytical solutions of the boundary value problem defined in the microstructure level of the inhomogeneous material and provide good predictions for the mean values over the RVE. Although originally designed for elastic materials, some approaches to deal with elastoplastic materials and even with viscoplastic materials have been developed over the years and compared with the results obtained using Finite Element Approaches. The

comparison between different methods of homogenization allows the definition of a range of validity between the different methods, which helps to discover the limitations of the various methods and aspects to take into account for future developments and research.

The main goal of this work is, firstly, to present a general overview of the different techniques that have been developed in the last years in order to obtain a prediction of the behavior of elastoplastic composites by taking into account geometrical and mechanical aspects. Secondly, a comparison between the different approaches is carried out through a numerical implementation of such techniques. Both objectives will be carried out through eight different chapters. The first chapter serves as an introduction and historical review of the advances that have been made in the field of micromechanics. On the other hand, the second chapter deals with some important theoretical background that is important in the field of *Continuum Micromechanics*, as well as a short introduction of the different approaches that traditionally have been considered to solve the problem. One group of methods, based on analytical solutions – the so-called *Mean Field Analysis* – will be commented in chapter 3. Chapter 4 is devoted to the implementation and validation of a numerical tool that solves the mean-field homogenization using analytical schemes for elastoplastic materials. Subsequent chapters are devoted to the comparison of the results with the results given by the Finite Element Method. The general formulation of such method – applied to multi-scale problems – is presented in chapter 5 from a theoretical point of view, as well as the corresponding numerical examples. Finally, last chapter will be dedicated to enumerate some conclusions extracted from the present work, including some aspects that can be object of future works or improvements.

The current work presents some important aspects about the theoretical concepts and the numerical implementation of some key approaches for solving the mechanical problem regarding composite materials. There exist a large number of possibilities to approximate the response of such complex materials, based in different assumptions. This document shows the general efficiency of the so-called mean-field homogenization schemes to capture correctly the macroscopic behavior of composites. Although these techniques show some limitations, like the incapability to provide results for the distribution of the different variables over the microgeometry or the low accuracy in the case of complex microgeometries (like porous materials), they represent an efficient way to predict the main general behavior of a composite material spending low computational effort. They are specially indicated to be used in the previous steps of an analysis or as a tool to validate the results with more involved approaches.

Table of Contents

Chapter 1

Introduction

1.1 Motivation

One of the most important engineering tasks over the years has been the discovery, development and mastery of increasingly sophisticated structural materials as a result of the requirements related to the technological progress. In the last decades, the growing needs for improved properties of products – in terms of energy consumption, reduced weight functionality, smaller dimensions, etc.– have been partially solved through the development of composite materials (i.e. an heterogeneous material made of two or more different constituents). A key to the success of many modern structural components is the tailored behavior of the material to given applications. Therefore, research efforts in material science engineering have been focused in the design of new materials either through the creation of new structures at the scale of single atoms and molecules – the realm of *nanotechnology* – or through the development of structural materials by changing the composition, size, arrangement and topology of the constituents at larger scales: the *microscopic/mesoscopic* level.

However, the idea of combining different materials in order to achieve different material properties is present in the nature since the dawn of the history. For instance, wood as such can be considered as a composite material made of very long fibers of cellulose that held together by a much weaker substance (lignin), while the bones of mammals, on the other hand, are made up by a porous mineral matrix reinforced with collagen fibers. Additionally, from a technological point of view, the concept of combining different materials to create an improved material is something that is not new. Thus, the very first composite produced by man was cob: a plastic matrix made of earth is reinforced by plant fibers, which have been used for over 5000 years. Concrete is also another composite, which have been used since Roman times and is the most important nowadays, at least in volume terms. Nevertheless, the composites industry can be considered as a new born industry, which has grown rapidly over the last forty years as a result of the manufacture of high modulus and high strength fibers, leading to materials with highly complex

microstructures.

Understanding the behavior of composite materials is not an easy task since the mechanical properties of such materials depend on an important number of factors, such as the mechanical properties of each phase and its interfaces, the volume fraction of each constituent, as well as its geometry and the spatial distribution within the composite. Furthermore, such materials are subjected to some effects produced by the appearance of highly complex phenomena, like damage in the composite material caused by fractures on the reinforcements or matrix or due to debonding along interfaces. Therefore, prediction of the properties of composite materials – obtained from the properties of its constituents and their geometry – is not trivial and requires the development of the so-called micromechanical models. Such models allow understanding the macroscopic behavior of the material and its dependence of the microscopic arrangement of the constituents, including the deformation and fracture mechanisms. Hence, micromechanics becomes an important tool in the design and study of new materials with an optimal microstructure, which is tailored to the final application.

1.2 Historical overview

The analysis of microheterogeneous materials is not a recent development. Within the last 150 years, estimates on effective responses of inhomogeneous materials have been made under a variety of different assumptions on the internal fields within the microstructure. The first theoretical studies of the performance of micromaterials date back to J.C. Maxwell (1831-1879), Lord Rayleigh, (1842-1919) and A. Einstein (1879-1955). While the former two were concerned with the determination of the overall electric conductivity of a heterogeneous material, the latter investigated the effective viscosity of a fluid that contains a suspension of solid spherical particles. In solid mechanics, however, emphasis was originally placed on the determination of the mechanical properties of a polycrystal from those of a single crystal with first theoretical considerations by W. Voigt (1850-1919) and A. Reuss (1900-1968). Within the last 50 years improved estimates have been pursued. For example, the so-called *Dilute* family methods are based on the assumption of no interaction between particles. With this assumption one requires only the solution to a single ellipsoidal particle embedded in an unbounded domain of material under uniform exterior loading. The solution of this problem was found through the Eshelby (1957) formalism, based on eigenstrain concepts (see section 3.2). By itself, this result is of little practical interest, however the solution is relatively compact and easy to use, and thus has been a basis for the development of many approximated analytical methods based on non-interacting and weakly interacting (particle) assumptions. In the second half of the last century, important contributions were supplied, among others, by E. Kröner (1919-2000) and R. Hill (1921-2011). Their theoretical concepts and analytical approximations, which also apply to modern composite materials, were later on extended and generalized to inelastic material behavior. Moreover, they serve as foundations for the treatment of the inverse problem, i.e., the design of new composite materials having an optimized microstructure

with regard to the overall performance. In this sense, development of numerical techniques such as the Finite Element Method has gained importance in the last years and research is now focused on solving micromechanical problems involving various scale levels. Such complex models imply a large number of numerical operations, which requires some model-reduction techniques in order to reduce the associated computational costs.

1.3 Objectives

The main goal of this work is, firstly, to present a general overview of the different techniques that have been developed in the last years in order to obtain a prediction of the behavior of elastoplastic composites by taking into account geometrical and mechanical aspects. Secondly, a comparison between the different approaches is carried out through a numerical implementation of such techniques. More especially, two approaches will be used throughout this work: finite element simulations and mean-field homogenization schemes. The study will be focused on inviscid inelastic materials and all the developments are made in the context of small perturbations.

1.4 Scope and Overview

The present document is divided into eight different chapters. The first chapter serves as an introduction and historical review of the advances that have been made in the field of micromechanics.

Second chapter deals with the scale transition problem, which involves the concepts of macroscopic structure and representative volume element (RVE) of the heterogeneous microstructure. In this section, the main concepts and nomenclature that will be used in the rest of the document will be presented, as well as a short introduction of the different approaches that traditionally have been considered to solve the problem. One group of methods, based on analytical solutions – the so-called *Mean Field Analysis* – will be commented in chapter 3. These techniques rely on simplifying hypotheses so that an approximate solution is found at a much lower computational cost than a corresponding FE simulation.

Chapter 4 is devoted to the development of mean-field homogenization schemes for elastoplastic materials, from a numerical point of view. In this section, the algorithms that have been implemented – using $Matlab^{©}$ tool – will be presented. Such algorithmic schemes correspond with the most usual approaches that are commonly used: the *secant approach* and the *incremental approach*. In addition, some results regarding the validation of such models will be shown, in order to justify and compare the effectiveness with the results that can be obtained from the literature.

Subsequent chapters are devoted to the comparison of the results with the results given by the Finite Element Method. The general formulation of such method – applied to multi-scale problems – is presented in chapter 5 from a theoretical point

of view, as well as the corresponding numerical examples.

Finally, last chapter will be dedicated to enumerate some conclusions extracted from the present work, including some aspects that can be object of future works or improvements.

Chapter 2

Multi-Scale Problems

2.1 Approximation to the Problem

The mission of computational micro-macro mechanics is to determine the relationships between the microstructure and the macroscopic response or "structural property" of a material. In order to obtain such relationships between the mechanical response of the different levels that are involved on the problem, some different approaches have been considered during the past years. The first attempts to obtain the behavior of the heterogeneous materials were based on phenomenological constitutive theories. Such methods are based on the definition of internal variables and the solution of differential equations in order to find the constitutive functional which links the macroscopic stress tensor with the history of the strain tensor at each point of the solid. However, the increasing demand for the modeling of problems of greater complexity has stretched the application of phenomenological problems, since it has been found large difficulties for the definition of internal variables that allow capturing the macroscopic effect of the most relevant micromechanisms.

A second alternative to solve the problem has been developed on the last years and consists on solving the micromechanical problem by means of the so-called multi-scale models, whereby microscopic information is incorporated into the constitutive description of the macroscopic behavior of the material. However, this task is not easy at all: if one were to attempt to perform a direct numerical simulation, for example of the mechanical response of a macroscopic engineering structure composed of a inhomogeneous material, incorporating all the microscope details (mechanical characteristics of the constituents, distribution, etc.), an extremely fine spatial discretization mesh, for example that of a finite element mesh, would be needed to capture all the influence and effects of the microscope heterogeneities. The resulting system of equations would contain a huge amount of numerical unknowns. Such problems are beyond the capacity of computing machines for the foreseeable future. Furthermore, the exact microgeometry is virtually impossible to determine throughout the structure. In addition, in case of solving such a sys-

tem, one should deal with an amount of complex data that should be processed in some way to provide useful information about the desired macroscopic behavior. It is important to notice that solutions to partial differential equations, even for the simplest cases of linear elastic models assuming infinitesimal strains and describing the response of small bodies containing a few heterogeneities are still open problems.

Because of these facts, models in practically all branches of the physical sciences are based on using regularized or homogenized material models (resulting in smooth coefficients in the partial differential equations). Usually, the problem is faced by computing a constitutive "relation between averages", relating volume averaged field variables in a first step. The regularized properties then can be used in a second step to carry out a macroscopic analysis of the structural element. In order to do this, a representative volume element (RVE) has to be defined, where the volume averaged of the internal fields will be computed through the solution of a series of boundary value problems with test loadings. Such regularization processes are referred to as "homogenization" and it will be explained in section 2.4.

The aforementioned method is based on the key concept of representative volume element (RVE). The condition that is required for defining a RVE is that it must be statistically representative of the material as a whole, which implies that a sample should be selected in such a way that contains a large number of heterogeneities. Therefore the computations over the RVE are extremely large, but are of reduced computational effort in comparison with a direct attack on the "real" problem. Historically, the first models used in micromechanics were based on analytical and semi-analytical mean-field homogenization approaches, since the computational cost was a real challenge. Most of these classical methods have a strongly phenomenological basis, and are in reality non-predictive of material responses that are unknown a-priori. Such models provide some good estimations of the effective properties of the inhomogeneous material with small computational effort, but require (due to their phenomenological nature) some extensive experimental data to "tune" parameters that have a little or no physical significance. Nowadays, with the increasing capacity of computers, computational approaches dominate the works in micromechanics field and new methods and techniques have come up in the last decades. Therefore, the phenomenological aspects of the material modeling have been reduced, with the burden of the work being shifted to high performance computational methods or reduced-model techniques.

2.2 Heterogeneity and Scale Separation

Generally speaking, engineering materials are heterogeneous, that is, they have a microstructure and they contain heterogeneities. However, what is considered as heterogeneity depends on the length scales used in the observation. Certain constituents or phases in a given inhomogeneous material are identifiable only at or below a specific length scale. Considering now such length scale, each of the constituents can be considered as homogeneous materials. However, each of the constituents may become heterogeneous when is observed at a smaller length scale.

An airplane spoiler made with some composite material, for example, may seem to be homogeneous to the naked eye ($\sim 10\ \mu m$). But, using an optical microscope ($\sim 1\ \mu m$), one can distinguish different phases (see Fig. 2.1), like the matrix phase and the inclusions made of fibers. At this length scale, although each of the inhomogeneities can be treated as a homogeneous material, the macroscopic material cannot be treated as a homogeneous material anymore because the microstructure attributes, such as the size, alignment and distribution of the fibers, which dictate how the material behaves at this length. When we go down further along the length scales, we know that each fiber (or even the matrix) also has its own microstructure. The behavior and properties of materials at each length scale are controlled by the observable microstructure at the corresponding length scale and the "heterogeneity" of a given material only depends on the length scale used in the observation. Therefore, when a material is studied, it is necessary to define the length scale at which the properties of interest are directly relevant. As a result, the microstructure features that cannot be observed at the length scale of interest can be neglected. In fact, for practical purposes, it is only certain averaged effects of the microstructure that are of interest. So, in micromechanics, the concept of *overall* properties is usually used to mention such properties of interest that are averaged over a certain volume of the heterogeneous material. The overall properties are meaningful only if the average taken over any arbitrary volume element comparable with the relevant length scale is the same with the heterogeneous material sample under consideration. Heterogeneous materials that meet this requirement are said to be macroscopically homogeneous.

Let us consider again the fiber-reinforced composite laminate of the example (Fig. 2.1). It seems to be quite impractical and unnecessary to deal with each individual fiber if the overall bending rigidity of the laminate is of primary interest. On the other hand, the bending rigidity of the laminate is very closely related to the lay up of the various layers within the laminate. To derive the overall rigidity of the composite, the laminate must be treated as a stack of fibers each being different in composition and/or orientation, albeit each fiber can be treated as a homogeneous material.

A requirement that should be fulfilled and that has been implicitly considered in the previous example is the existence of scale separation between the characteristic length of each scale L and l on which the macroscopic (e.g., bending rigidity of the composite laminate) and microscopic properties (elasticity of the plies) are defined, respectively. The microscale length d is defined through the size of the smallest constituent whose physical properties and arrangement have direct first-order effects on the macroscopic physical properties at the length scale L. The choice of the microscopic length scale l is not always clear and should be adapted to each problem. An appropriate choice should be guided by systematic "multi-scale" experimental observations. It is desirable to make a choice that includes a good balance between the definitions of such microgeometry that has a first-order effect on the overall properties and the simplicity of the resulting model. Additionally, it has to be considered that the macroscopic length scale L should be large enough so that the microscale fluctuations (or perturbations) of the main fields of

interest (in a mechanical problem, for instance, the strain and stress fields) due to the local variation at the microscale influence the overall effective property only through their averages. In fact, as it will be commented on section 2.4, in the framework of micromechanics, the stress and strain fields are split into contributions corresponding to different length scales. In this sense, the scale separation is required to assume that the order of magnitude of the fluctuations (micro or local quantities) at the smaller length scale influence the overall (or macroscopic) behavior at the larger length scale only through their averages. On the other hand, fluctuations of stress and strain fields as well as the compositional gradients at the large scale (macro or global quantities) are not significant at the microscale. As a result, the macrofields are considered as locally uniform and will be described as uniform boundary conditions when the boundary problem of the microstructure is solved. In order to achieve some conditions, the characteristic dimension of the microscale constituents should be orders of magnitude smaller than the macroscale element so that, $l/L \ll 1$. In the composite laminate example mentioned above, if the length of each single fiber is on the order $l \sim 0.1\ mm$, the characteristic length scale of the laminate should be at least on the order of $L \sim 1\ mm$ so that the macroscopic effective property (the bending rigidity) can be defined meaningfully.

Note that the identification of d and L is dependent of the length scale of interest. In the above example, since the interest is in the overall bending rigidity of the laminate, it could have been taken the overall thickness of the laminate to be the macroscopic length parameter and the length of each fiber to be the microscopic parameter. This way, it implies that each fiber is a homogeneous material with no microstructure. However, if the interest lies in the behavior of each individual fiber, i.e., the interest is in the length scale of the fiber length, the length of each fiber must be identified as the macroscopic length parameter. In this case, the microscopic length parameter l would be the diameter of the individual microfibers within the fiber. Each fiber as a whole can no longer be viewed as a homogeneous material. Instead, it becomes a composite consisting of polymer resin and the fibers. Each constituent can be considered a homogenous material (see Fig. 2.1).

2.3 Representative Volume Element (RVE)

The concept of Representative Volume Element has been already introduced in the previous chapters as a necessary feature that should be defined when an inhomogeneous material is modeled. The idea of representative volume is closely linked to the concept of microhomogeneity. The microstructure of heterogeneous materials is, at any given scale, very complex, and, to a certain extent, random. As it was pointed before, the precise description of the topologic features of the microstructure variation is usually impractical since it leads to a complex system of equations that involves a huge number of variables. As commented before, for practical purposes the study of inhomogeneous materials is carried out through certain averaged effects of the microstructure that are of interest. Thus, in the study of heterogeneous materials, it is common to speak of *overall* or *effective* properties.

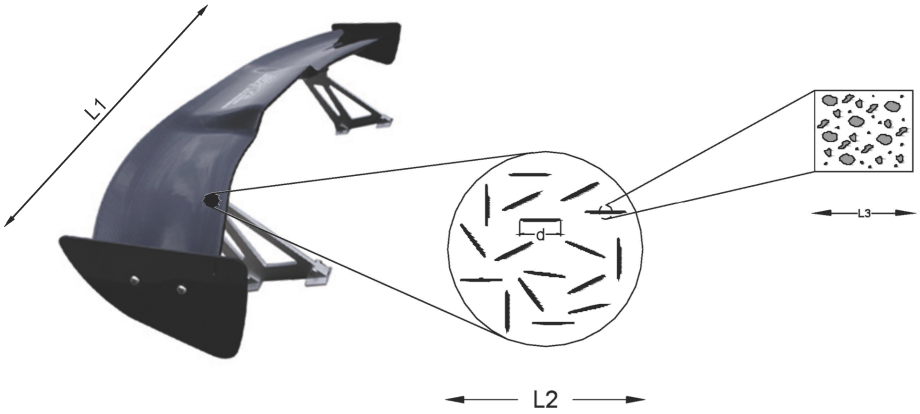

Figure 2.1: Scale separation and characteristic length scales: the material is viewed as homogeneous at the macroscopic level while heterogeneities can be seen at the level of the RVE. Fibers or inclusions can be seen, in turn, as homogeneous considering a new RVE in a lower scale.

Through this concept it is designated the properties averaged over a certain volume of the heterogeneous material. For such effective properties to be meaningful, the required size of the volume element must be such that the average taken over the arbitrary volume element V comparable with the relevant length scale d (here we consider only two different scales for simplicity) is the same with the heterogeneous material sample under consideration. In light of the above discussions (see Fig. 2.1), considering a Representative Volume Element characterized through the element size L_2, if in a heterogeneous material the microscopic length parameter d and the RVE length parameter are such that $d/L_2 \ll 1$, then the heterogeneous material can be considered as microscopically homogeneous at the length scale L_2. In other words, a volume element V with characteristic dimension of L_2 is called a representative volume element (RVE) if the overall properties on any RVE would be the same[1].

Therefore, the RVE in case of an irregular microstructure (defect distribution) must be selected in such a manner that it will contain a sufficiently large number of defects and, hence, its characteristic dimension L_2 has to be much larger than the characteristic length scale d of the microstructure. On the other hand, the volume V has to be small enough that it can approximately be regarded as a point on the macroscopic level (Gross [31]). A characteristic length L_1 on this level will vary depending on the problem and the required property and it may be given by the geometry, by the spatial variation of the loading, or by the stress and strain fields

[1]This condition often appears in the literature by considering that a RVE has to be sufficiently large to be *statically admissible*.

("macrofields") resulting in the macroscopically homogenous material[2].

In order to allow in a certain situation the selection of some volume V, which is suitable for the homogenization of the material, the characteristic length scales have to satisfy the size condition:

$$\boxed{d \ll L_2 \ll L_1}$$

As it can be extracted from the aforementioned requirements, defining the RVE is not a trivial task, even more considering that the microstructure of a composite material is not necessarily known a priori. In the case of random microstructure (Fig. 2.2a), the condition $d \ll L_2$ is taken into account so that a fictitious random microstructure of the RVE might be generated in order to provide a significant response from a statistical point of view. This random microgeometries are generated through the employment of some generators, which must take into account all the available information of the microstructure (volume fraction of each phase, orientations and shape of the inclusion,...). In the case of such random microstructures, defining the minimum size of the RVE is a crucial problem. In the literature there exists a large number of authors that discuss this subject and some of them have studied the factors that have a major influence on the selection of the minimum required size of a RVE (see Povirk [73] and Kanit [40] *et al.*) who define mathematical criteria to fix the cell size). The prerequisite of statistical homogeneity of a locally irregular microstructure is no longer necessary in the especial case of a *strictly* periodic microstructure (Fig. 2.2b) or periodic defect arrangement (Fig. 2.2c). Then a *unit cell* of this arrangement is already representative of the entire heterogeneous material. If assumptions are required to define such unit cell, different arrangements can sometimes be considered which lead to different predictions of the behavior. Also, either on the RVE or the periodic unit cell, various boundary conditions might apply which also influence the predictions. More information regarding the minimum size of the representative volume for practical purposes will be given in section 5.1.

Caution is required with some particular cases, such the so-called *functionally gradient materials* (FGM) with spatially varying macroscopic properties. In this case the distribution of microstructural details displays a spatial variation such that the condition of a statically homogeneous microstructure, which is necessary for the definition of the effective properties strictly speaking does not hold. The use of effective properties then has to be seen as a pragmatic approximation.

2.4 Homogenization approach

From the previous sections it can be deduced that the study of inhomogeneous materials implies various problems, defined in different scales. In order to solve such problems different models have been defined in the literature. In the present

[2]The size of the RVE must be much smaller than the fluctuation length of the prescribed mechanical loading of the whole body (i.e.: $L_2 \ll \lambda$) so that the use of the classical and differential tools of structural analysis remains valid. Here λ means the "wave length" of the prescribed mechanical loading over the structure.

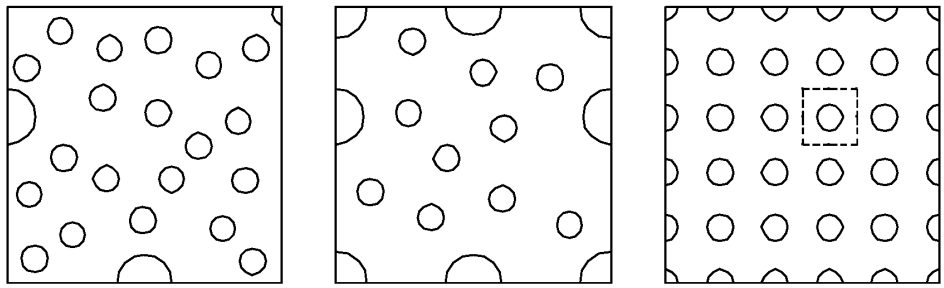

(a) RVE with a random microstructure.

(b) Periodic unit cell with random microstructure.

(c) Periodic unit cell and microstructural arrangement.

Figure 2.2: Periodicity of the unit cell and the microstructural arrangements (Pierard [68]).

document, only *hierarchical* approaches will be considered[3]. In such methods the problem is solved using a sequential approximation, where successive boundary value problems are solved from the finest scales to the coarsest scales. Therefore a mathematical tool is needed to connect the different levels, each of them characterized through a length scale parameter. The most common technique used in multi-scale problems for solving the micromechanical problem is the so-called *direct computational homogenization* and consists in solving some problems, through which the behavior or properties of some material at some larger scale can be estimated by using information from a smaller length scale. Homogenization can be viewed as using a (fictitious) *energetically equivalent*, homogeneous reference material at some higher length scale (called *effective* material) to describe the behavior of the real material that is inhomogeneous at lower length scales and presents a very complex composition (e.g. anisotropic crystallites, grain boundaries, dislocation, etc.). The general scheme of the *direct computational homogenization* can be summarized through the following four steps, as established by Suquet [87]:

- Definition of a microstructural representative volume element (RVE), of which the constitutive behavior of individual constituents is assumed to be known.
- Formulation of the microscopic boundary conditions from the macroscopic input variables and their application on the RVE (micro-to-macro transition).
- Calculation of the microscopic output variables from the analysis of the deformed microstructural RVE (micro-to-macro transition).
- Obtaining the relation between the macroscopic input and output variables.

Homogenization techniques are often used in materials characterization, i.e., simulating the overall response under simple loading conditions such as uniaxial tensile tests, and constitutive modeling, where the responses to general loads, load paths

[3]For a wider approach of the state of the art of multi-scale problems, see [34].

and loading sequences must be described. The description of the material is done through the *effective* properties, such that, for instance, Young's modulus and Poisson's ratio of certain material as experimentally determined with standard testing specimens. Measuring material properties, of course, is only justified if the result does not depend on the chosen testing specimen, i.e. the property the later has to be *representative* of the material. Analogous requirements hold when the effective material properties are theoretically derived from a given structure as will be discussed on the following.

The mathematical description of the basic principles used in the multi-scale problems that will be given in the following sections is based on the work of De Souza Neto and Feijó [86]. It will be assumed that for each point $\boldsymbol{x}$ of the macrocontinuum, a RVE can be found (which is not an easy task, as it was previously commented) and the geometrical arrangement and the material behaviors of the constituents are known. The RVE is denoted by Ω_μ and it consists of a solid part Ω_μ^s and a void part Ω_μ^v, which includes some features like cracks and pores:

$$\Omega_\mu = \Omega_\mu^s \cup \Omega_\mu^v \tag{2.1}$$

For simplicity, it is assumed that the void part does not intersect the boundary of the RVE, which can be expressed as:

$$\partial\Omega_\mu \cap \bar{\Omega}_\mu^v = \emptyset \tag{2.2}$$

where $\bar{\Omega}_\mu^v$ is the closure of the set Ω_μ^v. In the following, the microscopic variables are identified with the subindex μ and two different system of coordinates are defined: a reference system for the macroscopic scale (with position vector defined through $\boldsymbol{x}$) and other for the microscopic scale (with position vector defined through $\boldsymbol{y}$).

2.4.1 Homogenized Strain Tensor

The starting point from a kinematically based description of the multi-scale constitutive theories is the assumption that the strain tensor at each point in the macroscopic level $\boldsymbol{\varepsilon}$ can be obtained through the volume average of the microscopic strain field $\boldsymbol{\varepsilon}_\mu$ defined at each point $\boldsymbol{y}$ over the RVE associated with $\boldsymbol{x}$:

$$\boldsymbol{\varepsilon}(\boldsymbol{x}, t) = \frac{1}{V_\mu} \int_{\Omega_\mu} \boldsymbol{\varepsilon}_\mu(\boldsymbol{y}, t) \, \mathrm{d}V \tag{2.3}$$

where V_μ is the volume of the RVE. The microscopic strain can be expressed in terms of the microscopic displacement field such as:

$$\boldsymbol{\varepsilon}_\mu = \nabla^s \boldsymbol{u}_\mu \tag{2.4}$$

The microscopic displacement fields that satisfy (2.3) and (2.4) are said to be *kinematically admissible*. Substituting (2.4) into (2.3) and considering the Gauss theorem, one gets:

$$\boldsymbol{\varepsilon}(\boldsymbol{x}, t) = \frac{1}{V_\mu} \int_{\Omega_\mu} \nabla^s \boldsymbol{u}_\mu \, \mathrm{d}V = \frac{1}{V_\mu} \int_{\partial\Omega_\mu} \boldsymbol{u}_\mu \otimes_s \boldsymbol{n} \, \mathrm{d}A \tag{2.5}$$

where $\boldsymbol{n}$ is the unit outward normal vector to the boundary of the RVE (denoted through $\partial\Omega_\mu$) and the operator $\otimes_s$ is defined such as:

$$\boldsymbol{u} \otimes_s \boldsymbol{v} = \tfrac{1}{2}(\boldsymbol{u} \otimes \boldsymbol{v} + \boldsymbol{v} \otimes \boldsymbol{u}) \tag{2.6}$$

for two arbitrary vectors $\boldsymbol{u}$ and $\boldsymbol{v}$. In the context of small displacements theory it can be assumed, without loss of generality, that any microscopic displacement can be split into a sum of two terms:

$$\boldsymbol{u}_\mu(\boldsymbol{y}, t) = \boldsymbol{\varepsilon}(\boldsymbol{x}, t)\boldsymbol{y} + \boldsymbol{u}'_\mu(\boldsymbol{y}, t) \tag{2.7}$$

This assumption is based on the premise of scale separation (see section 2.2). Under this consideration, the microscopic displacement at each point of the RVE can be viewed as the composition of a linear displacement $\boldsymbol{\varepsilon}(\boldsymbol{x}, t)\boldsymbol{y}$ and a displacement fluctuation $\boldsymbol{u}'_\mu$. Accordingly, the microscopic strain field can be expressed through:

$$\boldsymbol{\varepsilon}_\mu(\boldsymbol{y}, t) = \boldsymbol{\varepsilon}(\boldsymbol{x}, t) + \nabla^s \boldsymbol{u}'_\mu(\boldsymbol{y}, t) = \boldsymbol{\varepsilon}(\boldsymbol{x}, t) + \boldsymbol{\varepsilon}'(\boldsymbol{y}, t) \tag{2.8}$$

In the previous equation it can be observed that the macroscopic strain is constant over the entire RVE, which is a consequence of the length scale separation. In this sense, a significant difference between length scales makes that the gradients of the fields as well as compositional gradients at the larger length scale (known as "slow variables") have a limited importance at the smaller scale and that they can be approximated as constants in the RVE. Inserting the eqn. (2.8) into the definition of the macroscopic strain (eqn. (2.3)), one gets:

$$\boldsymbol{\varepsilon}(\boldsymbol{x}, t) = \boldsymbol{\varepsilon}(\boldsymbol{x}, t) + \frac{1}{V_\mu} \int_{\Omega_\mu} \nabla^s \boldsymbol{u}'_\mu(\boldsymbol{y}, t)\ \mathrm{d}V \quad \rightsquigarrow \quad \int_{\Omega_\mu} \nabla^s \boldsymbol{u}'_\mu(\boldsymbol{y}, t)\ \mathrm{d}V = 0 \tag{2.9}$$

Using the Gauss theorem it can be found a new expression that provides the set of *kinematically admissible displacement fluctuations*:

$$\int_{\Omega_\mu} \nabla^s \boldsymbol{u}'_\mu(\boldsymbol{y}, t)\ \mathrm{d}V = \int_{\partial\Omega_\mu} \boldsymbol{u}'_\mu \otimes_s \boldsymbol{n}\ \mathrm{d}A = 0 \tag{2.10}$$

Consequently, all the microscopic displacement fields with the form (2.7) that satisfy (2.10) are said to be *kinematically admissible*. The set of kinematically admissible displacement fluctuations plays an important role in the variational characterization of the equilibrium of the RVE and here is denoted through $\mathscr{V}_\mu$. Depending on the choice of a particular subspace of the set of kinematically admissible displacement fluctuations various classes of multi-scale models can be defined (see section 2.4.7).

2.4.2 Equilibrium of the RVE

The RVE is in equilibrium at each instant t of its deformation history. In order to define the equilibrium state for the RVE it has to be considered a new variable: the microscopic stress field, which may be denoted through $\boldsymbol{\sigma}_\mu = \boldsymbol{\sigma}_\mu(\boldsymbol{y}, t)$. The

dynamic equilibrium state in the RVE satisfies the global form of the balance of linear momentum, given by:

$$\int_{\partial\Omega_\mu} \boldsymbol{t}(\boldsymbol{y},t)\ \mathrm{d}A + \int_{\Omega_\mu} \rho_0\big(\boldsymbol{b}(\boldsymbol{y},t) - \dot{\boldsymbol{v}}_\mu(\boldsymbol{y},t)\big)\ \mathrm{d}V \tag{2.11}$$

where $\boldsymbol{t}(\boldsymbol{y},t)$ is the is the traction field acting on the RVE, $\boldsymbol{b}(\boldsymbol{y},t)$ is the vector of body forces and $\dot{\boldsymbol{v}}_\mu(\boldsymbol{y},t)$ is the acceleration field. As stated by Miehe [53], due to the assumption of the existence of a scale separation between both considered levels[4], it can be proved that the inertial forces in the balance of linear momentum vanishes and the overall constitutive response of the microstructure can be based on a static equilibrium state. Based on this result, the static equilibrium of the RVE can be formulated in a more convenient way by considering the *Principle of Virtual Work* such as:

$$\int_{\Omega_\mu} \boldsymbol{\sigma}_\mu(\boldsymbol{y},t) : \nabla^s\boldsymbol{\eta}\ \mathrm{d}V - \int_{\Omega_\mu} \boldsymbol{b}(\boldsymbol{y},t)\cdot\boldsymbol{\eta}\ \mathrm{d}V - \int_{\partial\Omega_\mu} \boldsymbol{t}^e(\boldsymbol{y},t)\cdot\boldsymbol{\eta}\ \mathrm{d}A = 0 \qquad \forall\boldsymbol{\eta}\in\mathscr{V}_\mu \tag{2.12}$$

where $\boldsymbol{t}^e(\boldsymbol{y},t)$ is the external traction field exerted upon the RVE across its external boundary. The equilibrium equation represented by (2.12) holds at each time t for any virtual (i.e., kinematically admissible) displacement $\boldsymbol{\eta}$. The equilibrium equation can be split in order to express separately the equilibrium equation for the void part of the RVE:

$$\int_{\Omega_\mu^v} \boldsymbol{\sigma}_\mu(\boldsymbol{y},t) : \nabla^s\boldsymbol{\eta}\ \mathrm{d}V - \int_{\Omega_\mu^v} \boldsymbol{b}(\boldsymbol{y},t)\cdot\boldsymbol{\eta}\ \mathrm{d}V - \int_{\partial\Omega_\mu^v} \boldsymbol{t}^v(\boldsymbol{y},t)\cdot\boldsymbol{\eta}\ \mathrm{d}A = 0 \qquad \forall\boldsymbol{\eta}\in\mathscr{V}_\mu \tag{2.13}$$

where the vector $\boldsymbol{t}^v(\boldsymbol{y},t)$ represents the internal traction field, defined as the traction exerted upon the solid part of Ω_μ across the solid-void interface, denoted by $\partial\Omega_\mu^v$. The traction vector $\boldsymbol{t}^v$ will be equal to zero in the case of porous material and it will be prescribed as a pressure distribution in the case of a pressure fluid phase in the pores (or as functional of the displacement history in case of collapsing voids or closing micro-cracks due to the frictional contact). On the other hand, the equilibrium equation of the solid part of the RVE can be expressed as:

$$\begin{aligned}\int_{\Omega_\mu^s} \boldsymbol{\sigma}_\mu(\boldsymbol{y},t) : \nabla^s\boldsymbol{\eta}\ \mathrm{d}V - \int_{\Omega_\mu^s} \boldsymbol{b}(\boldsymbol{y},t)\cdot\boldsymbol{\eta}\ \mathrm{d}V \\ - \int_{\partial\Omega_\mu} \boldsymbol{t}^e(\boldsymbol{y},t)\cdot\boldsymbol{\eta}\ \mathrm{d}A - \int_{\partial\Omega_\mu^v} \boldsymbol{t}^v(\boldsymbol{y},t)\cdot\boldsymbol{\eta}\ \mathrm{d}A = 0 \qquad \forall\boldsymbol{\eta}\in\mathscr{V}_\mu\end{aligned} \tag{2.14}$$

[4] Stated through the condition: $\delta := l_\mu/l \ll 1$, where l_μ is the length scale for the microscopic level and l for the macroscopic level.

2.4.3 The Hill-Mandel condition

The Hill-Mandel condition [35] or macrohomogeneity condition is probably the most important principle used in micromechanics and plays a fundamental role in the mathematical description of multi-scale constitutive models[5]. It is a energy average theorem, based on physical arguments, and establishes that the local variation of macroscopic work is equal to the volume average of the variation of work over the RVE:

$$\boldsymbol{\sigma} : \dot{\boldsymbol{\varepsilon}} = \frac{1}{V_\mu} \int_{\Omega_\mu} \boldsymbol{\sigma}_\mu : \dot{\boldsymbol{\varepsilon}}_\mu \, \mathrm{d}V \tag{2.15}$$

The last equation holds for a microscopic stress field $\boldsymbol{\sigma}$ in equilibrium and for any *kinematically admissible* microscopic strain rate field $\dot{\boldsymbol{\varepsilon}}_\mu$, such that:

$$\dot{\boldsymbol{\varepsilon}}_\mu = \nabla^s \dot{\boldsymbol{u}}_\mu = \dot{\boldsymbol{\varepsilon}} + \nabla^s \dot{\boldsymbol{u}}'_\mu \qquad \forall \dot{\boldsymbol{u}}'_\mu \in \mathscr{V}_\mu \tag{2.16}$$

Introducing the fluctuation of displacements into (2.15), the Hill-Mandel condition can be interpreted to establish an energetic equivalence between the microfields fluctuation along the boundary of a RVE and their averages (see Fig. 2.3). As it was commented on the previous sections, the averaging domain Ω_μ should be sufficiently large with respect to the heterogeneities and for suitable boundary conditions (see 2.4.7) in order to assume the aforementioned equivalence.

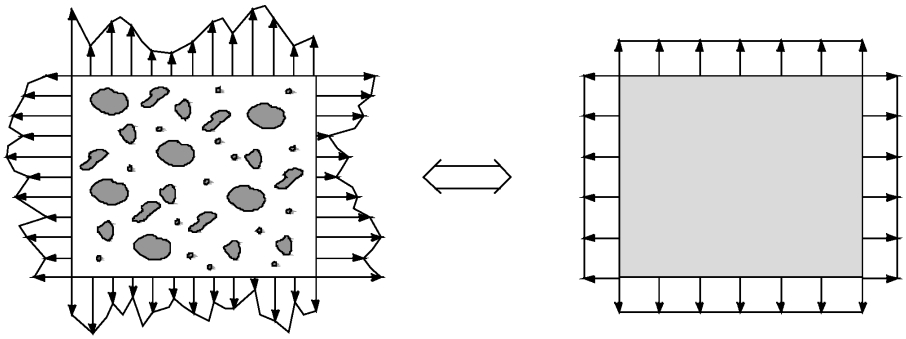

Figure 2.3: RVE with fluctuating microscopic fields and averages (Gross [31]).

Considering the Hill-Mandel condition (2.15) and using (2.16), it easy to prove that the Hill-Mandel condition is equivalent to the following identity[6]:

$$\frac{1}{V_\mu} \int_{\Omega_\mu} \boldsymbol{\sigma}_\mu : \nabla^s \dot{\boldsymbol{u}}'_\mu \, \mathrm{d}V = 0 \tag{2.17}$$

[5] Quoting the words of Bohm [10]: *"The Mandel-Hill condition forms the basis of the interpretation of homogenization procedures in terms of a homogeneous comparison material (or "reference medium") that is energetically equivalent to a given inhomogeneous material".*

[6] For more details, see [86].

Integrating by parts and considering the equilibrium state of the RVE, the Hill-Mandel condition can be stated through the following variational equations:

$$\int_{\partial\Omega_\mu} \boldsymbol{t}^e \cdot \boldsymbol{\eta} \, \mathrm{d}A = 0, \qquad \int_{\Omega_\mu} \boldsymbol{b} \cdot \boldsymbol{\eta} \, \mathrm{d}V = 0, \qquad \forall \boldsymbol{\eta} \in \mathscr{V}_\mu \tag{2.18}$$

From the last equalities it can be inferred an important result: the Hill-Mandel condition is equivalent to requiring that the external surface traction $\boldsymbol{t}^e$ and body force field $\boldsymbol{b}$ of the RVE be purely reactive, i.e., they are a reaction to the imposed kinematical constraints (when $\mathscr{V}_\mu$ is chosen) and cannot be prescribed independently, since they are automatically obtained when $\mathscr{V}_\mu$ is prescribed (and they belong to the functional space orthogonal to $\mathscr{V}_\mu$). Accordingly to the previous result, the equilibrium equation for the RVE (2.14) can be written without considering the external boundary traction nor body force terms:

$$\int_{\Omega^s_\mu} \boldsymbol{\sigma}_\mu(\boldsymbol{y}, t) : \nabla^s \boldsymbol{\eta} \, \mathrm{d}V - \int_{\partial\Omega^v_\mu} \boldsymbol{t}^v(\boldsymbol{y}, t) \cdot \boldsymbol{\eta} \, \mathrm{d}A = 0 \qquad \forall \boldsymbol{\eta} \in \mathscr{V}_\mu \tag{2.19}$$

2.4.4 Homogenized Stress

Considering the Hill-Mandel condition given by (2.15) and the additive decomposition of the microscopic strain tensor (2.16) it can be written:

$$\boldsymbol{\sigma} : \dot{\boldsymbol{\varepsilon}} = \frac{1}{V_\mu} \int_{\Omega_\mu} \boldsymbol{\sigma}_\mu : \dot{\boldsymbol{\varepsilon}} \, \mathrm{d}V + \frac{1}{V_\mu} \int_{\Omega_\mu} \boldsymbol{\sigma}_\mu : \nabla^s \dot{\boldsymbol{u}}'_\mu \, \mathrm{d}V \qquad \forall \dot{\boldsymbol{u}}'_\mu \in \mathscr{V}_\mu \tag{2.20}$$

Last equality is valid for any kinematically admissible $\dot{\boldsymbol{u}}'_\mu$. Considering the particular case $\dot{\boldsymbol{u}}'_\mu = 0$, one gets:

$$\boldsymbol{\sigma} : \dot{\boldsymbol{\varepsilon}} = \frac{1}{V_\mu} \int_{\Omega_\mu} \boldsymbol{\sigma}_\mu : \dot{\boldsymbol{\varepsilon}} \, \mathrm{d}V \qquad \forall \dot{\boldsymbol{\varepsilon}} \tag{2.21}$$

Since the last equation holds for any value of the macroscopic strain rate field, then it is inferred that the following equality holds:

$$\boldsymbol{\sigma}(\boldsymbol{x}, t) = \frac{1}{V_\mu} \int_{\Omega_\mu} \boldsymbol{\sigma}_\mu(\boldsymbol{y}, t) \, \mathrm{d}V \tag{2.22}$$

Accordingly to equation (2.22), the macroscopic stress field is equal to the volume average of the microscopic stress field over the associated RVE. However, as stated by Hernández *et al.* [34], this definition is obtained as a corollary of the Hill-Mandel Principle and the additive decomposition of the microscopic strain and not as an assumption of the model. Considering the equilibrium of the RVE and the symmetry of the stress tensor, an alternative formulation of the homogenized stress in terms of RVE boundary tractions and body forces can be obtained:

$$\boldsymbol{\sigma}(\boldsymbol{x}, t) = \frac{1}{V_\mu} \Big[\int_{\partial\Omega_\mu} \boldsymbol{t}^e(\boldsymbol{y}, t) \otimes_s \boldsymbol{y} \, \mathrm{d}A - \int_{\Omega^s_\mu} \boldsymbol{b}(\boldsymbol{y}, t) \otimes_s \boldsymbol{y} \, \mathrm{d}V - \int_{\Omega^v_\mu} \boldsymbol{b}(\boldsymbol{y}, t) \otimes_s \boldsymbol{y} \, \mathrm{d}V \Big] \tag{2.23}$$

2.4.5 Microscopic constitutive response

Another important ingredient to define completely a multi-scale constitutive model is fixing the constitutive relations of the RVE material. In general, the link between the microscopic stress field and the microscopic strain field history can be expressed through a relation of the type:

$$\boldsymbol{\sigma}_\mu(\boldsymbol{y}) = \mathscr{F}_y(\boldsymbol{\varepsilon}^t_\mu(\boldsymbol{y})) = \mathscr{F}_y\Big\{\big[\boldsymbol{\varepsilon}(\boldsymbol{x},t), \nabla^s \boldsymbol{u}'_\mu(\boldsymbol{y},t)\big]^t\Big\} \tag{2.24}$$

where the superscript t denotes the history up to instant t and the subscript y denotes the point $\boldsymbol{y} \in \Omega^s_\mu$ where the functional is defined, since the material response will vary from point to point of the RVE. Substituting the last expression for the constitutive relation in the equilibrium equation for the solid part of the RVE given by (2.19) the microscopic equilibrium problem can be stated as:

$$\mathcal{G}(\boldsymbol{\varepsilon}, \boldsymbol{u}'_\mu, \boldsymbol{\eta}) \equiv \int_{\Omega^s_\mu} \mathscr{F}_y\Big\{\big[\boldsymbol{\varepsilon}(\boldsymbol{x},t), \nabla^s \boldsymbol{u}'_\mu(\boldsymbol{y},t)\big]^t\Big\} : \nabla^s \boldsymbol{\eta}\, \mathrm{d}V - \int_{\partial\Omega^v_\mu} \boldsymbol{t}^v(\boldsymbol{y},t)\cdot\boldsymbol{\eta}\, \mathrm{d}A = 0 \qquad \forall \boldsymbol{\eta} \in \mathscr{V}_\mu \tag{2.25}$$

where $\mathcal{G}(\boldsymbol{\varepsilon}, \boldsymbol{u}'_\mu, \boldsymbol{\eta})$ is the virtual work functional. The problem will consist on finding, for a given history of macroscopic strain $\boldsymbol{\epsilon}(\boldsymbol{x},t)$ at point $\boldsymbol{x}$ of the macrocontinuum, a kinematically admissible microscopic displacement fluctuation $\boldsymbol{u}'_\mu \in \mathscr{V}_\mu$ such that, for each t, makes $\mathcal{G}$ equal to zero.

2.4.6 Multi-scale model

The multi-scale model is defined through the ingredients provided on the previous sections. Hence, the problem can be stated as choosing an appropriate space $\mathscr{V}_\mu$ of kinematically admissible displacement fluctuations, which should satisfy the minimum kinematical constraint given by (2.10) and should make the microscopic equilibrium problem well-posed. Once the set $\mathscr{V}_\mu$ is defined, the problem will consist on finding, for a given history of macroscopic strain, the macroscopic stress fields in the solid. In order to do that, firstly a kinematically admissible microscopic displacement fluctuation $\boldsymbol{u}'_\mu \in \mathscr{V}_\mu$ such that, for each t, fulfills eqn. (2.25) must be found. With the values of $\boldsymbol{u}'_\mu$ and the functional the microscopic stress can be obtained using eqn. (2.24). Finally, by virtue of equality (2.22), the macroscopic stress field can be computed.

2.4.7 Boundary conditions on the RVE

As it has been commented on the previous section, the multi-scale problem is well-posed when the set of kinematically admissible displacement fluctuations are chosen, i.e., the kinematical constraints have to be imposed on the RVE, which can be seen as setting the boundary conditions on the RVE. Based on the work of De Souza Neto and Feijó [86], four different constitutive models are presented:

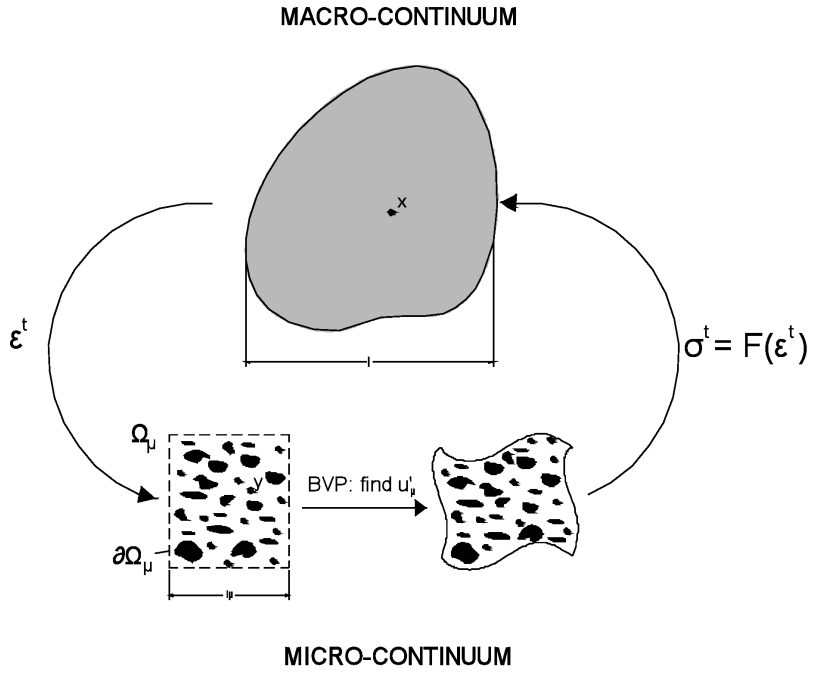

Figure 2.4: Scheme of the solving procedure for a generic multi-scale problem.

homogeneous micro-cell strain model, linear RVE boundary displacement model, periodic RVE boundary displacement fluctuations model (Fig. 2.2b) and uniform RVE boundary traction model (Fig. 2.2a).

Homogeneous micro-cell strain model. In the case of the homogeneous micro-cell strain model, the set of kinematically admissible displacement fluctuations is chosen such as: $\mathscr{V}_\mu \equiv \{0\}$. This choice of the kinematically admissible displacement fluctuations implies:

$$\boldsymbol{u}'_\mu = \boldsymbol{0} \qquad \forall \boldsymbol{y} \in \Omega^s_\mu \tag{2.26}$$

Taking into account the additive decomposition of the microscopic displacement field:

$$\boldsymbol{u}_\mu(\boldsymbol{y}, t) = \boldsymbol{\varepsilon}(\boldsymbol{x}, t)\boldsymbol{y} \qquad \forall \boldsymbol{y} \in \Omega^s_\mu \tag{2.27}$$

It can be observed from the last equation that the microscopic displacement field is linear in $\boldsymbol{y}$, which implies a homogeneous micro-cell strain field:

$$\boldsymbol{\varepsilon}_\mu(\boldsymbol{y}, t) = \boldsymbol{\varepsilon}(\boldsymbol{x}, t) \tag{2.28}$$

The value of the microscopic strain field coincides with the value of the macroscopic strain field at point $\boldsymbol{x}$ of the macro-continuum. The microscopic stress field is obtained directly by considering the constitutive relation on the RVE such as:

$$\boldsymbol{\sigma}_\mu(\boldsymbol{y}, t) = \mathscr{F}_y(\boldsymbol{\varepsilon}^t) \tag{2.29}$$

As it can be observed, the model provides a quite simple solution for the microscopic strain and stress fields. However, the assumption of homogeneous strain field is far away from the real behavior in the microstructure, since it has been observed some complex behaviors due to the interaction of constituents within the RVE. Furthermore, in the current model, the body force $\boldsymbol{b}$, external surface traction $\boldsymbol{t}^e$ and the internal surface traction $\boldsymbol{t}^v$ are all reactions to the imposed kinematical constraint. Therefore, since the traction $\boldsymbol{t}^v$ cannot be imposed, this model is not suitable to describe the interaction between solid and fluid phases in saturated porous media or the crack closure effects in microstructures with cracks. Taking into account the limitations of the model, the homogeneous micro-cell strain model can be used to provide a first estimation for the real problem, . The macroscopic stress field will be computed by considering the volume average of the microscopic stress field:

$$\boldsymbol{\sigma}(t) = \frac{1}{V_\mu} \int_{\Omega_\mu^s} \mathscr{F}_y(\boldsymbol{\varepsilon}^t) \, \mathrm{d}V \tag{2.30}$$

An instance of the above functional of particular practical interest arises when the solid part of the RVE is made of a number N of non-overlapping distinct materials with constitutive response functional $\mathscr{F}^{(p)}$ independent of coordinate $\boldsymbol{y}$.

$$\begin{aligned} \boldsymbol{\sigma}(t) &= \sum_{p=1}^{N} \frac{1}{V_\mu^{(p)}} \int_{\Omega_\mu^{(p)}} \mathscr{F}^{(p)}(\boldsymbol{\varepsilon}^t) \, \mathrm{d}V \\ &= \sum_{p=1}^{N} \frac{\mathscr{F}^{(p)}(\boldsymbol{\varepsilon}^t)}{V_\mu^{(p)}} \int_{\Omega_\mu^{(p)}} \mathrm{d}V \\ &= \sum_{p=1}^{N} c^{(p)} \boldsymbol{\sigma}_\mu^{(p)} \end{aligned} \tag{2.31}$$

where $c^{(p)} = \frac{V_\mu^{(p)}}{V_\mu}$ is the volume fraction and $\boldsymbol{\sigma}_\mu^{(p)}$ is the microscopic stress of phase (p). As it can be observed, the macroscopic stress is computed through the weighted average of the stress acting at the different solid phases. This way to compute the macroscopic stress is known as the *rule of mixtures* and it is widely used in the previous computations.

Linear RVE boundary displacement model. This particular multi-scale model is based on the assumption that the boundary displacement fluctuations vanish, which can be expressed as: $\mathscr{V}_\mu \equiv \{\boldsymbol{u}'_\mu \in \mathscr{K}_\mu^* \mid \boldsymbol{u}'_\mu(\boldsymbol{y}, t) = 0 \ \forall \boldsymbol{y} \in \partial\Omega_\mu\}$, where $\mathscr{K}_\mu^*$ is the minimally constrained vector space of kinematically admissible displacement fluctuations of the RVE.

This choice implies that the microscopic strain field along the boundary of the RVE is linear in $\boldsymbol{y}$, i.e.,

$$\boldsymbol{\varepsilon}_\mu(\boldsymbol{y}, t) = \boldsymbol{\varepsilon}(\boldsymbol{x}, t)\boldsymbol{y} \qquad \forall \boldsymbol{y} \in \partial\Omega_\mu \tag{2.32}$$

For this particular case, the external surface traction $\boldsymbol{t}^e$ belongs to the space of all sufficiently regular fields over $\partial\Omega_\mu$ while the only body force field $\boldsymbol{b}$ orthogonal to the

space of kinematically admissible displacement fluctuation (in virtue of eqn. (2.18)) is the null-vector:

$$\boldsymbol{b}(\boldsymbol{y},t)=\boldsymbol{0} \qquad \forall \boldsymbol{y}\in\Omega_\mu \tag{2.33}$$

Periodic boundary displacement fluctuations model. A third possibility is to consider periodic boundary conditions for the displacement fluctuations. This typology of boundary conditions require the periodicity of the microstructure in all directions, such that it is possible to define a *unit cell* whose periodic repetition generates the microstructure in the vicinity of each macroscopic point $\boldsymbol{x}$. The way to impose periodic boundary conditions is through applying periodic displacement fluctuations on the boundary of the RVE:

$$\boldsymbol{u}'_\mu(\boldsymbol{y}^R,t)=\boldsymbol{u}'_\mu(\boldsymbol{y}^L,t) \tag{2.34}$$

Accordingly, the space of kinematically admissible displacements fluctuations is defined as: $\mathscr{V}_\mu \equiv \{\boldsymbol{u}'_\mu \in \mathscr{K}^*_\mu \mid \boldsymbol{u}'_\mu(\boldsymbol{y}^R,t)=\boldsymbol{u}'_\mu(\boldsymbol{y}^L,t)\ \forall \text{ pairs } \{\boldsymbol{y}^R,\boldsymbol{y}^L\}\in\partial\Omega_\mu\}$. It can be proved (see [86]) that this particular choice of the space of kinematically admissible displacements fluctuations implies anti-periodic tractions at each corresponding pair of nodes lying on opposite faces of the RVE boundary (see Fig. 2.5c):

$$\boldsymbol{t}^e(\boldsymbol{y}^R,t)=-\boldsymbol{t}^e(\boldsymbol{y}^L,t) \tag{2.35}$$

For this particular case, the body force orthogonal to the space $\mathscr{V}_\mu$ for the particular case of periodic boundary displacement fluctuations is the null vector too, as it happened in the previous case:

$$\boldsymbol{b}(\boldsymbol{y},t)=\boldsymbol{0} \qquad \forall \boldsymbol{y}\in\Omega_\mu \tag{2.36}$$

Uniform boundary traction. The last class of multi-scale model corresponds to the assumption of *minimum kinematical constraint* on the RVE, i.e., the space $\mathscr{V}_\mu$ coincides with the space $\mathscr{K}^*_\mu$. As occurred in the two previous models, the prescribed set of kinematically admissible displacement fluctuation implies that the body force vector $\boldsymbol{b}$ located on the orthogonal space of $\mathscr{V}_\mu$ is the null-vector again:

$$\boldsymbol{b}(\boldsymbol{y},t)=\boldsymbol{0} \qquad \forall \boldsymbol{y}\in\Omega_\mu \tag{2.37}$$

On the other hand, the external surface traction $\boldsymbol{t}^e$ compatible with the current kinematical constraint is[7]:

$$\boldsymbol{t}^e(\boldsymbol{y},t)=\boldsymbol{\sigma}_\mu(\boldsymbol{y},t)=\boldsymbol{\sigma}(\boldsymbol{x},t)\ \boldsymbol{n}(\boldsymbol{y}) \qquad \forall \boldsymbol{y}\in\partial\Omega_\mu \tag{2.38}$$

where $\boldsymbol{\sigma}(\boldsymbol{x},t)$ is the macroscopic stress at the point $\boldsymbol{x}$ of the macro-continuum. As it can be observed, the result obtained in the previous equation is a mere consequence of the prescribed kinematical constraint and, in a strictly kinematical framework, the traction boundary condition given by eqn (2.38) is not imposed a priori.

[7] For the mathematical proof of eqn. (2.38) see [86].

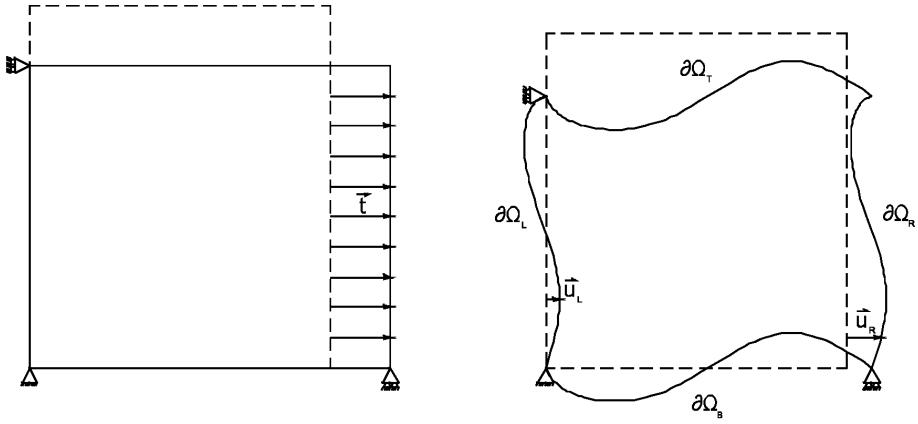

(a) Prescribed uniaxial tractions.

(b) Periodic boundary conditions.

Figure 2.5: Imposition of boundary conditions to a 2D rectangular RVE. Initial configuration is in dots and final one in continuous lines (Pierard [68]).

The solution of the boundary value problem over the RVE is not necessarily the same depending on the selected kinematical constraints. Thus, the solution for the microscopic equilibrium problem using the most kinematically constrained models will lead to stiffer solutions for the problem, while reducing the kinematical constraints produces more compliant solutions. In fact, as stated by Miehe [53]: *"linear deformation and uniform tractions provide upper and lower bounds of the overall stiffness of the finite-sized RVEs of heterogeneous materials which converge to each other if the size of the RVE becomes infinitely large"*. On the other hand, periodic boundary conditions generally lead to an intermediate and more accurate response, which means that a smaller cell size can be considered: the so-called *repeating unit cell (RUC)*. This is even more true during an analysis of the microscopic fields. In addition, when imposing periodic boundary conditions there no exists difference between the treatment of the lateral faces and the sections located in the middle of the RVE. On the contrary, prescribed linear displacements or uniform tractions on the boundary give an inaccurate response close to the boundaries (e.g.: if uniform tractions are prescribed, the stress will be uniform on the faces which is obviously not correct). These facts have been observed numerically in numerous studies, including Kanit *et al.* [40] in linear elasticity, Jiang *et al.* [38, 39] in elastoplasticity and Ostoja-Starzewski [64] for a wide range of constitutive behaviors.

2.5 Major Modeling Strategies in Continuum Micromechanics of Materials

All micromechanical methods described in the present document can be used to do materials characterization and many of them can also be employed directly as micromechanically based constitutive models at higher length scales. Materials characterization only provides the effective properties of the energetically equivalent homogeneous material by simulating the overall material response under simple loading conditions. On the other hand, micromechanical constitutive models can supply the full response of the material through the stress and strain tensors for any given loading condition or any loading path. Obviously, micromechanical constitutive models are more demanding than materials characterization but they have both a clear physical basis and an inherent capacity to provide the phase strains and stresses for each constituent by using localization techniques. On the contrary, some simplified models such as semiempirical constitutive laws (see Davis [16]) do not posses such qualities.

Several criteria must be taken into account when choosing a solution method: arrangement and periodicity of the microstructure, computational cost, desired information on the local fields, accuracy of the predictions,... A comparison of all the presented methods is given at the end of this section.

2.5.1 Mean-field homogenization schemes

Semi-analytical mean-field homogenization methods appeared some years ago when the computational cost supposed a real problem. These methods are based on some assumptions for the interaction between constituents: several methods have been proposed by different authors and the difference among them is founded on their interaction laws. As their name indicates, these methods enable to provide the macroscopic behavior of the material (through the homogenization) and the strain and stress tensors for each phase, in terms of averages (expressed through the term "mean-field"). Such methods were developed initially for linear constituents and they enable to get some accurate predictions of the macroscopic behavior in the linear elastic regime with a small computational cost, especially for inclusion-reinforced materials and polycrystals. In the last years these approaches have been extended to inelastic materials by linearizing the local constitutive laws of nonlinear materials.

Mean-field homogenization techniques are commonly based on the Eshelby result [24], which is valid for ellipsoidal inclusions only and assume a perfect bonding between constituents. This theoretical result will be explained in section 3.2. Disadvantages of such techniques lies in their incapacity to predict any strain or stress distribution in the microgeometry and to recover some effects like clustering, percolation and size effects. These methods will be explained in detail in chapter 3 and the extension to rate independent elastoplastic behavior will be commented in chapter 4.

2.5.2 Finite Element methods

Classical finite element approaches can be used to solve the boundary value problem on a RVE. The Finite Element Method is nowadays the most popular scheme for evaluating full field models, especially in the nonlinear range, due to the fact that it is a flexible model and enables supporting a wide range of constitutive description for the constituents and for the interfaces. Such approach is even more suited when periodic microstructure is assumed, since very simple unit cells subjected to periodic boundary conditions can be considered, leading to an important reduction of the computational costs. The Finite Element Method provides good results for both the macroscopic response and the local fields. However, some disadvantages like the impossibility of taking into account size effects have been detected. In addition, the generation of an appropriate finite element mesh for some complex problems is a very hard task and may lead to high computational costs, especially when the problem is coupled to another one on a different scale. Therefore, some authors have studied some simplified methods or have developed some additional techniques to avoid some problems. For instance, a simplification can consist on reducing the real three dimensional (3D) RVE to a simplified two dimensional (2D) axisymmetric or planar one, when the conditions of symmetry allow it. Another alternative, that can be considered if difficulties in modeling the microstructure arise, consists of using the Voronoi cell finite element method, proposed by Ghosh [28] and based on a Dirichlet tessellation of the microstructure into a network of multi-sided Voronoi polygons (see Fig. 2.6)[8]. Formulation in linear and some nonlinear regimes have been developed for such elements and applied to some different constitutive behaviors.

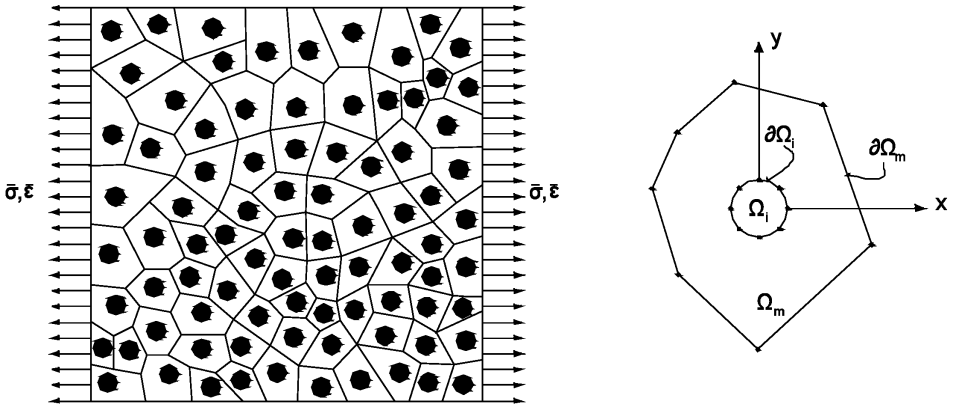

Figure 2.6: Tesellation of the microstructure into Voronoi cells.

[8]This approach is well-suited to study the microstructure of polycrystals and sometimes for the one of two-phase materials (Kanit *et al* [40]).

2.5.3 Asymptotic homogenization method

Another technique that allows predicting the macroscopic and microscopic properties of an inhomogeneous material is the so-called asymptotic homogenization method, developed by Bensoussan *et al.* [7] and Sanchez-Palencia [77]. The method relies on the assumption of separation between scales, which can be described through the condition given by the ratio between the characteristic length of the RVE (l) and the one of the real structure (L) such that: $\varepsilon = l/L \ll 1$. The technique is based on a dependence of all variables with respect to both length scales, due to the fact that the presence of heterogeneities in a periodic microstructure produces rapid variation of strain and stresses in a small neighborhood ε of a macroscopic point $\bar{\boldsymbol{x}}$, as described by Ghosh *et al.* [29]). Therefore, one can write the variables in terms of the coordinates at the macroscopic level ($\bar{\boldsymbol{x}}$) and at the microscopic one ($\bar{\boldsymbol{x}}/\varepsilon$). Using asymptotical expansions of displacement and stress fields with respect to ε in the equilibrium equation and constitutive relations leads to a set of partial differential equations with periodic boundary conditions. This system can be solved numerically using, for instance, Finite Element algorithms. They also have been combined with other methods like the unit-cell scheme for linear problems, leading to the Variational Asymptotical Method for Unit Cell Homogenization (see Yu and Tang [98]) or together with a Voronoi cell tessellation (see Ghosh *et al.* [29]). For a historical review of the method, see Chung *et al.* [15] and references therein.

2.5.4 Generalized method of cells

The generalized method of cells was introduced by Aboudi [1], Paley and Aboudi [65] and Dvorak [22] (termed the transformation field analysis) and allows computing the microscopic and macroscopic properties of heterogeneous inelastic materials subjected to multiaxial mechanical loadings as well as spatially constant thermal loading. The method is based on dividing a repeating unit cell into an arbitrary number of generic cells, which are divided again into 4 (or 8) rectangular (or parallelepipedal) subcells (see Fig. 2.7). Each subcell only contains a homogeneous material, which is different from one cell to each other. The global response of the material is calculated using a classical volume average and assuming that the displacement vector on each subcell varies linearly with the local subcell coordinates. Moreover, the continuity of displacements and tractions between adjacent subcells and repeating unit cells is imposed. Generalized method of cells is very efficient from an algorithmic point of view and provides accurate results for the global response of the solid, although the quality of the local fields is not that high due to the linear assumption of the displacements fields. Some authors have developed improvements of the generalized method of cells in order to apply it to nonlinear problems. For instance, Aboudi *et al.* [2, 3] have created the so-called high-fidelity general method of cells, which uses higher order displacement fields, which leads to much higher computational costs (although they are still lower than an equivalent finite element simulation). In this point, one should consider if it is convenient to use this improved method of cells or, on the contrary, it is better to spend much

computational cost using a finite element approach (this method provides better accuracy of the microfields due to the imposed rectangular shape of the subcells).

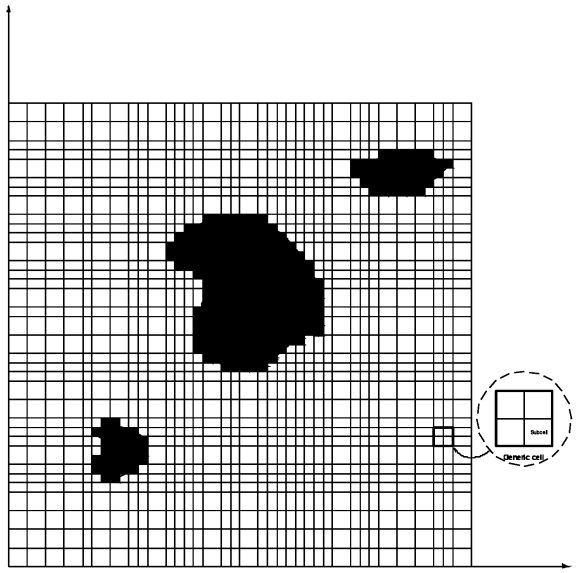

Figure 2.7: Typical discretization of a repeating unit cell, generic cell and subcell of the generalized method of cells (Pierard [68]).

2.5.5 Fast Fourier transform method

Fast Fourier transform method is a meshless method introduced by Moulinec and Suquet [56, 57] that is restricted to periodic microstructures. The method is based on the use of the fast Fourier Transform and Discrete Fourier Transforms (see [59]) to solve the problem at the microscopic level and it can be combined together with image digitalization techniques to discretize the microstructure. In practical applications, the RVE is digitalized into a given number of pixels (2D) or voxels (3D), which contain some mechanical properties associated to each of them. After discretizing the RVE, the constitutive and equilibrium equations can be written in an integral form by introducing the Green tensor. Using a Fourier transformation of this expression, the problem can be solved by means of an iterative process over the stress tensor (if macroscopic strain is prescribed) in the Fourier space. After solving the nonlinear periodic equation (known as Lippmann-Schwinger equation) a solution at each pixel (or voxel) is obtained. This method implies less computational cost than an equivalent finite element simulation. The Fast Fourier transform method has been also adapted to take into account some difficult cases liked the nonlinear response of the heterogeneous materials, leading to the Transformation Field Analysis of Dvorak [22], which is characterized by its high computational

efficiency. However, the method of Dvorak is based on piecewise uniform transformation fields and very fine discretizations of the phases are required to achieve good accuracy (see Dvorak *et al.* [23]). Due to this, Michel and Suquet [52]) have developed the so-called Nonuniform Transformation Field Analysis, which is an improved version of the TFA, based on nonuniform, incompressible and orthogonal "plastic flow modes" to provide better results in the case of nonlinear mechanical behavior of materials.

2.5.6 Embedded Cell or Embedding Approaches

The embedding approaches are used for materials characterization but maybe the most common application for such methods is the study of some special regions of interest in inhomogeneous materials, such as the tips of macroscopic cracks or their surroundings. These strategies are based on an approximation of the real material through a model that consists on a "core" containing a discrete phase arrangement (known as "local heterogeneous region") embedded in an outer region ("embedding" or "effective' region") where far field loads or strains are applied (Böhm [10]). A self-consistent or quasi-self-consistent approach is used to calculate the problem, in which the core is described with high detail while the material properties of the outer region may be described by some macroscopic constitutive law. Embedded cell approaches can resolve local stress and strain fields in the core region at high detail and do not require that the microgeometry and all microfields must be strictly periodic. However, they tend to be computationally expensive and are characterized by the appearance of spurious boundary layers, which occur at the "interfaces" between the core and the embedding region and perturb the local stress and strain fields.

In the literature (see [10]) three basic types of embedding approaches are differentiated. One of them uses discrete microstructures in both the core region and the surrounding material, the latter, however, being discretized by a much coarser mesh, see, e.g., Sautter *et al.* [78]. Such models can avoid boundary layers to a large extent by using appropriately graded meshes. They tend to be relatively expensive computationally. Some authors have developed Finite Element Models with mesh superposition techniques, which use a coarser mesh over the macroscopic model together with a geometrically independent, much finer mesh in regions of interest (Takano *et al.* [90]). This methods are conceptually equivalent to the first type of Embedding Approaches.

In the second group of embedding methods the behavior of the outer regions is described via appropriated "smeared out" constitutive models. These typically take the form of semiempirical or micromechanically based constitutive laws that are prescribed a priori for the embedding zone and which must be chosen to correspond closely to the overall behavior of the core[9]. This way, conceptually simple models are obtained that are very well suited to studying local phenomena. For such applications, loads may be introduced via macrohomogeneous stress and/or

[9]The material parameters used with these constitutive laws may be obtained from modeling or from experiments.

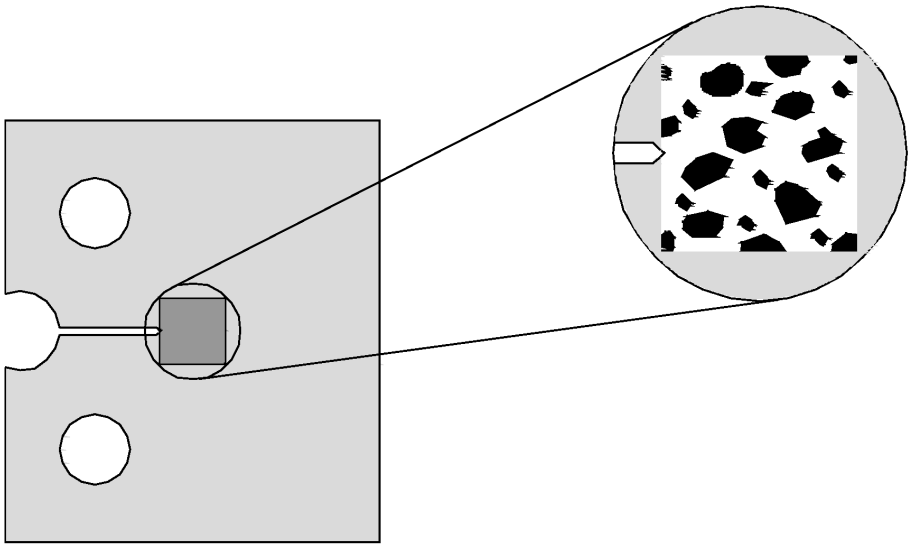

Figure 2.8: Schematic depiction of the arrangement of core and embedding region in a embedded cell model of a tensile test specimen (Böhm [10]).

strain fields or via displacement boundary conditions that impose a far field behavior obtained from a suitable analytical or numerical solution pertinent to the appropriate effective material behavior.

The third type employs the homogenized mechanical response of the core for determining the effective behavior of the surrounding medium in a self-consistent way. Models of this type have been mainly employed for materials characterization (see section 3.5). Such self-consistent methods need some requirements that can be easily fulfilled in the linear range but may lead to considerable complexity when at least one of the constituents shows elastoplastic or viscoplastic material behavior. In such complex cases, some authors have proposed several approximations, obtaining the so-called "quasi-self-consistent schemes".

2.5.7 Windowing Approaches

Windowing approaches are employed to obtain estimates or bounds for the macroscopic properties of heterogeneous materials by randomly selecting special nonperiodic subregions (called "windows", typically of rectangular or hexahedral shape) that are subjected to boundary conditions that guarantee energy equivalence between the micro- and macroscales. These volume elements typically have simple shapes, are extracted at random positions from a given phase arrangement and, in the case of macroscopically homogeneous materials, with random orientations from an inhomogeneous medium (see Fig. 2.9), and are smaller than RVEs. Windowing

methods are based on a surface integral version of the Hill condition, which can be fulfilled via uniform boundary conditions or periodic boundary conditions. For the special cases of macrohomogeneous stress and strain boundary conditions, respectively, lower and upper estimates for the overall properties of a given window[10]. Choosing several different windows of comparable size and taking the averages of the estimates may provide upper and lower bounds for the effective properties of the material.

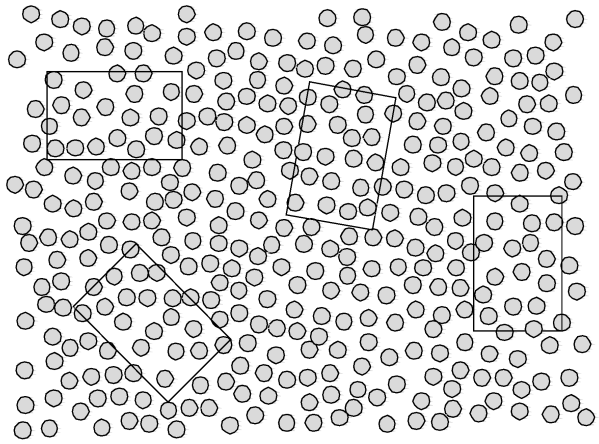

Figure 2.9: Schematic depiction of a composite and four rectangular windows of equal size (Böhm [10]).

Like embedding methods windowing gives rise to perturbed boundary layer near the surfaces of the volume element, which may influence the results of phase averages of microfields. The principal strength of windowing methods lies in providing an approach to study the linear behavior of non-periodic volume.

2.5.8 Comparison of the various methods

Finally a overview of the aforementioned methods can be observed in the table 2.1(the table has been collected from [68] and completed with some of the aforementioned methods). The table shows the different capabilities and levels of the accuracy of the different approaches that are commonly used for homogenization purposes. The criteria that have been selected to make the comparison is:

- Complex geometries: possibility of the method to deal with complex microstructures.

[10]The generation of lower and upper estimates by windowing using such boundary conditions can be shown to be valid in the context of nonlinear elasticity and deformation plasticity. Mixed boundary conditions, however, rely on the superposition principle and, accordingly, cannot be used for general load paths in the inelastic regime.

- Ease of discretization: most methods require a discretization of the RVE, which can be tricky in some cases.
- Accuracy of the macroscopic response: this is the main goal of the homogenization methods, so its accuracy is of first importance.
- Accuracy of the microfields: some methods, in addition to the prediction of the macroscopic response can give accurate information about microfields as well.
- Computational cost: varies from a fraction of second to several hours on a multiprocessor computer so that it might be a huge limitation for applications of the method in practice.
- Nonlinear behaviors: the difficulty of extensions to nonlinear behavior greatly depends on the method.

The table only pretends to be a rough summary of the different methods, due to the difficulty of collecting all the different methods and their variants. Moreover, it is important to realize that some methods are more appropriate than others depending on the type of problem to solve.

Homogenization Method	2DFE	3DFE	2DVCFE	AHM	WA
Complex Geometries	⋆	⋆	⋆	⋆	⋆⋆
Ease of discretization	⋆⋆	⋆	⋆⋆⋆	⋆⋆	⋆⋆⋆
Accuracy macro response	⋆⋆	⋆⋆⋆	⋆⋆	⋆⋆	⋆
Accuracy microfields	⋆⋆	⋆⋆⋆	⋆	⋆⋆	⋆
Computational cost	⋆⋆	⋆	⋆⋆	⋆	⋆⋆
Nonlinear behaviors	⋆⋆⋆	⋆⋆⋆	⋆⋆⋆	⋆⋆	⋆
Homogenization Method	**FFTM**	**GMC**	**HFGC**	**MFHM**	**ECA**
Complex Geometries	⋆⋆	⋆⋆	⋆⋆⋆	⋆⋆	⋆
Ease of discretization	⋆⋆	⋆⋆	⋆⋆⋆	⋆⋆⋆	⋆⋆
Accuracy macro response	⋆⋆⋆	⋆⋆⋆	⋆⋆	⋆⋆	⋆
Accuracy microfields	⋆	⋆⋆	⋆⋆	⋆	⋆⋆
Computational cost	⋆⋆	⋆	⋆	⋆⋆⋆	⋆
Nonlinear behaviors	⋆⋆⋆	⋆⋆⋆	⋆⋆	⋆⋆	⋆

Table 2.1: Comparison of different homogenization methods over various criteria (adapted from Pierard [68]). 2DFE: two-Dimensional Finite Element method, 3DFE: three-Dimensional Finite Element method, 2DVCFE: two-Dimensional Voronoi Cell Finite Element method, AHM: Asymptotic Homogenization Method, WA: Windowing Approach, FFTM: Fast Fourier Transform Method, GMC: Generalized Method of Cells, HFGC: High Fidelity Generalized Method of Cells, MFHM: Mean-Field Homogenization Method and ECA: Embedded Cell Approach. Evaluations are: ⋆: weak, ⋆⋆: fair, ⋆⋆⋆: good.

Chapter 3

Mean-Field Analysis (M.F.A)

Mean-field homogenization schemes are an efficient way to predict the behavior of heterogeneous materials. They range from the simplest hypotheses on the stress or strain sharing among the phases which do not require analytical solution on the associated boundary-value problem (Voigt and Reuss estimates), to more involved geometric models based on the solution of a boundary-value problem involving a single or composite inclusion embedded in an equivalent homogenized medium whose elastic module become part of the solution procedure (Self-Consistent schemes). In general, they are based on analytical solutions of the boundary value problem defined in the microstructure level of the inhomogeneous material, defined in section 2.4. Such techniques are formulated in the context of linear elasticity, where the solution of the boundary value problem is known to be unique and the fields inside the domain Ω_μ^s can be represented through a linear dependency such as:

$$\boldsymbol{\varepsilon}_\mu(\boldsymbol{y},t) = \mathbb{A}(\boldsymbol{y}) : \boldsymbol{\varepsilon}(\boldsymbol{x},t) \qquad \text{and} \qquad \boldsymbol{\sigma}_\mu(\boldsymbol{y},t) = \mathbb{B}(\boldsymbol{y}) : \boldsymbol{\sigma}(\boldsymbol{x},t) \tag{3.1}$$

$\mathbb{A}(\boldsymbol{y})$ and $\mathbb{B}(\boldsymbol{y})$ are fourth order tensors known as mechanical strain and stress concentration tensors (or influence functions, see Hill [35]) and represent the complete solution of the respective boundary value problems. When they are known, the solution of the multi-scale problem is trivial. However, microgeometries of real inhomogeneous materials are characterized, in the majority of cases of practical relevance, through their complexity and randomness and exact expressions for $\mathbb{A}(\boldsymbol{y})$, $\mathbb{B}(\boldsymbol{y})$, $\boldsymbol{\varepsilon}_\mu(\boldsymbol{y},t)$, $\boldsymbol{\sigma}_\mu(\boldsymbol{y},t)$, etc., in general cannot be given with reasonable effort. As a consequence, approximations have to be introduced. Therefore, it is important to consider the RVE, since it can be applied the *ergodic* hypothesis, i.e., the heterogeneous material is assumed to be statically homogeneous[1].

[1] A simple definition of the RVE was given by Drugan and Willis [21]: *"It is the smallest material volume element of the composite for which the usual spatially constant (overall modulus) macroscopic constitutive representation is a sufficiently accurate model to represent mean constitutive response"*.

In fact, mean-field approaches (MFAs) approximate the microfields within each constituents by their volume phase averages $\boldsymbol{\varepsilon}_\mu^{(p)}$ and $\boldsymbol{\sigma}_\mu^{(p)}$, i.e., *uniform strain and stress fields* on each phase are used. The main geometrical characteristics of each phase, given by the volume fraction of each constituent, phase topology, aspect ratio of inclusions, ... are considered by using statistical descriptors. In MFAs the relations between the micro- and macro-fields are given by the following expressions (the dependance on the macroscopic coordinate $\boldsymbol{x}$ is omitted for clarity):

$$\begin{aligned} \boldsymbol{\varepsilon}_\mu^{(p)} &= \bar{\mathbb{A}}^{(p)} : \boldsymbol{\varepsilon} \\ \boldsymbol{\sigma}_\mu^{(p)} &= \bar{\mathbb{B}}^{(p)} : \boldsymbol{\sigma} \end{aligned} \tag{3.2}$$

and the homogenization relations can be written as:

$$\begin{aligned} \boldsymbol{\varepsilon}_\mu^{(p)} &= \frac{1}{V_\mu^{(p)}} \int_{\Omega_\mu^{(p)}} \boldsymbol{\varepsilon}(\boldsymbol{y},t)\mathrm{d}V \quad \text{with} \quad \boldsymbol{\varepsilon} = \sum\nolimits_p c^{(p)} \boldsymbol{\varepsilon}_\mu^{(p)} \\ \boldsymbol{\sigma}_\mu^{(p)} &= \frac{1}{V_\mu^{(p)}} \int_{\Omega_\mu^{(p)}} \boldsymbol{\sigma}(\boldsymbol{y},t)\mathrm{d}V \quad \text{with} \quad \boldsymbol{\sigma} = \sum\nolimits_p c^{(p)} \boldsymbol{\sigma}_\mu^{(p)} \end{aligned} \tag{3.3}$$

where $^{(p)}$ denotes a given phase of the material (see Fig. 3.1), $V^{(p)}$ is the volume occupied by this phase, and $c^{(p)} = V^{(p)}/\sum_N V^{(k)}$ is the volume fraction of the phase (it is easy to see that $\sum_N c^{(p)} = 1$). In contrast to equation (3.1) the phase concentration tensors $\bar{\mathbb{A}}$ and $\bar{\mathbb{B}}$ used in MFAs are not functions of the spatial coordinates of the microstructure and they are considered to be constant over each phase.

Mean-field approaches tend to be formulated in terms of the phase concentration tensors (in fact, different methods differ from each other by the selection of the concentration tensors), they require low computational requirements and they have been successful in describing the thermoelastic response of inhomogeneous materials. Because they do not explicitly account for n-particle interactions they are sometimes referred to as "noninteracting approximations" in the literature. They are based on the existence of an RVE and typically assume some idealized statistics of the phase arrangement at the microscale. Furthermore, perfect bonding between the constituents is assumed in all cases.

Such methods are based on a procedure involving two different steps. In a first step, a local problem for a single inclusion is solved in order to obtain approximations for the local field behavior as was derived by Eshelby for elastic fields of an ellipsoidal inclusion [24]. The second step consists on averaging the local fields to obtain the global effective properties. In this context, the main requirements on homogenization methods, according to Zheng and Du [99] are:

a) a simple structure which can be solved explicitly, such that a physical interpretations for the behavior of all the components involved is possible;

b) a valid structure for multiphase composites with various inclusion geometries, isotropy and anisotropies;

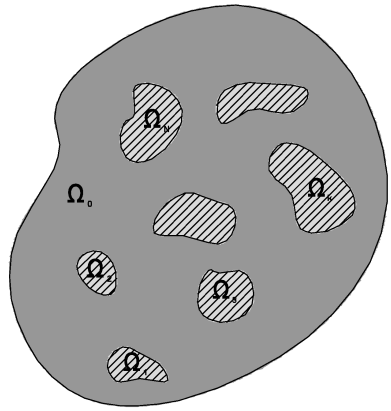

Figure 3.1: Multiphase composite. The matrix is represented through the index 0 while the inclusions are denoted through indexes 1 to N.

c) an accurate model for the influence of various inclusion distributions and interactions between inclusions and their immediately surrounding matrix.

Various mean-field homogenization schemes are presented in this section and their application to linear elastoplastic composites will be examined in chapter 4. Furthermore, some theoretical bounds of the real response can be developed, which enable to check some approximations made by the predictive methods. These bounds, based on variational principles will be also commented at the end of the present chapter.

3.1 General Relations between Mean Fiels in Elastic Multi-phase materials

Throughout this document additive decomposition of strains is used. For example, for the case of elastoplastic material behavior the total strain tensor can be accordingly written as:

$$\boldsymbol{\varepsilon}(\boldsymbol{x},t) = \boldsymbol{\varepsilon}_{el}(\boldsymbol{x},t) + \boldsymbol{\varepsilon}_{pl}(\boldsymbol{x},t) \tag{3.4}$$

where $\boldsymbol{\varepsilon}_{el}(\boldsymbol{x},t)$ and $\boldsymbol{\varepsilon}_{pl}(\boldsymbol{x},t)$ denote the elastic and plastic strains, respectively.

For elastic inhomogeneous materials and isothermal process, the macroscopic stress-strain relations can be written in the form:

$$\boldsymbol{\sigma}(\boldsymbol{x},t) = \mathbb{C}^*(\boldsymbol{x},t) : \boldsymbol{\varepsilon}(\boldsymbol{x},t)$$

$$\boldsymbol{\varepsilon}(\boldsymbol{x},t) = \mathbb{M}^*(\boldsymbol{x},t) : \boldsymbol{\sigma}(\boldsymbol{x},t) \tag{3.5}$$

Each constituent of the multi-phase material is assumed to behave elastically, so that:

$$\begin{aligned}\boldsymbol{\sigma}_{\mu}^{(p)} &= \mathbb{C}^{*}(\boldsymbol{x},t) : \boldsymbol{\varepsilon}_{\mu}^{(p)} \\ \boldsymbol{\varepsilon}_{\mu}^{(p)} &= \mathbb{M}^{*}(\boldsymbol{x},t) : \boldsymbol{\sigma}_{\mu}^{(p)}\end{aligned} \tag{3.6}$$

From the definition of phase averaging, the relations between the phase averaged fields,

$$\begin{aligned}\boldsymbol{\varepsilon}(\boldsymbol{x},t) &= \sum\nolimits_{p} c^{(p)} \boldsymbol{\varepsilon}_{\mu}^{(p)} = \boldsymbol{\varepsilon}^{0}(\boldsymbol{x},t) \\ \boldsymbol{\sigma}(\boldsymbol{x},t) &= \sum\nolimits_{p} c^{(p)} \boldsymbol{\varepsilon}_{\mu}^{(p)} = \boldsymbol{\sigma}^{0}(\boldsymbol{x},t)\end{aligned} \tag{3.7}$$

follow immediately, where $\boldsymbol{\varepsilon}^{0}(\boldsymbol{x},t)$ and $\boldsymbol{\sigma}^{0}(\boldsymbol{x},t)$ denote the far field (applied) homogeneous stress and strain tensors, respectively, with $\boldsymbol{\sigma}^{0}(\boldsymbol{x},t) = \mathbb{C}^{*}(\boldsymbol{x},t) : \boldsymbol{\varepsilon}^{0}(\boldsymbol{x},t)$. Perfect interfaces between the phases are assumed in expressing the macroscopic strain of the composite as the weighted sum of the average strains.

By using last expression and considering the concentration tensors (equation (3.2)), the strain and stress concentration tensors can be shown to fulfill the relations (in the following, the dependence of the macroscopic coordinate $\boldsymbol{x}$ and time t is omitted for clarity):

$$\sum_{(p)} c^{(p)} \bar{\mathbb{A}}^{(p)} = \mathbb{I} \qquad \text{and} \qquad \sum_{(p)} c^{(p)} \bar{\mathbb{B}}^{(p)} = \mathbb{I} \tag{3.8}$$

where $\mathbb{I}$ stands for the symmetric rank four unit tensor and $c^{(p)} = V^{(p)}/\sum_{N} V^{(k)}$ is the volume fraction of each phase.

The effective and compliance tensors of the composite can be obtained from the properties of the phases and from the mechanical concentration tensors as:

$$\mathbb{C}^{*} = \sum_{(p)} c^{(p)} \mathbb{C}^{(p)} : \bar{\mathbb{A}}^{(p)} \qquad \mathbb{M}^{*} = \sum_{(p)} c^{(p)} \mathbb{M}^{(p)} : \bar{\mathbb{B}}^{(p)} \tag{3.9}$$

The mechanical stress and strain concentration tensors for a given phase are linked to each other by expressions of the type:

$$\bar{\mathbb{A}}^{(p)} = \mathbb{M}^{(p)} : \bar{\mathbb{B}}^{(p)} : \mathbb{C}^{*} \qquad \text{and} \qquad \bar{\mathbb{B}}^{(p)} = \mathbb{C}^{(p)} : \bar{\mathbb{A}}^{(p)} : \mathbb{M}^{*} \tag{3.10}$$

In the above expressions, it can be observed that only the influence tensors of $n-1$ phases are needed for the representation of the effective elastic constants.

For simplicity, we consider in the following a material which consists of two phases only. One of the phases is referred to as the matrix (index M) and the other as the inhomogeneity (I). The expressions aforementioned can be rewritten for this particular case in a very simple way:

$$\begin{aligned}\boldsymbol{\varepsilon} &= \xi\ \boldsymbol{\varepsilon}_{\mu}^{(i)} + (1-\xi)\ \boldsymbol{\varepsilon}_{\mu}^{(m)} = \boldsymbol{\varepsilon}^{0} \\ \boldsymbol{\sigma} &= \xi\ \boldsymbol{\sigma}_{\mu}^{(i)} + (1-\xi)\ \boldsymbol{\sigma}_{\mu}^{(m)} = \boldsymbol{\sigma}^{0}\end{aligned} \tag{3.11}$$

where $\xi = c^{(i)} = V^{(i)}/\sum_{N} V^{(k)}$ stands for the volume fraction of the inclusions and $1-\xi = c^{(m)} = V^{(m)}/\sum_{N} V^{(k)}$ for the volume fraction of the matrix. Now, the

relations between the concentration tensor of the different phases can be written as:

$$\xi\ \bar{\mathbb{A}}^{(i)} + (1-\xi)\ \bar{\mathbb{A}}^{(m)} = \mathbb{I} \qquad \text{and} \qquad \xi\ \bar{\mathbb{B}}^{(i)} + (1-\xi)\ \bar{\mathbb{B}}^{(m)} = \mathbb{I} \tag{3.12}$$

The effective elasticity and compliance tensors of the composite in the case of a two-phase composite can be obtained from the phases and from the mechanical concentration tensors as:

$$\begin{aligned} \mathbb{C}^* &= \xi\ \bar{\mathbb{C}}^{(i)} : \bar{\mathbb{A}}^{(i)} + (1-\xi)\ \mathbb{C}^{(m)} : \bar{\mathbb{A}}^{(m)} \\ &= \mathbb{C}^{(m)} + \xi\ [\mathbb{C}^{(i)} - \mathbb{C}^{(m)}] : \bar{\mathbb{A}}^{(i)} \\ &= \mathbb{C}^{(i)} + (1-\xi)\ [\mathbb{C}^{(m)} - \mathbb{C}^{(i)}] : \bar{\mathbb{A}}^{(m)} \end{aligned} \tag{3.13}$$

$$\begin{aligned} \mathbb{M}^* &= \xi\ \bar{\mathbb{M}}^{(i)} : \bar{\mathbb{B}}^{(i)} + (1-\xi)\ \mathbb{M}^{(m)} : \bar{\mathbb{B}}^{(m)} \\ &= \mathbb{M}^{(m)} + \xi\ [\mathbb{M}^{(i)} - \mathbb{M}^{(m)}] : \bar{\mathbb{B}}^{(i)} \\ &= \mathbb{M}^{(i)} + (1-\xi)\ [\mathbb{M}^{(m)} - \mathbb{M}^{(i)}] : \bar{\mathbb{B}}^{(m)} \end{aligned} \tag{3.14}$$

Finally, the relations between strain and stress concentration tensors for each of the two phases can be written as:

$$\begin{aligned} (1-\xi)\ \bar{A}^{(m)} &= (\mathbb{C}^{(m)} - \mathbb{C}^{(i)})^{-1} : (\mathbb{C}^* - \mathbb{C}^{(i)}) \\ \xi\ \bar{A}^{(i)} &= (\mathbb{C}^{(i)} - \mathbb{C}^{(m)})^{-1} : (\mathbb{C}^* - \mathbb{C}^{(m)}) \end{aligned} \tag{3.15}$$

$$\begin{aligned} (1-\xi)\ \bar{B}^{(m)} &= (\mathbb{M}^{(m)} - \mathbb{M}^{(i)})^{-1} : (\mathbb{M}^* - \mathbb{M}^{(i)}) \\ \xi\ \bar{B}^{(i)} &= (\mathbb{M}^{(i)} - \mathbb{M}^{(m)})^{-1} : (\mathbb{M}^* - \mathbb{M}^{(m)}) \end{aligned} \tag{3.16}$$

In this particular case, only it is necessary to know one concentration tensor for describing the full elastic behavior of the inhomogeneous material within the mean-field methods.

3.2 Eshelby's result

3.2.1 Eshelby's problem

A large proportion of the mean field descriptions used in continuum micromechanics of materials are based on the work of Eshelby [24], who studied the stress and strain distributions in homogeneous media that contains a subregion that spontaneously changes its shape and/or size so that it no longer fits into it previous space in the "parent medium". Eshelby's result show that if an elastic *homogeneous* ellipsoidal inclusion (i.e., an inclusion consisting of the same material as the matrix) in an *infinite* matrix is subjected to a homogeneous strain $\boldsymbol{\varepsilon}_t$ (called the "stress-free strain", "unconstrained strain", "eigenstrain" or "transformation strain"), the stress and strain states in the constrained inclusion are uniform, i.e., $\boldsymbol{\sigma}_\mu^{(i)}$ and $\boldsymbol{\varepsilon}_\mu^{(i)}$

do not depend on the microscopic coordinate $\boldsymbol{y}$. The uniform strain in the constrained inclusion (the "constrained strain"), $\boldsymbol{\varepsilon}_c$, is related to the stress-free strain $\boldsymbol{\varepsilon}_t$ by the expression:

$$\boldsymbol{\varepsilon}_c = \mathbb{S} : \boldsymbol{\varepsilon}_t \tag{3.17}$$

where $\mathbb{S}$ is referred to as the (interior point) Eshelby tensor. For eqn. (3.17) to hold, $\boldsymbol{\varepsilon}_t$ may be any kind of eigenstrain that involves no changes in the elastic constant of the inclusion. Eshelby illustrated the problem through a set of cut and weld operations (see Fig. 3.2):

- Firstly the inclusion is removed from the solid and it is deformed freely with a value that is represented through the eigenstrain tensor $\boldsymbol{\varepsilon}_t$. This strain does not induce any stress in the inclusion (the inclusion is unconstrained) neither in the solid (Fig. 3.2a).
- The inclusion cannot be directly introduced into its original position and some stress should be applied to return the inclusion to its original shape (Fig. 3.2b).
- Once the inclusion is returned to the initial configuration, it can be placed again in the original hole and it can be welded with the rest of the solid, removing the stresses until a new equilibrium configuration in the inclusion (characterized through $\boldsymbol{\varepsilon}_c$) is found (Fig. 3.2c).

The stresses in the inclusion can be determined directly applying Hooke's law (as it was commented before, Eshelby's result is based on linear elastic materials). Due to the fact that the strain in the inclusion is uniform:

$$\boldsymbol{\sigma}_{\mu}^{(i)} = \mathbb{C}^{(m)} : [\boldsymbol{\varepsilon}_c - \boldsymbol{\varepsilon}_t] = \mathbb{C}^{(m)} : [\mathbb{S} - \mathbb{I}] : \boldsymbol{\varepsilon}_t \tag{3.18}$$

Eshelby's tensor only depends on the elastic properties of the matrix and on the relation between the major and minor axis of the ellipsoid. The Eshelby tensor is symmetric in the first and second pair of indices, but in general it is not symmetric with regard to an exchange of these pairs (minor symmetry condition). There exist very simple analytical expressions for some particular cases, such as for spheres, disks and long fibers embedded into an isotropic matrix. Some authors have found analytical expressions for transversely isotropic matrix with the restriction that the direction of anisotropy is aligned with the revolution direction of the spheroid. In all other general cases, a numerical evaluation of the tensor is necessary [58].

3.2.2 Equivalent homogeneous inclusion

Eshelby's result is based on the assumption of a homogeneous inclusion. However, for mean field descriptions of dilute matrix-inclusion composites, the interest is focused on the stress and strain fields in inhomogeneous inclusions that are embedded in a matrix. Such cases can be handled on the basis of Eshelby's theory for homogeneous inclusions, by means of the concept of equivalent homogeneous inclusions. The main idea is to consider the solid subjected to a macroscopic strain field $\boldsymbol{\varepsilon}^0$ and

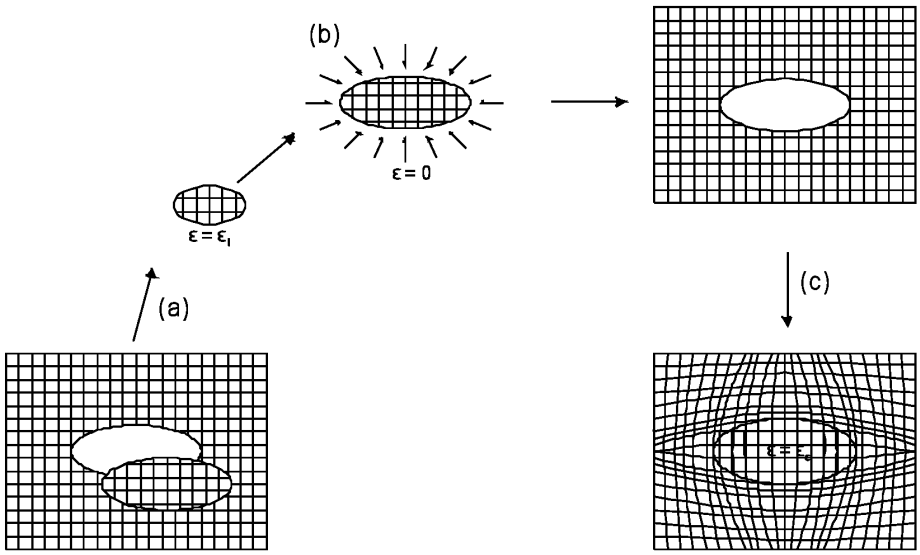

Figure 3.2: Solution of the Eshelby's problem. The ellipsoidal inclusion is subjected to a transformation represented through the strain tensor $\boldsymbol{\varepsilon}_t$ (Segurado [81]).

compute the strain in the inclusion by replacing the real inhomogeneity through a "fictitious" equivalent inclusion, whose mechanical properties are exactly the same as the effective medium, which is subjected to a strain field $\boldsymbol{\varepsilon}_t$. The strain field $\boldsymbol{\varepsilon}_t$ is obtained through imposing that the stress fields and the constrained strains in both inclusions (the real one and the equivalent "fictitious") are the same. Accordingly to the figure 3.3a, the stress and the strain field in the "equivalent homogeneous inclusion" are given by:

$$\boldsymbol{\varepsilon}_{\mu}^{(i)} = \boldsymbol{\varepsilon}_c + \boldsymbol{\varepsilon}^0 \qquad \text{and} \qquad \boldsymbol{\sigma}_{\mu}^{(i)} = \mathbb{C}^{(m)} : [\boldsymbol{\varepsilon}_c + \boldsymbol{\varepsilon}^0 - \boldsymbol{\varepsilon}_t] \tag{3.19}$$

The strain field in the real inclusion should be equal to the strain field in the "fictitious" inclusion, i.e. $\boldsymbol{\varepsilon}_c + \boldsymbol{\varepsilon}^0$. Therefore the stress field in the real inhomogeneity may be:

$$\boldsymbol{\sigma}_{\mu}^{(i)} = \mathbb{C}^{(i)} : [\boldsymbol{\varepsilon}_c + \boldsymbol{\varepsilon}^0] \tag{3.20}$$

where $\mathbb{C}^{(i)}$ is the constitutive tensor of the inhomogeneity. The strain $\boldsymbol{\varepsilon}_t$ that should be imposed in order to get the same strains in both inclusions (Fig. 3.3) is obtained through making equal the stresses in both states (eqn. (3.19) and (3.20)). Hence:

$$\boldsymbol{\varepsilon}_t = \left[(\mathbb{C}^{(i)} - \mathbb{C}^{(m)}) : \mathbb{S}^{(i)} + \mathbb{C}^{(m)}\right]^{-1} : (\mathbb{C}^{(i)} - \mathbb{C}^{(m)}) : \boldsymbol{\varepsilon}^0. \tag{3.21}$$

where the Eshelby's result (eqn. (3.17)) has been taken into account. The most important result from the previous identities is the strain concentration tensor in

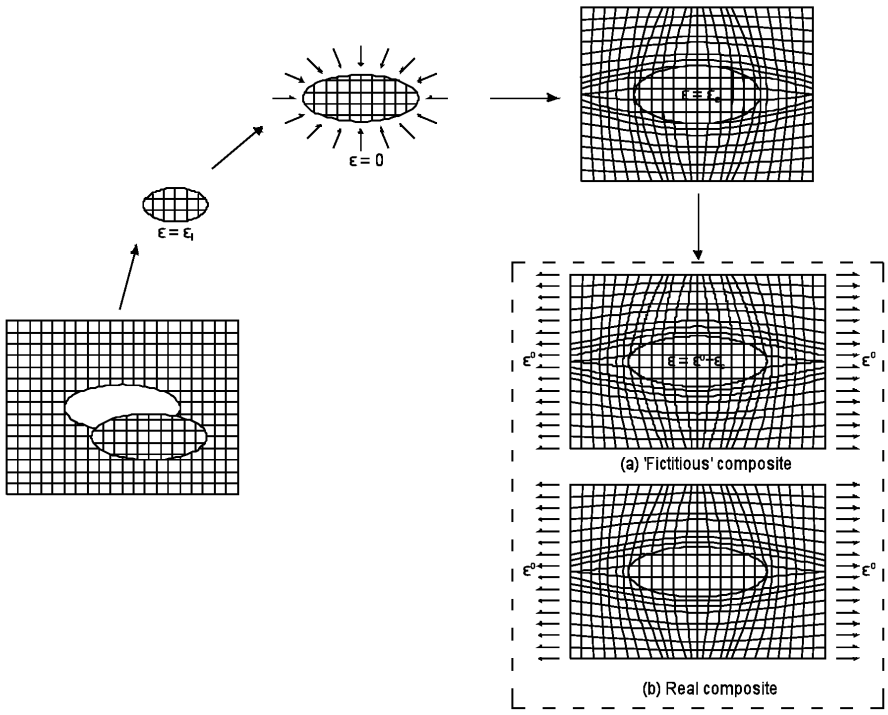

Figure 3.3: Equivalent operations that illustrates the "equivalent" problem that should be solved to compute the strain localization tensor $\mathbb{A}^{(i)}$ (Segurado [81]).

the inclusion. Indeed, combining equations (3.19) and (3.21) one obtains:

$$\begin{aligned} \boldsymbol{\varepsilon}_{\mu}^{(i)} &= \boldsymbol{\varepsilon}^{0} + \boldsymbol{\varepsilon}_{c} = \boldsymbol{\varepsilon}^{0} + \mathbb{S} : \boldsymbol{\varepsilon}_{t} \\ &= \left[\mathbb{I} + \mathbb{S}^{(i)} : \mathbb{C}^{(m)^{-1}} : (\mathbb{C}^{(i)} - \mathbb{C}^{(m)})\right]^{-1} : \boldsymbol{\varepsilon}^{0} = \bar{\mathbb{A}}_{dil}^{(i)} : \boldsymbol{\varepsilon}^{0} \end{aligned} \tag{3.22}$$

where the subindex "*dil*" indicates that last expression is only exact when the inclusion is embedded into an infinite matrix (as assumed by Eshelby). Equation (3.22) is one of the simplest expressions for the strain concentration tensor. It does not take into account the perturbations in the stress fields, produced by the neighboring inhomogeneities and it should be applied strictly when $\xi \to 0$, i.e. it does not consider the interaction between particles. By setting $\boldsymbol{\varepsilon}_{\mu}^{(i)} = \mathbb{M}^{i} : \boldsymbol{\sigma}_{\mu}^{(i)}$ and using $\boldsymbol{\varepsilon}^{0} = \mathbb{M}^{m} : \boldsymbol{\sigma}^{0}$, the dilute stress concentration tensor for the inhomogeneities is found from equation (3.22) as:

$$\begin{aligned} \bar{\mathbb{B}}_{dil}^{(i)} &= \mathbb{C}^{(i)} : \left[\mathbb{I} + \mathbb{S} : \mathbb{M}^{(m)} : (\mathbb{C}^{(i)} - \mathbb{C}^{(m)})\right]^{-1} : \mathbb{M}^{(m)} \\ &= \left[\mathbb{I} + \mathbb{C}^{(m)} : (\mathbb{I} - \mathbb{S}) : (\mathbb{M}^{(i)} - \mathbb{M}^{(m)})\right]^{-1} \end{aligned} \tag{3.23}$$

Once the expression for the strain concentration tensor is obtained, the elastic properties of the composite material are computed using equations (3.9) and (3.22)

$$\mathbb{C}^* = \mathbb{C}^{(m)} + \sum_N c^{(p)}(\mathbb{C}^{(p)} - \mathbb{C}^{(m)}) : \left[\mathbb{I} + \mathbb{S}^{(p)} : \mathbb{C}^{(m)^{-1}} : (\mathbb{C}^{(p)} - \mathbb{C}^{(m)})\right]^{-1} \quad (3.24)$$

where $\mathbb{S}^{(p)}$ is the Eshelby tensor corresponding to the phase (p), which is embedded into a matrix with elastic properties $\mathbb{C}^{(m)}$. As illustrated in Fig. 3.4 each defect can be considered in an unbounded domain subjected to a uniform far-field loading $\boldsymbol{\varepsilon}^0$ or $\boldsymbol{\sigma}^0$.

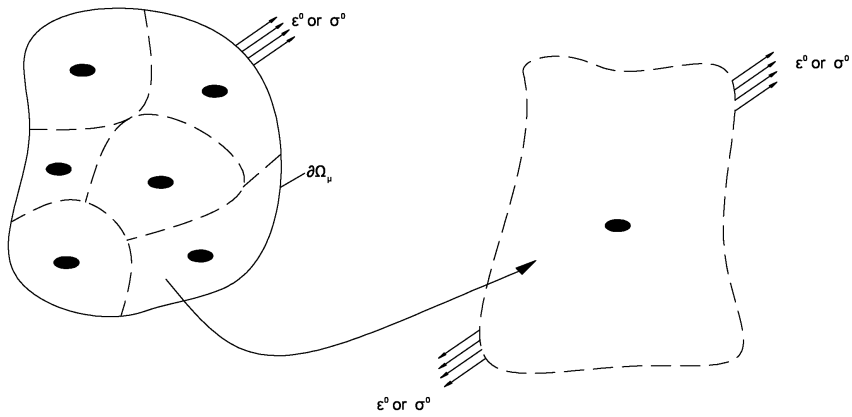

Figure 3.4: Model of dilute defect distribution (Gross [31]).

3.3 Voigt and Reuss estimations

The simplest mean-field schemes are Voigt and Reuss estimates, where isostrain and isostress conditions among the phases are assumed, respectively. Hence in the Voigt scheme all the strain concentration tensors are equal to unity, i.e., $\bar{\mathbb{A}}^{(p)} = \mathbb{I}$. Thus, the effective constitutive tensor of the composite is the volume average of the per phase uniform local stiffness:

$$\mathbb{C}^*_{Voigt} = \langle \mathbb{C} \rangle = \sum\nolimits_p c^{(p)} \mathbb{C}^{(p)} \quad (3.25)$$

This scheme provides an upper bound for the stress response of the composite (see 3.10.3). Similarly in the Reuss scheme the stress concentration tensors are equal to the unity, i.e., $\bar{\mathbb{B}}^{(p)} = \mathbb{I}$ and it gives a lower bound for the stress response. For this particular case, the compliance effective tensor of the composite is given by the volume average of the per phase uniform local compliance tensors:

$$\mathbb{C}^*_{Reuss} = \langle \mathbb{M}^{-1} \rangle = \left[\sum\nolimits_p c^{(p)} \mathbb{M}^{(p)}\right]^{-1} \quad (3.26)$$

Both results can be combined into a simple expression to express the upper and lower limits for the effective constitutive tensor:

$$\mathbb{C}^*_{(Voigt)} \geq \mathbb{C}^* \geq \mathbb{C}^*_{(Reuss)} \tag{3.27}$$

The Voigt and Reuss bounds are based on the *principle of minimum potential energy* and on the *principle of minimum complementary energy*. They are valid irrespective of the actual microstructure, but the underlying approximations of a constant stress or strain field in general violate the compatibility of deformation or the local equilibrium, respectively.

3.4 Mori-Tanaka model

Mori-Tanaka model is based on the Eshelby result for a non-interacting dilute defect distribution. In this case, interactions between inhomogeneities are introduced by means of approximating the stress acting on an inhomogeneity by an appropriate average matrix stress. This method maintains the same approach that was developed for dilute inhomogeneities and the interactions among the inclusions are considered through the modification of the stress or strain fields acting on each inhomogeneity. As it can be observed in Fig. 3.5, in the Mori-Tanaka model the macroscopic strain or stress fields acting on the RVE ($\boldsymbol{\varepsilon}^0$ or $\boldsymbol{\sigma}^0$) is replaced by the phase averaged matrix strain or stress field ($\boldsymbol{\varepsilon}_\mu^{(m)}$ or $\boldsymbol{\sigma}_\mu^{(m)}$). This assumption can be expressed mathematically by the following equations, as indicated by Benveniste [8]:

$$\begin{aligned} \boldsymbol{\varepsilon}_\mu^{(i)} &= \bar{\mathbb{A}}_{dil}^{(i)} : \boldsymbol{\varepsilon}_\mu^{(m)} \\ \boldsymbol{\sigma}_\mu^{(i)} &= \bar{\mathbb{B}}_{dil}^{(i)} : \boldsymbol{\sigma}_\mu^{(m)} \end{aligned} \tag{3.28}$$

Considering the previous equations and the expression (3.11), for a composite with only two phases (similar expressions can be easily derived for a composite with n phases), some expressions to determine the effective material properties can be obtained:

$$\begin{aligned} \boldsymbol{\varepsilon}_\mu^{(m)} &= \bar{\mathbb{A}}_{MT}^{(m)} : \boldsymbol{\varepsilon} = \left[(1-\xi)\ \mathbb{I} + \xi\ \bar{\mathbb{A}}_{dil}^{(i)}\right]^{-1} : \boldsymbol{\varepsilon} \\ &= \left[(1-\xi)\ \mathbb{I} + \xi\ [\mathbb{I} + \mathbb{S} : \mathbb{M}^{(m)} : (\mathbb{C}^{(i)} - \mathbb{C}^{(m)})]^{-1}\right]^{-1} : \boldsymbol{\varepsilon} \end{aligned} \tag{3.29}$$

$$\begin{aligned} \boldsymbol{\sigma}_\mu^{(m)} &= \bar{\mathbb{B}}_{MT}^{(m)} : \boldsymbol{\sigma} = \left[(1-\xi)\ \mathbb{I} + \xi\ \bar{\mathbb{B}}_{dil}^{(i)}\right]^{-1} : \boldsymbol{\sigma} \\ &= \left[(1-\xi)\mathbb{I} + \xi\ \mathbb{C}^{(i)} : [\mathbb{I} + \mathbb{S} : \mathbb{M}^{(m)} : (\mathbb{C}^{(i)} - \mathbb{C}^{(m)})]^{-1}\right]^{-1} : \mathbb{M}^{(m)} : \boldsymbol{\sigma} \end{aligned} \tag{3.30}$$

Similar expressions can be obtained if now the strain concentration tensors for the inclusions are considered:

$$\begin{aligned} \boldsymbol{\varepsilon}_\mu^{(i)} &= \bar{\mathbb{A}}_{MT}^{(i)} : \boldsymbol{\varepsilon} = \bar{\mathbb{A}}_{dil}^{(i)} : \left[(1-\xi)\ \mathbb{I} + \xi\ \bar{\mathbb{A}}_{dil}^{(i)}\right]^{-1} : \boldsymbol{\varepsilon} \\ \boldsymbol{\sigma}_\mu^{(i)} &= \bar{\mathbb{B}}_{MT}^{(i)} : \boldsymbol{\sigma} = \bar{\mathbb{B}}_{dil}^{(i)} : \left[(1-\xi)\ \mathbb{I} + \xi\ \bar{\mathbb{B}}_{dil}^{(i)}\right]^{-1} : \boldsymbol{\sigma} \end{aligned} \tag{3.31}$$

The expressions for the Mori-Tanaka model can be obtained explicitly by considering the expression for the strain and stress concentration tensors in the case of a dilute defect distribution (see (3.22)). Mori-Tanaka model, in contrast to the model of a dilute distribution, correctly covers the extreme cases of $\xi = 0$ and $\xi = 1$ (homogeneous material) and therefore can be applied for arbitrary volume fractions (although the model only provides accurate results for low values of ξ). In case of having high values of the concentration of inhomogeneities (in the literature some authors set the limit value around 25-30%), materials can be reversed and the matrix assumes the role of inclusions (and viceversa). This method is known as "inverse" Mori-Tanaka method and it will be used hereafter in order to explain the Lielens Method (see 3.8). Mori-Tanaka is one of the most used method in micromechanics when one implements an analytical method, since it is an explicit method that can be implemented into computer programs in a very straight-forward way and provides enough accuracy for the effective properties in some common materials.

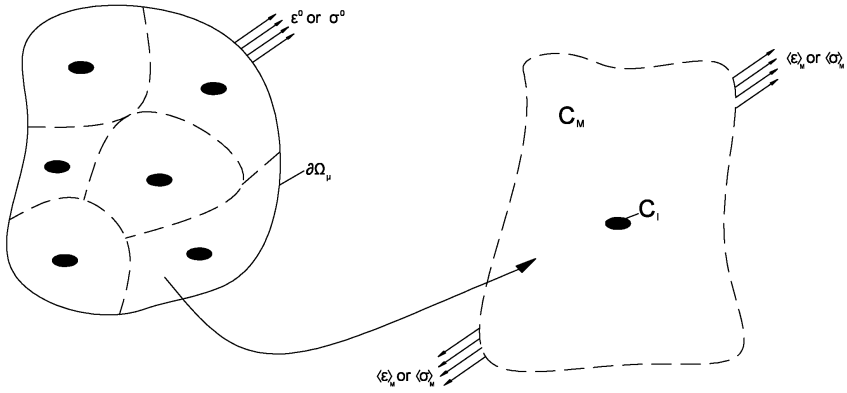

Figure 3.5: Defect interaction in the Mori-Tanaka model (Gross [31]).

It has been proven that, in some simple cases, the Mori-Tanaka method leads to the same results given by the Hashin-Shtrikman bounds. This fact will be commented in section 3.10.3.

3.5 Self-Consistent Scheme

Self-consistent method is based on the existence of a sufficient distance among the inhomogeneities embedded in a homogeneous matrix. Thus self-consistent method approximates the interaction between the different phases by assuming that each inhomogeneity is embedded in an infinite volume of an effective medium, whose properties coincide with the ones of the composite (which are not known a priori). The defect is subjected to the macroscopic strain or macroscopic stress and the

boundary problem is computed by solving an implicit nonlinear system of equations for the unknown elastic tensors $(\mathbb{C}^*, \mathbb{M}^*)$, which describe the behavior of the effective medium. The expression of the strain and stress concentration tensors can be obtained easily by substituting the values regarding the matrix phase by the effective values of the composite:

$$\begin{aligned} \bar{\mathbb{A}}^{(p)} &= \left[\mathbb{I} + \mathbb{S} : \mathbb{M}^* : (\mathbb{C}^{(p)} - \mathbb{C}^*)\right]^{-1} \\ \bar{\mathbb{B}}^{(p)} &= \left[\mathbb{I} + (\mathbb{I} - \mathbb{S}) : \mathbb{C}^* : (\mathbb{M}^{(p)} - \mathbb{M}^*)\right]^{-1} \end{aligned} \tag{3.32}$$

Algorithmically, the classical self-consistent method implies an additional iterative

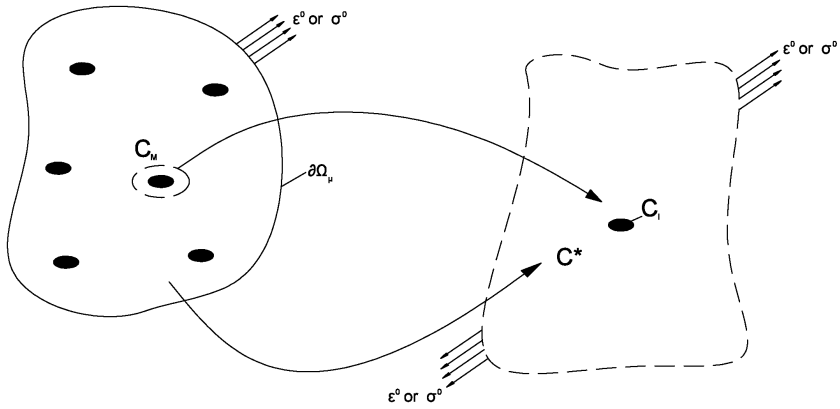

Figure 3.6: Model of the self-consistent method (Gross [31]).

loop to calculate the effective tensors of the composite. This system can be solved by self-consistent iterative schemes, based on eqn. (3.13) and (3.14) for two phase composites:

$$\begin{aligned} \mathbb{C}^*_{SC,n+1} &= \mathbb{C}^{(m)} + \xi \left(\mathbb{C}^{(i)} - \mathbb{C}^{(m)}\right) : \left[\mathbb{I} + \mathbb{S}_n : \mathbb{M}_n : (\mathbb{C}^{(i)} - \mathbb{C}_n)\right]^{-1} \\ \mathbb{M}^*_{SC,n+1} &= \left[\mathbb{C}^*_{SC,n+1}\right]^{-1} \end{aligned} \tag{3.33}$$

where $\mathbb{S}_n$ is the Eshelby tensor that should be computed on each iteration and describes the behavior of an inhomogeneity embedded in the n-th iteration of the effective medium.

Self-consistent methods were developed initially to describe the behavior of polycrystals and they are well-suited to study such materials like Functionally Graded Materials, in which the volume fraction of a constituent can vary from 0 to 1 through the thickness of a sample[2]. However, classical self-consistent schemes present some problems when describing the behavior of matrix-inclusion composites, such as porous materials, where they predict a breakdown of the stiffness

[2]Like the Mori-Tanaka model, the self-consistent method covers the limit cases of a homogeneous material.

due to the phenomena of *percolation* of the pores. Another drawback of the self-consistent method is related to the fact that the method is based on a mixing of the microscopic and macroscopic level, which strictly should be separated. In this sense, the classical self-consistent method does not fulfill the first condition described at the beginning of the current chapter. In order to reduce this physical inconsistency the *generalized self-consistent method* was developed some authors.

3.6 Generalized Self-Consistent Scheme

The Generalized Self-Consistent model or Three-phase model was developed by Christensen and Lo [9] in 1979 and it can be considered as an improved version of the Classical Self-Consistent scheme. This method, which cannot be considered strictly as a Mean-Field Analysis[3], was developed to compute the effective properties of a composite material reinforced with spheroidal inclusions or aligned fibers.[4] As it can be observed in the Fig. 3.9 the particle or fiber is surrounded by a constant-thickness layer of matrix, which is in turn embedded in the composite material (whose effective properties are unknown). The thickness of the matrix layer is chosen in a way that the relationship with the radius of the inclusion is constant and it is determined by the volumetric fraction of the inhomogeneity in the composite material.

This method is based on an energy approach in which the related elasticity problem is solved. The model leads to a set of differential equations, which describe the behavior of the three-phase material and should be solved in order to obtain the value of the effective properties of the composite. This method provides excellent results for inhomogeneous materials with matrix-inclusion topologies and is a highly appropriated method to compute the material characterization of heterogeneous materials reinforced by spherical or equiaxed particles or aligned continuous fibers.

3.7 Differential Scheme

The differential scheme is based on a succession of infinitesimal steps. In each of these steps, small concentrations of inhomogeneities are added to a composite material and then homogenizing. This procedure, originally set out by Roscoe [76] and developed by Hashin [33], is illustrated in Fig. 3.8. As it can be observed, an infinitesimal volume $\mathrm{d}V$ of the inclusion with mechanical properties $\mathbb{C}^{(i)}$ is embedded in the matrix, which has effective properties $\mathbb{C}^{*}$. The effective properties

[3] Such methods cannot be considered Mean-Field Analysis since they are not based on the volumetric averages of the strains and stresses in each phase.

[4] This family of models study the behavior of complex geometrical entities, called *patterns* or *motifs*, embedded in a matrix. The Generalized Self-Consistent model covers partially the second and third condition commented in 3.1 but does not fulfill the first condition, since a set of differential equations must be solved to obtain a solution. For a general case, the stress and strain fields of these entities are inhomogeneous even in the dilute case and numerical methods have to be considered to calculate the overall constraint tensors.

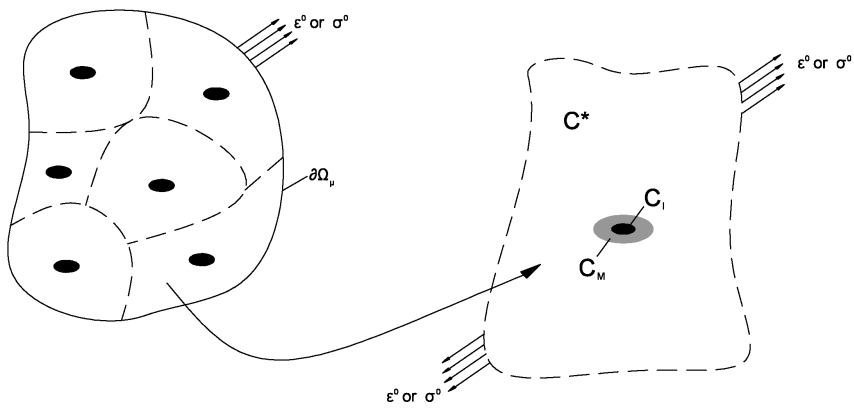

Figure 3.7: Three phase or Generalized Self-Consistent model (Klusemann [42]).

of the matrix depends on each step on the volume fraction of the inclusion $c^{(i)}$ and then should be computed at each step, due to the variation of such fraction. The method is based on the conservation of volume equation for the total volume V, when an infinitesimal volume of the inclusion is added, then the same volume of the matrix material has to be removed. The volume balance at each step is given by:

$$(c^{(i)} + \mathrm{d}c^{(i)})V = c^{(i)}V - c^{(i)}\mathrm{d}V + \mathrm{d}V \quad \Longrightarrow \quad \frac{\mathrm{d}V}{V} = \frac{\mathrm{d}c^{(i)}}{1 - c^{(i)}} \tag{3.34}$$

Since the method is based on infinitesimal volumes, the equations of the model of dilute distribution is exact at each step and it can be written as:

$$\begin{aligned} \mathbb{C}^*\big(c^{(i)} + \mathrm{d}c^{(i)}\big) &= \mathbb{C}^*(c^{(i)}) + \frac{\mathrm{d}V}{V}\big(\mathbb{C}^{(i)} - \mathbb{C}^*(c^{(i)})\big) : \bar{\mathbb{A}}^{(i)}_{dil} \\ \mathbb{M}^*\big(c^{(i)} + \mathrm{d}c^{(i)}\big) &= \mathbb{M}^*(c^{(i)}) + \frac{\mathrm{d}V}{V}\big(\mathbb{M}^{(i)} - \mathbb{M}^*(c^{(i)})\big) : \bar{\mathbb{B}}^{(i)}_{dil} \end{aligned} \tag{3.35}$$

In the last equation, the concentration strain and stress tensors $\bar{\mathbb{A}}^{(i)}_{dil}$ and $\bar{\mathbb{B}}^{(i)}_{dil}$ depend on the effective matrix material. Considering the volume balance equation (3.34) and the equality $\mathbb{C}^*(c^{(i)} + \mathrm{d}c^{(i)}) = \mathbb{C}^*(c^{(i)}) + \mathrm{d}\mathbb{C}^*(c^{(i)})$ (respectively $\mathbb{M}^*(c^{(i)} + \mathrm{d}c^{(i)}) = \mathbb{M}^*(c^{(i)}) + \mathrm{d}\mathbb{M}^*(c^{(i)})$), the equations can be expressed as:

$$\begin{aligned} \frac{\mathrm{d}\mathbb{C}^*(c^{(i)})}{\mathrm{d}c^{(i)}} &= \frac{1}{1 - c^{(i)}}\big(\mathbb{C}^{(i)} - \mathbb{C}^*(c^{(i)})\big) : \bar{\mathbb{A}}^{(i)}_{dil} \\ \frac{\mathrm{d}\mathbb{M}^*(c^{(i)})}{\mathrm{d}c^{(i)}} &= \frac{1}{1 - c^{(i)}}\big(\mathbb{M}^{(i)} - \mathbb{M}^*(c^{(i)})\big) : \bar{\mathbb{B}}^{(i)}_{dil} \end{aligned} \tag{3.36}$$

The differential scheme then leads to a system of nonlinear ordinary differential equations for the constitutive and compliance tensors as a function of the volume

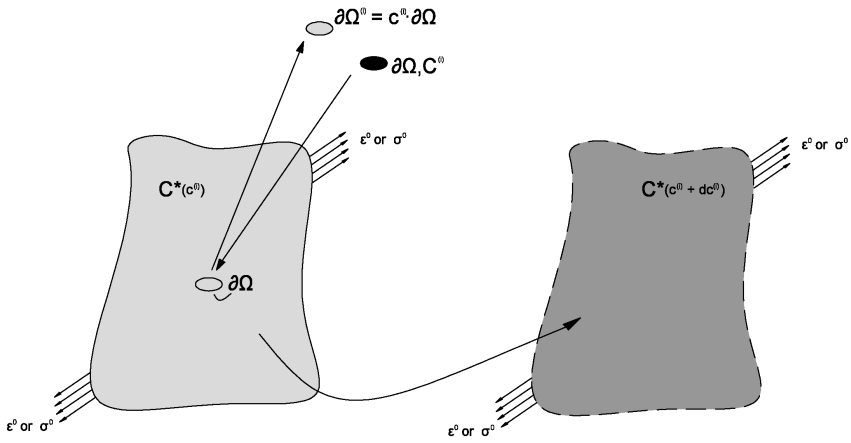

Figure 3.8: Differential scheme (Gross [31]).

fraction $c^{(i)}$ of the embedded phase, which can be solved with standard numerical techniques for initial value problems, such as Runge-Kutta schemes. The initial conditions can be set as:

$$\mathbb{C}^*\left(c^{(i)}=0\right)=\mathbb{C}^{(m)} \qquad \text{and} \qquad \mathbb{M}^*\left(c^{(i)}=0\right)=\mathbb{M}^{(m)} \tag{3.37}$$

Differential schemes are not very used in the study of the mechanical behavior of composite materials due to the mathematical complexity (in this aspect, this scheme does not fulfill partially the first requirement for an ideal MFA) if we compare them with the rest of the aforementioned models. Differential schemes, as it happens with the Self-Consistent methods and Mori-Tanaka method, do not consider neither the distribution of the inclusions nor the interaction among them, therefore it provides only accurate results for low values of the volume fraction of the inhomogeneities.

3.8 Double Inclusion Model

The Double Inclusion Model, which was proposed by Nemat-Nasser and Hori [62], is based on a model in which each spheroidal inclusion (with volume average $c^{(i)}$) is surrounded by a hollow inclusion (volume average $c^{(m)}$), whose stiffness is $\mathbb{C}^{(m)}$. Both inclusions are embedded into the composite, whose effective properties are $\mathbb{C}_R$, and present the same aspect ratio, symmetry axis and center, and the ratio between their volume averages is equal to that of the inclusions and the matrix in the actual composite ($c^{(i)}/c^{(m)}$). By choosing $\mathbb{C}_R = \mathbb{C}^{(m)}$ it is easy to observe that the Mori-Tanaka model is recovered. On the other hand, if $\mathbb{C}_R = \mathbb{C}^{(i)}$ is chosen, then it can be proven that the "inverse" Mori-Tanaka model is obtained: it corresponds to Mori-Tanaka for a composite where the material properties of the inclusions

and matrix are permuted. The real behavior of the composite material will be

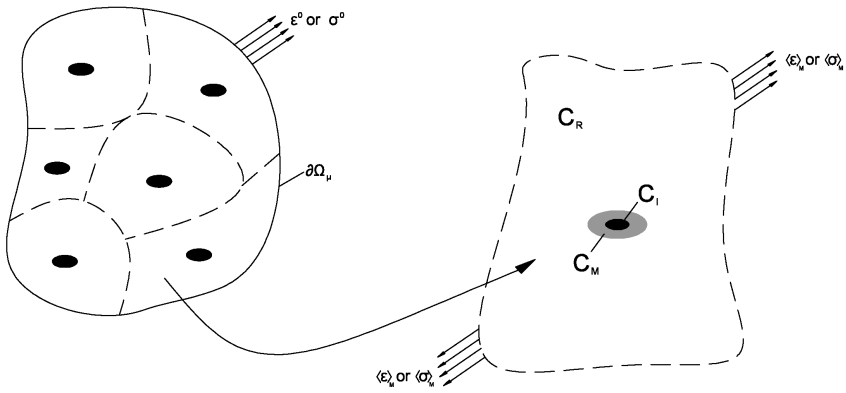

Figure 3.9: Scheme of the Double Inclusion model developed by Lielens (Klusemann [42]).

close to the solution given by the "direct" Mori-Tanaka model for small values of the fraction volume of the inhomogeneities, while for large values the "inverse" Mori-Tanaka formulation will provide a better approximation. As a consequence of such conclusions, Lielens [50] proposed an interpolation between both Mori-Tanaka estimates, in order to obtain the strain concentration tensor:

$$\bar{\mathbb{A}}_{DI}^{(m)} = [(1-\phi(c^{(i)}))\ (\bar{\mathbb{A}}_{MT}^{(m)})^{-1} + \phi(c^{(i)})\ (\bar{\mathbb{A}}_{MT^{-1}}^{(m)})^{-1}]^{-1} \tag{3.38}$$

where $\phi(c^{(i)})$ is a smooth interpolation function, which depends on the volumetric fraction of the inhomogeneity phase and satisfies the following properties:

$$\phi(c^{(i)}) > 0, \qquad \frac{\mathrm{d}\phi}{\mathrm{d}c^{(i)}}(c^{(i)}) > 0, \qquad \lim_{c^{(i)}\to 0}\phi(c^{(i)}) = 0, \qquad \lim_{c^{(i)}\to 1}\phi(c^{(i)}) = 1. \tag{3.39}$$

Lielens proposed a simple quadratic expression for the smooth interpolation function:

$$\phi(c^{(i)}) = \frac{1}{2}c^{(i)}(1+c^{(i)}) \tag{3.40}$$

On the following equations, the expressions for the strain concentration tensors of the "direct" Mori-Tanaka and the "inverse" Mori-Tanaka method are recalled:

$$\begin{aligned}\bar{\mathbb{A}}_{MT}^{(m)} &= [\mathbb{I} + \mathbb{S}^{(m)} : \mathbb{M}^{(m)} : (\mathbb{C}^{(i)} - \mathbb{C}^{(m)})]^{-1} \\ \bar{\mathbb{A}}_{MT^{-1}}^{(m)} &= [\mathbb{I} + \mathbb{S}^{(i)} : \mathbb{M}^{(i)} : (\mathbb{C}^{(m)} - \mathbb{C}^{(i)})]^{-1}\end{aligned} \tag{3.41}$$

In the previous equations, a distinction has been done between the Eshelby tensor $\mathbb{S}^{(m)}$, calculated using the material properties of the matrix phase, and the Eshelby tensor $\mathbb{S}^{(i)}$, calculated using the material properties of the inclusions.

The Double Inclusion Model provides good estimations for inhomogeneous materials with matrix-inclusion topologies, independently of the volume fraction of the inhomogeneities. However, the method posses the drawback of not having a theoretical basis, since the expressions of the strain concentration tensors are obtained through a simple interpolation of two different methods and the terms "matrix" and "inclusion" become irrelevant. Due to the fact that the method is based on the Mori-Tanaka method, it has the same drawbacks: no interaction among particles taken into account and not considering the inhomogeneities distribution. However, this method provides better results for a wider range of the volume fraction of the inclusions, since it considers both "direct" and the "inverse" Mori-Tanaka method in the same expression.

3.9 Effective Self-Consistent Scheme

The Effective Self-Consistent Scheme was proposed by Zheng and Du [99] and is based on the three-phase model (or Generalized Self-Consistent Scheme). As it was explained in 3.6, the three phase model considers an inclusion that is surrounded by a matrix finite material, which in turn is embedded in the unbounded effective medium. In the following the inclusion together with its matrix atmosphere will be called inclusion-matrix cell and it will be denoted by a subscript 'D'.

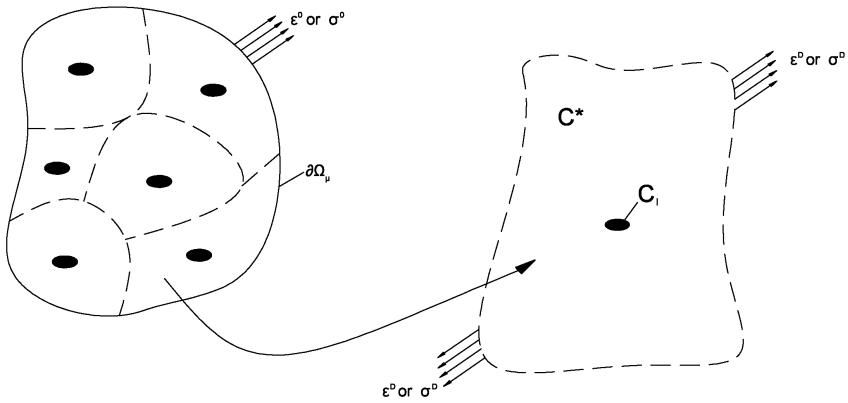

Figure 3.10: Scheme of the Effective Self-Consistent Scheme (ESCS) (Klusemann [42]).

As it has been considered in the rest of the methods, the Representative Volume Element is subjected to a uniform macroscopic stress $(\boldsymbol{\sigma}^0)$[5]. Firstly, it is assumed that the inclusion-matrix cell only consists of the matrix material and, considering the Eshelby's solution, the stress and strain fields in the cell are uniform and can be related using the following expressions:

$$\boldsymbol{\varepsilon}^D = \mathbb{M}^{(m)} : \boldsymbol{\sigma}^D \qquad \text{with} \qquad \boldsymbol{\sigma}^D = [\mathbb{I} - \Omega^D : \mathbb{H}]^{-1} : \boldsymbol{\sigma}^0 \tag{3.42}$$

[5]The method can be also formulated in terms of uniform macroscopic strains.

where Ω^D is the so-called *eigenstiffness tensor* of the cell with respect to the unknown effective medium and $\mathbb{H}$ describes the increment of the compliance in the composite. The expressions of both tensors are given by:

$$\Omega^D = \mathbb{C}^* : (\mathbb{I} - \mathbb{S}^*); \qquad \mathbb{H} = \mathbb{M}^* - \mathbb{M}^{(m)} \tag{3.43}$$

In the last expression, $\mathbb{S}^*$ represents the Eshelby tensor for the cell (inclusion+matrix) embedded in the effective medium.

The next step of the method recovers the original three-phase model, considering the effect of the uniform strain field $\boldsymbol{\varepsilon}^D$ in the inclusion. In order to do that, some extra tractions are calculated and applied on the inclusion boundary, using the following expression:

$$\boldsymbol{\tau}^D = \mathbb{C}^{(i)} - \mathbb{C}^{(m)} : \boldsymbol{\varepsilon}^D \tag{3.44}$$

The tractions will be applied along the boundary of the inclusion, considering

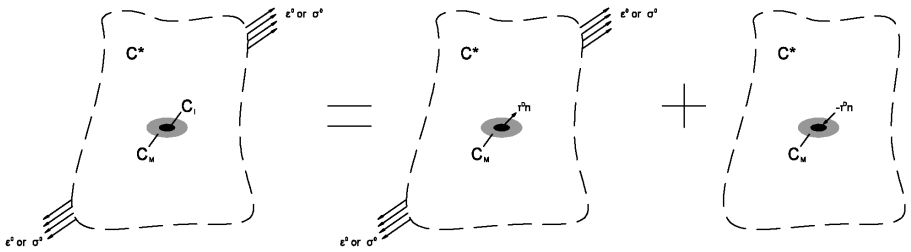

Figure 3.11: Decomposition of the original problem into two separate problems (ESCS) (Klusemann [42]).

the unit outward normal vector $\boldsymbol{n}$. Through this considerations, the original three-phase problem is decomposed into two different problems, as can be seen in Fig. 3.11. An additional approximation is carried out in order to simplify the original problem, leading to a two-phase problem. The key of such approximation consists on substituting the average stress field in the inclusion $\boldsymbol{\sigma}_\mu^{(i)}$ due to the traction $-\boldsymbol{\tau}^D n$ by a new averaged stress field $\boldsymbol{\sigma}_\mu^{*(i)}$, which occurs in a two-phase problem where the effective material is replaced by the matrix material. The simplified two-phase problem is depicted in Fig. 3.12, where it can be observed that the RVE is now subjected to the uniform stress field $\boldsymbol{\sigma}^D$, corresponding to the averaged stress field of the matrix atmosphere in the original problem. The approximation to the new problem leads to a much simpler boundary value problem, characterized through a matrix-inclusion problem type. The average stress over the inclusion can be obtained through the expression:

$$\boldsymbol{\sigma}_{\mu,ESCS}^{(i)} = [\mathbb{I} + \Omega^{(m)} : \mathbb{H}^{(i)}]^{-1}[\mathbb{I} - \Omega^{(D)} : \mathbb{H}]^{-1} : \boldsymbol{\sigma}^0 \tag{3.45}$$

The aforementioned approximation leads to an error of $\mathcal{O}(c^2)$ (see Zheng and Du [99]) compared to $\boldsymbol{\sigma}_{\mu,ESCS}^{(i)}$ and the exact average stress $\boldsymbol{\sigma}_{\mu}^{(i)}$ in the inclusion for the whole estimate. Therefore $\boldsymbol{\sigma}_{\mu}^{(i)}$ can be replaced by $\boldsymbol{\sigma}_{\mu,ESCS}^{(i)}$ and the macroscopic strain tensor $\boldsymbol{\varepsilon}$ can be expressed by:

$$\boldsymbol{\varepsilon} = \mathbb{M}^{(m)} : \boldsymbol{\varepsilon}^0 + c^{(i)}(\mathbb{M}^{(i)} - \mathbb{C}^{(m)}) : \boldsymbol{\sigma}_{\mu}^{(i)} \tag{3.46}$$

Taking into account the strain-equivalence $\boldsymbol{\varepsilon} = \mathbb{M} : \boldsymbol{\sigma}^0$ yields to the relation:

$$\mathbb{H} : \boldsymbol{\sigma}^0 = \mathbb{H}^{(i)} : \boldsymbol{\varepsilon}_{\mu}^{(i)} \tag{3.47}$$

where $\mathbb{H}^{(i)}$ is defined as the *compliance fluctuations tensor*:

$$\mathbb{H}^{(i)} = \mathbb{M}^{(i)} - \mathbb{C}^{(m)} \tag{3.48}$$

Using equations (3.42) and (3.48) an *implicit* equation for the compliance incre-

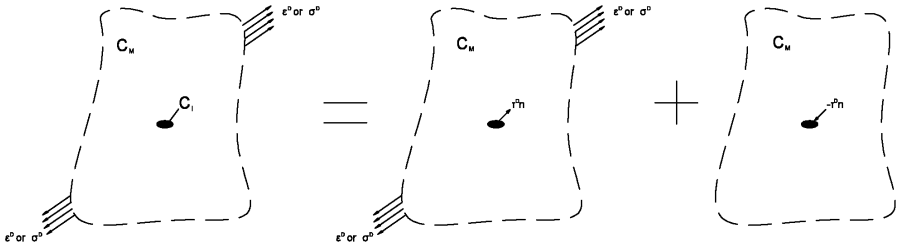

Figure 3.12: Approximation of the three-phase model by a simplified two-phase model (Klusemann [42]).

ment tensor can be obtained:

$$\mathbb{H} = \mathbb{H}_{dil}^{(i)} : [\mathbb{I} - \Omega^D \mathbb{H}]^{-1} \tag{3.49}$$

Here $\mathbb{H}_{dil}^{(i)}$ can be considered as the dilute estimate compliance tensor, which can be calculated by:

$$\mathbb{H}_{dil}^{(i)} = c^{(i)}[\mathbb{H}^{-1} + \Omega^0]^{-1} \tag{3.50}$$

Finally, this relation can be used to determine the effective constitutive tensor $\mathbb{C}^*$, thereby obtaining the relation:

$$\mathbb{C}_{ESCS}^* = [\mathbb{H} + \mathbb{C}^{(m)}]^{-1} \tag{3.51}$$

The solution of the ESCS method coincides with an effective stress model for the estimation of the average stress over any inclusion, which is embedded in the unbounded matrix material, which is subjected to a modified uniform stress field $\boldsymbol{\sigma}^D$ rather than the real macroscopic stress field $\boldsymbol{\sigma}^0$.

As it has been commented before, the simplification of the initial problems leads to an implicit equation for the compliance increment tensor $\mathbb{H}$, which is not desirable after seeing the three main requirement for a Mean-Field Approach. In order to simplify the problem, Zheng and Du developed a new and explicit version of the Effective Self-Consistent Scheme. This new version of the method is called *Interaction Direct Derivative (IDD)* and is based on an expansion of the right side of eqn. (3.49), leading to a expression of $\mathbb{H}$ that can be solved in a simple way. This method is the only one that has the three desired properties for an ideal MFA and provides good results for a large variety of microstructures[6]. For more details, see [99].

3.10 Variational bounds

In the previous sections the classical approaches to compute the effective elastic properties of heterogeneous materials have been presented. All the aforementioned methods are based on solving a boundary value problem and considering some simplifying assumptions: the RVE has been assumed to be infinitely large and methods are based on the fundamental solution for a single defect formulated by Eshelby, without taking into account the distribution, orientation, number and sizes of the different inclusions. Furthermore, different assumptions within the micromechanical models lead to different approximated solutions for the effective properties of the composite materials which may differ from each other and in some particular cases may display a qualitatively different behavior. On the other hand, such models formulate very complex micromechanical problems using only a limited amount of information, leading to a very simple analytical formulation that can be easily implemented in quite simple codes. However, one may be interested on computing an exact range within which the effective properties of a heterogeneous material are located, instead of having some analytical estimations that provides some results whose accuracy cannot be determined. This task is very useful as a previous step in the computation of a micromechanical model using complex techniques (as described in 2.5) and it can be accomplished by means of extremum principles of elasticity theory. These methods are based on energetic expressions and provide upper and lower bounds for the effective properties of the composite material.

3.10.1 Voigt and Reuss bounds

Voigt and Reuss bounds were presented in section 3.3. As it was commented before, both schemes are based on the consideration of isostrain and isostress condition among the phases, which leads to simple expressions of the strain ($\bar{\mathbb{A}}^{(p)} = \mathbb{I}$) and stress concentration tensors ($\bar{\mathbb{B}}^{(p)} = \mathbb{I}$). However, both methods can be studied from a energetic point of view, using the principle of minimum potential energy

[6] As indicated in [99], this is not the only method that covers all three requirements. In this sense, the method developed by Ponte-Castañeda and Willis [72] also fulfills the three commented aspects for an ideal MFA.

(Voigt) and on the principle of minimum complementary energy (Reuss) in order to show that these expressions provide an upper and a lower bound for the effective properties of the heterogeneous material.

Firstly, the principle of minimum potential energy will be considered. This principle states that among all kinematically admissible strain fields, the *true* strains render the total potential energy a minimum. We consider now a Representative Volume Element whose boundary conditions consist on prescribed displacements along the entire boundary $\partial\Omega_\mu$. For this particular case, the potential due to the tractions along the boundary vanishes and the total potential energy in case of a kinematically admissible strain field ε_μ is given by:

$$\hat{\prod}(\boldsymbol{\varepsilon}) = \frac{1}{2}\int_\Omega \boldsymbol{\varepsilon}_\mu : \mathbb{C} : \boldsymbol{\varepsilon}_\mu \, \mathrm{d}V = \frac{V_\mu}{2}\langle \boldsymbol{\varepsilon}_\mu : \mathbb{C} : \boldsymbol{\varepsilon}_\mu \rangle \tag{3.52}$$

Assuming now the hypotheses of linear displacements as a special case of boundary conditions $\boldsymbol{u}|_{\partial\Omega} = \boldsymbol{\varepsilon}^0 \boldsymbol{y}$ where $\boldsymbol{\varepsilon}^0 = const.$ and considering the Hill-Mandel condition given by eqn. (2.15), then the strain energy condition can be written as $\prod = \frac{V_\mu}{2}\boldsymbol{\varepsilon}^0 : \mathbb{C}^* : \boldsymbol{\varepsilon}^0$. From the extremum principle $\hat{\prod}(\boldsymbol{\varepsilon}_\mu) \geq \prod$ it then follows that:

$$\langle \boldsymbol{\varepsilon}_\mu : \mathbb{C} : \boldsymbol{\varepsilon}_\mu \rangle \geq \boldsymbol{\varepsilon}^0 : \mathbb{C}^* : \boldsymbol{\varepsilon}^0 \tag{3.53}$$

The preceeding equation is fulfilled by all the strain fields $\boldsymbol{\epsilon}_\mu$ which satisfy the aforementioned boundary condition. Such a strain field is given by the Voigt approximation $\boldsymbol{\varepsilon}_\mu = const. = \boldsymbol{\varepsilon}^0$. Particularizing (3.53) for this strain field:

$$\boldsymbol{\varepsilon}^0 : \langle \mathbb{C} \rangle : \boldsymbol{\varepsilon}^0 \geq \boldsymbol{\varepsilon}^0 : \mathbb{C}^* : \boldsymbol{\varepsilon}^0 \quad \Longrightarrow \quad \boldsymbol{\varepsilon}^0 : (\langle \mathbb{C} \rangle - \mathbb{C}^*) : \boldsymbol{\varepsilon}^0 \geq 0 \tag{3.54}$$

Hence the average constitutive tensor $\langle \mathbb{C} \rangle$ is larger than $\mathbb{C}^*$ and therefore represents an upper bound for the effective properties of the heterogeneous material.

A similar result can be formulated by setting out the problem in terms of the complementary energy, by considering stress fields ($\boldsymbol{\sigma}_\mu$) that satisfy the equilibrium and prescribed traction boundary conditions. For this case, the expression of the complementary energy is given by:

$$\hat{\widetilde{\prod}}(\boldsymbol{\sigma}^0) = \frac{1}{2}\int_\Omega \boldsymbol{\sigma}_\mu : \mathbb{C}^{-1} : \boldsymbol{\sigma}_\mu \, \mathrm{d}V = \frac{V_\mu}{2}\langle \boldsymbol{\sigma}_\mu : \mathbb{C}^{-1} : \boldsymbol{\sigma}_\mu \rangle \tag{3.55}$$

In this particular case, if we assume a case of uniform traction boundary condition $\boldsymbol{t}|_{\partial\Omega} = \boldsymbol{\sigma}^0 \boldsymbol{n}$ where $\boldsymbol{\sigma}^0 = const.$, then the complementary energy according to the Hill-Mandel principle can be written as $\widetilde{\prod} = \frac{V_\mu}{2}\boldsymbol{\sigma}^0 : \mathbb{C}^{*-1} : \boldsymbol{\sigma}^0$. From the extremum principle $\hat{\widetilde{\prod}}(\boldsymbol{\sigma}_\mu) \geq \widetilde{\prod}$ it follows that:

$$\langle \boldsymbol{\sigma}_\mu : \mathbb{C}^{-1} : \boldsymbol{\sigma}_\mu \rangle \geq \boldsymbol{\sigma}^0 : \mathbb{C}^{*-1} : \boldsymbol{\sigma}^0 \tag{3.56}$$

Equation (3.56) is fulfilled by all the admissible stress fields $\boldsymbol{\sigma}_\mu$. Such a strain field is given by the Reuss approximation $\boldsymbol{\sigma}_\mu = const.$. Particularizing (3.56) for this stress field:

$$\boldsymbol{\sigma}^0 : \langle \mathbb{C}^{-1} \rangle : \boldsymbol{\sigma}^0 \geq \boldsymbol{\sigma}^0 : \mathbb{C}^{*-1} : \boldsymbol{\sigma}^0 \quad \Longrightarrow \quad \boldsymbol{\sigma}^0 : (\langle \mathbb{C}^{-1} \rangle - \mathbb{C}^{*-1}) : \boldsymbol{\sigma}^0 \geq 0 \tag{3.57}$$

Hence the average compliance tensor $\langle \mathbb{C}^{-1} \rangle$ is larger than $\mathbb{C}^{*-1}$ and therefore represents an upper bound for the effective compliance tensor of the heterogeneous material. In terms of the constitutive tensor $\langle \mathbb{C} \rangle$, it is easy to observe that the Reuss approximation represents a lower bound for $\mathbb{C}^*$.

Then, combining both results, we have obtained some bounds and the real effective properties of the heterogeneous material have to be always in between these values (for kinematically admissible strain fields and admissible stresses). Recalling the expressions:

$$\mathbb{C}^*_{(Voigt)} = \langle \mathbb{C} \rangle \geq \mathbb{C}^* \geq \langle \mathbb{C}^{-1} \rangle^{-1} = \mathbb{C}^*_{(Reuss)} \tag{3.58}$$

These bounds, which are based on simple expressions, do not contain any information on the microgeometry beyond the phase volume fractions and therefore are too slack for practical purposes.

3.10.2 Hashin-Shtrikman bounds

Hashin-Shtrikman bounds are based on a variational principle [32] and provide much information since the bounds are tighter. They are formulated in terms of a homogeneous reference material and some auxiliary fields (the so-called stress polarization fields $\boldsymbol{\tau}(\boldsymbol{y})$) that describe the differences between the stress fields in the inhomogeneous microscopic material (*fast variables*) and the stress field in the homogeneous reference medium (*slow variables*). This auxiliary variables allow separating the "fast" and "slow" contributions in the expression of the complementary energy of the composite and together with the Hill-Mandel condition provide an expression of a functional, known as the *Hashin-Shtrikman variational principle*:

$$\mathcal{F}\big(\boldsymbol{\tau}(\boldsymbol{y})\big) = \frac{1}{V_\mu} \int_\Omega \Big\{ \boldsymbol{\tau}^T(\boldsymbol{y}) : [\mathbb{C}^0 - \mathbb{C}(\boldsymbol{y})]^{-1} : \boldsymbol{\tau}(\boldsymbol{y}) + [\boldsymbol{\tau}(\boldsymbol{y}) - \langle \boldsymbol{\tau} \rangle^*]^T : \boldsymbol{\varepsilon}'_\mu : (\boldsymbol{\tau}(\boldsymbol{y})) + 2\boldsymbol{\tau}^T : \boldsymbol{\varepsilon}^0 \Big\} \mathrm{d}V \tag{3.59}$$

where the stress polarization tensor can be obtained by expressing the stress field $\boldsymbol{\sigma}_\mu(\boldsymbol{y})$ in an inhomogeneous material ($\mathbb{C}(\boldsymbol{y})$) in terms of a homogeneous reference material ($\mathbb{C}^0$) as:

$$\boldsymbol{\sigma}_\mu(\boldsymbol{y}) = \mathbb{C}(\boldsymbol{y}) : \boldsymbol{\varepsilon}_\mu(\boldsymbol{y}) = \mathbb{C}^0 : \boldsymbol{\varepsilon}_\mu(\boldsymbol{y}) + \boldsymbol{\tau}(\boldsymbol{y}) \quad \rightsquigarrow \quad \boldsymbol{\tau}(\boldsymbol{y}) = (\mathbb{C}(\boldsymbol{y}) - \mathbb{C}^0) : \boldsymbol{\varepsilon}_\mu(\boldsymbol{y}) \tag{3.60}$$

As it can be observed in eqn. (3.59), $\mathcal{F}$ depends on $\boldsymbol{\tau}(\boldsymbol{y})$. In order to obtain some information, it has to be computed the values of $\boldsymbol{\tau}(\boldsymbol{y})$ in order to make the functional $\mathcal{F}$ stationary. By doing this, the stationary values of $\mathcal{F}$ take the form $\mathcal{F} = \boldsymbol{\varepsilon}^{0^T} : (\mathbb{C}(\boldsymbol{y}) - \mathbb{C}^0) : \boldsymbol{\varepsilon}^0$. Hence, if the difference $(\mathbb{C}(\boldsymbol{y}) - \mathbb{C}^0)$ is positive definite the functional reaches a maximum. Conversely, the functional attains a minimum when the expression $(\mathbb{C}(\boldsymbol{y}) - \mathbb{C}^0)$ is negative definite.

The evaluation of the Hashin-Shtrikman bounds can be done only for particular cases, since the expressions for the stress polarization tensors are highly complex.

One option is to approximate the stress polarization tensors through their phase-averages: $\boldsymbol{\tau}^{(p)} = [\mathbb{C}^{(p)} - \mathbb{C}^0] : \langle \boldsymbol{\varepsilon}_\mu \rangle^{(p)}$, which leads to a simpler expression for the strain fluctuations $\boldsymbol{\varepsilon}'_\mu(\boldsymbol{\tau}^{(p)})$ that can be evaluated with a procedure based on the Eshelby problem. By optimizing the functional $\mathcal{F}$ with respect to the approximated expression for the stress polarization tensor, the tightest possible bounds within the Hashin-Shtrikman scheme are found[7].

As a particular case, it can be considered a composite which consists of *two isotropic phases* with elastic constants $\mathbb{C}^{(m)}$ and $\mathbb{C}^{(i)}$. If we assume that the matrix phase is softer than the inclusions and the matrix material is taken as comparison material ($\mathbb{C}^0 = \mathbb{C}^{(m)}$), then the aforementioned procedure leads to the following lower bound for the constitutive tensor:

$$\mathbb{C}^*_{HS-} = \mathbb{C}^{(m)} + \xi[(\mathbb{C}^{(i)} - \mathbb{C}^{(m)})^{-1} + (1-\xi)\, \mathbb{S}^{(m)} : \mathbb{M}^{(m)}]^{-1} \tag{3.61}$$

This expression coincides with the expression obtained in the Mori-Tanaka model. On the other hand, if the inclusions are taken as comparison material ($\mathbb{C}^0 = \mathbb{C}^{(i)}$), the above procedure leads to the upper bound for the effective constitutive tensor:

$$\mathbb{C}^*_{HS+} = \mathbb{C}^{(i)} + (1-\xi)[(\mathbb{C}^{(m)} - \mathbb{C}^{(i)})^{-1} + \xi\, \mathbb{S}^{(i)} : \mathbb{M}^{(i)}]^{-1} \tag{3.62}$$

This expression is equivalent to the same expression obtained in the so-called "inverse" Mori-Tanaka model, where the roles of the matrix phase and inclusions are exchanged. According to this, the Double Inclusion model can be seen as a properly chosen interpolation between the Hashin-Shtrikman bounds. In the case of porous materials, the Mori-Tanaka approach corresponds to the upper Hashin-Shtrikman bound, while the lower bound is trivial.

Hashin-Shtrikman bounds can also be employed when modeling materials that do not contain matrix-inclusion topologies, since the method holds for any phase arrangement of the appropriate symmetry and phase volume fraction, because is based on energetic principles. In this context, the bounds obtained through this variational principle are the tightest bounds that can be obtained using only the geometrical information provided by the volume fraction and the overall symmetry. When complex phase patterns are to be considered, numerical methods must be used in order to evaluate correctly the stress polarization tensor.

3.10.3 Improved Bounds

Some improved variational methods have been developed in the last years by a considerable number of authors. These methods use more complex trial functions and the required optimization, which is necessary to obtain the bounds of the effective properties for a inhomogeneous materials, needs some statistical information on the phase arrangement in the form of n-point correlations. Using a bigger amount of information allows to generate variational bounds that are significantly tighter than Hashin-Shtrikman estimates, although at a significantly larger computational cost.

[7] As it has been explained, only for simple cases such as a material with n discrete isotropic phases and piecewise constant elastic properties.

One of the most important methods is the so-called *Three-point bounds* for isotropic two-phase materials. This approach is based on the information of the phase arrangement (geometry and distribution of the particles) contained in two three-point microstructural parameters, $\eta(\xi)$ and $\zeta(\xi)$. These parameters can be evaluated for any given microstructure, although it is a considerable task. However, there exists in the literature some analytical formulation for an important number of generic microstructures of practical importance[8].

[8] For a discussion of the different improved variational bounds and the value of the parameters see, e.g., Bohm [10] and the literature contained on it.

Chapter 4

Homogenization of elastoplastic materials

The Mean-Field Approaches presented in the Chapter 3 are based in the assumption of a linear elastic material behavior and cannot be directly applied to most common materials, due to the fact that they often show an inelastic behavior. Therefore, some considerations have to be taken into account in order to extent the homogenization methods to nonlinear behaviors such elastoplasticity. Elastoplastic materials show a high dependence on loading paths and markedly fluctuations of the microfields for each phase. These two factors lead to different behaviors on each material point in an elastoplastic phase since each one follows a different trajectory in stress space. Therefore, the inhomogeneous material should be theoretically treated as a multiphase material, in which each point of the microstructure can be considered as a different phase. This fact causes the impossibility of using the phase averages to describe the mechanical behavior of the inhomogeneous material, as is done for the linear elastic case. As a consequence, some simplifications has to be done.

The first attempt of homogenization for elastoplastic composites was made by Kröner [47], who proposed a self-consistent model for polycrystals in which interactions between the phases are only elastic. Another approach was proposed by Hill [36], who defined a linear comparison material (LCC) with the same geometry as the original inhomogeneous material and linearized the local constitutive laws of its various phases in rate form, in such a way that the mean-field homogenization schemes in linear elasticity are valid. The work of Hill was developed by some other authors (Hutchinson [37], Petterman *et al.* [66]) containing as a result a step-by-step iterative procedure to compute the mechanical response of elastoplastic materials through the use of the tangent stiffness tensor of the phases. It was early recognized that such approaches overestimated the flow stress of the inhomogeneous material, due to the anisotropic nature of the tangent stiffness tensor during plastic deformation. This limitation led to the development of secant methods (Tandon and Weng [92], Berveiller and Zaoui [6] and Suquet [89]), which deal with

the elastoplastic behavior of the material within the framework of nonlinear elasticity. During the last years some improvements of the tangent and secant methods have been developed, leading to second order secant methods (see Suquet [88]) and new versions of the tangent method using the isotropic projection of the tangent stiffness method (see Doghri and Ouaar [17]). More recently, a new method based on using the tangent stiffness in a non-incremental form has been developed. This method is known as the "affine" approximation (Masson *et al.* [51]) and it provides a good approach for studying elastoviscoplastic materials.

As can be observed, the description of elastoplastic materials through analytical techniques involves the selection of the linearization procedure (tangent, incremental, ...), the linear homogenization model (Mori-Tanaka, Self-Consistent, Differential Scheme, ...) and the phase-wise equivalent stresses and equivalent strains to be used in evaluating the elastoplastic constitutive material behavior (first-order equivalent stress, second-order equivalent stress, ...). In the following sections some comments about the main methods and the implementation in a numerical software of such methods will be done.

4.1 Theoretical Background

In the following chapter some ideas about the macroscopic behavior regarding the elastoplastic inhomogeneous materials are given. The aim of the present section is to describe the macroscopic *effective* behavior of a inhomogeneous material by considering relations between the volume averages of the macroscopic stresses and the macroscopic strains, just as it was done for linear elastic materials. This section is based on the concepts described in Gross [31] and they will be used to understand the theoretical treatment of the elastoplasticity in heterogeneous materials. Let's consider a volume V_μ on the microscopic level of a inhomogeneous material. The elastoplastic behavior of such volume can be characterized through the spatially varying constitutive tensor $\mathbb{C}(\boldsymbol{y})$ and the spatially varying yield condition:

$$\mathcal{F}(\boldsymbol{\sigma}_\mu(\boldsymbol{y},t),\boldsymbol{y}) \leq 0 \tag{4.1}$$

The yield condition describes the set of all admissible stress states which in addition must satisfy the microscopic equilibrium ($\nabla \cdot \boldsymbol{\sigma}_\mu(\boldsymbol{y},t) = \boldsymbol{0}$). The relation with the elastic strains can be obtained through the elasticity law. In the following, the additive decomposition of the strain fields is assumed ($\boldsymbol{\varepsilon}_\mu(\boldsymbol{y},t) = \boldsymbol{\varepsilon}_{\mu,el}(\boldsymbol{y},t) + \boldsymbol{\varepsilon}_{\mu,pl}(\boldsymbol{y},t)$):

$$\boldsymbol{\sigma}_\mu(\boldsymbol{y},t) = \mathbb{C}(\boldsymbol{y}) : \boldsymbol{\varepsilon}_{\mu,el}(\boldsymbol{y},t) = \mathbb{C}(\boldsymbol{y}) : \big(\boldsymbol{\varepsilon}(\boldsymbol{y},t) - \boldsymbol{\varepsilon}_{\mu,pl}(\boldsymbol{y},t)\big) \tag{4.2}$$

The model is completed by considering the flow rule for the plastic strain increments $\dot{\boldsymbol{\varepsilon}}_\mu^{\,p}$, which will depend on the framework adopted to study the material (either incremental theory or deformation theory). As it can be in the Fig. 4.1, the volume element is considered to be subjected to prescribed strains $\boldsymbol{\varepsilon}^0$ or stresses $\boldsymbol{\sigma}^0$. For a linear elastic material, the macrostrains $\boldsymbol{\varepsilon}(\boldsymbol{x},t)$ could be defined as the volume average of the microscopic strains $\boldsymbol{\varepsilon}_\mu(\boldsymbol{y},t)$. However, this simple relation does

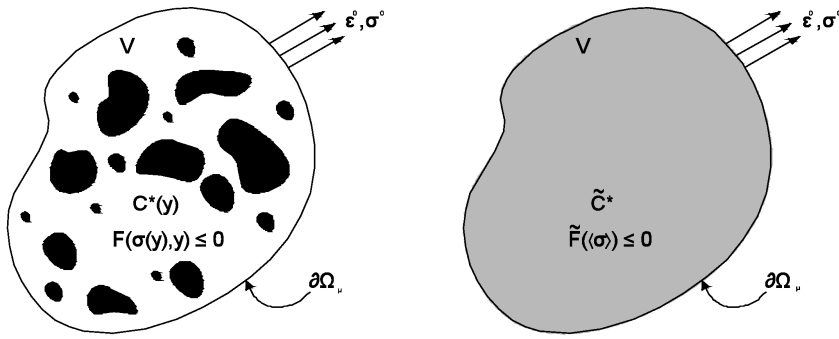

Figure 4.1: Inhomogeneous elastoplastic material (left) and homogenized comparison material (right) (Gross [31]).

not hold for the elastic and plastic parts of the macroscopic strains. The aim of the present section is to determine how the spatially distributed plastic and elastic strains $\boldsymbol{\varepsilon}_{\mu,pl}(\boldsymbol{y},t)$ and $\boldsymbol{\varepsilon}_{\mu,el}(\boldsymbol{y},t)$ are transferred to the microscale. In order to determine such relations, a purely *elastic comparison material* is defined in the same volume V_μ, subjected to the same boundary conditions. For this material, the equations defined in the previous chapter hold and the problem can be formulated as:

$$\begin{aligned} \boldsymbol{u}|_{\partial\Omega} &= \boldsymbol{\varepsilon}^0 \cdot \boldsymbol{y} \qquad \tilde{\boldsymbol{\varepsilon}}_\mu^{(a)} = \mathbb{A}(\boldsymbol{y}) : \boldsymbol{\varepsilon}^0 \qquad \langle \tilde{\boldsymbol{\varepsilon}}_\mu^{(a)} \rangle = \langle \boldsymbol{\varepsilon}_\mu \rangle = \boldsymbol{\varepsilon}^0 \\ \boldsymbol{t}|_{\partial V} &= \boldsymbol{\sigma}^0 \cdot \boldsymbol{n} \qquad \tilde{\boldsymbol{\sigma}}_\mu^{(b)} = \mathbb{B}(\boldsymbol{y}) : \boldsymbol{\sigma}^0 \qquad \langle \tilde{\boldsymbol{\sigma}}_\mu^{(a)} \rangle = \langle \boldsymbol{\sigma}_\mu \rangle = \boldsymbol{\sigma}^0 \end{aligned} \tag{4.3}$$

For simplicity, it will assumed now that macrostrains are imposed in the problem (similar results can be obtained through imposing macrostresses, see [31]). Considering the elasticity law, the macroscopic stresses will be given by: $\langle \boldsymbol{\sigma}_\mu^{(a)} \rangle = \mathbb{C}^* : \langle \tilde{\boldsymbol{\varepsilon}}_\mu^{(a)} \rangle$. The volume average over the volume V_μ can be obtained by multiplying the previous expressions by $\langle \tilde{\boldsymbol{\varepsilon}}_\mu^{(a)} \rangle$:

$$\langle \boldsymbol{\sigma}_\mu : \tilde{\boldsymbol{\varepsilon}}_\mu^{(a)} \rangle = \langle \boldsymbol{\varepsilon}_\mu : \overbrace{\mathbb{C} : \underbrace{\mathbb{A} : \boldsymbol{\varepsilon}^0}_{\tilde{\boldsymbol{\varepsilon}}_\mu^{(a)}}}^{\tilde{\boldsymbol{\sigma}}_\mu^{(a)}} \rangle - \langle \boldsymbol{\varepsilon}_{\mu,pl} : \overbrace{\mathbb{C} : \underbrace{\mathbb{A} : \boldsymbol{\varepsilon}^0}_{\tilde{\boldsymbol{\varepsilon}}_\mu^{(a)}}}^{\tilde{\boldsymbol{\sigma}}_\mu^{(a)}} \rangle \tag{4.4}$$

Since the fields $\tilde{\boldsymbol{\varepsilon}}_\mu^{(a)}$ and $\tilde{\boldsymbol{\sigma}}_\mu^{(a)}$ as well as $\boldsymbol{\varepsilon}_\mu$ and $\boldsymbol{\sigma}_\mu$ are kinematically and statically admissible the above relation can be varied considering the Hill-Mandel condition:

$$\begin{aligned} \langle \boldsymbol{\sigma}_\mu \rangle : \boldsymbol{\varepsilon}^0 &= \langle \boldsymbol{\varepsilon}_\mu \rangle : \langle \mathbb{C} : \mathbb{A} \rangle : \boldsymbol{\varepsilon}^0 - \langle \boldsymbol{\varepsilon}_{\mu,pl} : \mathbb{C} : \mathbb{A} \rangle : \boldsymbol{\varepsilon}^0 \\ &= \langle \boldsymbol{\varepsilon}_\mu \rangle : \mathbb{C}^* : \boldsymbol{\varepsilon}^0 - \langle \boldsymbol{\varepsilon}_{\mu,pl} : \mathbb{C} : \mathbb{A} \rangle : \boldsymbol{\varepsilon}^0 \end{aligned} \tag{4.5}$$

The previous expression holds for any arbitrary applied far-field strain $\boldsymbol{\varepsilon}^0$ and allows obtaining a relation between the macroscopic stress and the macroscopic strain:

$$\langle \boldsymbol{\sigma}_\mu \rangle = \mathbb{C}^* : \Big(\langle \boldsymbol{\varepsilon}_\mu \rangle - \boldsymbol{\mathcal{E}}_{pl} \Big) \tag{4.6}$$

with the expression for the macroscopic plastic strain:

$$\boldsymbol{\mathcal{E}}_{pl} = \mathbb{C}^{*^{-1}} : \langle \boldsymbol{\varepsilon}_{\mu,pl} : \mathbb{C} : \mathbb{A} \rangle \tag{4.7}$$

Considering the addition split for the macroscopic strain field, the expression for the macroscopic elastic strain can be found easily:

$$\boldsymbol{\mathcal{E}}_{el} = \langle \boldsymbol{\varepsilon}_\mu \rangle - \boldsymbol{\mathcal{E}}_{pl} = \mathbb{C}^{*^{-1}} : \langle \boldsymbol{\varepsilon}_{\mu,el} : \mathbb{C} : \mathbb{A} \rangle \tag{4.8}$$

As it can be observed through the previous expression, in the elastoplastic case the macroscopic elastic and plastic strains are not the ordinary volume average but the weighted averages of the respective microfields where the elastic heterogeneity in terms of the tensors $\mathbb{C}$ and $\mathbb{A}$ serves as the weighting factor[1].

Another interesting result that can be derived now is the expression of the elastic energy and the dissipation in a elastoplastic inhomogeneous material. In order to do that, let's consider a material that behaves elastic-perfectly plastic on the microscopic field. The strain energy density is given by:

$$U(\boldsymbol{y}) = \frac{1}{2} \boldsymbol{\varepsilon}_{\mu,el} : \mathbb{C} : \boldsymbol{\varepsilon}_{\mu,el} \tag{4.9}$$

Now we consider a Representative Volume Element V_μ subjected to prescribed macroscopic strain $\langle \boldsymbol{\varepsilon}_\mu \rangle = \boldsymbol{\varepsilon}^0$. A new auxiliary field $\boldsymbol{\varepsilon}_{\mu,res}(\boldsymbol{y}, t)$ is defined in order to describe the deviation of the true strain $\boldsymbol{\varepsilon}(\boldsymbol{y}, t)$ of the elastoplastic problem with respect to the strain field $\tilde{\boldsymbol{\varepsilon}}_\mu^{(a)}(\boldsymbol{y}, t)$ in a purely elastic comparison problem:

$$\boldsymbol{\varepsilon}_{\mu,res}(\boldsymbol{y}) = \boldsymbol{\varepsilon}_\mu(\boldsymbol{y}, t) - \tilde{\boldsymbol{\varepsilon}}_\mu^{(a)}(\boldsymbol{y}, t) = \boldsymbol{\varepsilon}_{\mu,el}(\boldsymbol{y}, t) - \mathbb{A} : \boldsymbol{\mathcal{E}}_{el} \tag{4.10}$$

The new variable is defined to study the behavior of the microstructure when the inhomogeneous material is subject to a complete macroscopically unloading ($\langle \boldsymbol{\varepsilon}_\mu \rangle \to 0$). From the eqn. (4.10) the expression for the microscopic strain field can be derived:

$$\boldsymbol{\varepsilon}_{\mu,el} = \boldsymbol{\varepsilon}_{\mu,res}(\boldsymbol{y}, t) + \mathbb{A} : \boldsymbol{\mathcal{E}}_{el} \tag{4.11}$$

Equation (4.11) can be used to calculate the volume average over of the energy density V_μ:

$$\begin{aligned} \langle U \rangle &= \frac{1}{2} \langle \big(\boldsymbol{\varepsilon}_{\mu,res}(\boldsymbol{y}, t) + \mathbb{A} : \boldsymbol{\mathcal{E}}_{el} \big) : \mathbb{C} : \big(\boldsymbol{\varepsilon}_{\mu,res}(\boldsymbol{y}, t) + \mathbb{A} : \boldsymbol{\mathcal{E}}_{el} \big) \rangle \\ &= \frac{1}{2} \langle \boldsymbol{\varepsilon}_{\mu,res} : \mathbb{C} : \boldsymbol{\varepsilon}_{\mu,res} \rangle + \frac{1}{2} \boldsymbol{\mathcal{E}}_{el} \underbrace{\langle \mathbb{A}^T : \mathbb{C} : \mathbb{A} \rangle}_{\mathbb{C}^*} \boldsymbol{\mathcal{E}}_{el} + \langle \boldsymbol{\varepsilon}_{\mu,res} : \mathbb{C} : \mathbb{A} : \boldsymbol{\mathcal{E}}_{el} \rangle \end{aligned} \tag{4.12}$$

[1] In the case of having the macroscopic stresses as the applied far-field, the tensors that serve as weighting factors are $\mathbb{B}$ and $\mathbb{M}$.

It can be proven, using the Hill-Mandel condition and the fact that the volume average of the residual strains vanishes[2], that the last expression in brackets vanishes (for more details, see [31]) and the average strain density in the RVE (with volume V_μ) reads:

$$\langle U \rangle = \frac{1}{2}\boldsymbol{\mathcal{E}}_{el} : \mathbb{C}^* : \boldsymbol{\mathcal{E}}_{el} + \frac{1}{2}\langle \boldsymbol{\varepsilon}_{\mu,res} : \mathbb{C} : \boldsymbol{\varepsilon}_{\mu,res} \rangle = \frac{1}{2}\boldsymbol{\mathcal{E}}_{el} : \mathbb{C}^* : \boldsymbol{\mathcal{E}}_{el} + \frac{1}{2}\langle \boldsymbol{\varepsilon}_{\mu,res} : \boldsymbol{\sigma}_{\mu,res} \rangle \quad (4.13)$$

where the identity $\boldsymbol{\sigma}_{\mu,res} = \mathbb{C}(\boldsymbol{y}) : \boldsymbol{\varepsilon}_{\mu,res}$ has been used. The first term describes the energy due to the macroscopic elastic strains $\boldsymbol{\mathcal{E}}_{el}$ while the second term represents the averaged strain density due to the heterogeneous residual fields.

The previous results can be used in order to calculate the dissipation. If the material behavior on the microscopic level is perfectly plastic the work done by the stresses on the plastic strains is entirely dissipated and the expression to compute the dissipation is given by:

$$\mathcal{D} = \langle \boldsymbol{\sigma}_\mu : \dot{\boldsymbol{\varepsilon}}_{\mu,pl} \rangle \quad (4.14)$$

It can be proven (see [31]) that this expression can be formulated in terms of the macroscopic volume averaged fields as:

$$\mathcal{D} = \langle \boldsymbol{\sigma}_\mu \rangle : \dot{\boldsymbol{\mathcal{E}}}_{pl} - \frac{1}{2}\langle \boldsymbol{\varepsilon}_{\mu,res} : \mathbb{C} : \boldsymbol{\varepsilon}_{\mu,res} \rangle^{\cdot} \quad (4.15)$$

From the last equation, it can be observed that the last term coincides with the elastic energy of the residual strain field. Therefore, not all the entire power done by the macroscopic stresses on the plastic strains is dissipated since a part is stored as elastic energy of the residual strain field (given by the second term on the right hand side).

The last ingredient that should be contemplated in order to state the elasto-plastic model for a inhomogeneous material is the definition of the macroscopic yield condition. If at some point of the microstructure plastic flow takes place with $\dot{\boldsymbol{\varepsilon}}^p_\mu \neq 0$ the stress state corresponding to this point is located on the yield surface, i.e., $\mathcal{F}(\boldsymbol{\sigma}_\mu(\boldsymbol{y}, t), \boldsymbol{y}) = 0$. For the rest of the points, whose stress states lie inside the yield surface such that $\mathcal{F}(\boldsymbol{\sigma}_\mu(\boldsymbol{y}, t), \boldsymbol{y}) < 0$, the inhomogeneous material behaves elastically. For simplicity, on the following it will be considered again a RVE of heterogeneous material with elastic-perfect plastic constituents (no hardening on the microscopic level), subjected to a far-field stress boundary condition $\langle \boldsymbol{\sigma}_\mu \rangle = \boldsymbol{\sigma}^0$.

Let us assume now that the stress level is imposed through some loading steps. The first stress loading steps will not cause plastic flow $\dot{\boldsymbol{\varepsilon}}^p_\mu = 0$ and the stress field throughout the RVE will be purely elastic. Since the material behaves as a linear elastic material, the localization relationships given in the previous chapters hold and the macroscopic yield condition can be easily obtained:

$$\mathcal{F}(\boldsymbol{\sigma}_\mu(\boldsymbol{y}, t), \boldsymbol{y}) = \mathcal{F}(\mathbb{B}(\boldsymbol{y}) : \langle \boldsymbol{\sigma}_\mu \rangle, \boldsymbol{y}) \equiv \tilde{\mathcal{F}}(\boldsymbol{y}) \leq 0 \qquad \forall \boldsymbol{y} \in V_\mu \quad (4.16)$$

[2] This identity can be obtained by considering the RVE in the case of macroscopic unloading, i.e., $\boldsymbol{\varepsilon}^0 = 0$.

It has to be taken into account that the macroscopic yield condition is defined for all the points located in the RVE. The set of all admissible macroscopic stress states that fulfill the eqn. (4.16) is formed by the intersection of all the macrostresses $\langle \boldsymbol{\sigma} \rangle$ for which the equation (4.16) holds in every point $\boldsymbol{y}$ of the RVE. The previous statement can be clarified through a simple example: let us consider two different points $\boldsymbol{y}_a$ and $\boldsymbol{y}_b$ and their corresponding yield surfaces represented in the plane of the two first components for the principal stress space (see Fig. 4.2). As it can

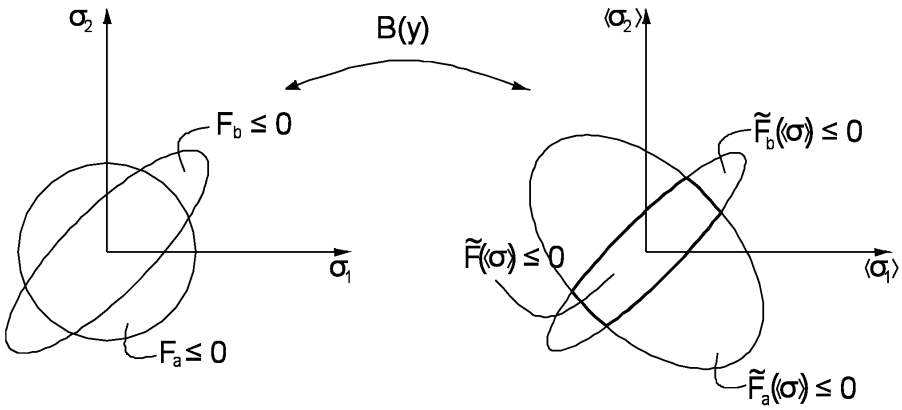

Figure 4.2: Elastic domains and yield surfaces on the microscopic (left) and macroscopic (right) scales (Gross [31]).

be appreciated, the stress localization tensor $\mathbb{B}$ transforms, as a linear mapping, the convex microscopic yield surfaces $\mathcal{F}_{a,b} = 0$ into the likewise convex surfaces $\tilde{\mathcal{F}}_{a,b} = 0$, being the latter defined in the plane of the principal macroscopic stress space. The intersection of two surfaces (the shaded region in Fig. 4.2) represents the set of all macroscopic stress states for which the resulting microscopic stress fields $\boldsymbol{\sigma}(\boldsymbol{y}, t)$ satisfy the condition given by eqn (4.16) at the points $\boldsymbol{y}_a$ and $\boldsymbol{y}_b$. The shaded region can be considered as the macroscopic yield surface $\tilde{\mathcal{F}}(\boldsymbol{y}) = 0$, since the macroscopic stress states that cause plastic flow are necessarily located on the boundary of such region.

After defining the concept of macroscopic yield surface through a simple situation characterized by the non-existence of plastic flow, it is important to analyze the effect of plasticity on the aforementioned yield surface. In order to do that, a microscopic point $\boldsymbol{y}$ is considered, where the stress state $\boldsymbol{\sigma}_\mu$ is located on the yield surface and produces some amount of plastic flow $\dot{\boldsymbol{\varepsilon}}^p_\mu \neq 0$. Through the stress concentration tensor $\mathbb{B}$ we can map the stress field in order to achieve the value for the corresponding macroscopic stress state $\langle \boldsymbol{\sigma}_\mu \rangle$, which will lie on the macroscopic yield surface. The plastic state produces that the residual stress variable is no longer zero:

$$\boldsymbol{\sigma}_{\mu,res}(\boldsymbol{y}, t) = \boldsymbol{\sigma}_\mu(\boldsymbol{y}, t) - \tilde{\boldsymbol{\sigma}}^{(b)}_\mu(\boldsymbol{y}, t) \neq \mathbf{0} \tag{4.17}$$

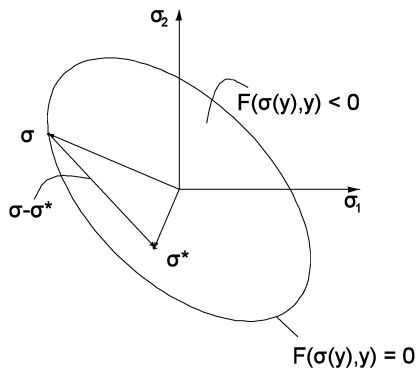

Figure 4.3: Elastic unloading on the microscopic level (Gross [31]).

If an unloading process is considered, the new stress state $\boldsymbol{\sigma}_\mu^*$ will lie into the elastic regime (Fig. 4.3). The difference between the previous two states is given by:

$$\boldsymbol{\sigma}_\mu(\boldsymbol{y},t) - \boldsymbol{\sigma}_\mu^*(\boldsymbol{y},t) = \mathbb{B}(\boldsymbol{y}) : \left(\langle\boldsymbol{\sigma}_\mu\rangle - \langle\boldsymbol{\sigma}_\mu^*\rangle\right) \tag{4.18}$$

Using the definition of the residual stress field:

$$\mathbb{B}(\boldsymbol{y}) : \langle\boldsymbol{\sigma}_\mu^*\rangle = \boldsymbol{\sigma}_\mu^*(\boldsymbol{y},t) - \boldsymbol{\sigma}_{\mu,res}(\boldsymbol{y},t) \tag{4.19}$$

This equality is valid for all the macroscopic stress states $\langle\boldsymbol{\sigma}_\mu^*\rangle$ inside the elastic domain, i.e., all the macroscopic stress states which cause a stress state in all the microscopic points $\boldsymbol{y}$ located inside the microscopic yield surface. Accordingly, the macroscopic yield surface is determined at each point $\boldsymbol{y}$ from each admissible microscopic stress state $\boldsymbol{\sigma}_\mu^*(\boldsymbol{y},t)$ through subtracting $\boldsymbol{\sigma}_{\mu,res}(\boldsymbol{y},t)$ and mapping using the linear transformation introduced by the tensor $\mathbb{B}(\boldsymbol{y})$. Finally, the result at all the points should be intersected. As is indicated in [31], the subtraction of the residual stress can be viewed as a translation by $\boldsymbol{\sigma}_{\mu,res}(\boldsymbol{y},t)$, which introduces additional kinematic hardening that can be appreciated in the macroscopic level.

The results obtained in the present section are based on the existence of the strain and stress concentration tensors $\mathbb{A}(\boldsymbol{y})$ and $\mathbb{B}(\boldsymbol{y})$. In the case of linear elasticity, it was sufficient to know the explicit formulation for such tensors in terms of the Eshelby tensor for ellipsoidal inhomogeneities embedded in a homogeneous matrix. However, when one takes into account the plastic behavior of the materials a new variable has to be considered: the plastic strains. This variable is spatially variable (depends on each point of the microstructure), although in most cases could be observed as an eigenstrain. As a result, further approximations should be considered in order to adapt some analytical homogenization methods to elastoplastic materials. As commented in the introduction of the present chapter, the approximation for elastoplastic materials are based on the concept of linear comparison composite, in which the nonlinear laws of its various phases are linearized in such a way that the mean-field homogenization schemes valid for linear elasticity

can be applied. In the following sections the most used methods for elastoplastic inhomogeneous materials will be presented, which differ between them according to the linearization scheme adopted for each case.

In the following sections, the elastoplastic behavior of materials will be based on the J_2 model, which relies on the Von Mises equivalent stress that coincides with the second invariant of the deviatoric stress tensor. The model is based on the hypotheses of additive decomposition of the total strain field and Hookean law:

$$\boldsymbol{\varepsilon}_\mu = \boldsymbol{\varepsilon}_{\mu,el} + \boldsymbol{\varepsilon}_{\mu,pl}, \qquad \boldsymbol{\sigma}_\mu = \mathbb{C} : \boldsymbol{\varepsilon}_{\mu,el} \tag{4.20}$$

The description for the yield function of each constituent will be given by:

$$\mathcal{F}(\boldsymbol{\sigma}_\mu) \doteq \sigma_{eq} - \sigma_Y - \mathcal{R}(\psi) \tag{4.21}$$

where σ_Y is the initial yield stress of the material, σ_{eq} is the equivalent stress of the material and $\mathcal{R}(\psi)$ is the hardening function. The yield function defines the set of admissible stresses ($\mathbb{E}_\sigma \doteq \boldsymbol{\sigma}_\mu | \mathcal{F}(\boldsymbol{\sigma}_\mu) \leq 0$), which interior defines the elastic domain ($int(\mathbb{E}_\sigma) \doteq \boldsymbol{\sigma}_\mu | \mathcal{F}(\boldsymbol{\sigma}_\mu) < 0$) and the yield surface ($\partial\mathbb{E}_\sigma \doteq \boldsymbol{\sigma}_\mu | \mathcal{F}(\boldsymbol{\sigma}_\mu) = 0$). The plastic flow rule governs the evolution of the plastic strain as:

$$\dot{\boldsymbol{\varepsilon}}_{\mu,pl} = \dot{\gamma} \frac{\partial \mathcal{F}}{\partial \boldsymbol{\sigma}_\mu} \tag{4.22}$$

where the scalar $\dot{\gamma} \geq 0$ is the plastic multiplier. Its sign is positive if $\mathcal{F} = 0$ and $\dot{\mathcal{F}} = 0$ (yielding in plasticity) or nil if $\mathcal{F} < 0$ (elasticity) or $\mathcal{F} = 0$ and $\dot{\mathcal{F}} < 0$ (elastic unloading).

The internal variable ψ is called accumulated plasticity and keeps track of the past history undergone by the material; it is linked to the plastic strain rate through the following expression:

$$\dot{\psi} = \left(\frac{2}{3}\, \dot{\boldsymbol{\varepsilon}}_\mu : \dot{\boldsymbol{\varepsilon}}_\mu\right)^{\frac{1}{2}} = \dot{\gamma} \tag{4.23}$$

Finally, the last variable that should be characterized in order to complete the definition of the constitutive elastoplastic model is the normal vector to the yield surface in stress space, whose expression is given by:

$$\boldsymbol{N} = \frac{\partial \mathcal{F}}{\partial \boldsymbol{\sigma}_\mu} = \frac{3}{2} \frac{\boldsymbol{\sigma}_{\mu,dev}}{\sigma_{\mu,eq}} \tag{4.24}$$

4.2 Secant Method

Secant formulations of elastoplasticity in inhomogeneous materials deal with the problem within the context of deformation theory of plasticity, approximating the elastoplastic behavior of materials through a set of nonlinear elastic models. Consequently, secant methods are not able to adequately model the mechanical behavior of the material under nonproportional loading paths (e.g. cyclic deformation), which supposes a large drawback in the use of such methods in practical applications. However, secant methods provide good results in the case of monotonous

and proportional loading paths and their use has been extended in a considerable number of theoretical studies.

The secant formulation determines for each phase a secant operator which links the total strain to the total stress. The problem is divided in a succession of loading steps, defined through increasing values of the applied effective stress tensor $\boldsymbol{\sigma}^0$ (in the case of a stress-driven problem) or the applied effective strain tensor $\boldsymbol{\varepsilon}^0$ (in the case of a strain-driven problem). In the following, the formulation of the problem will be presented in a strain-driven way, due to the fact that the models implemented have been done using this approach[3]. As commented before, the secant formulation is based on the deformation theory of plasticity, where the following relation between plastic strains and deviatoric stresses is assumed:

$$\boldsymbol{\varepsilon}^{(p)}_{\mu,pl} = \gamma^{(p)} \boldsymbol{\sigma}^{(p)}_{\mu,dev} \tag{4.25}$$

where $\gamma^{(p)}$ is the plastic multiplier and $\boldsymbol{\sigma}^{(p)}_{\mu,dev}$ designates the deviatoric part of the stress tensor for the phase $^{(p)}$. According to the Von Mises' yield condition in conjunction with the definition of equivalent stress and equivalent plastic strain (see section 4.1), the multiplier can be easily obtained as $\gamma^{(p)} = 3\varepsilon^{(p)}_{\mu,pl,eq}/2\sigma^{(p)}_{\mu,eq}$. The previous result leads to the so-called *Hencky-Ilyushin law*, which can be expressed as:

$$\boldsymbol{\sigma}^{(p)}_{\mu,dev} = 2\mu^{(p)}_{sec} \boldsymbol{e}^{(p)}, \qquad \text{with} \qquad \boldsymbol{e}^{(p)} = \Big[\frac{1}{2\mu^{(p)}} + \frac{3}{2}\frac{\varepsilon^{(p)}_{\mu,pl,eq}}{\sigma^{(p)}_{\mu,eq}}\Big] \boldsymbol{\sigma}^{(p)}_{\mu,dev} \tag{4.26}$$

As it can be observed, the formulation has the structure of a nonlinear elastic constitutive law with the secant modulus $\mu^{(p)}_{sec}\big(\varepsilon^{(p)}_{\mu,pl,eq}\big)$, which depends on the reference equivalent plastic strain of each phase. In fact, through the choice of the equivalent plastic strain the spatial dependence of the constitutive tensor is removed and the constitutive law for an elastoplastic phase denoted by $^{(p)}$ can be expressed as:

$$\boldsymbol{\sigma}^{(p)}_{\mu} = \mathbb{C}^{(p)}_{sec} : \boldsymbol{\varepsilon}^{(p)}_{\mu} \qquad \text{with} \qquad \mathbb{C}^{(p)}_{sec} = 3\kappa^{(p)} : \mathbb{J} + 2\mu^{(p)}_{sec}\big(\varepsilon^{(p)}_{\mu,pl,eq}\big) : \mathbb{K} \tag{4.27}$$

where $\mathbb{J}$ and $\mathbb{K}$ are the fourth-order volumetric and deviatoric projection tensors, respectively. The expressions for these tensors are: $\mathbb{J} = \frac{1}{3}\ \mathbf{1} \otimes \mathbf{1}$ and $\mathbb{K} = \mathbb{I} - \mathbb{J}$.

The macroscopic relation can be computed by considering linear homogenization, using the classical expressions commented on chapter 3. The macroscopic constitutive expression can be formulated as:

$$\boldsymbol{\sigma} = \mathbb{C}^*\big(\varepsilon^{(1)}_{\mu,pl,eq}, \varepsilon^{(2)}_{\mu,pl,eq}, \ \ldots\ , \varepsilon^{(p)}_{\mu,pl,eq}\big) : \boldsymbol{\varepsilon} \qquad \text{with} \qquad \mathbb{C}^* = \sum_{(p)} c^{(p)} \bar{\mathbb{A}}^{(p)}_{(sec)} : \mathbb{C}^{(p)}_{sec} \tag{4.28}$$

In the last expression, the strain concentration tensor will depend on the choice of the homogenization method and it will be also a function of the plastic equivalent

[3]This aspect will be commented again in the following sections, when the numerical implementation is described.

strain of each phase. The homogenization of elastoplastic composites is thus reduced to solving a set of nonlinear algebraic equations in $\varepsilon^{(p)}_{\mu,pl,eq}$. For each value of the applied far-field strain $\boldsymbol{\varepsilon}$, the secant effective stiffness tensor of the composite is computed and the effective response of the material can be determined through eqn. (4.28). The numerical implementation of the problem is done through an iterative fixed-point algorithm, which begins with a trivial value of the secant stiffness tensor of each phase.

The only ingredient that should be defined in order to describe completely the secant method is the definition of the reference state, i.e., the definition of the equivalent plastic strain for each phase. In the classic homogenization problems, this reference state is determined for each phase $^{(p)}$ from the deviatoric part of the average strain tensor of that phase:

$$\varepsilon^{(p)}_{\mu,pl,eq} = \left[\frac{2}{3}\langle\boldsymbol{\varepsilon}_\mu\rangle^{(p)}_{dev} : \langle\boldsymbol{\varepsilon}_\mu\rangle^{(p)}_{dev}\right]^{1/2} \tag{4.29}$$

This approximation is known as *first-order secant method*. However, this way to determine the equivalent plastic strain leads to lower values for the equivalent plastic strain in comparison with the phase average of the equivalent strain. It was observed that such deviation of the values was due to the large strain gradients, which develop during plastic deformation, and hence the composite yield and flow stresses were in practice overestimated. This problem was investigated and several approaches were made to determine the equivalent state from energy considerations or statistically-based theories. Finally, Suquet [88] and Ponte-Castañeda [71] developed the so-called "modified" secant approximation, where the reference equivalent strain in each phase $^{(p)}$ is determined from the volumetric average of second order moment of the effective strain tensor, instead of the classical first order moment. This method is also known in literature as *second order secant method*. The expression of the equivalent plastic strain is given by:

$$\varepsilon^{(p)}_{\mu,pl,eq} = \left[\frac{2}{3}\mathbb{K} :: \langle\boldsymbol{\varepsilon}_\mu \otimes \boldsymbol{\varepsilon}_\mu\rangle^{(p)}\right]^{1/2} \tag{4.30}$$

An analytical approximation was given by Kreher [46] and Buryachenko [13], who demonstrated that the second order moment of the equivalent plastic strain can be computed from the secant elastic tensor according to:

$$\varepsilon^{(p)}_{\mu,pl,eq} \simeq \left[\frac{1}{3c^{(p)}}\ \boldsymbol{\varepsilon}\ \frac{\partial\mathbb{C}^*}{\partial\mu^{(p)}_{sec}}\ \boldsymbol{\varepsilon}\right]^{1/2} \tag{4.31}$$

This second order approach of the secant method leads to better approximation when results are compared with "exact" results (results obtained using Finite Element Approximations), as it was proven in recent papers by Segurado *et al.* [79] and Pierard *et al.* [69].

4.3 Tangent Method

Tangent or incremental methods are based on a linearization of the local constitutive laws written in rate form, so homogenization models valid in linear elasticity

can apply in each time interval. Therefore, incremental models can take into account rigorously the effect of the loading history on the deformation and can be used to simulate the mechanical behavior under non-proportional loading paths.

The incremental formulation determines for each phase a tangent operator which links the strain rate to the stress rate. The problem is divided in a succession of loading steps, defined through the effective stress rate $\dot{\boldsymbol{\sigma}}^0$ (in the case of a stress-driven problem) or the effective strain rate $\dot{\boldsymbol{\varepsilon}}^0$ (in the case of a strain-driven problem). At the starting point, the *Prandtl-Reuss law* is employed for each phase:

$$\dot{\boldsymbol{e}}^{(p)} = \Big[\frac{1}{2\mu^{(p)}}\mathbb{I} + \frac{3}{2g^{(p)}}\frac{\boldsymbol{\sigma}^{(p)}_{\mu,dev} \otimes \boldsymbol{\sigma}^{(p)}_{\mu,dev}}{\boldsymbol{\sigma}^{(p)}_{\mu,dev} : \boldsymbol{\sigma}^{(p)}_{\mu,dev}}\Big] : \dot{\boldsymbol{\sigma}}^{(p)}_{\mu,dev} \tag{4.32}$$

where the variable $g^{(p)}$ denotes the plastic tangent modulus, defined by the expression: $g^{(p)} = \dot{\boldsymbol{\sigma}}^{(p)}_{\mu,eq}/\dot{\boldsymbol{\varepsilon}}^{(p)}_{\mu,eq,pl}$. The rate form of the elastoplastic behavior for each phase reads:

$$\dot{\boldsymbol{\sigma}}^{(p)}_{\mu} = \mathbb{C}^{(p)}_{ep} : \dot{\boldsymbol{\varepsilon}}^{(p)}_{\mu} \tag{4.33}$$

where $\mathbb{C}^{(p)}_{ep}$ is the so-called continuum elastoplastic tangent operator. When only a finite number of time increments are considered (for numerical implementation purposes), the previous equation can be written taking into account a discretization in time over each time interval:

$$\Delta\boldsymbol{\sigma}^{(p)}_{\mu} = \mathbb{C}^{(p)}_{alg} : \Delta\boldsymbol{\varepsilon}^{(p)}_{\mu} \tag{4.34}$$

where $\Delta\boldsymbol{\sigma}^{(p)}_{\mu}$ and $\Delta\boldsymbol{\varepsilon}^{(p)}_{\mu}$ are the stress and strain increments of each phase over the time interval and $\mathbb{C}^{(p)}_{alg}$ is the algorithmic tangent operator. It has to be emphasized that both tangent operators, $\mathbb{C}^{(p)}_{ep}$ and $\mathbb{C}^{(p)}_{alg}$, are different in general and become close for vanishingly small plastic strain increments. The tangent tensors show a dependence of the actual stress distribution, i.e., $\mathbb{C}^{(p)}_{ep} = \mathbb{C}^{(p)}_{ep}(\boldsymbol{y})$ and they are, even in case of an elastically isotropic material, *anisotropic* since they depend on the direction of the plastic flow, as it can be observed on the second part of the eqn. (4.32). At this point, for solving the problem, the linearization process is introduced through substituting the stress dependence of the tangent tensors by a dependence on the average stress in the respective case. This assumption leads to an incrementally linear material behavior with a spatially constant tangent stiffness tensor for each phase:

$$\dot{\boldsymbol{\sigma}}^{(p)}_{\mu} = \mathbb{C}^{(p)}_{ep}\Big(\langle\boldsymbol{\sigma}^{(p)}_{\mu,dev}\rangle\Big) : \dot{\boldsymbol{\varepsilon}}^{(p)}_{\mu} \tag{4.35}$$

The analytical expressions for the elastoplastic (also known as *continuum*) tangent operator and the algorithmic (also known as *consistent*) tangent operators can be then computed for most constitutive models. For the J_2 elastoplastic model they read:

$$\begin{aligned}
\mathbb{C}^{(p)}_{ep} &= \mathbb{C}^{(p)} - \frac{(2\mu^{(p)})^2}{h}\boldsymbol{N^{(p)}} \otimes \boldsymbol{N^{(p)}} \quad \text{with} \quad h = 3\mu^{(p)} + \frac{\mathrm{d}R}{\mathrm{d}\psi} \\
\mathbb{C}^{(p)}_{alg} &= \mathbb{C}^{(p)}_{ep} - (2\mu^{(p)})^2(\Delta\psi)\frac{\sigma^{(p)}_{\mu,eq}}{\sigma^{(p)}_{\mu,eq,tr}}\frac{\partial \boldsymbol{N}^{(p)}}{\partial \boldsymbol{\sigma}^{(p)}_{\mu}}
\end{aligned} \tag{4.36}$$

with $\sigma^{(p)}_{\mu,eq,tr}$ a trial (elastic predictor) value of $\sigma^{(p)}_{\mu,eq}$. In the last equations, the different variables coincide with the ones described in section 4.1. The expression for the partial derivative of the normal vector $\boldsymbol{N}$ with respect to $\boldsymbol{\sigma}_\mu$ is given by:

$$\frac{\partial \boldsymbol{N}^{(p)}}{\partial \boldsymbol{\sigma}^{(p)}_\mu} = \frac{1}{\sigma^{(p)}_{\mu,eq}}\Big(\frac{3}{2}\mathbb{K} - \boldsymbol{N}^{(p)} \otimes \boldsymbol{N}^{(p)}\Big) \tag{4.37}$$

The last equations ((4.34), (4.36)) can be written for each phase and form a set of linearized constitutive equations over the time step. Given the state of deformation at the beginning of the time step, homogenization models defined in the previous chapter can be applied over the current time interval, so that the macroscopic constitutive equation reads:

$$\Delta\boldsymbol{\sigma} = \mathbb{C}^*\Big(\langle\sigma_\mu\rangle^{(0)}_{eq}, \langle\sigma_\mu\rangle^{(1)}_{eq}, \ldots, \langle\sigma_\mu\rangle^{(p)}_{eq}\Big) : \Delta\boldsymbol{\varepsilon} \tag{4.38}$$

where $\mathbb{C}^*$ is the macroscopic tangent operator. For the present method, the reference equivalent stresses in each phase is computed from the average stress tensor (first-order moment)[4]. At each phase, the phase concentration tensors are obtained at each time increment considering the elastoplastic tangent operators as arguments and the macroscopic tangent operator can be then calculated through:

$$\mathbb{C}^* = \sum_{(p)} c^{(p)} \bar{\mathbb{A}}^{(p)}_t : \mathbb{C}^{(p)}_t \tag{4.39}$$

At the end, a set of equations is solved in a strain driven way. For each time step, given a macroscopic strain increment, a trial value of the average strain increment in the inclusions is computed. A fixed-point iterative scheme converges to average strain values in the phases from which the effective stiffness and the macroscopic response can be computed.

It has been proved that incremental main-field approaches tend to overestimate the macroscopic strain hardening in the plastic regime, i.e., the prediction of the macroscopic behavior is too stiff. Several attempts have been done in order to soften the macroscopic response by considering "isotropized" operators as well as algorithmic modifications (see Doghri and Ouaar [17] and Doghri and Friebel [18]). Basically, the idea consists on modifying the anisotropic algorithmic tangent operator and extracting the isotropic part of this tensor. The results that have been obtained through this approximation lead to better results due to the fact that they reduce the overprediction of the strain hardening behavior. From all the proposed methods, the one that will be applied in the present study corresponds with the a general method defined by Bornert [11], who proposed a method which consists on a projection of the anisotropic tangent operator onto the subspace of isotropic tangent operators. The tensor is defined by using the scalars κ_t and μ_t, defined as:

$$\mathbb{C}_{iso} = 3\kappa_t\mathbb{J} + 2\mu_t\mathbb{K} \quad \text{with} \quad \kappa_t = \kappa, \quad \mu_t = \mu - \frac{3}{5}\mu^2\Big(\frac{1}{h} + 4\frac{\Delta\psi}{\sigma_{\mu,eq,tr}}\Big) \tag{4.40}$$

[4]The extension of the incremental approach considering the second-order moment for the computation of the equivalent stresses in each phase is still an open subject.

This tensor is used in each phase to compute the tangent Eshelby tensor at each time step, while the previous definition of the algorithmic tangent operator (anisotropic) is used in the rest of the computations. Some authors have proposed using the "isotropized" constitutive tensor also in the expressions for the strain concentration tensors of each phase and also in the expressions for computing the effective constitutive tensor. Depending on the choice, different results are obtained (see [68]).

4.4 Numerical Implementation

One of the most important objectives of the present document is to give a definition of the most important concepts that should be considered for computing multiscale problems using micromechanical models. In the previous section, it has been explained the theoretical framework of the main models that are used for an analytical description of the main problem, as well as the main assumptions and hypothesis, on which those models are based. These analytical methods have been implemented in a Matlab© code, in order to provide a numerical tool to solve the micromechanical model using analytical models. In this section a description of the main aspects of the code will be given, as well as the numerical tools developed to transfer the theoretical expressions to a complete algorithm. The program will be used in the next chapters to provide a comparison between analytical tools for solving the micromechanical problem and the Finite Element Method.

4.4.1 General Description of the Code

The main code, implemented in Matlab©, has been written to compute the general response of a heterogeneous material composed by two different phases with matrix-inclusions arrangement. A material with an elastoplastic behavior and isotropic hardening forms the matrix phase, while the inclusions are purely elastic. Both materials are characterized through their mechanical parameters (Young modulus and Poisson's ratio). Two different hardening laws have been implemented on the code for the matrix phase:

- A linear-exponential law given by:

$$R(\psi) = \theta \bar{H} \psi + (\bar{K}_\infty - \bar{K}_0)[1 - \mathrm{e}^{-\delta\psi}],$$

  where $\bar{H} \geq 0$,$\bar{K}_\infty > \bar{K}_0 > 0$ and $\delta \geq 0$ are material constants.

- A power law given by:

$$R(\psi) = A\psi^m,$$

  where A is the strength coefficient and m the matrix strain hardening exponent.

The user should define the hardening law (exponential or power law) through an internal variable of the program and the corresponding values for the different

hardening parameters. The program takes into account the hardening law automatically.

The program solves the micromechanical problem using the secant and the incremental scheme using the J_2 plasticity model. As mentioned before, both methods are based on a linearization of the problem, in order to apply the homogenization techniques valid for linear elastic materials. Different Mean-Field approaches have been considered in the code, whose implementation will be commented in the next section. All the considered methods are based on the Eshelby's result to compute the concentration tensors for each phase. In all of them, the Eshelby tensor should be computed using the mechanical properties of the matrix phase (except for the Double Inclusion method, which additionally requires the Eshelby tensor computed with the properties of the inclusions). Six different types of inclusions have been considered in the formulation of the problem, based on the analytical expressions for the components of the Eshelby tensor (see Appendix A): spherical inclusions, ellipsoidal inclusions (oblate and prolate), flat disks, long fibers, long cylindrical fibers with circular and elliptical cross-section. The last two cases are only valid for 2D problems while the rest of them can be used to formulate a complete 3D model.

The program has been completely written using Voigt's notation, in order to save computational resources and simplify the operations between tensors. The stress and strain tensors are written in vector form according to:

$$\begin{bmatrix}\sigma_1\\ \sigma_2\\ \sigma_3\\ \sigma_4\\ \sigma_5\\ \sigma_6\end{bmatrix} = \begin{bmatrix}\sigma_{11}\\ \sigma_{22}\\ \sigma_{33}\\ \sigma_{23}\\ \sigma_{31}\\ \sigma_{12}\end{bmatrix} \qquad \begin{bmatrix}\varepsilon_1\\ \varepsilon_2\\ \varepsilon_3\\ \varepsilon_4\\ \varepsilon_5\\ \varepsilon_6\end{bmatrix} = \begin{bmatrix}\varepsilon_{11}\\ \varepsilon_{22}\\ \varepsilon_{33}\\ 2\,\varepsilon_{23}\\ 2\,\varepsilon_{31}\\ 2\,\varepsilon_{12}\end{bmatrix}$$

The program has been coded in a strain driven way: the input data consists on a strain increment law, which can be monotonic or cyclic (for those cases the secant methods are not considered). The macroscopic strain field is imposed by defining the magnitude of each component through a vector and defining the loading steps through a matrix, whose first column includes the initial time for each interval and the second column serves as a loading factor. The user can also define the number of points in which each interval will be divided (the loading steps are divided uniformly by the number of loading increments), in order to provide more accuracy in the results (but spending more computational resources). The program solves the nonlinear problem and calculates the macroscopic stress vector and the stress vector for each phase at each time step.

4.4.2 Homogenization Methods

Among all the possible homogenization techniques that have been commented in Chapter 3, only some of them have been implemented: classical Eshelby homogenization (for dilute inclusions), Mori-Tanaka approach, Classical Self-Consistent

Method, Differential Scheme and Double-Inclusion Scheme (Lielens Method). These techniques have been selected due to the fact that they are the most extended in the literature[5] Input data in all the implemented methods are the constitutive tensors for each phase (elastic and compliance tensors, $\mathbb{C}$ and $\mathbb{M}$, respectively), the Eshelby tensor $\mathbb{S}$[6] and the volume fraction of the inclusions ξ. On the other hand, the output data consists on the strain and stress concentration tensors for each phase, i.e., $\mathbb{A}^{(p)}$ and $\mathbb{B}^{(p)}$, and the effective constitutive tensors (elastic and compliance tensors, $\mathbb{C}^*$ and $\mathbb{M}^*$, respectively).

All it was commented in the previous chapter, all the Mean-Field methods may be written in an explicit way except the Classical Self-Consistent and the Differential Scheme. The Self-Consistent Method needs an iterative scheme to compute the effective properties of the homogenized material, while the Differential Scheme needs some numerical techniques in order to solve an ordinary differential equation. The Self-Consistent Method has been coded using an iterative fixed-point algorithm, which begins with a value of the effective properties of the heterogeneous solid obtained using the expression for the strain concentration with the matrix as effective material. The scheme for solving this method is given in the following chart:

- Input data: ξ, $\mathbb{S}^{(m)}$, $\mathbb{C}^{(i)}$, $\mathbb{M}^{(i)}$, $\mathbb{C}^{(m)}$, $\mathbb{M}^{(m)}$.
- Inizialitation: $\mathbb{C}^*$, $\mathbb{M}^* \leftarrow \mathbb{A}^{(i)}_{dil}(\mathbb{S}^{(m)}, \mathbb{C}^{(i)}, \mathbb{C}^{(m)})$, $\mathbb{B}^{(i)}_{dil}(\mathbb{S}^{(m)}, \mathbb{M}^{(i)}, \mathbb{M}^{(m)})$.
- Iterations:
  1. Using the previous results as starting point:

     $$\mathbb{C}_* = \mathbb{C}^*_{k-1}; \qquad \mathbb{M}_* = \mathbb{M}^*_{k-1}$$

  2. Computing the Poisson's ratio and the Eshelby tensor for the iteration k:

     $$\nu_k = -\frac{\mathbb{M}^*_{1,2}}{\mathbb{M}^*_{1,1}} \qquad \rightarrow \qquad \mathbb{S}^*_k$$

  3. Compute the new effective properties using the effective tensors for the previous iteration:

     $$\mathbb{C}^*_k, \mathbb{M}^*_k \qquad \leftarrow \qquad \mathbb{A}^{(i)}_{dil}(\mathbb{S}^{(m)}_k, \mathbb{C}^{(i)}, \mathbb{C}^*), \mathbb{B}^{(i)}_{dil}(\mathbb{S}^*_k, \mathbb{M}^{(i)}, \mathbb{M}^*)$$

  4. Check the error between iterations:

     $$||\mathbb{C}^*_k - \mathbb{C}^*|| < TOL \qquad ||\mathbb{M}^*_k - \mathbb{M}^*|| < TOL$$

- The values obtained after convergence are the final values for: $\mathbb{C}^*$, $\mathbb{M}^*$, $\mathbb{A}^{(i)}_{dil}$ and $\mathbb{B}^{(i)}_{dil}$.

---

[5] In fact, the Mori-Tanaka method is the one that is used almost exclusively in the literature (as well as the approaches based on the Mori-Tanaka method, such as the Double-Inclusion Scheme).

[6] In the case of the Double-Inclusion method, two different Eshelby tensors should be defined: one computed using the mechanical properties of the matrix and other with the inclusion properties.

The Differential Scheme is solved using a Runge-Kutta 4 procedure to solve numerically the ordinary differential equations given by eqn. (3.36). The main scheme to solve the method is given on the following lines of pseudo-code. As it can be observed, the scheme computes firstly the effective constitutive tensor using a zero value for the volume fraction of the inclusions. Subsequently, at each iteration, the method computes new values for the constitutive tensor by considering increasingly values for the volume fraction of the inclusion, until reaching the "true value" ξ:

- Input data: ξ, $\mathbb{S}^{(m)}$, $\mathbb{C}^{(i)}$, $\mathbb{M}^{(i)}$, $\mathbb{C}^{(m)}$, $\mathbb{M}^{(m)}$.
- Inizialitation: $\mathbb{C}^*$, $\mathbb{M}^* \leftarrow \mathbb{A}^{(i)}_{dil}\big(\mathbb{S}^{(m)}, \mathbb{C}^{(i)}, \mathbb{C}^{(m)}\big)$, $\mathbb{B}^{(i)}_{dil}\big(\mathbb{S}^{(m)}, \mathbb{M}^{(i)}, \mathbb{M}^{(m)}\big)$.
- Fixing the increment for each step and the number of intervals: $h,\ n = \xi/h$.
- Iterations: for each value of the volume fraction of the inclusions $\xi_k = k \cdot h$

  1. First evaluation at the current point:

     $$\mathbb{A}^{(i)}_{dil,k} = \big[\mathbb{I} + \mathbb{S}_k : \mathbb{M}^{(m)}_k : (\mathbb{C}^{(i)}_k - \mathbb{C}^{(m)}_k)\big]^{-1}$$
     $$\mathbb{B}^{(i)}_{dil,k} = \mathbb{C}^{(i)}_k : \big[\mathbb{I} + \mathbb{S}_k : \mathbb{M}^{(m)}_k : (\mathbb{C}^{(i)}_k - \mathbb{C}^{(m)}_k)\big]^{-1} : \mathbb{M}^{(m)}_k$$

  2. Computing the new point, in which the second evaluation will be done:

     $$\xi_{k+h/2} = \xi_k + 0.5 \cdot h$$
     $$k^{\mathbb{A}}_1 = \frac{1}{1-\xi_k}(\mathbb{C}^{(i)}_k - \mathbb{C}^{(m)}_k) : \mathbb{A}^{(i)}_{dil,k} \rightarrow \mathbb{C}^m_{k+h/2} = \mathbb{C}^m_k + 0.5 \cdot h \cdot k^{\mathbb{A}}_1$$
     $$k^{\mathbb{B}}_1 = \frac{1}{1-\xi_k}(\mathbb{M}^{(i)}_k - \mathbb{M}^{(m)}_k) : \mathbb{B}^{(i)}_{dil,k} \rightarrow \mathbb{M}^m_{k+h/2} = \mathbb{M}^m_k + 0.5 \cdot h \cdot k^{\mathbb{B}}_1$$

  3. Computing the Eshelby tensor in the second point:

     $$\nu_{k+h/2} = -\frac{\mathbb{M}^{(m)}_{1,2\ k+h/2}}{\mathbb{M}^{(m)}_{1,1\ k+h/2}} \qquad \rightarrow \qquad \mathbb{S}^{(m)}_{k+h/2}$$

  4. Computing the concentration tensors at the second point:

     $$\mathbb{A}^{(i)}_{dil,k+h/2} = \big[\mathbb{I} + \mathbb{S}_{k+h/2} : \mathbb{M}^{(m)}_{k+h/2} : (\mathbb{C}^{(i)}_{k+h/2} - \mathbb{C}^{(m)}_{k+h/2})\big]^{-1}$$
     $$\mathbb{B}^{(i)}_{dil,k+h/2} = \mathbb{C}^{(i)}_k : \big[\mathbb{I} + \mathbb{S}_{k+h/2} : \mathbb{M}^{(m)}_{k+h/2} : (\mathbb{C}^{(i)}_k - \mathbb{C}^{(m)}_{k+h/2})\big]^{-1} : \mathbb{M}^{(m)}_{k+h/2}$$

  5. Computing the new point, in which the third evaluation will be done:

     $$\xi_{k+h^*/2} = \xi_k + 0.5 \cdot h$$
     $$k^{\mathbb{A}}_2 = \frac{1}{1-\xi_{k+h/2}}(\mathbb{C}^{(i)} - \mathbb{C}^{(m)}_{k+h/2}) : \mathbb{A}^{(i)}_{dil,k+h/2} \rightarrow \mathbb{C}^m_{k+h^*/2} = \mathbb{C}^m + 0.5 \cdot h \cdot k^{\mathbb{A}}_2$$
     $$k^{\mathbb{B}}_2 = \frac{1}{1-\xi_{k+h/2}}(\mathbb{M}^{(i)} - \mathbb{M}^{(m)}_{k+h/2}) : \mathbb{B}^{(i)}_{dil,k+h/2} \rightarrow \mathbb{M}^m_{k+h^*/2} = \mathbb{M}^m + 0.5 \cdot h \cdot k^{\mathbb{B}}_2$$

  6. Computing the Eshelby tensor in the new point:

     $$\nu_{k+h^*/2} = -\frac{\mathbb{M}^{(m)}_{1,2\ k+h^*/2}}{\mathbb{M}^{(m)}_{1,1\ k+h^*/2}} \qquad \rightarrow \qquad \mathbb{S}^{(m)}_{k+h^*/2}$$

7. Computing the concentration tensors at the third point:

$$\mathbb{A}^{(i)}_{dil,k+h^*/_2} = \left[\mathbb{I} + \mathbb{S}_{k+h^*/_2} : \mathbb{M}^{(m)}_{k+h^*/_2} : (\mathbb{C}^{(i)}_k - \mathbb{C}^{(m)}_{k+h^*/_2})\right]^{-1}$$
$$\mathbb{B}^{(i)}_{dil,k+h^*/_2} = \mathbb{C}^{(i)}_k : \left[\mathbb{I} + \mathbb{S}_{k+h^*/_2} : \mathbb{M}^{(m)}_{k+h^*/_2} : (\mathbb{C}^{(i)}_k - \mathbb{C}^{(m)}_{k+h^*/_2})\right]^{-1} : \mathbb{M}^{(m)}_{k+h^*/_2}$$

8. Computing the new point, in which the fourth evaluation will be done:

$$\xi_{k+h} = \xi_k + h$$
$$k_3^{\mathbb{A}} = \frac{1}{1-\xi_{k+h^*/_2}}(\mathbb{C}^{(i)} - \mathbb{C}^{(m)}_{k+h^*/_2}) : \mathbb{A}^{(i)}_{dil,k+h^*/_2} \rightarrow \mathbb{C}^m_{k+h} = \mathbb{C}^m + h \cdot k_3^{\mathbb{A}}$$
$$k_3^{\mathbb{B}} = \frac{1}{1-\xi_{k+h^*/_2}}(\mathbb{M}^{(i)} - \mathbb{M}^{(m)}_{k+h^*/_2}) : \mathbb{B}^{(i)}_{dil,k+h^*/_2} \rightarrow \mathbb{M}^m_{k+h} = \mathbb{M}^m + h \cdot k_3^{\mathbb{B}}$$

9. Computing the Eshelby tensor in the new point:

$$\nu_{k+h} = -\frac{\mathbb{M}^{(m)}_{1,2\ k+h}}{\mathbb{M}\ 1,1_{k+h}{}^{(m)}} \qquad \rightarrow \qquad \mathbb{S}^{(m)}_{k+h}$$

10. Computing the concentration tensors at the fourth point:

$$\mathbb{A}^{(i)}_{dil,k+h} = \left[\mathbb{I} + \mathbb{S}_{k+h} : \mathbb{M}^{(m)}_{k+h} : (\mathbb{C}^{(i)}_k - \mathbb{C}^{(m)}_{k+h})\right]^{-1}$$
$$\mathbb{B}^{(i)}_{dil,k+h} = \mathbb{C}^{(i)}_k : \left[\mathbb{I} + \mathbb{S}_{k+h} : \mathbb{M}^{(m)}_{k+h} : (\mathbb{C}^{(i)}_k - \mathbb{C}^{(m)}_{k+h})\right]^{-1} : \mathbb{M}^{(m)}_{k+h}$$

11. Computing the fourth evaluation

$$k_4^{\mathbb{A}} = \frac{1}{1-\xi_{k+h}}(\mathbb{C}^{(i)} - \mathbb{C}^{(m)}_{k+h}) : \mathbb{A}^{(i)}_{dil,k+h}$$
$$k_4^{\mathbb{B}} = \frac{1}{1-\xi_{k+h}}(\mathbb{M}^{(i)} - \mathbb{M}^{(m)}_{k+h}) : \mathbb{B}^{(i)}_{dil,k+h}$$

12. Calculating the effective constitutive tensors using Runge-Kutta scheme:

$$\mathbb{C}^{(m)}_{k+1} = \mathbb{C}^{(m)}_k + \frac{h}{6}\left(k_1^{\mathbb{A}} + 2k_2^{\mathbb{A}} + 2k_3^{\mathbb{A}} + k_4^{\mathbb{A}}\right)$$
$$\mathbb{M}^{(m)}_{k+1} = \mathbb{M}^{(m)}_k + \frac{h}{6}\left(k_1^{\mathbb{B}} + 2k_2^{\mathbb{B}} + 2k_3^{\mathbb{B}} + k_4^{\mathbb{B}}\right)$$

- The values obtained for the last iteration ($\xi_k = \xi$) are the final values for: $\mathbb{C}^*$, $\mathbb{M}^*$, $\mathbb{A}^{(i)}_{dil}$ and $\mathbb{B}^{(i)}_{dil}$.

4.4.3 Secant method

The program computes the micromechanical problem using two different approaches: the secant method and the incremental method. As it was commented before, the secant approach is based on deformation theory of plasticity and determines for each phase a secant operator which links the total strain to the total stress. Considering the formulation given in the section 4.2, a function has been coded using Matlab© in order to solve the micromechanical problem using the secant method. The program takes as input data the value of the macrostrain field at each time step and the mechanical properties for each of the constituents. As output data,

the program provides the strain and stress fields for the constituents and the inhomogeneous material, for each time step. The code is based on a fixed-point algorithm, which takes a trial value of the secant elastic tensor of the matrix at each time step and solves a nonlinear set of algebraic equations in $\varepsilon^{(m)}_{\mu,pl,eq}$. On the following lines the implemented strategy is described in a pseudo-code form:

- Input data: ξ, Material parameters ($E^{(m)}, \nu^{(m)}, E^{(i)}, \nu^{(i)}$, hardening parameters, ...) and $\boldsymbol{\varepsilon}$.
- Computation of the constitutive tensors of the constituents considering elastic behavior: $\mathbb{C}^{(m)}$, $\mathbb{M}^{(m)}$, $\mathbb{C}^{(i)}$ and $\mathbb{M}^{(i)}$.
- Computation of the Eshelby tensor considering elastic behavior of the matrix: $\mathbb{S}^{(m)} \leftarrow \nu^{(m)}$.
- Obtaining the strain and stress concentration tensor using elastic properties of materials: $\bar{\mathbb{A}}^{(m)}, \bar{\mathbb{B}}^{(m)}, \bar{\mathbb{A}}^{(i)}$ and $\bar{\mathbb{B}}^{(i)} \leftarrow \mathbb{C}^{(m)}, \mathbb{M}^{(m)}, \mathbb{C}^{(i)}, \mathbb{M}^{(i)}, \mathbb{M}^{(i)}, \mathbb{S}^{(m)}$ and ξ.
- Computation of the effective constitutive tensor os the heterogeneous material considering elastic behavior of the constituents: $\mathbb{C}^*$, $\mathbb{M}^* \leftarrow \bar{\mathbb{A}}^{(m)}, \bar{\mathbb{B}}^{(m)}, \bar{\mathbb{A}}^{(i)}, \bar{\mathbb{B}}^{(i)}$.
- Iterations: for each loading step (the counter is omitted for clarity)

  1. Trial state: obtaining the strain and stress fields in the matrix considering elastic material:

     $$\boldsymbol{\varepsilon}^m_{\mu,k} = \bar{\mathbb{A}}^{(m)} : \boldsymbol{\varepsilon}_k; \qquad \boldsymbol{\sigma}^m_{\mu,k} = \mathbb{C}^{(m)} : \boldsymbol{\varepsilon}^m_{\mu,k}$$

  2. Computing the equivalent stress:

     a) Using a first order approximation:

     $$\varepsilon^{(m)}_{\mu,pl,eq\ k} = \Big[\frac{2}{3}\ \boldsymbol{\varepsilon}_{\mu,dev\ k} : \boldsymbol{\varepsilon}_{\mu,dev\ k}\Big]^{1/2} \rightsquigarrow \sigma^{(m)}_{\mu,eq\ k}$$

     b) Using a second order approximation:

     $$\varepsilon^{(m)}_{\mu,pl,eq\ k} = \Big[\frac{3}{1-\xi}\ \boldsymbol{\varepsilon}_k : \frac{\partial \mathbb{C}^*}{\partial \mu^{(m)}} : \boldsymbol{\varepsilon}_k\Big]^{1/2} \rightsquigarrow \sigma^{(m)}_{\mu,eq\ k}$$

  3. If the loading corresponds to a elastic case ($\sigma^{(m)}_{\mu,eq\ k} \leq \sigma_Y$). The trial state is valid: the secant properties are equal to the elastic properties.
  4. Else ($\sigma^{(m)}_{\mu,eq\ k} > \sigma_Y$). Iterations: while $Error > TOL$

     i. Computing the value of the secant shear modulus:

     $$\mu^{(m)}_{sec} = \frac{\sigma^{(m)}_{\mu,eq\ k}\mu^{(m)}}{\sigma^{(m)}_{\mu,eq\ k} + 3\mu^{(m)}\varepsilon^{(m)}_{\mu,pl,eq\ k}}$$

     ii. Obtaining the secant Poisson ratio and the secant Eshelby tensor:
     $\mathbb{S}^{(m)}_{sec} \leftarrow k^{(m)}, \mu^{(m)}_{sec}$

     iii. Computing the constitutive secant tensors for the matrix phase:
     $\mathbb{C}^{(m)}_{sec}, \mathbb{M}^{(m)}_{sec} \leftarrow k^{(m)}, \mu^{(m)}_{sec}$

     iv. Calculation of the secant strain and stress concentration tensors:
     $\bar{\mathbb{A}}^{(m)}_{sec}, \bar{\mathbb{B}}^{(m)}_{sec}, \bar{\mathbb{A}}^{(i)}_{sec}, \bar{\mathbb{B}}^{(i)}_{sec} \leftarrow \mathbb{C}^{(m)}_{sec}, \mathbb{M}^{(m)}_{sec}, \mathbb{C}^{(i)}, \mathbb{M}^{(i)}, \mathbb{S}^{(m)}_{sec}$

     v. Secant effective properties of the heterogeneous material:
     $\mathbb{C}^*_{sec}, \mathbb{M}^*_{sec} \leftarrow \bar{\mathbb{A}}^{(m)}_{sec}, \bar{\mathbb{B}}^{(m)}_{sec}, \bar{\mathbb{A}}^{(i)}_{sec}, \bar{\mathbb{B}}^{(i)}_{sec}$.

     vi. Computation of the new value of the equivalent strain:

a) Using a first order approximation:

$$\boldsymbol{\varepsilon}^{(m)}_{\mu,pl\ k+1} = \mathbb{M}^{(m)} : \left[\mathbb{C}^{m} - \mathbb{C}^{m}_{sec}\right] : \left(\mathbb{A}^{(m)}_{sec} : \boldsymbol{\varepsilon}\right)$$
$$\varepsilon^{(m)}_{\mu,pl,eq\ k+1} = \left[\frac{2}{3}\ \boldsymbol{\varepsilon}^{(m)}_{\mu,pl\ k+1} : \boldsymbol{\varepsilon}^{(m)}_{\mu,pl\ k+1}\right]^{1/2}$$

b) Using a second order approximation:

$$\varepsilon^{(m)}_{\mu,pl,eq\ k+1} = \left[\frac{3}{1-\xi}\ \boldsymbol{\varepsilon} : \frac{\partial \mathbb{C}^{*}_{sec}}{\partial \mu^{(m)}_{sec}} : \boldsymbol{\varepsilon}\right]^{1/2}$$

vii. Computing the error and updating variables for the next iteration:

$$Error = || \frac{\varepsilon^{(m)}_{\mu,pl,eq\ k+1} - \varepsilon^{(m)}_{\mu,pl,eq\ k}}{\varepsilon^{(m)}_{\mu,pl,eq\ k}} ||$$

viii. If $Error \leq TOL$, then exit the loop.
ix. Else: new iteration after updating the variables:

$$\varepsilon^{(m)}_{\mu,pl,eq\ k} = \varepsilon^{(m)}_{\mu,pl,eq\ k+1}$$

5. After the convergence, computation of the macrostresses using the effective secant constitutive tensor:

$$\boldsymbol{\sigma} = \mathbb{C}^{*}_{sec} : \boldsymbol{\varepsilon} \quad .$$

6. Computation of the microstrains and microstresses for each constituent using the secant concentration tensors:

$$\boldsymbol{\varepsilon}^{(m)}_{\mu} = \bar{\mathbb{A}}^{(m)}_{sec} : \boldsymbol{\varepsilon} \quad \longrightarrow \quad \boldsymbol{\sigma}^{(m)}_{\mu} = \mathbb{C}^{(m)}_{sec} : \boldsymbol{\varepsilon}^{(m)}_{\mu}$$
$$\boldsymbol{\varepsilon}^{(i)}_{\mu} = \bar{\mathbb{A}}^{(i)}_{sec} : \boldsymbol{\varepsilon} \quad \longrightarrow \quad \boldsymbol{\sigma}^{(i)}_{\mu} = \mathbb{C}^{(i)}_{sec} : \boldsymbol{\varepsilon}^{(i)}_{\mu}$$

The main scheme of the code is valid for both first order and second order secant methods, although the computation of the equivalent plastic strain is different for each of them. As it was commented before, the first order secant method provides lower values for the equivalent plastic stress and hence the composite yield and flow stresses were in practice overestimated. The second-order moment is computed in a new function using the expression indicated in equation (4.31):

$$\varepsilon^{(m)}_{\mu,pl,eq} \simeq \left[\frac{1}{3(1-\xi)}\ \boldsymbol{\varepsilon}\ \frac{\partial \mathbb{C}^{*}_{sec}}{\partial \mu^{(m)}_{sec}}\ \boldsymbol{\varepsilon}\right]^{1/2} \tag{4.41}$$

In this equation the expression for the derivative of the effective elastic tensor is needed with respect to the secant shear modulus. Taking into account that the effective elastic tensor of a two phase composite can be written as:

$$\begin{aligned} \mathbb{C}^{*}_{sec} &= (1-\xi)\ \bar{\mathbb{A}}^{(m)}_{sec} : \mathbb{C}^{(m)}_{sec} + \xi\ \bar{\mathbb{A}}^{(i)}_{sec} : \mathbb{C}^{(i)} \\ &= \mathbb{C}^{(m)}_{sec} + \xi\ \mathbb{A}^{(i)}_{sec} : \left(\mathbb{C}^{(i)} - \mathbb{C}^{(m)}_{sec}\right) \end{aligned} \tag{4.42}$$

The derivative of the effective elastic tensor with respect to the secant shear modulus can be written in terms of the derivatives of the concentration tensors and the elastic tensors of each constituent:

$$\begin{aligned}\frac{\partial \mathbb{C}^{*}_{sec}}{\partial \mu^{(m)}_{sec}} &= \left[\frac{\partial \mathbb{C}^{(m)}_{sec}}{\partial \mu^{(m)}_{sec}} : (1-\bar{\mathbb{A}}^{(i)}_{sec}) + \xi\ \frac{\partial \bar{\mathbb{A}}^{(i)}_{sec}}{\partial \mu^{(m)}_{sec}} : (\mathbb{C}^{(i)} - \mathbb{C}^{(m)}_{sec})\right] \\ &= \left[2\mathbb{K} : (1-\bar{\mathbb{A}}^{(i)}_{sec}) + \xi\ \frac{\partial \bar{\mathbb{A}}^{(i)}_{sec}}{\partial \mu^{(m)}_{sec}} : (\mathbb{C}^{(i)} - \mathbb{C}^{(m)}_{sec})\right] \end{aligned} \tag{4.43}$$

In the last expression it has been considered that the constitutive tensor can be expressed as a sum between a volumetric term, which does not depend on the shear modulus, and a deviatoric term, which depends linearly on the secant shear modulus. In order to compute the eqn. (4.43) is necessary to know the derivative of the strain concentration tensor with respect to the secant shear modulus, which can be derived from the definition of the strain localization method (using, for example, the definition given by Mori-Tanaka approach):

$$\begin{aligned}\bar{\mathbb{A}}^{(i)}_{sec} &= \left[\mathbb{I} + (1-\xi)\ \mathbb{S}^{(m)}_{sec}\mathbb{M}^{(m)}_{sec}(\mathbb{C}^{(i)} - \mathbb{C}^{(m)}_{sec})\right]^{-1} \\ \frac{\partial \bar{\mathbb{A}}^{(i)}_{sec}}{\partial \mu^{(m)}_{sec}} &= -(1-\xi)\ \bar{\mathbb{A}}^{(i)}_{sec} : \left\{\left[\frac{\partial \mathbb{S}^{(m)}_{sec}}{\partial \mu^{(m)}_{sec}} : \mathbb{M}^{(m)}_{sec} + \mathbb{S}^{(m)}_{sec} : \frac{\partial \mathbb{M}^{(m)}_{sec}}{\partial \mu^{(m)}_{sec}}\right](\mathbb{C}^{(i)} - \mathbb{C}^{(m)}_{sec}) \right. \\ &\quad \left. - \mathbb{S}^{(m)}_{sec} : \mathbb{M}^{(m)}_{sec} : \frac{\partial \mathbb{C}^{(m)}_{sec}}{\partial \mu^{(m)}_{sec}}\right\} : \bar{\mathbb{A}}^{(i)}_{sec} \end{aligned} \tag{4.44}$$

Rearranging the previous expression:

$$\begin{aligned}\frac{\partial \bar{\mathbb{A}}^{(i)}_{sec}}{\partial \mu^{(m)}_{sec}} &= (1-\xi)\ \bar{\mathbb{A}}^{(i)}_{sec} : \left\{\left[\mathbb{S}^{(m)}_{sec} : \frac{1}{2{\mu^{(m)}_{sec}}^2}\mathbb{K} - \frac{\partial \mathbb{S}^{(m)}_{sec}}{\partial \mu^{(m)}_{sec}} : \mathbb{M}^{(m)}_{sec}\right](\mathbb{C}^{(i)} - \mathbb{C}^{(m)}_{sec}) \right. \\ &\quad \left. + \mathbb{S}^{(m)}_{sec} : \mathbb{M}^{(m)}_{sec} : 2\mathbb{K}\right\} : \bar{\mathbb{A}}^{(i)}_{sec} \end{aligned} \tag{4.45}$$

where the value of the derivative of Eshelby's tensor with respect to the secant shear modulus can be obtained easily by considering the chain rule and the relation between the secant shear modulus and the Poisson's ratio:

$$\frac{\partial \mathbb{S}^{(m)}_{sec}}{\partial \mu^{(m)}_{sec}} = \frac{\partial \nu^{(m)}_{sec}}{\partial \mu^{(m)}_{sec}}\frac{\partial \mathbb{S}^{(m)}_{sec}}{\partial \nu^{(m)}_{sec}} = -\frac{9k^{(m)}}{2(3k^{(m)} + 2\mu^{(m)}_{sec})^2}\frac{\partial \mathbb{S}^{(m)}_{sec}}{\partial \nu^{(m)}_{sec}} \tag{4.46}$$

where the analytical expression for the partial derivatives of Eshelby's tensor with respect to $\nu^{(m)}_{sec}$ can be found in the Appendix A.

4.4.4 Incremental method

The second main procedure to solve the micromechanical model is the incremental method. This approach is based on the constitutive equations written in rate form,

which can be discretized over a time interval $[t_n, t_{n+1}]$ as follows:

$$\Delta\boldsymbol{\varepsilon}^{(i)} = \bar{\mathbb{A}}^{(i)}(t_{n+\alpha})\Delta\bar{\boldsymbol{\varepsilon}}, \qquad t_{n+\alpha} = (1-\alpha)\ t_n + \alpha\ t_{n+1}, \quad \alpha \in]0,1] \tag{4.47}$$

where a generalized mid-point rule is used. Explicit and implicit integrations correspond to $\alpha = 0$ and $\alpha > 0$, respectively, with special cases: $\alpha = 1$(backward Euler) and $\alpha = 1/2$ (mid-point rule). Input data are the state of deformation at the beginning of a time step and the prescribed increment of macrostrain at the time step, as well as the per-phase history variables at t_n. The numerical implementation of the incremental approach is more complex since it involves calling two different constitutive models (elastic for the inclusions and J_2 elastoplastic for the matrix) and dealing with the anisotropic algorithmic tangent constitutive tensor. The step-by step incremental procedure that has been coded using Matlab© is described in the following lines of pseudo-code:

- Input data: ξ, Material parameters ($E^{(m)}, \nu^{(m)}, E^{(i)}, \nu^{(i)}$, hardening parameters, ...) and $\boldsymbol{\varepsilon}$.
- Inizialization: $\Delta\boldsymbol{\varepsilon} = \boldsymbol{\varepsilon}_{n+1} - \boldsymbol{\varepsilon}_n$; $\Delta\boldsymbol{\varepsilon}_\mu^{(i)} \leftarrow \Delta\boldsymbol{\varepsilon}$
- Iterations: while $Error > TOL$ (index for the iteration counter omitted for simplicity).
  1. Computing the constitutive tensors for the inclusions using the elastic properties of the material and the stress tensor:

     $\mathbb{C}_{n+1}^{(i)}, \mathbb{M}_{n+1}^{(i)} \leftarrow E^{(i)}, \nu^{(i)}$.
     $\boldsymbol{\varepsilon}_{\mu\ n+1}^{(i)} = \boldsymbol{\varepsilon}_{\mu\ n}^{(i)} + \Delta\boldsymbol{\varepsilon}_\mu^{(i)}$.
     $\boldsymbol{\sigma}_{\mu\ n+1}^{(i)} = \boldsymbol{\sigma}_{\mu\ n}^{(i)} + \mathbb{C}^{(i)} : \Delta\boldsymbol{\varepsilon}_\mu^{(i)}$.

  2. Compute the increment of average strain in matrix phase:

     $$\Delta\boldsymbol{\varepsilon}_\mu^{(m)} = \frac{\boldsymbol{\varepsilon} - \xi\ \Delta\boldsymbol{\varepsilon}_\mu^{(i)}}{1-\xi}$$

  3. Call the implemented code with the J_2 plastic model. Input data are $\Delta\boldsymbol{\varepsilon}_\mu^{(m)}$, $\boldsymbol{\varepsilon}_{\mu\ n}^{(m)}$ and ψ_n. The program gives the value for the algorithm (consistent) constitutive tensors: $\mathbb{C}_{alg,n+1}^{(m)}$ and $\mathbb{M}_{alg,n+1}^{(m)}$.
  4. Computing the values for the constitutive tensors at time $t_{n+\alpha}$:

     $$\mathbb{C}_{alg,n+\alpha}^{(m)} = (1-\alpha)\mathbb{C}_{alg,n}^{(m)} + \alpha\mathbb{C}_{alg,n+1}^{(m)}; \qquad \alpha \in]0,1]$$

  5. Projecting the algorithm constitutive tensor onto the subspace of isotropic tangent operators: $\mathbb{C}_{iso,n+1}^{(m)}$.
  6. Computing the Eshelby tensor with the isotropic constitutive tensor:
     $\mathbb{S}_{n+1}^{(m)} \leftarrow \nu_{n+1}^{(m)} \leftarrow (\mathbb{C}_{iso,n+1}^{(m)})$.
  7. Compute the strain concentration tensors:
     $\bar{\mathbb{A}}_{n+\alpha}^{(m)}, \bar{\mathbb{B}}_{n+\alpha}^{(m)}, \bar{\mathbb{A}}_{n+\alpha}^{(i)}, \bar{\mathbb{B}}_{n+\alpha}^{(i)} \leftarrow \mathbb{C}_{n+\alpha}^{(m)}, \mathbb{M}_{n+\alpha}^{(m)}, \mathbb{C}^{(i)}, \mathbb{M}^{(i)}, \mathbb{S}_{n+1}^{(m)}$
  8. Check the compability of average strain in inclusions phase by computing the error:
     $Error = ||\bar{\mathbb{A}}_{n+\alpha}^{(i)} : \Delta\boldsymbol{\varepsilon} - \Delta\boldsymbol{\varepsilon}_\mu^{(i)}||$
  9. If $Error \leq TOL$, then exit the loop.

10. Else: new iteration with a new value $\Delta\boldsymbol{\varepsilon}_{\mu}^{(i)}$:

$$\Delta\boldsymbol{\varepsilon}_{\mu}^{(i)} \leftarrow \Delta\boldsymbol{\varepsilon}_{\mu}^{(i)} + \zeta \cdot Error \qquad \zeta \in]0,1].$$

- After convergence, compute the effective constitutive tensor and the macrostress increment.

$$\mathbb{C}^{*}_{n+\alpha} = (1-\xi)\ \mathbb{C}^{(m)}_{n+\alpha} : \bar{\mathbb{A}}^{(m)}_{n+\alpha} + \xi\ \mathbb{C}^{(i)}_{n+\alpha} : \bar{\mathbb{A}}^{(i)}_{n+\alpha}.$$
$$\Delta\boldsymbol{\sigma} = \mathbb{C}^{*}_{n+\alpha} : \Delta\boldsymbol{\varepsilon}$$

After describing the main scheme of the code, some remarks have to be done. Firstly, according to Ortiz and Popov [63] the generalized mid-point rule provides first-order accuracy always except for $\alpha = 1/2$, which leads to second-order accuracy. Furthermore, for $\alpha \geq 1/2$ the generalized mid-point rule is unconditionally stable regardless of the considered yield function. As shown in [19], good predictions are obtained with $\alpha = 1/2$ or $\alpha = 2/3$. As commented in 4.3, the elastoplastic consistent tangent operator is used in all the operations except for computing Eshelby's tensor, where an isotropic projection of the tensor is considered. This approximation leads to softer results (avoiding part of the overstiffness predicted using anisotropic tensors) and allows computing $\mathbb{S}^{(m)}$ using analytical expressions, since the closed forms of the Eshelby's tensor only exist for isotropic matrix or transversely isotropic matrix whose anisotropy axis is aligned with the axis of revolution of the spheroid (see [58]).

As it can be observed through the pseudo-code, the program iterates over the average strain increment in the inclusions (it is considered as the main variable). However, the code can be modified easily to iterate over the average strain increment in the matrix phase (the definition of the error should be changed). Another important aspect is the starting assumption, which consists on making equal the composite strain increment and the inclusions strain increment. As it is commented in [19], this procedure "gives a stiff starting response, which is iteratively brought down to the final and the softer solution". Finally, it must be commented that the algorithm is based in a fixed-point iterative procedure, which has been proved (see [17],[18]) that works in a robust and fast manner. Nevertheless, this scheme can be inappropriate for some cases and the development of a Newton-type method is desirable, although it involves very complex equations, as commented in [19].

4.4.5 Output Data

The program provides the values of the stress field at each time step for each of the constituents (microstresses) and for the heterogeneous material (macrostresses). The input file allows selecting different representations to plot the evolution of the stress field both in the matrix phase and in the inhomogeneous material. The user can select among different options in order to obtain the desired results. Three different graphs can be plot with the program: stress-strain diagrams, stress-time diagrams and first invariant-second invariant diagram. The stress representation can be done for all the required components of the stress (and strain) tensor.

4.5 Validation of the Model

Prior to the comparison between methods for solving the micromechanical problem, it is necessary to carry out a validation of the implemented model to ensure that the numerical methods provide correct results. To carry out this task, it has been taken into account some of the research works done by some authors. Specifically, the validation process and the comments made below are based on the work of Doghri and Ouaar [17] and Pierard *et al.* [69]. The results presented in those papers have been digitalized in Matlab© in order to compare the results in the same graphs. In the following sections the results that have been obtained to carry out the validation of the model will be shown, taking into account most of the variables involved in the problem and that can cause some discrepancies when the micromechanical model is implemented.

The example that has been used for the validation of the model corresponds with a metal matrix composite (MMC), specifically an aluminum alloy matrix reinforced with spherical ceramic inclusions of volume fraction ξ, whose value varies and will be indicated specifically on each example. The matrix has the following mechanical properties: $E^{(m)} = 75\ GPa., \nu^{(m)} = 0.3, \sigma_Y = 75\ MPa$, with power-law isotropic hardening ($R(\psi) = A\psi^m$) with $A = 416\ MPa$ and $m = 0.40$. The mechanical properties of the elastic inclusions are: $E^{(i)} = 400\ GPa., \nu^{(i)} = 0.2$.

4.5.1 Validation of the homogenization techniques

As it was commented in the previous sections, the program that has been coded uses the incremental and the secant approach (both first and second order methods) to solve the micromechanical model. Those methods are based on a linearization process using the concept of linear comparison material (LCC), which allows the subsequently use of homogenization techniques for linear elastic materials. Therefore, the first process of the validation consists on contrast the results of the effective properties of the material using different mean-field methods. In this case, different values of the effective Young modulus have been obtained by varying the volume fraction of the inclusions. The first results are shown in the Fig. 4.4: As it can be observed, the predicted values of the effective Young Modulus for the MMC for all the methods coincide with those obtained from [17]. As it can be observed, the values obtained using Voigt and Reuss approaches represent respectively upper and lower bounds for the real solution, although these bounds could be tighter if one uses the Hashin-Shtrikman. On the other side, both Mori-Tanaka and Double-Inclusion methods provide good results and it can be observed how the values given by both methods coincide for low values of volume fraction of the inclusions, as it was expected. However, for higher values of the volume fraction the Double-Inclusion method is preferred for computing the effective properties of the composite.

The homogenization techniques that have been validated through the previous example are the most used in the literature, since they are based in an explicit scheme that is easy to implement and give accurate solution with low computational cost. However, as it was commented in the previous sections, the implementation

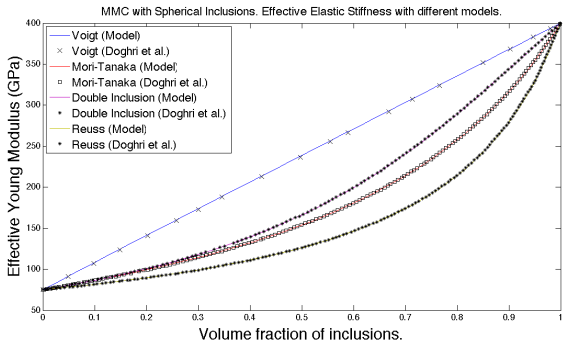

Figure 4.4: Validation of homogenization techniques for predicting the MMC effective Young modulus.

of such methods is trivial and can be done directly without excessive difficulties. On the contrary, more complicated is the implementation of the implicit methods (Classical Self-Consistent Scheme y Differential Scheme) since they require iterative numerical schemes as was shown in section 4.4.2. In order to check the correct implementation of such methods, a new example has been computed. For this particular case it has been modeled a composite formed by an epoxy matrix ($E^{(m)} = 3.5\ GPa., \nu^{(m)} = 0.35$) and glass spherical inclusions $E^{(i)} = 74\ GPa., \nu^{(i)} = 0.2$, like the material studied by Böhm [10].

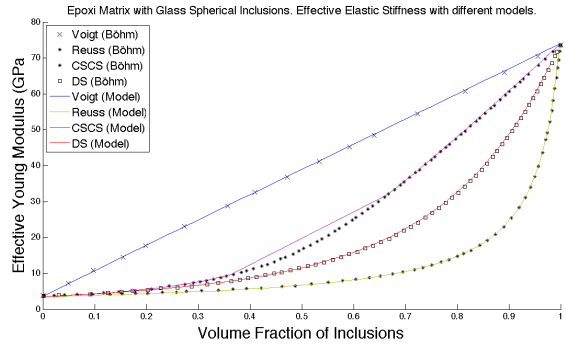

Figure 4.5: Validation of homogenization techniques for predicting the effective Young modulus of a composite with epoxy matrix and glass spherical inclusions.

For this case, it has been also represented the values given using the Voigt and Reuss bounds, in order to show that they always provide upper and lower bounds. The effective Young modulus of the composite obtained using the implemented model coincide with that ones obtained through a digitalization of the results that can be found in [10]. Nevertheless, during the validation it has been found that the self-consistent method becomes unstable for those values of the volume fraction.

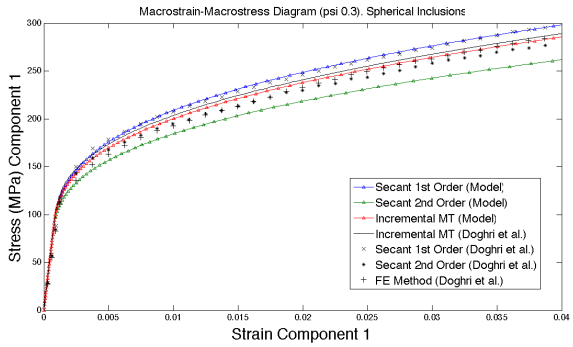

Figure 4.6: Validation of elastoplastic strategies for predicting the behavior of a MMC (Spherical inclusions: $\xi = 30\%$) under macro-tension.

Therefore, there exist some values of the volume fraction of the inclusions where the values of the model do not coincide exactly with the values extracted from the literature (when $\xi \in [0.35, 0.65]$), as it can be observed in Fig. 4.5. The main reason for such behavior is the high value of the ratio $E^{(i)}/E^{(m)}$. In order to obtain the desired results, it has been computed separately those intervals where the method is stable and the critical zone is approximated by a linear function, giving some discordances with respect to the theoretical results. However, it has been proven that the self-consistent scheme provides good results for lower values of the ratio between Young modulus of the constituents.

4.5.2 Validation of the elastoplastic strategies

After checking the Mean-Field Methods for computing the homogenization of the effective properties, the strategies for computing the elastoplastic problem has been also validated. In order to do this, it has been simulated the behavior of the same MMC under a tension test and the results has been compared with those ones obtained by Doghri *et al.* [17] and Segurado *et al.* [79]. In all cases, the homogenization has been performed using the Mori-Tanaka method combined with the three main strategies commented in the current chapter: secant method (first and second order) and incremental method. Fig. 4.6 shows the results obtained imposing macrostresses in the RVE, corresponding to a uniaxial tension test.

The values extracted from the model are very similar to that ones digitalized from [17] and it can be concluded that the problem is correctly implemented. It has to be commented that the validation of the main strategies to model the elastoplastic behavior are based on a *stress driven algorithm*, in order to impose uniaxial tension in an easy way. The code is completely equivalent to those shown in the previous section, but the implementation has been modified in order to adapt the variables to the new input data. This way to impose boundary conditions is not usual since the most of available codes are based on strain driven algorithms, where displacements are imposed on the RVE. In this sense, the FE results obtained by

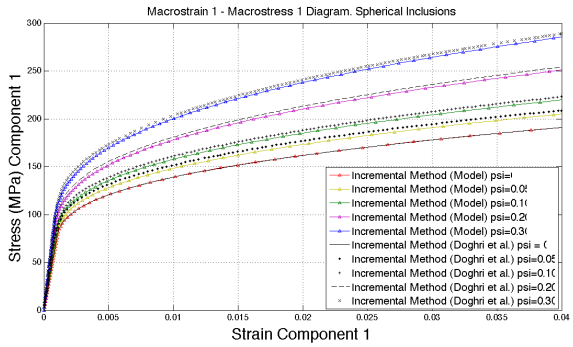

Figure 4.7: Validation of incremental approach for predicting the behavior of a MMC under macro-tension for various volume fraction of inclusions.

Segurado *et al.* are based on a simulation of a tridimensional cube containing 30 spheres, in which the boundary conditions are imposed in terms of displacements. The values of the prescribed displacements are obtained by imposing the values of the stresses in the RVE. This way to impose boundary conditions is not usual in practical simulations, where a multiscale analysis is implemented and both problems (macromechanical and micromechanical) are coupled. However, it has been verified that the theoretical works based on the simulation of an isolated RVE (see [69], [79], ...), where only the micromechanical problem is studied, use the aforementioned boundary conditions to impose loading tests.

Due to the importance of the incremental method, it has been simulated the behavior of the same MMC under uniaxial tensile test, this time using only the incremental approach and varying the values of the volume fraction of the inclusions. Once again, only small differences are appreciated between the values of the model and the reference values from [17], as it is shown in the Fig. 4.7:

As it can be observed, the values for the situation in which only exists matrix material ($\xi = 0$) are exactly the same than the reference ones and it can be concluded that the J_2 elastoplastic model is correctly implemented. In the rest of the cases, the values are very close to the reference solution, but they are not exactly the same. In this sense, it has to be commented that, in general, this methods are very sensitive with respect to the input data and the errors are accumulated in the successive iterations, which leads to some noticeable differences when the value of the plastic strains are large.

In order to conclude the validation of the model it has been carried out another simulation of a MMC, but this time considering ellipsoidal inclusions and a volume fraction of $\xi = 25\%$. This simulation allows checking the different expressions for the Eshelby's tensor, at least for the most common cases. The characteristics of the constituents are exactly the same than on the other cases. The results can be observed in Fig. 4.8, where a tensile uniaxial test has been considered and the same stress driven model has been used to compute the results.

In this case, the results obtained using the model are exactly the same that

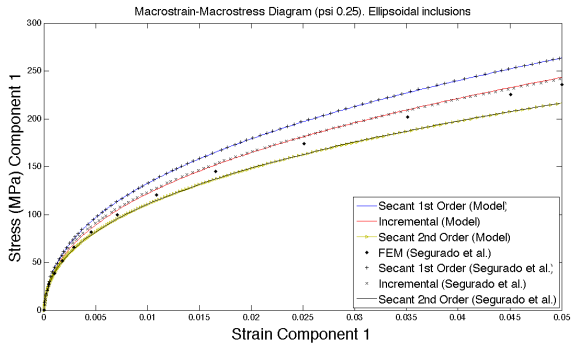

Figure 4.8: Validation of elastoplastic strategies for predicting the behavior of a MMC (Ellipsoidal inclusions: $\xi = 25\%$) under macro-tension. Hardening parameter: $m = 0.40$.

those ones digitalized from [69] and it can be observed that the values provided by the incremental method are the closest ones with respect to the "exact" results provided by a FEM simulation. The simulation has been repeated modifying the value of the exponent in the isotropic hardening law (from $m = 0.40$ to $m = 0.05$) and the results can be observed in the Fig. 4.9. Once again, the validation is successful because the values obtained are consistent with those obtained by Pierard *et al.*. However, during the different simulations it has been observed that some numerical problems appear in the results given by the first order secant method when the value of the exponent m grows and the behavior of the matrix is stiffer. This fact only affects to a small region of the results, but should be considered in the following, when a comparison between the different methods will be done.

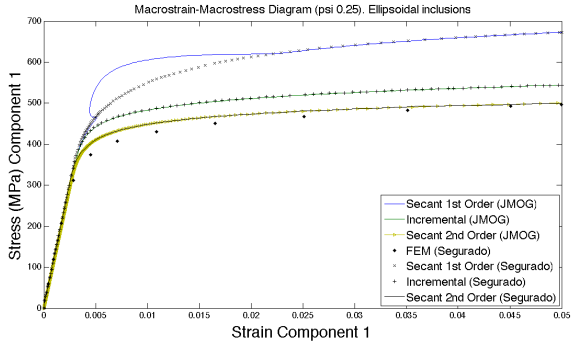

Figure 4.9: Validation of elastoplastic strategies for predicting the behavior of a MMC (Ellipsoidal inclusions: $\xi = 25\%$) under macro-tension. Hardening parameter: $m = 0.05$.

It is considered that the results provided in the current section are enough

to prove the validation of the implemented model. In the following chapters the practical aspects of a Finite Element Implementation will be described and a comparison between analytical and numerical techniques will be described, assuming that the differences between the results obtained with such methods are produced by the limitations of each technique. Therefore, no comments about the differences between the results provided for each technique (secant, incremental and FEM) are given at this point.

Chapter 5

Numerical Simulations

In the previous chapters the theoretical background of such methods has been presented, putting special emphasis in the simplifications and assumptions that are included. A numerical implementation of the most important strategies has been carried out subsequently and the main algorithms and their validation have been already commented. In the current chapter some numerical simulations will be presented in order to compare the accuracy of the Mean-Field homogenization schemes for solving multi-scale problems with respect to the results that are provided using the Finite Element Method. The Finite Element program that has been used to extract the results for each simulation was already implemented. However, some theoretical aspects and numerical aspects will be commented in the first sections, in order to clarify the philosophy of the method when it is applied to multi-scale problems. Finally, some illustrative examples will be presented and the results will be discussed in the last sections.

5.1 F.E.M.: some theoretical background

The Finite Element Method for multi-scale problems is based on the theoretical aspects described in section 2.4. The multi-scale implementation of the Finite Element Method is done by discretizing, firstly, the macro-continuum in finite elements and, for each Gauss point of the "macroscopic" mesh, defining a Representative Volume Element, where the microscopic equilibrium should be determined using in turn the Finite Element Method. This way to compute multi-scale problems is known in literature as FE^2 method and is widely used for solving multi-scale mechanical problems. The continuum RVE equilibrium problem will consist on finding, for a given history of macroscopic strain $\boldsymbol{\varepsilon}(\boldsymbol{x}, t)$ at point $\boldsymbol{x}$ of the macro-continuum, a kinematically admissible microscopic displacement fluctu-

ation $\boldsymbol{u}'_\mu \in \mathscr{V}_\mu$ such that:

$$\mathcal{G}(\boldsymbol{\varepsilon}, \boldsymbol{u}'_\mu, \boldsymbol{\eta}) \equiv \int_{\Omega^s_\mu} \mathscr{F}_y \Big\{ \big[\boldsymbol{\varepsilon}(\boldsymbol{x},t), \nabla^s \boldsymbol{u}'_\mu(\boldsymbol{y},t)\big]^t \Big\} : \nabla^s \boldsymbol{\eta} \; \mathrm{d}V - \int_{\partial\Omega^v_\mu} \boldsymbol{t}^v(\boldsymbol{y},t) \cdot \boldsymbol{\eta} \; \mathrm{d}A = 0 \qquad \forall \boldsymbol{\eta} \in \mathscr{V}_\mu \quad (5.1)$$

where $\mathcal{G}(\boldsymbol{\varepsilon}, \boldsymbol{u}'_\mu, \boldsymbol{\eta})$ is the virtual work functional. Eqn. (5.1) can be discretized with respect to the time variable, obtaining an incremental form of the RVE equilibrium for an interval of interest defined by $[t_0, t_f] = \bigcup_{n=1}^{N} [t_n, t_{n+1}]$, such as:

$$\hat{\mathcal{G}}_{n+1} = \int_{\Omega^s_\mu} \mathscr{F}_y \Big\{ \big[\boldsymbol{\varepsilon}_{n+1}, \nabla^s \boldsymbol{u}'_\mu|_{n+1}\big]^t \Big\} : \nabla^s \boldsymbol{\eta} \; \mathrm{d}V - \int_{\partial\Omega^v_\mu} \boldsymbol{t}^v_{n+1} \cdot \boldsymbol{\eta} \; \mathrm{d}A = 0 \qquad \forall \boldsymbol{\eta} \in \mathscr{V}_\mu \quad (5.2)$$

where $\hat{\mathcal{G}}_{n+1}$ is the incremental virtual work functional at time t_{n+1} and $\boldsymbol{\eta}$ denotes the test function. As it was commented in section 2.4, the value of the microscopic stress tensor will be entirely determined by choosing the form of the functional constitutive relation represented by $\mathscr{F}$. In most of cases, the functional will be established by (phenomenological) incremental constitutive equations, using the microscopic strain tensor $\boldsymbol{\varepsilon}_\mu|_{n+1}$ and a set of microscopic internal variables $\boldsymbol{\xi}_\mu|_{n+1}$ as input data. In this work, only solid materials will be considered and the term related to the contribution of internal tractions due to the presence of pressurized fluids can be eliminated from the previous equation:

$$\hat{\mathcal{G}}_{n+1} = \int_{\Omega^s_\mu} \mathscr{F}_y \Big\{ \big[\boldsymbol{\varepsilon}_{n+1}, \nabla^s \boldsymbol{u}'_\mu|_{n+1}\big]^t \Big\} : \nabla^s \boldsymbol{\eta} \; \mathrm{d}V \qquad \forall \boldsymbol{\eta} \in \mathscr{V}_\mu \quad (5.3)$$

At this point, the finite element discretization can be introduced in the model, looking for the form of the last equation in the finite dimensional space defined by $\mathscr{V}^h_\mu \subset \mathscr{V}_\mu$ and spanned by linearly independent functions $\{N_1, N_2, \ldots, N_n\}$ (n is the number of nodes corresponding to the discretization of the RVE). The projection of the continuum variables $\boldsymbol{u}'_\mu$ and $\boldsymbol{\eta}$ is carried out through a linear combination of the basis functions:

$$\boldsymbol{u}'^h_\mu = \sum_{I=1}^{n} \hat{\boldsymbol{u}}'^h_{\mu,I} N_I(\boldsymbol{y}) \quad (5.4)$$

$$\boldsymbol{\eta}^h = \sum_{I=1}^{n} \hat{\boldsymbol{\eta}}^h_I N_I(\boldsymbol{y}) \quad (5.5)$$

Inserting (5.4,5.5) in (5.3) and considering the arbitrariness of the coefficients $\hat{\boldsymbol{\eta}}^h_I$ an expression for the $i-th$ component of the residual at the $I-th$ node is obtained:

$$R_{iI} = \int_{\Omega^s_\mu} \frac{\partial N_I}{\partial y_j} (\boldsymbol{\sigma}_\mu)_{ji} \; \mathrm{d}\Omega \quad (5.6)$$

In the last expression the functional $\mathscr{F}$ have been substituted by $\boldsymbol{\sigma}_\mu$ just for clarity. Introducing the so-called "$\boldsymbol{B}$-matrix" connecting strain tensor and nodal displacements in (5.6) and expressing the result in Voigt notation, the following expression for the residual is obtained:

$$R_{iI} = \int_{\Omega^s_\mu} \boldsymbol{B}^T \{\boldsymbol{\sigma}_\mu\} \, \mathrm{d}\Omega \tag{5.7}$$

where $\{\boldsymbol{\sigma}_\mu\}$ represents the microscopic stress tensor written in Voigt's notation. Because of the non-linear dependency of the microscopic stress tensor with respect to the nodal displacements, the equation (5.7) must be solved by using a iterative procedure. Considering the classical Newton-Raphson iterative method, the final equation that must be solved to compute the displacements for each time step is given by:

$$\boldsymbol{0} = \{\boldsymbol{R}\}^{(k)} + \{\boldsymbol{K}_\mu\}^{(k)} \left(\left\{ \hat{\boldsymbol{u}}'^h_\mu \right\}^{(k+1)} - \left\{ \hat{\boldsymbol{u}}'^h_\mu \right\}^{(k)} \right) \tag{5.8}$$

where $\boldsymbol{K}_\mu$ denotes the tangent stiffness matrix, which is given by:

$$\{\boldsymbol{K}_\mu\} = \int_{\Omega^s_\mu} \{\boldsymbol{B}^T\}\{\boldsymbol{C}_\mu\}\{\boldsymbol{B}\} \, \mathrm{d}\Omega \tag{5.9}$$

where $\boldsymbol{C}_\mu$ is the *algorithmic tangent operator* consistent with the microscopic incremental constitutive law. The expression for $\boldsymbol{C}_\mu$ is obtained by considering the directional derivative of the constitutive functional for each constituent. However, more interesting is to consider the definition of the *homogenized tangent constitutive operator* $\boldsymbol{C}$. As stated in [86], $\boldsymbol{C}$ is a *"fourth order tensor that expresses the tangential relationship between the macroscopic stress and macroscopic strain tensor at t_{n+1}, consistently with the homogenized incremental form of the constitutive function"*, given by:

$$\boldsymbol{\sigma}(\boldsymbol{\varepsilon}_{n+1}, \bar{\boldsymbol{\xi}}_{n+1}) \equiv \frac{1}{V_\mu} \int_{\Omega^s_\mu} \boldsymbol{\sigma}_\mu(\boldsymbol{\varepsilon}_{n+1}, \nabla^s \boldsymbol{u}'_\mu|_{n+1}, \boldsymbol{\xi}_\mu|_{n+1}) \, \mathrm{d}V \tag{5.10}$$

The analytical expression for the homogenized tangent operator can be derived by considering the directional derivative of the *homogenized constitutive functional* over the RVE. It can be proved (see [86]), that the expression for the algorithmic tangent operator considering the time discretization is given by:

$$\begin{aligned} \boldsymbol{C} &= \boldsymbol{C}_{Taylor} + \boldsymbol{C}' \\ &= \left[\frac{1}{V_\mu} \int_{\Omega^s_\mu} \boldsymbol{C}_\mu \, \mathrm{d}V \right] + \left[\frac{1}{V_\mu} \int_{\Omega^s_\mu} (\boldsymbol{C}_\mu)_{ijpq} (\Delta \boldsymbol{u}')_{pq} \, \mathrm{d}V \right] \boldsymbol{e}_i \otimes \boldsymbol{e}_j \otimes \boldsymbol{e}_k \otimes \boldsymbol{e}_l \end{aligned} \tag{5.11}$$

As it can be observed in eqn. (5.11), the homogenized tangent operator is the sum of two different terms: one term, known as the *Taylor contribution*[1], which corresponds with the volume average of the microscopic constitutive tangent operator

[1] The name for this term is given because it corresponds with the expression of the homogenized tangent operator under Taylor assumption ($\mathscr{V}_\mu = \{\boldsymbol{0}\}$).

and a second term, known as *Tangential fluctuation contribution*, which depends on the choice of the space $\mathscr{V}_\mu$. As it can be observed through the aforementioned expressions, for the multi-scale problem solved through a computational homogenization technique no explicit assumptions are required associated to the macroscopic local constitutive response at the macroscale, since it is derived from the equilibrium boundary value problem associated to each RVE. There exist various ways to compute the value of the homogenized tangent operator in the practice, as indicated in [44], like , for instance, a direct numerical differentiation of the macroscopic stress-strain relation using a forward difference approximation or using a condensation of the constrained degrees of freedom.

5.2 F.E.M.: computational aspects

Prior to start with the comparison of the results, some of the features related to the Finite Element program used to compare results will be given in the current section. The program has been developed using the theoretical concepts described in the previous sections and allows solving the boundary value problem associated with the equilibrium of the Representative Volume Element[2]. The input data of the program is implemented using the software $GiD^{©}$, where the user should introduce the geometry of the RVE and create the mesh using quadrilateral elements (see Fig. 5.1). The program $GiD^{©}$ creates a file containing the relevant information in order to define the boundary value problem, which is used by the solver in order to provide the solution of the problem. The numerical implementation of the Finite Element Method has been done using the program $Matlab^{©}$. In this case, the user indicates the name of the file containing the geometrical description of the RVE and provides the imposed macrostrain history. The program solves the equilibrium at each step considering periodic boundary conditions (the boundary conditions are automatically generated by the program) and provides some figures that give information about the results of the homogenization problem (macrostresses, equivalent plastic strain, ...), which can be used to compare the accuracy of the mean-field methods described in chapter 4. Additionally, the program also provides the distribution of the stress and strain fields over the entire domain of the RVE, which will give important information about the behavior of the inhomogeneous material in the microscopic level. This results can be visualized using the post-processing tool of the program $GiD^{©}$ (see Fig. 5.2), since the numerical solver creates automatically the corresponding files containing the aforementioned information.

Perhaps one of the most important aspects of the implementation for a such Finite Element program is the definition of an RVE. As it was commented in the section 2.3, fixing the characteristics of a Representative Volume Element is not an easy task since the volume must be large enough to be considered as *statistically homogeneous*, but small enough to fulfill the requirement of the separation of scales and to lead to comprehensible computational costs. This issue has been

[2]This program has been created in CIMNE and its implementation was outside the scope of the current work.

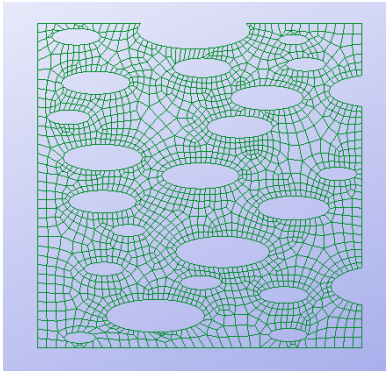

Figure 5.1: Example of input geometrical description of a unit cell using the problem type of the GiD.

extensively treated in different works and some rules are given in order to generate statistically homogeneous microstructures. In this particular work, where only ellipsoidal inclusions will be considered, it has been taken into account the work of Pierard *et al.* [69]. The distribution of ellipsoids is generated by using a program implemented in *Matlab*©: for a given value of the size of the RVE, the user defines the eccentricity of the ellipsoidal inclusions and the range of the values for the major axis of the inclusions. The program generates a random distribution of the ellipsoids in such a way that the position for each ellipsoidal inclusion fulfills some geometrical restrictions (minimum distance between inclusions, distance between inclusions and boundary of the RVE, ...). The program evaluates the position for each inclusion using an iterative process, known as *Random Sequential Adsorption Algorithm* (see [69]), and it stops when the value of the prescribed volume fraction for the inclusions is reached.

As it was commented previously, the program uses periodic boundary conditions on the RVE in order to prescribe the kinematically admissible set of displacements fluctuations. The boundary conditions are automatically generated along the boundary of the RVE by the solver program, using as input data the prescribed value for the macroscopic strain history. In the last years the definition of the prescribed boundary conditions on the microstructural BVP has been widely discussed. Some authors (see, for instance, Segurado and Llorca [79]) have demonstrated that better approximations to the effective composite properties are obtained if periodic boundary conditions are applied on the RVE[3]. Moreover, the use of periodic boundary conditions and the assumption of periodic microstructure lead to the concept of *Representative Unit Cell*. The assumption of periodic microstructure is widely used in the computational homogenization approach since it leads to smaller representative microstructures and, in consequence, less computa-

[3]The consideration of such periodic boundary conditions requires modifying the RVE generation algorithm, due to the fact that the presence of identical inclusions in each pair of the RVE boundary faces has to be ensured.

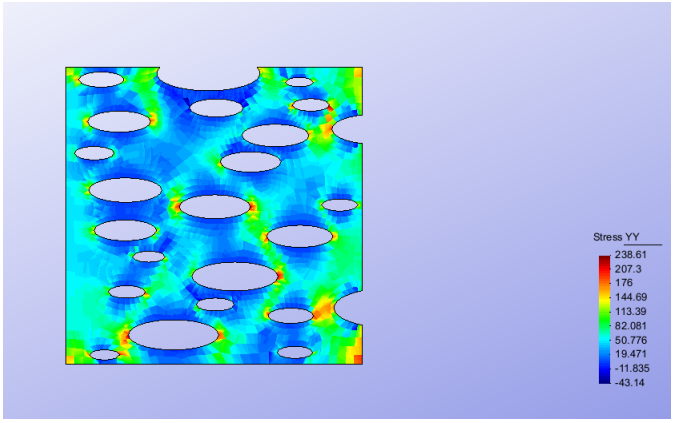

Figure 5.2: Example of output values for the distribution of the component over the RVE σ_{yy} for a porous material.

tional cost. The assumption of periodic microstructures is not very restrictive if one considers that, for a multi-scale problem, a unit cell is defined in every Gauss point of the macroscopic mesh. Therefore, the periodicity is only considered in the vicinity of each macroscopic point, i.e., only a local periodicity is assumed, which is not a very strong assumption in the case of usual Finite Element models. Some interesting notes about the differences between a RVE and a RUC for practical applications are given in the work of Pindera *et al.* [70].

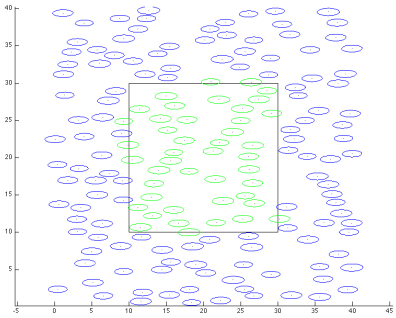

Figure 5.3: Generation of a RVE using the implemented program to create random positions for the inclusions.

5.3 Numerical Simulations: comparison of results

In the current work, numerous simulations have been carried out to try to check the range of validity of the analytical methods of mean field in the macroscopic response of different composite materials. The comparative study comprises the analysis of some factors that can be decisive in the accuracy of results. The qualitative influence of such factors, such as the volume fraction of the inclusions or the ratio between the properties of materials, has been commented on the previous chapters. However, some quantitative results are necessary to state the goodness of mean-field analysis, in order to determine the validity of such methods in the initial stages prior to the determination of the macroscopic behavior of composite materials.

The comparative study of this work is restricted to a 2D-case, corresponding to a plane-strain problem where only four components of the macro-stress tensor have to be computed. The study could be extended to a 3D problem since the implemented program is designed to deal with such problems and the plane-strain case could be viewed as a particular case. This limitation is due to the fact that the available FE program is only prepared to manage this kind of problems. However, in the current work it has been considered that the comparative study of 2D models is sufficient to obtain some useful conclusions about the accuracy of the Mean-Field homogenization methods.

5.3.1 Previous verifications

The first examples that have been carried out correspond to extreme cases from the point of view of the distribution of materials, i.e., the cases when the composite material consists only of a single phase. These cases have been implemented in order to verify the accuracy of the method in the simplest cases, i.e., when the composite is constituted only by a single material. The example that has been used for the previous verifications of the implemented program corresponds to a metal matrix composite (MMC), specifically an aluminum alloy matrix reinforced with elliptical ceramic inclusions. The matrix has the following mechanical properties: $E^{(m)} = 75\ GPa., \nu^{(m)} = 0.3, \sigma_Y = 75\ MPa$, with exponential-law isotropic hardening ($R(\psi) = \theta\bar{H}\psi + (\bar{K}_\infty - \bar{K}_0)[1 - \mathrm{e}^{-\delta\psi}]$) with $\theta = 1$, $\bar{H} = 5000$, $\bar{K}_\infty = 100$, $\bar{K}_0 = 75$ and $\delta = 2500$. The mechanical properties of the elastic inclusions are: $E^{(i)} = 400\ GPa., \nu^{(i)} = 0.20$. The Representative Unit Cell that has been chosen for this particular example corresponds with a 20x20 mm. square of a uniform material.

The microgeometry is subjected to an imposed uniaxial cyclic macro-strain, whose maximum value corresponds to a level of macro-strains in the direction 1 equal to $6.25 \cdot 10^{-3}$. The imposed macro-strain is showed in the Fig. 5.4, where the four different components of the macro-strain tensor (input data) are shown. The problem has been solved using a Finite Element Procedure and selecting two different sets of kinematically admissible displacement fluctuations. The models that have been considered are a Periodic Boundary Displacement Fluctuations Model and an Homogeneous Micro-Cell strain model (concretely the so-called *Rule of Mixtures*, see 2.4.7). These two models are compared with an analytical approach using

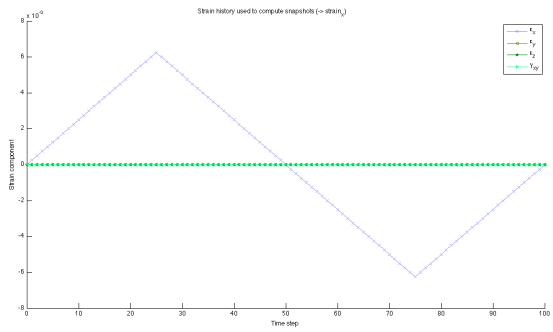

Figure 5.4: Cyclic uniaxial macro-strain imposed in the microgeometry to carry out the previous verifications.

Mori-Tanaka, since this is the most extended technique for solving problems using Mean-Field methods. For this particular case, where the loading path is cyclic, it can be only considered an incremental approach for solving the elastoplastic problem. In Fig. 5.5 can be observed the strain-stress diagram corresponding to the first components of the macro-strain and macro-stress: As it can be observed in

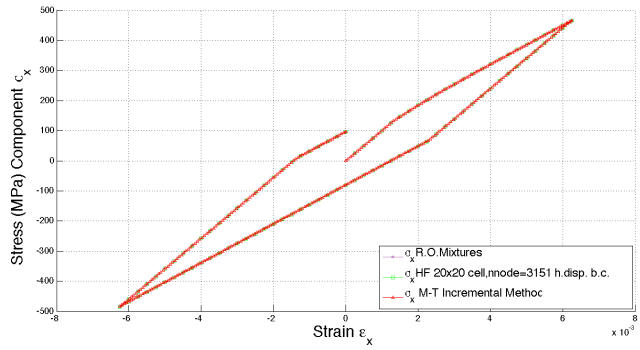

Figure 5.5: MMC ($\xi = 0$) under uniaxial cyclic macro-strain. Comparison of the results obtained for the first component of the macro-stresses ($\varepsilon_x - \sigma_x$).

the Fig 5.5, the three different methods provide exactly the same results, which coincide with the response of a composite material that it is only formed by a metal matrix. The figure shows an initial elastic path until a level of stress of 120 MPa, followed by an exponential hardening path that reaches a maximum level of stress of approximately 480 MPa, corresponding with the maximum level of imposed macro-strain. When the material reaches the maximum strain, the stresses descend following again the elastic path until reaching a value of 60 MPa, from which again it shows a new nonlinear behavior characterized by a hardening law, which is extended until reaching the minimum value of the imposed macro-strain.

The minimum value of the stresses in this situation is approximately 490 MPa. The material is loaded again with increasing increments of the macro-strain, showing an elastic behavior. Finally, when the level of stresses is almost zero, the material behavior is inelastic until reaching the final value of the imposed macro-strain, showing a final value of the stress equal to 100 MPa for a null value of the imposed strains.

Figs. 5.6 and 5.7 show the strain-stress diagram for the second and third components of the stress tensor. As it can be observed, again the predictions of the three models are exactly the same. The other two components of the stress tensor show a similar behavior, although the hardening path differs from the observed in the previous case. In this particular case, the final value of the stresses in the directions y and z are approximately -50 MPa, which was expected taking into account that the material is stretched only in the x direction. The fourth component of

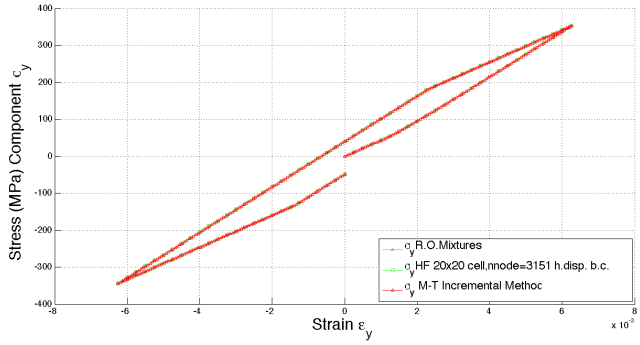

Figure 5.6: MMC ($\xi = 0$) under uniaxial cyclic macro-strain. Comparison of the results obtained for the second component of the macro-stresses ($\varepsilon_x - \sigma_y$).

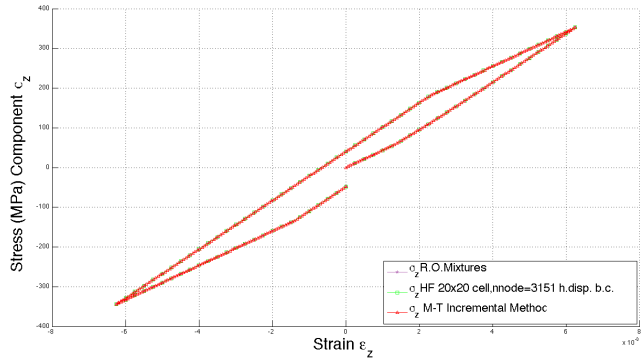

Figure 5.7: MMC ($\xi = 0$) under uniaxial cyclic macro-strain. Comparison of the results obtained for the third component of the macro-stresses ($\varepsilon_x - \sigma_z$).

the stress tensor (τ_{xy}), according to the assumption of plane strain and an imposed macro-strain only in the first direction, is equal to zero in the case of an isotropic material. Therefore, the results regarding this component will not be shown in the current work.

Similarly an analysis was made of the composite material, this time consisting of a single material whose characteristics coincide with the elastic material of the inclusions. It is expected to obtain a pure elastic behavior of the material, for that reason not all the results will be provided in the current work. In the following figure it can be observed the strain-stress curve for the first components of both tensors. As it was expected, the diagram shows a straight line whose slope coincides with the value of the Young modulus of the material ($E^{(i)} = 400\ GPa.$).

The three methods provide exactly the same results, characterized by a maximum value of approximately 2800 MPa and a minimum value of -2800 MPa. In this case, the observed behavior in the fourth component of the stress tensor is similar to the previous case, where some negligible values of the shear stress appear in the results of the Periodic Boundary Displacement Fluctuations Model.

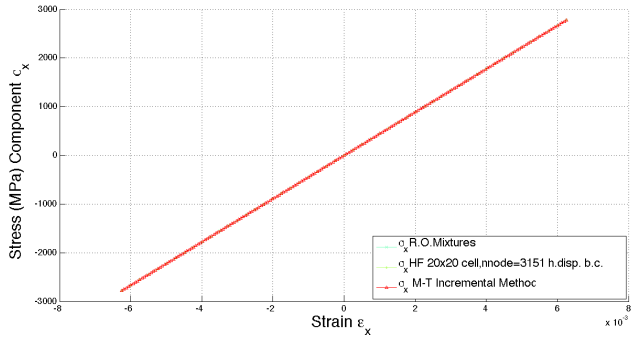

Figure 5.8: MMC ($\xi = 1$) under uniaxial cyclic macro-strain. Comparison of the results obtained for the first component of the macro-stresses ($\varepsilon_x - \sigma_x$).

The programs also provide some information that can be very useful in the case of more complicated examples. For instance, the representation of the two first invariants gives some important information about the inelastic behavior of the material. Figs. 5.9 and 5.10 show the representation of the two first invariants for the previous examples. The graphics show the inelastic behavior of the metal matrix and the pure elastic behavior of the inclusions and coincide in the three different methods. It is expected that a "real" MMC, i.e., a MMC with values of the volume fraction of the inclusions between 0 and 1, may show a behavior that will lay between this two "extreme" situations.

For these particular cases, the representation of the accumulated plastic strains with respect the time also can be a good indicator about the differences between solving the problem using a Mean-Field method or a Finite Element Approach. The Mean-Field method, as it has been commented during the current work, pro-

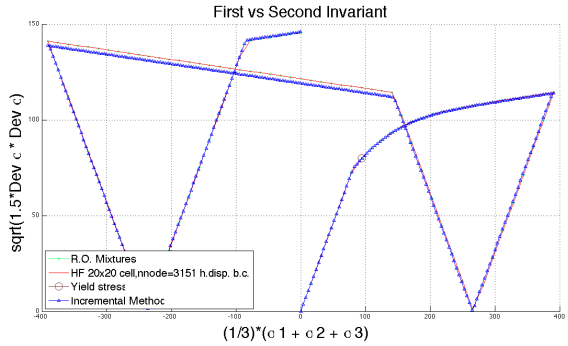

Figure 5.9: MMC ($\xi = 0$) under uniaxial cyclic macro-strain.Representation of the two first invariants.

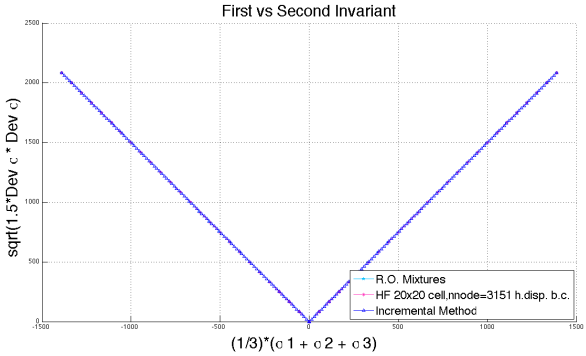

Figure 5.10: MMC ($\xi = 1$) under uniaxial cyclic macro-strain.Representation of the two first invariants.

vides information about the mean behavior of the microstructure, while the Finite Element approach allows solving the distribution of the plastic strains on the entire RCU, which will depend on several factors like the distribution and shape of inclusions, for instance. Therefore, a significant difference in the results obtained in the representation of the accumulated plastic strain will be associated with the concentration of plastic strains in some elements, which will lead to significant differences in the results provided by the different methods. In this particular case, the material that has been studied is homogeneous and, as it is shown in the Figs. 5.11 and 5.12, the results using both methods (Mean-Field Approach and Finite Element Approach) coincide. Nevertheless, the Finite Element program does not provide the volume average response for the accumulated plastic strain and the accumulated plastic strain may not be compared for the rest of the examples.

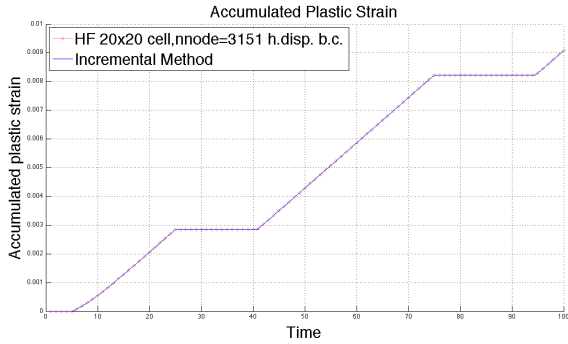

Figure 5.11: MMC ($\xi = 0$) under uniaxial cyclic macro-strain.Representation of the accumulated plastic strain.

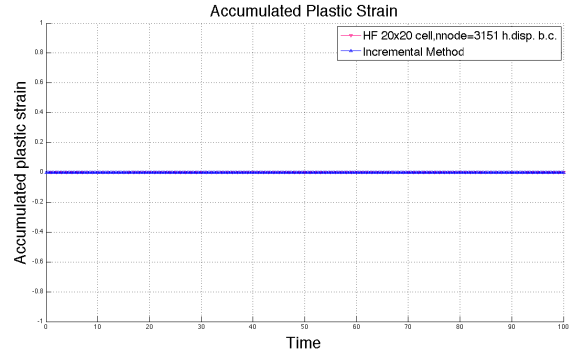

Figure 5.12: MMC ($\xi = 1$) under uniaxial cyclic macro-strain.Representation of the accumulated plastic strain.

5.3.2 Influence of the material

The previous examples have been presented in order to observe the behavior of the different methods in such cases in which the macroscopic behavior of the material is given by the characteristics of a single phase. In this section the results obtained with the different homogenization methods using different mechanical properties of the constituent materials are analyzed. To do this, three different materials have been modeling: firstly, a metal matrix composite with ceramic inclusions, secondly, an epoxy matrix composite reinforced with E-glass inclusions and, finally, a porous metal matrix composite. The choice of the different properties of the materials has been done in order to observe the differences in the results when the stiffness ratio (defined as the ratio of the Young modulus of the two constituents) is increased. The following table shows the different properties that has been considered for each material.

Three different arrangements have been used for each material, in order to

	Matrix								Inclusions		Ratio
	Young	Poisson	Yield	HardeningParameters					Young	Poisson	$E^{(i)}/$
	$E^{(m)}$	$\mu^{(m)}$	σ_Y	θ	$\bar{H}$	$\bar{K}_\infty$	$\bar{K}_0$	δ	$E^{(i)}$	$\mu^{(i)}$	$E^{(m)}$
MMC	$75 \cdot 10^3$	0.3	75	1	5000	100	75	2500	$400 \cdot 10^3$	0.2	5.333
EMC	$3.5 \cdot 10^3$	0.35	25	1	500	10	7.5	250	$74 \cdot 10^3$	0.2	21.14
Porous	$75 \cdot 10^3$	0.3	75	1	5000	100	75	2500	$--$	$--$	∞

Table 5.1: Properties of the different materials use in the analysis. The units for the stress-like variables are MPa.

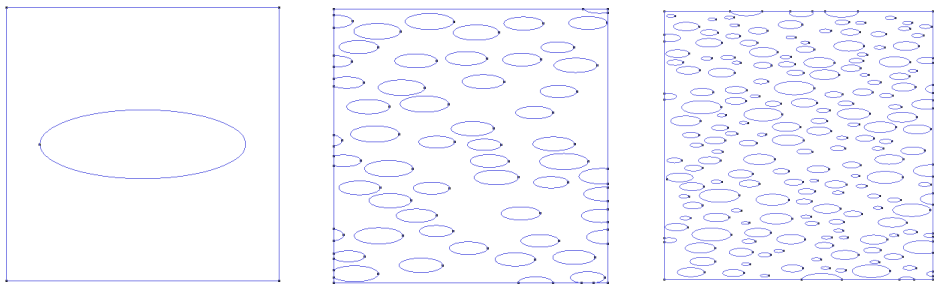

Table 5.2: Different arrangements used to model the different composites.

observe the predictions of the results when the distribution, number and size of inclusions vary. The aspect of each of the modeled microstructures can be observed in the Fig. 5.2, corresponding to a square 20x20 mm. domain. The first geometry corresponds with a RCU that contains only one elliptical inclusion centered in the cell. The volume fraction in this first case is 0.15 and the aspect ratio of the axis is 1/3. The second domain used in this analysis corresponds to a microgeometry formed by 54 elliptical inclusions whose aspect ratio equal to 1/3. In this case the size of each ellipse is almost the same and the volume fraction of the inclusions is almost 0.30 (it is difficult to obtain the exact value due to the procedure to generate the Representative Unit Cell. In this case, the exact value for the volume fraction of the inclusions is 0.284178). The last arrangement consists on a RCU composed by a matrix and 182 elliptical inclusions with aspect ratio equal to 1/3. The size of the inclusions changes considerably in the microstructure, but the volume fraction of the inclusions is again 0.30 (the exact value in this case is 0.26989425).

Each material and each microgeometry has been subjected to three different loading paths. The first loading path consists in an elongation in the direction of the main axis of the elliptical inclusions (in the current work, it coincides with the Cartesian "x" axis). The imposed strain trajectory is uniform (see Fig. 5.13) and the maximum value is 0.00625. The second loading path is a uniaxial cyclic elongation/compression test (see Fig. 5.14), coinciding with the loading path that was used in the section 5.3.1. Finally, a biaxial tension test has been applied in order to compare results when more complicated loading paths are involved in the problem. In this case (see Fig. 5.15), the maximum value coincides with the other two cases (0.00625) and the monotonic trajectory is imposed in the two axis in

which the main axis of the elliptical inclusions are defined (in the current work, they coincide with the Cartesian “x” and “y” axes).

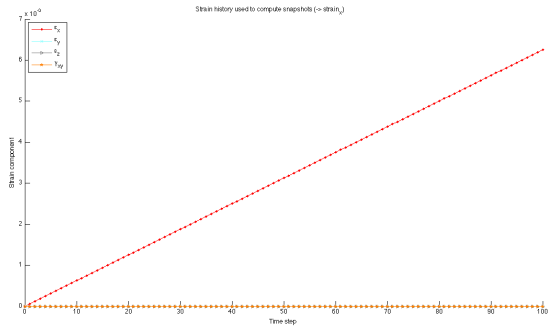

Figure 5.13: Monotonic uniaxial macro-strain imposed in the microgeometry.

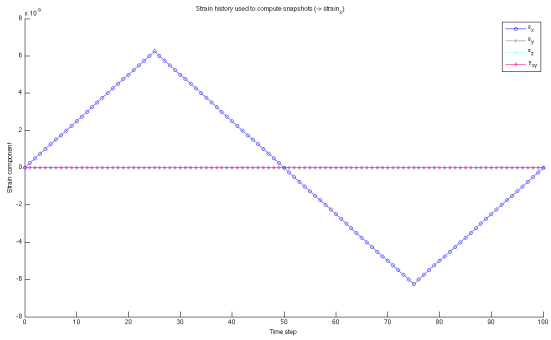

Figure 5.14: Cyclic uniaxial macro-strain imposed in the microgeometry.

The most relevant results for each material will be presented on the following paragraphs. The results are organized following an order in which the stiffness ratio is increased, due to the fact that it is expected a greater divergence of the results when the ratio is increased. Moreover, for each material, the results are shown from the simplest arrangement of the microgeometry (only one inclusion) to the most complex arrangement (with 182 elliptical inclusions). In this case, it is also expected to obtain an increasing number of differences in the results of each model. In all the cases, the results have been computed using a Mean-Field method (Mori-Tanaka) and two different Finite Element models: Periodic Boundary Displacement Fluctuations Model (from now on, *High-Fidelity model*) and Homogeneous Micro-Cell strain model (in the following, designated as *Rule of Mixtures*).

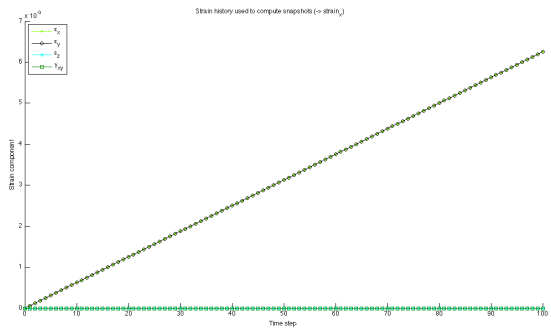

Figure 5.15: Monotonic biaxial macro-strain imposed in the microgeometry.

Material 1: Metal Matrix Composite

Firstly, the results corresponding to the first arrangement will be analyzed. The volume fraction of the inclusions has a value of 0.15 and then it is expected to obtain accurate values using Mean-Field methods (according to different authors, the limit value for the different methods is around 0.30). Theoretically, the first arrangement coincides with the microgeometry in which the mean-field methods are based (according to Eshelby's result, see 3.2) and due to this reason, the analytical expressions may provide the exact solution (at least, in the elastic domain). The number of elements of the Finite Element approaches are given in such a way that the results can be considered as exact. The Fig. 5.16 shows the strain-stress diagram for the first component when the first loading path is applied. The figure shows the high accuracy of the secant method using the first order approach and the incremental method, whose results coincide almost exactly with the results provided by the High Fidelity method. However, the Rule of Mixtures gives a stiffer response of the material, as was mentioned in the previous sections 2.4. In this case, the elastic region of the composite is larger than on the other cases and the final value of the stress in the x-direction is approximately 47% higher than the exact value. On the other hand, the secant method with second order approach provides a softer behavior of the material, if we compare with the exact results. As it can be observed, the yield stress of the composite has a lower value and then the inelastic branch covers a wider region. As it was mentioned before, this method is based on the second order moment to calculate the equivalent plastic strain and it was developed to obtain more accurate results, since it was observed a very rigid response with the conventional methods.

The analytical methods only provide information about the mean value of the different variables, while the Finite Element Approaches give information about the distribution of the different variables in the whole domain of the problem. Hence, as it can be appreciated in the Fig. 5.17, the maximum values for the equivalent plastic strain are concentrated in the two edges of the major axis, i.e., in the interface between the two constituents of the composite material. The concentration of

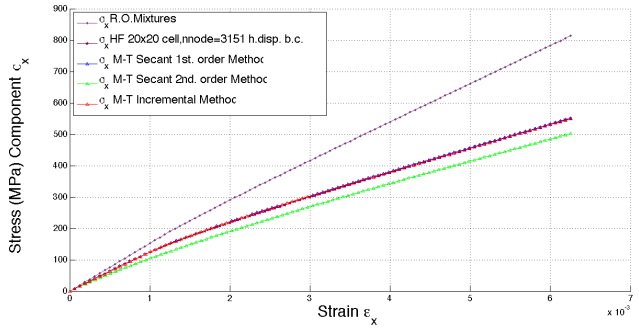

Figure 5.16: MMC ($\xi = 0.15$) under uniaxial monotonic macro-strain. Comparison of the results obtained for the first component of the macro-stresses ($\varepsilon_x - \sigma_x$).

the equivalent strain in such zones of the microgeometry can cause the failure of the material due to the debonding of both phases, which shows the importance of considering the Mean-Field methods only as appropriate to study the general behavior of the material, in a preliminary phase.

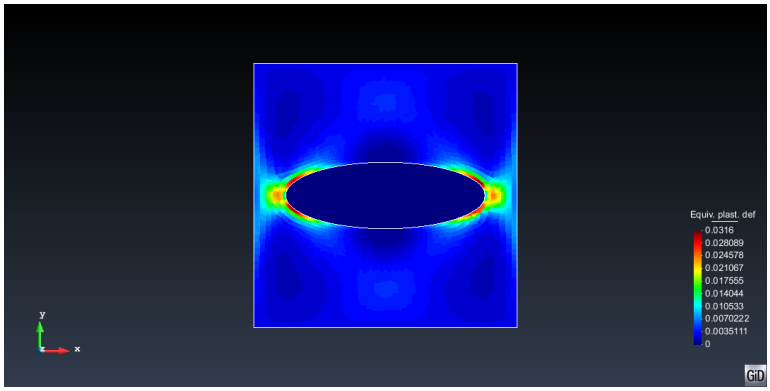

Figure 5.17: MMC ($\xi = 0.15$) under uniaxial monotonic macro-strain. Distribution of the equivalent plastic strain in the microgeometry.

The study of the remaining components of the stress tensor can also provide some useful information about the accuracy of the different methods. In case of the second component, which coincides with the direction of the minor axis of the elliptical inclusion, the Rule of Mixtures gives the best approximation among the simplified models. As it can be observed in the Figure 5.18, the values that are given by the Rule of Mixtures almost coincide with the exact values given by the High Fidelity method, especially for the higher values of the imposed macro-strain. The first order secant method also gives good results and the accuracy in the elastic domain is even better. However, both secant method using a second order approach

and the incremental method show a higher stiffness of the composite material and the accuracy of the results is worse (the maximum error is almost 6%). On the other

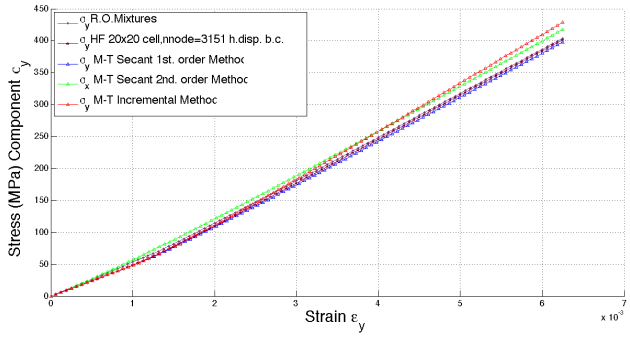

Figure 5.18: MMC ($\xi = 0.15$) under uniaxial monotonic macro-strain. Comparison of the results obtained for the second component of the macro-stresses ($\varepsilon_x - \sigma_y$).

hand, the results obtained for the out-of-plane stress component (corresponding with the assumption of plain strain) are quite accurate. In this case (see Fig. 5.19) the Rule of Mixtures again shows a higher rigidity for the homogenized material and the values of the stresses are overestimated. The higher accuracy in the results is obtained again using the first order secant method, while the incremental method also gives quite good results. The secant method using a second order approach provides a very stiff response of the material, although the final error is only around 5%.

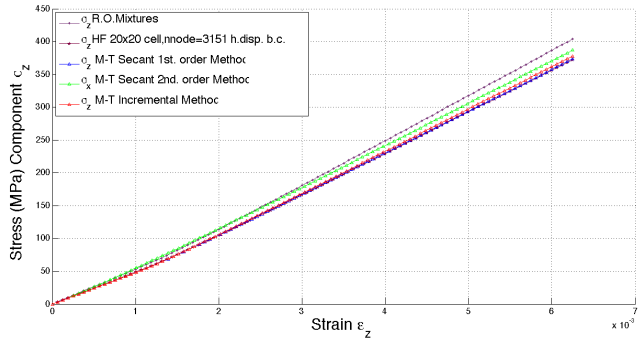

Figure 5.19: MMC ($\xi = 0.15$) under uniaxial monotonic macro-strain. Comparison of the results obtained for the third component of the macro-stresses ($\varepsilon_x - \sigma_z$).

The best results for this first example have been given by using the first order secant method, while the incremental method provides good accuracy, although in some cases the response of the homogeneous material may be very stiff. However, as it was indicated on previous chapters, the incremental method is the unique

approach that can be used for modeling non-uniform loading paths and it is the only alternative that has to be considered in such cases. Figure 5.20 shows the strain-stress diagram that has been obtained when a cyclic strain path is considered. In this particular case, the diagram for the first component of the macro-stresses reveals that the Rule of Mixtures is not a good choice to model a composite material that is subjected to a cyclic load. As occurred in the previous case, the response of the homogenized material is very stiff and the trajectory of the stresses is quite different with respect to the exact results provided by the High Fidelity method. Nevertheless, the incremental method provides a good estimation for the stresses along the entire loading path, although some differences can be observed for the plastic region when the material is compressed. The final value of the stresses is almost the exact value and it can be concluded that the results given by the incremental method are quite accurate.

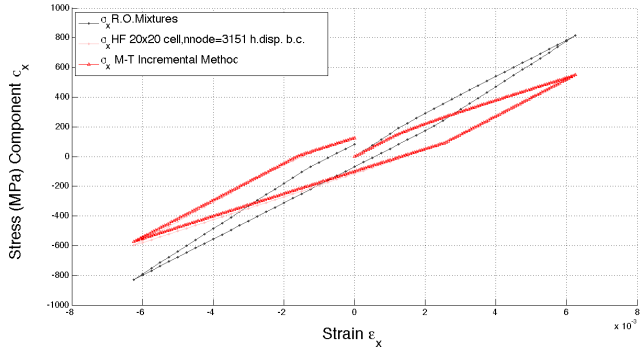

Figure 5.20: MMC ($\xi = 0.15$) under uniaxial cyclic macro-strain. Comparison of the results obtained for the first component of the macro-stresses ($\varepsilon_x - \sigma_x$).

On the other hand, the results for the second component of the macroscopic stress tensor are more accurate when the Rule of Mixtures is considered. As occurred with the monotonic uniaxial strain path, the results obtained using the Rule of Mixtures almost coincide with the exact response of the material. However, the differences between both F.E. approaches start increasing when the increments of the imposed strain become negative. The results using the incremental method, on the other hand, show a stiffer behavior of the composite material, even in the first part of the loading cycle. As it can be observed in the Fig. 5.21, the macrostresses obtained with the analytical method are overestimated, which can be inappropriated in real applications (these results lie out of the safe-side).

The results regarding the out-of-plane component of the macro-stresses are shown in the Fig. 5.22. Once again, the approximated results given by the incremental method are very accurate and it cannot be observed any differences with respect to the exact results. The response using the Rule of Mixtures is more rigid than the real response of the composite, which lead to an overestimation of the out-of-plane macro-stresses.

The conclusions that can be deducted when studying the behavior of the dif-

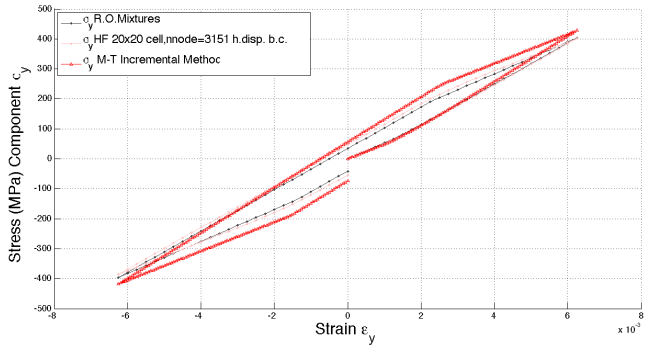

Figure 5.21: MMC ($\xi = 0.15$) under uniaxial cyclic macro-strain. Comparison of the results obtained for the second component of the macro-stresses ($\varepsilon_x - \sigma_y$).

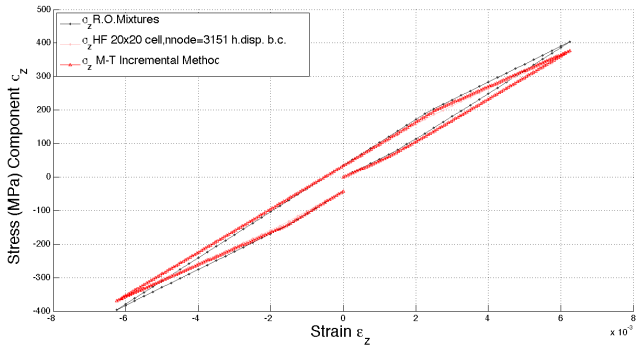

Figure 5.22: MMC ($\xi = 0.15$) under uniaxial cyclic macro-strain. Comparison of the results obtained for the third component of the macro-stresses ($\varepsilon_x - \sigma_z$).

ferent models in the case of a biaxial load are not very different with respect to the previously discussed. In this case, the main differences are obtained in the case of the results regarding with the macrostresses in the direction of the second component. In this case, the secant method provides the most accurate results, being again the first order approach the best approximation among the analytical methods. Nevertheless, the second order approach for the secant method provides better results than the incremental approach, as it can be observed in the Fig. 5.23. The results provided by the incremental approach are more accurate in the elastic region and also for low values of the plastic strain. However, when the plastic strain is increased, the incremental method gives a softer behavior of the composite material, while the response using the secant method with a second order approach for computing the equivalent plastic strain provides more accurate results.

After analyzing the behavior in the simplest case insofar as the microgeometry is concerned, now it is time to compare the results obtained in the case of two complex microgeometries with a value of the volume fraction of inclusions near

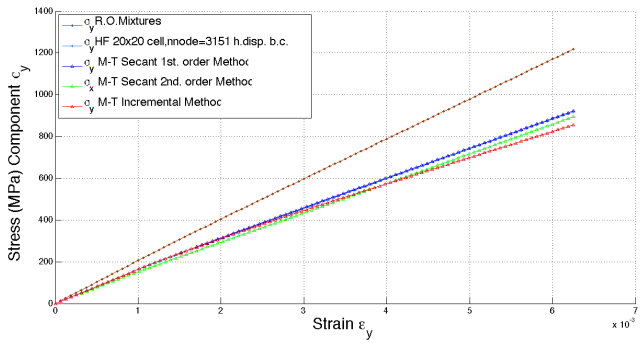

Figure 5.23: MMC ($\xi = 0.15$) under biaxial monotonic macro-strain. Comparison of the results obtained for the second component of the macro-stresses ($\varepsilon_x - \sigma_y$).

the maximum considered as suitable for the use of Mean-Field methods. For these cases, only the most relevant results will be displayed so as to maintain the highest possible conciseness of the text. The first results that will be shown correspond with the samples subjected to a uniaxial monotonic strain trajectory. The conclusions in this case are very similar to those commented before: the volume average for the first component of the macrostress tensor is well modeled by the first order secant method and the incremental method, while the Rule of Mixtures provides a high stiff response of the material and the second order secant method provides a soft behavior of the composite (see Fig 5.24). This tendency changes when the second component of the macrostresses is considered. In this case, the best results are given by the Rule of Mixtures, while the first order secant method provides the best approximation among the analytical methods. The rest of the implemented approaches (incremental method and second order secant method) lead to stiffer response of the homogenized material, giving the incremental method the worst response of the analyzed methods. The out-of-plane stress (macrostress in the z-direction) is perfectly modeled by the first order secant method, while the rest of analytical approximations give accurate results, although the homogenized material shows a stiffer response.

However, the most relevant conclusions when such involved geometries are studied are related with the local distribution of the stresses and strains in the material. As it was described before, the Mean-Field methods do not provide the local distribution over the volume and some relevant information is missed. Nevertheless, the unique variables that are transferred in the macro-scale are those related with the volume-average values. Due to this fact, for practical purposes, it may not be necessary to implement a strategy based on a Finite Element Approach to solve the problem.

The same conclusions as in the previous case can be collected for the case of cyclic loading. For this particular imposed macrostrains, the incremental method provides good results in regard to the volume average for the first and third components of the stress tensor. However, the results for the second component show

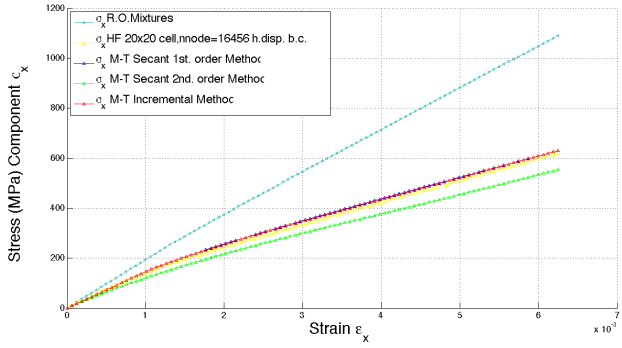

Figure 5.24: MMC ($\xi = 0.2699$) under uniaxial monotonic macro-strain. Comparison of the results obtained for the first component of the macro-stresses ($\varepsilon_x - \sigma_x$).

a stiffer prediction of the incremental method, as occurred in the first microgeometry. The differences between the methods can be better observed through the representation of the first two invariants: as it can be observed in Fig. 5.25, the incremental method gives a good approximation when the level of plastic strains in the microgeometry is low. For increasingly values of the plastic strain, the homogenized material modeled through the incremental method behaves stiffer and the level of stresses that it reaches is higher in comparison with the results provided using the High Fidelity approach. This fact can be seen with great clarity from the moment when the material is unloaded and when the subsequent compression is applied. As it can be appreciated, the divergences of both curves become greater and greater, which can be observed in the present differences regarding the slope of the plastic branch, which changes between both models because it depends directly on the reached level of plastic strain.

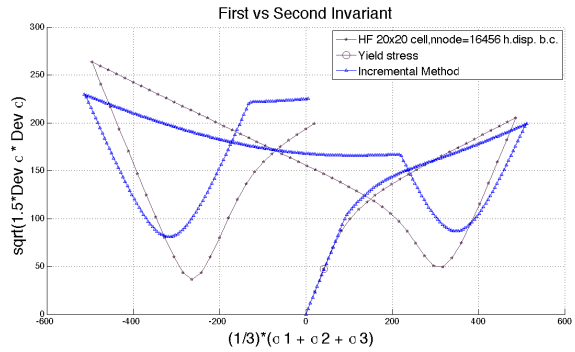

Figure 5.25: MMC ($\xi = 0.2699$) under uniaxial cyclic macro-strain. Representation of the first invariant vs. second invariant.

The Fig. 5.3 shows the number of elements whose level of accumulated plastic

strain is above a given threshold for both previous cases (monotonic and cyclic loading paths). As it can be observed, the curves differ from each other, especially in terms of the number of elements that exceed the highest value of accumulated plastic strain. The number of items that exceed the maximum threshold considered in the study grows, especially during the plastic branch of the unloading process and subsequent compression. This zone of the diagram was, precisely, the part of the diagram where the greatest differences between the different models were observed.

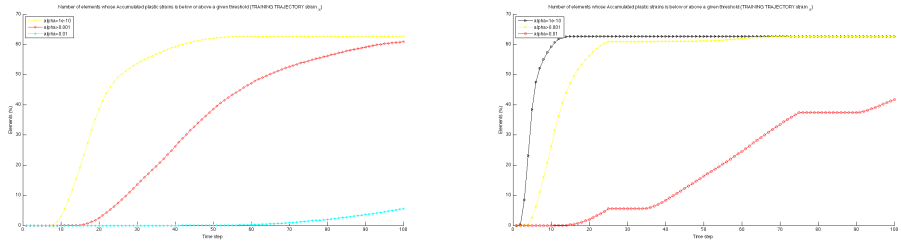

Table 5.3: Comparison between the accumulated plastic strain in the elements for the third microgeometry in the monotonic case (left) and the cyclic case (right).

The last case that will be commented for the first material refers to the case of a biaxial monotonic strain trajectory. For this particular case, the volume average of the macro stresses is very similar in both cases and the same conclusions that were commented for the previous case (only one elliptical inclusion) are valid for both arrangements (see Fig. 5.26). Once again, the better approximation is given by the first order secant method and the incremental method, while the second order secant method provides a much softer response of the material.

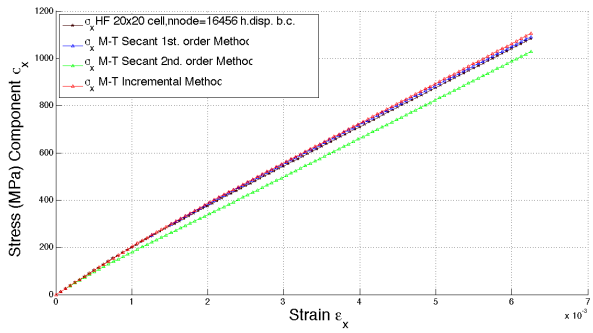

Figure 5.26: MMC ($\xi = 0.2842$) under uniaxial monotonic macro-strain. Comparison of the results obtained for the first component of the macro-stresses ($\varepsilon_x - \sigma_x$).

As occurred with the cyclic loading path, the maximum value of the accumulated plastic strain is different depending on which arrangement is considered.

Although the results cannot be strictly compared due to the fact that the volume fraction of inclusions is not exactly the same, it can be assumed that the values for the volume fraction are close enough to analyze the differences in the values of the accumulated strain. Through the observation of the maximum accumulated plastic strain in both microgeometries, it is possible to observe that the maximum value of the accumulated plastic strain in case of the RCU with less number of inclusions is almost the double that in case of the microgeometry with major number of inclusions. Although the "mean" behavior of both models is the same, these kind of singularities in the microscopic level can lead to important features that should be considered in order to model the response of a composite material, especially when one is looking for optimizing the properties of a new material. Therefore it is very important to choose correctly the arrangement and characteristics of each RCU (or RVE, depending on the model used in the analysis), which has to be equilibrated with the computational effort that is needed to solve the problem: for this particular case, the second arrangement is modeled using a F.E. mesh with 5297 elements, while the third RCE needs 16456 elements. The differences in the number of elements imply high computational costs, since the inelastic problem is a nonlinear problem that should be computed using an iterative process.

Material 2: Epoxy Matrix Composite

In the previous section has been shown the results obtained on the study of a Metal Matrix Composite, which is characterized by a low value of the stiffness ratio. It has been observed that for all three microgeometries the results provided by the different methods are very accurate. In the current section the diagrams for the same arrangements and load cases will be presented, although the material for both the matrix and inclusions has been changed. The properties of the different phases are based on an epoxy matrix composite reinforced with elliptical E-glass inclusions, which results in a higher ratio of the stiffness coefficient. The hardening parameters have also been modified with respect to the previous example. The values for such parameters do not correspond to real values, and the modification responds to the necessity of obtaining some "clear" graphical results.

As it was done for the previous material, the first results that will be commented correspond with the first microgeometry (only one elliptical inclusion), which coincides with the theoretical geometry used by Eshelby to define the theoretical background of the Mean-Field homogenization methods. Fig. 5.27 shows the strain-stress diagram for the first component of the macroscopic stress tensor in the case of a monotonic uniaxial imposed macroscopic strain. In this case it can be observed a higher discrepancy in the results, being the response of the composite material modeled with the analytical methods softer than the real behavior predicted by the High Fidelity method. Another important feature to be considered is the agreement between the results predicted by the first order secant method and the incremental method. The explanation of this fact can be made through the analysis of the accumulated plastic strain. The results obtained in this particular case show how the incremental method and the first order secant method do not predict the appearance of plastic strains in the matrix phase and only the

second order secant method takes into consideration this fact, although the mean value provided by such method is overestimated. As a consequence, the material modeled using Mean-Field approaches (first order secant method and incremental method) does not present any hardening branch and thus the level of macroscopic stresses in the material are lower.

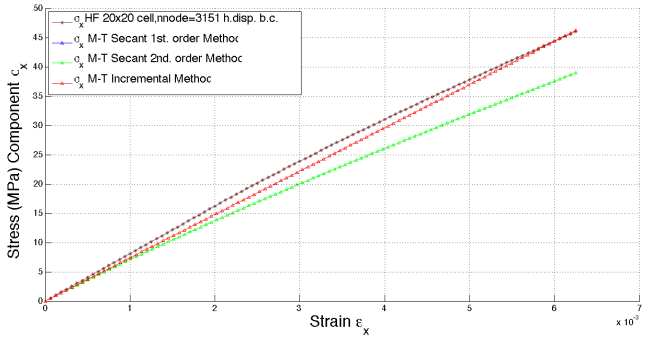

Figure 5.27: MMC ($\xi = 0.15$) under uniaxial monotonic macro-strain. Comparison of the results obtained for the first component of the macro-stresses ($\varepsilon_x - \sigma_x$).

Although in the case of a uniaxial monotonic load the previous considerations do not seem to be very problematic since the obtained results do not differ very much with respect to the theoretical results, in the case of a uniaxial cyclic load the performance of the analytical methods starts showing higher discrepancies (see Fig. 5.28). As it can be deducted from the results, the analytical methods (both incremental and first order secant method) underestimate the equivalent stress of the composite material. This fact was already analyzed by different authors (see Segurado et al. [79]) and it was the main reason to propose an alternative method to evaluate the equivalent stress, like using the second order secant method. However, no alternative method for the incremental approach has been obtained yet, and thus the results for such cases like cyclic imposed macroscopic strain cannot be analyzed in a proper way using Mean-Field techniques.

The main reason for the divergence in the results seems to be the different properties of the material, since the rest of the factors that can make some influence in the results remain constant. Moreover, the study of some microscopic variables like the distribution of the equivalent plastic strain over the microgeometry shows the same behavior of the material, being the plastic deformation concentrated around the edges of the major axis of the inclusion (see Fig. 5.29).

The last result that will be shown in relation with the study of the simplest geometry corresponds with the case of a imposed biaxial monotonic macroscopic strain. In this case, the strain-stress diagram for the first component of the macroscopic stress tensor shows a similar behavior as it was observed in the uniaxial monotonic case. However, the second component of the macroscopic stress tensor, i.e., the component in the y-direction, shows a pure elastic behavior (see Fig. 5.34) and the results provided by the incremental method and the first order secant

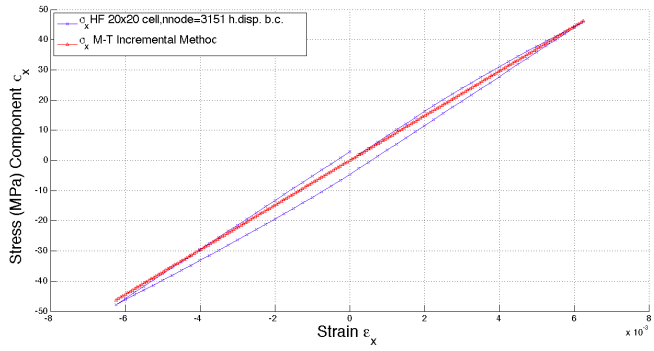

Figure 5.28: EMC ($\xi = 0.15$) under uniaxial cyclic macro-strain. Comparison of the results obtained for the first component of the macro-stresses ($\varepsilon_x - \sigma_x$).

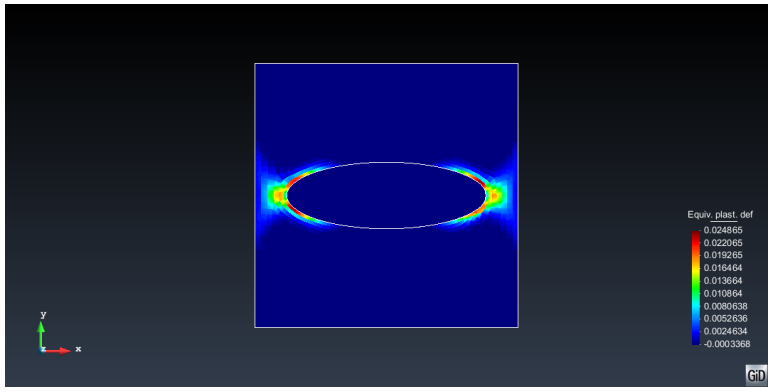

Figure 5.29: EMC ($\xi = 0.15$) under uniaxial monotonic macro-strain. Distribution of the equivalent plastic strain over the microgeometry.

method coincide with the exact results. The second order secant method predicts an inelastic behavior of the material and the response of the composite is softer than the real behavior, leading to an underestimation of the macroscopic stresses.

Similar results were obtained in the case of more complicated microgeometries and higher volume fraction of inclusions. The simulations computed with the first order secant method and incremental method predict an elastic behavior of the composite material, which does not correspond with the exact behavior predicted by the High Fidelity method. The values for the macroscopic stresses observed in the results obtained using analytical methods are very close to the real solution, although the real behavior of the material is better modeled using the second order secant method, since it is the unique analytical method that predicts an inelastic response of the composite material.

A theoretical comparison between microgeometries can provide some information about the influence in the results of the chosen arrangement for the microge-

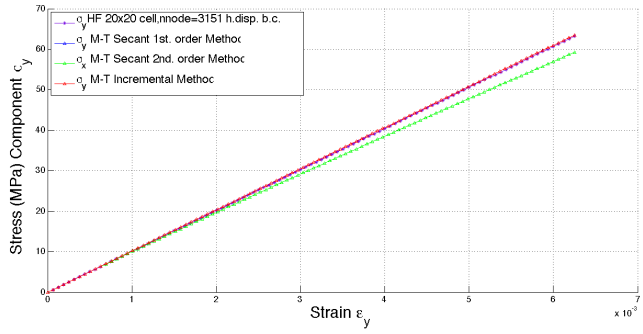

Figure 5.30: EMC ($\xi = 0.15$) under biaxial monotonic macro-strain. Comparison of the results obtained for the second component of the macro-stresses ($\varepsilon_x - \sigma_y$).

ometry. Fig. 5.33 and 5.32 show the distribution of the equivalent plastic strain over the unit cell for the last loading step. As it was occurred for the first material, the size of the inclusions has a very significant influence in the peak values for the macroscopic variables, since the concentration of some stresses is higher in those inclusions with greater size. For this particular case, the first order analytical methods not only do not provide the distribution of the equivalent plastic strain in the microgeometry, but also they do not even predict the plastic behavior of the composite.

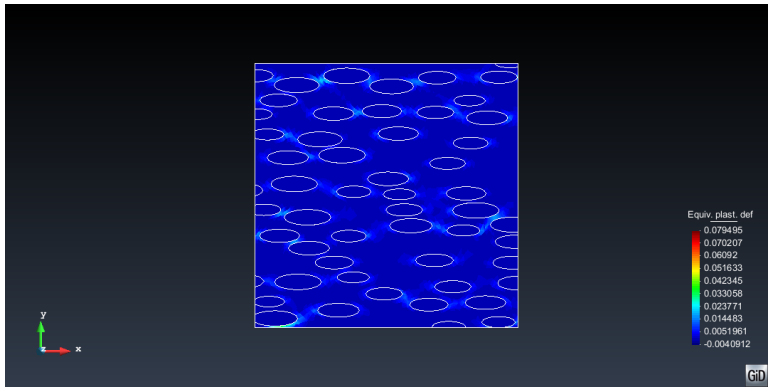

Figure 5.31: EMC ($\xi = 0.2842$) under uniaxial monotonic macro-strain. Distribution of the equivalent plastic strain over the second microgeometry.

In the previous comments nothing has been commented about the results provided by the Rule of Mixtures. For the first material it has been observed that the Rule of Mixtures overestimates the macroscopic stresses on the material, although in some particular cases the level of the stresses was similar to the exact values provided by the High Fidelity method. However, for the second material, charac-

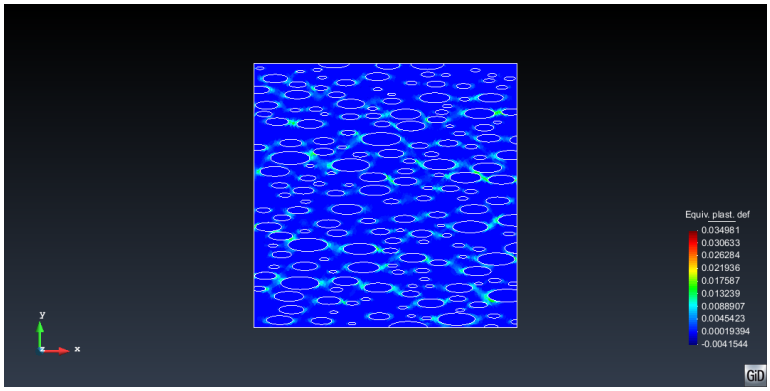

Figure 5.32: EMC ($\xi = 0.2699$) under uniaxial monotonic macro-strain. Distribution of the equivalent plastic strain over the third microgeometry.

terized by the high value of the stiffness coefficient, the Rule of Mixtures seems to be very inappropriate to predict the overall response of the material, since the level of stresses lies far away from the exact results. Due to this, the results regarding such method are not provided in the current section. The divergence observed between the different homogenization methods is even more patent in the case of an imposed uniaxial cyclic macrostrain. As it can be observed through the study of the representation of the two first invariants, the incremental method predicts an elastic response of the homogenized material, while the real response is inelastic, as it can be inferred through the observation of the curve obtained using the High Fidelity method. In the case of the Rule of Mixtures, the material behaves in a much stiffer way in comparison with the other methods, which can cause some problems in the case of taking into account the Rule of Mixtures to design the current composite material.

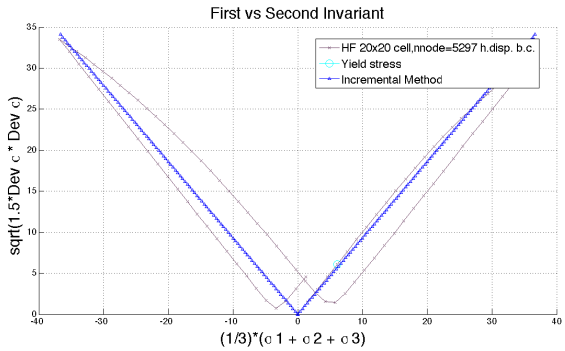

Figure 5.33: EMC ($\xi = 0.2842$) under uniaxial cyclic macro-strain. Representation of the two first invariants.

Finally, in the case of a biaxial monotonic load the conclusions that can be extracted from the study of the second material are exactly the same that those commented for the first microgeometry. As it was previously indicated, the first component of the macroscopic stress tensor follows the same behavior observed in the first analyzed loading path, while the second component shows an elastic behavior that coincides with the results provided by the analytical methods. This particular example allows observing the anisotropic behavior of the homogenized material, due to the fact that the geometry of the aligned ellipsoids provide different stiffness depending on the direction of the imposed macrostrains. For this particular case, the material shows larger stiffness in the y-direction, where the minor axis is defined.

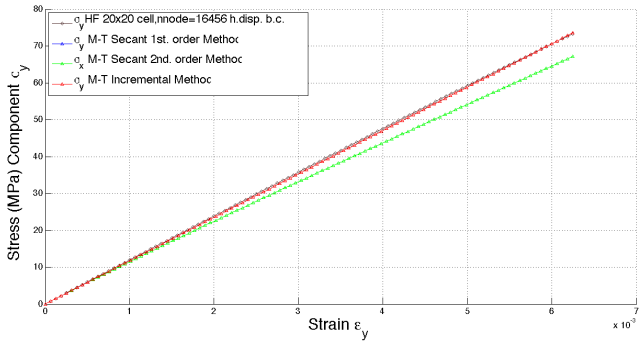

Figure 5.34: EMC ($\xi = 0.2699$) under biaxial monotonic macro-strain. Comparison of the results obtained for the second component of the macro-stresses ($\varepsilon_x - \sigma_y$).

Material 3: Porous Material

The latter case that will be studied, with regard to the influence of the material in the results obtained using the different methods of homogenization, corresponds to an extreme case: a porous material. This new feature is easily implemented in the High Fidelity model just by eliminating the inclusion in the pre-processor (GiD©), while in the Rule of Mixtures and the analytical model it has to be included a "fictious" material that simulate the void (giving quasi-null properties to the material of the inclusion). It is expected to obtain some discordances in the results, which so far have been fairly good, due to the fact that the stiffness coefficient reach the maximum value. Different authors state that the Mean-Field homogenization methods are perfectly valid to predict the behavior of porous materials, although it is very hard to find examples in the literature.

The presentation of the results for the porous material will begin, as in the rest of the cases, with the simplest microgeometry and the simplest imposed strain path (uniaxial and monotonic). The results for the first component of the macroscopic stress tensor (see Fig. 5.35) show some particularities for the current case that were not observable in the previous examples. Firstly, it can be observed

that none of the analytical methods predict correctly the elastic branch. All of them underestimate the properties of the composite, giving a value for the effective Young Modulus that is smaller than the real value. Nevertheless, the Rule of Mixtures and the High Fidelity method provide the same value for the effective Young Modulus, as occurred for the first material (see Fig. 5.16). However, if the results regarding the inelastic branch are now analyzed, it can be observed that the Rule of Mixtures overestimates again the macroscopic stresses of the material. On the other hand, the second order secant method underestimates the real response of the material and the homogenized material in this case is much softer with respect to the exact behavior of the composite. The incremental method, for this particular case, is very inaccurate in comparison with the results that were obtained in the rest of materials, while the first order secant method gives the most accurate results, although the error tends to increase with increasing values of the imposed macrostrain.

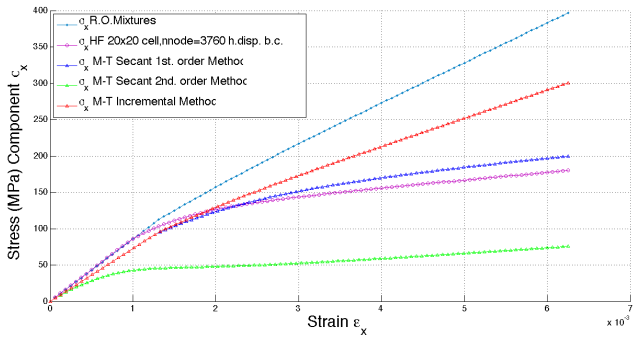

Figure 5.35: Porous material ($\xi = 0.15$) under uniaxial monotonic macro-strain. Comparison of the results obtained for the first component of the macro-stresses ($\varepsilon_x - \sigma_x$).

A similar tendency appears in the case of the second component of the macroscopic stress tensor (see Fig. 5.36). For this particular case, the Rule of Mixtures does not simulate correctly the elastic behavior of the homogenized material, giving a stiffer response. However, the analytical methods predict correctly the macroscopic properties and the values of the stress for the second component are equal to the exact values in the elastic regime. In the post-yield regime the situation changes drastically, especially in the case of the results provided by the incremental method: it can be observed a sharply increment in the level of macroscopic stresses and the curvature of the strain stress curve has the opposite sign in comparison with the real response of the porous material. On the other hand, the secant methods model much better the inelastic regime, although the accuracy of the first order method continues being the most accurate.

In the case of the out-of-plane component of the macroscopic stress tensor the situation is even worse in comparison with the values observed in the rest of materials. In this case, in which the accuracy of the analytical methods were quite high, the results get even worse. Fig. 5.37 shows the curves obtained using the

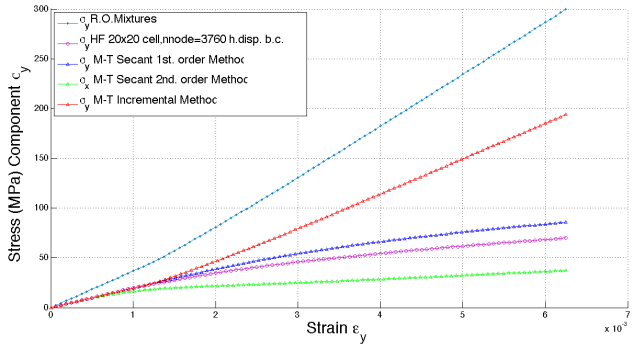

Figure 5.36: Porous material ($\xi = 0.15$) under uniaxial monotonic macro-strain. Comparison of the results obtained for the second component of the macro-stresses ($\varepsilon_x - \sigma_y$).

different methods, where it can be noticed that the distribution of the results are very similar to those ones obtained for the second component of the macroscopic stress tensor.

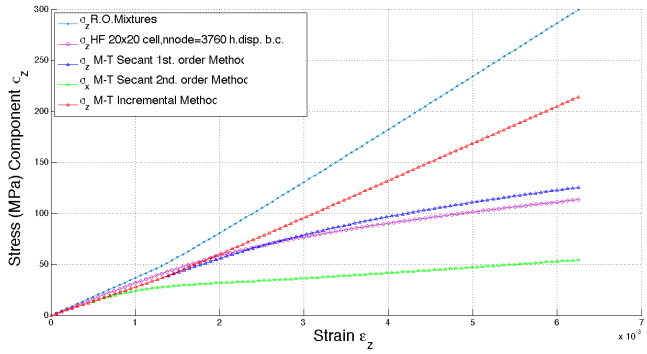

Figure 5.37: Porous material ($\xi = 0.15$) under uniaxial monotonic macro-strain. Comparison of the results obtained for the third component of the macro-stresses ($\varepsilon_x - \sigma_z$).

Further conclusions can be deducted by attending to some variables provided by the Finite Element Approaches, like the distribution of the equivalent plastic strain. For this particular variable, the fact of eliminating the inclusion produces severe changes on the behavior of the composite, which were not appreciated for the second material (see 5.4). As it can be appreciated, there exists a much bigger zone in the microgeometry that is affected by plastic strains, although the edges of the major axis are again the location of the highest values for such variable. On the other hand, the lowest values are located close to the lateral sides of the unit cell, which does not occur for the MMC.

When considering the actions of a cyclic load, the prediction of the mean-field approaches is even worse. As it was indicated on the previous analyzed cases,

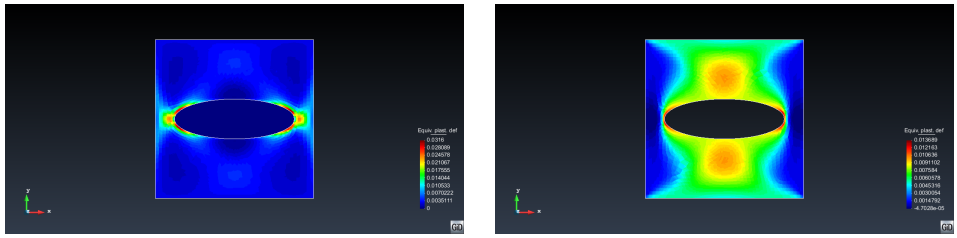

Table 5.4: Comparison between the equivalent plastic strain for the first (left) and third (right) material in the monotonic uniaxial case.

the cyclic load makes that a greater number of elements may present high values of the plastic strain. This causes some divergence of the results, which is more pronounced in the case of studying a porous material, as it can be observed through the analysis of the first and second invariant (see Fig. 5.38). The curve for the incremental method coincides exactly with the exact values when the level of macroscopic stresses lies below the yield stress of the material, while the curve Rule of Mixtures differs considerably from the theoretical results. Above the yield stress the accuracy of the incremental method starts going down and the predicted behavior looks like the one predicted by the Rule of Mixtures.

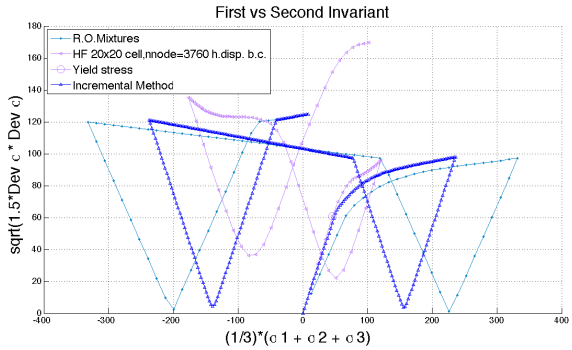

Figure 5.38: Porous material ($\xi = 0.15$) under uniaxial cyclic macro-strain. Representation of the two firsts invariants.

The previous conclusions can be visualized in the macroscopic strain-stress diagram (see Fig. 5.39). For all the three components, the elastic behavior is perfectly described by the incremental method. However, the inelastic branch for the incremental method consider a stiffness that is not real since the material tends to be softer, as shows the results using the High Fidelity method. For this situation, contrary to what occurred with the rest of the materials, the results obtained with the incremental method are very close to those obtained with the Rule of Mixtures.

The last case that will be analyzed for this first microgeometry corresponds to the biaxial monotonic imposed macro strain. For this particular case, the conclu-

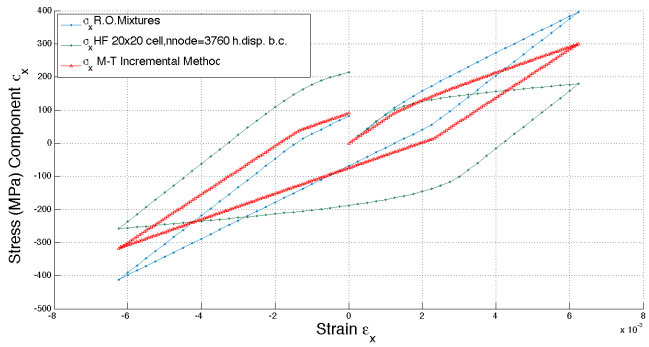

Figure 5.39: Porous material ($\xi = 0.15$) under uniaxial cyclic macro-strain. Comparison of the results obtained for the first component of the macro-stresses ($\varepsilon_x - \sigma_x$).

sions are very similar to those ones commented in the uniaxial case, particularly for the first and third components of the macroscopic stress tensor (see Fig. 5.40): the Rule of Mixtures provides a stiffer response of the material in comparison with the real behavior of the composite material, even in the elastic regime. The values obtained with the incremental and the first order secant method for the macroscopic stresses are also higher than the exact values, although the behavior of the material seems to be much closer to the real one. Maybe an important aspect that should be commented with respect to the predicted results is the differences between the yield stress that are obtained depending on the method. As it can be observed in Fig. 5.40, the plastic domain starts firstly in the second order secant method, since this method overestimates the value for the equivalent plastic strain and that leads to a softer behavior of the homogenized material. On the other hand, the plastic domain is given for higher values of the imposed macroscopic strain in the case of the incremental method and the first order secant method, which underestimate the behavior of the equivalent plastic strain and predict a stiffer response for the composite, being the response given by the first order secant method much better than the one provided by the incremental method. In the case of the second component, the situation is quite different, since the rigidity shown by the composite drops sharply and the level of stresses in the material is very small. As Fig. 5.21 shows, the best method to approximate the real behavior of the porous material is the second order secant method, due to the fact that is the only one that predicts the existence of high levels of plastic strain over the geometry. The difference between the results in this case can be explained through the distribution of the equivalent plastic strain when the inclusions are removed. As it was previously commented, higher values for the equivalent plastic strain are located over the entire domain of the material (see Fig. 5.4), which affects the distribution of stresses over the RCU and causes the loss of rigidity in the y-direction.

Unexpected results are found in the case of more involved microstructures, as it can be observed in the results obtained for the second and third microgeometries. In the previous examples it was observed that the changes in the distribution and

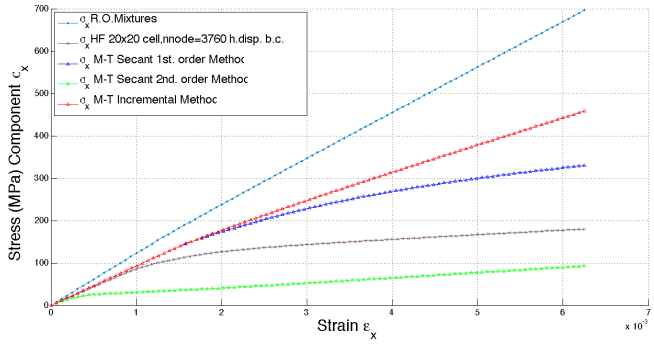

Figure 5.40: Porous material ($\xi = 0.15$) under biaxial monotonic macro-strain. Comparison of the results obtained for the first component of the macro-stresses ($\varepsilon_x - \sigma_x$).

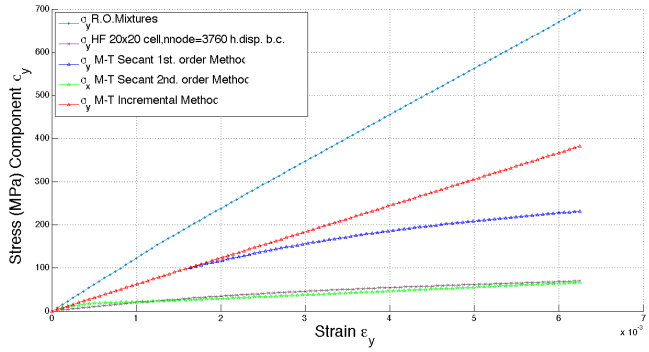

Figure 5.41: Porous material ($\xi = 0.15$) under biaxial monotonic macro-strain. Comparison of the results obtained for the second component of the macro-stresses ($\varepsilon_x - \sigma_y$).

volume fraction of the inclusions were not a determinant factor for the accuracy of the results. However, in the case of a porous material, it has been found that the arrangement of the phases plays an important role for the prediction of the different models. As it can be observed in the figure 5.42, the results obtained for the third microgeometry are more accurate in comparison with those obtained for the first arrangement, which in principle corresponds with the theoretical basis of the Mean-Field methods. Although the strain-stress diagram for the macroscopic prediction shows a similar tendency in comparison with the previous results (the Rule of Mixtures provides the exact response for the elastic regime, while the analytical methods predict a lower value for the Young Modulus), the response regarding the first order secant method in the case of plastic regime are very close to the real response of the composite material.

Moreover, it has not been found significant differences between the results obtained with the second and third arrangement. In the case of the second component of the macroscopic stress tensor the conclusions that are extracted after the analy-

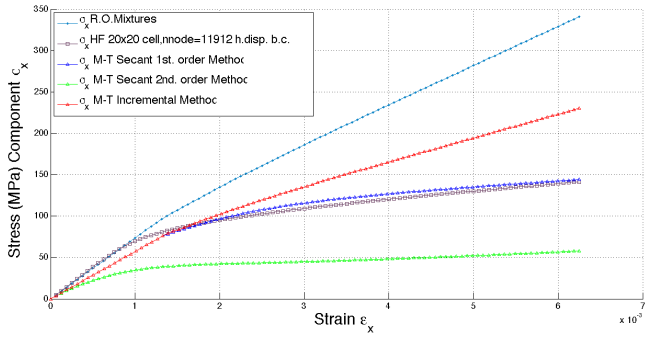

Figure 5.42: Porous material ($\xi = 0.2699$) under uniaxial monotonic macro-strain. Comparison of the results obtained for the first component of the macro-stresses ($\varepsilon_x - \sigma_x$).

sis of the results are very similar: firstly, as it occurred in the first microgeometry, for this second component the elastic response of the composite is well predicted by all three analytical methods, while the Rule of Mixtures gives a higher value for the effective Young Modulus. The incremental method shows a quite stiffer behavior regarding the inelastic behavior of the material, as it was also observed for previous cases. However, the first order secant method provides accurate results also for this particular case, being the divergence between the results lower than for the case of a unique pore. The same conclusions can be deducted for the second order secant method, although the accuracy of this approach is worse in comparison with the first order approach (see Fig. 5.43). Once again, the differences in the results for both microgeometries (second and third arrangement of pores) are almost imperceptible.

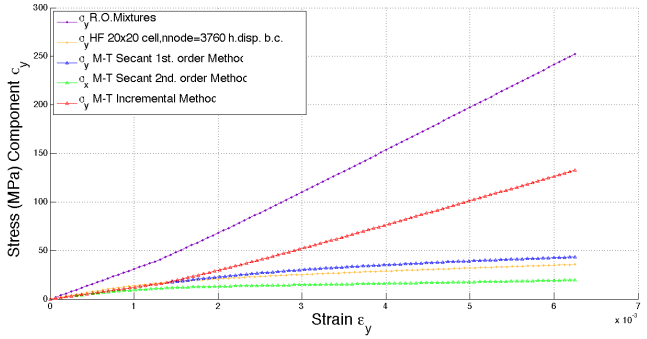

Figure 5.43: Porous material ($\xi = 0.2842$) under uniaxial monotonic macro-strain. Comparison of the results obtained for the second component of the macro-stresses ($\varepsilon_x - \sigma_y$).

The values for the second component of the macroscopic stress tensor are much lower than the values obtained for the first component. This also occurred for

the first microgeometry and the justification for such behavior were found in the "redistribution" of the stresses in the case of a porous material, which are concentrated in the vertical direction. This phenomena is also found for the more complex microgeometries, as it is shown in the Fig. 5.5, where it can be observed a predominance of the distribution for the equivalent plastic strain in the second direction.

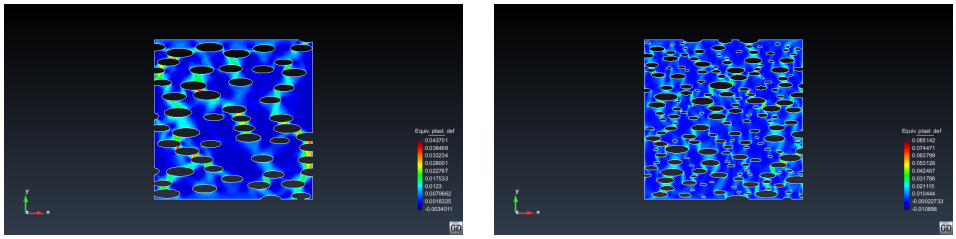

Table 5.5: Comparison between the distribution of the equivalent plastic strain for the second (left) and third (right) microgeometries in the monotonic uniaxial case.

Similar results are obtained in the study for the third component of the macroscopic stress tensor. As occurred for the previous components, the highest accuracy for the out-of-plane stress is given by the first order secant method, which predicts quite well the behavior of the composite in the inelastic regime. The incremental method gives a stiffer response, while the second order secant method provides lower values for the stresses in the material. The prediction for the value of the Young Modulus is underestimated for all three analytical methods, being the Rule of Mixtures the unique approach that models correctly the elastic regime in this particular case (see Fig. 5.44).

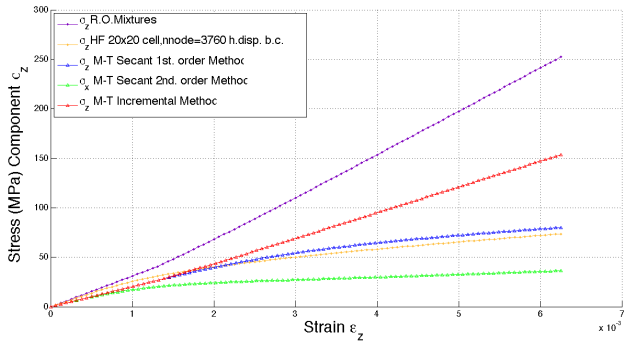

Figure 5.44: Porous material ($\xi = 0.2842$) under uniaxial monotonic macro-strain. Comparison of the results obtained for the third component of the macro-stresses ($\varepsilon_x - \sigma_z$).

Although the results for the first load case (uniaxial monotonic imposed macroscopic strain) were definitely better for the second and third microgeometries in the case of a porous material, it has been observed that the accuracy of the analytical

methods for such material arrangements is inferior when a cyclic macroscopic strain is imposed. As it occurred in the first microgeometry, the incremental method predicts a much stiffer behavior of the material and the level of the macroscopic stresses lies between the exact results and the results given by the Rule of Mixtures, as it can be observed through the strain-stress diagram for the first component of the macroscopic stresses (see Fig. 5.45). Once again, the predicted value of the effective Young Modulus is lower for the case of the incremental approach, in comparison with the real value, which coincides exactly with the result provided by the Rule of Mixtures. Moreover, the slope of the hardening path for the incremental method is overestimated and the residual value for the macroscopic stress (when the material is unloaded) is clearly higher for the analytical approach, which almost coincides with the residual value for the stresses predicted by the Rule of Mixtures.

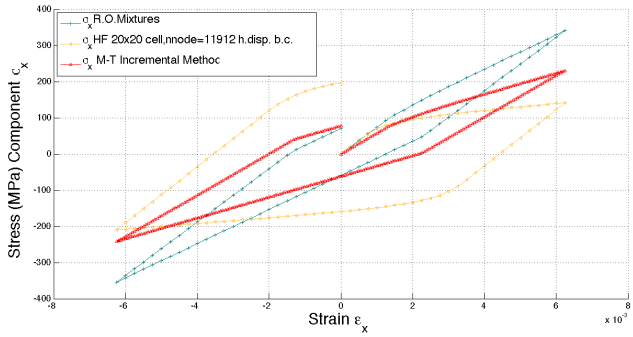

Figure 5.45: Porous material ($\xi = 0.2699$) under uniaxial cyclic macro-strain. Comparison of the results obtained for the first component of the macro-stresses ($\varepsilon_x - \sigma_x$).

Fig. 5.6 shows the distribution of the equivalent plastic strain in each RCU for the last time step. It can be appreciated on the results, that the distribution of the equivalent plastic strain on the third microgeometry is more uniform than in the second one, in which the zones where the plastic strain appear are concentrated around the pores. Once again, the distribution for the plastic strain appears to have a predominant direction, coinciding with the vertical axis (y-direction in this case). This behavior justifies again the lower stiffness observed in the pore material, when the macroscopic stresses in the y-direction are analyzed.

The observation of the diagram corresponding the first and second invariants (see Fig. 5.46) brings some interesting conclusions that it is necessary to comment. The branch corresponding the elastic regime for the first loading steps coincides exactly for both the incremental and the High Fidelity methods. However, in the post-yield regime the differences between both approaches start increasing, especially in the hardening branch, where it can be appreciated a quite different shape between both curves, being the curve regarding the High Fidelity method quite irregular in comparison with the curves corresponding the Rule of Mixtures and the incremental method.

Finally, the analysis of the influence of the different material will be finished

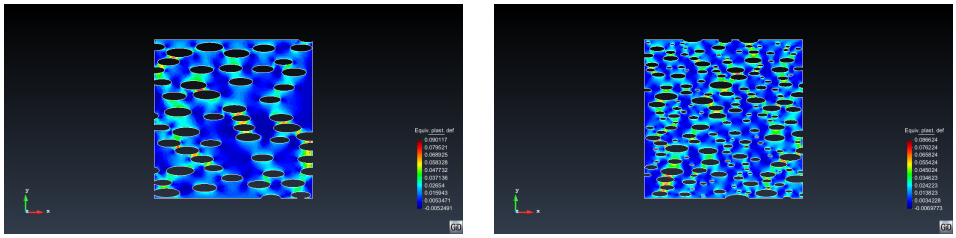

Table 5.6: Comparison between the distribution of the equivalent plastic strain for the second (left) and third (right) microgeometries in the cyclic uniaxial case.

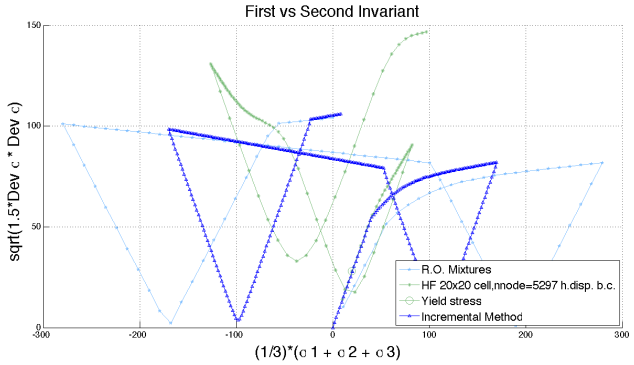

Figure 5.46: Porous material ($\xi = 0.2842$) under uniaxial cyclic macro-strain. Representation of the two firsts invariants.

with the results regarding the biaxial monotonic imposed strain in the porous material. In this case, the results are very similar to those obtained for the simplest microgeometry, where it was observed that any of the analytical methods reproduced the exact behavior observed for the macroscopic stresses. Contrary to what was observed in the case of a single pore, in the case of most involved microgeometries there is no coincidence in the results observed for the second component of the macroscopic strain (see Fig. 5.47), due to the fact that the new imposed macrostrain causes the appearance of high values of the accumulated plastic strain, which reach values that are comparable with those observed for the cyclic load.

5.3.3 Influence of the loading path

Some important conclusions have been extracted from the study of the accuracy of the different methods regarding the properties of the constituents and the arrangement of the microgeometry. Although in the previous examples it has been analyzed different types of loading cases, it has not be considered the magnitude of the imposed macro-strain as a parameter to determine the accuracy of the Mean-Field homogenization methods (maintaining the rest of parameters as constants).

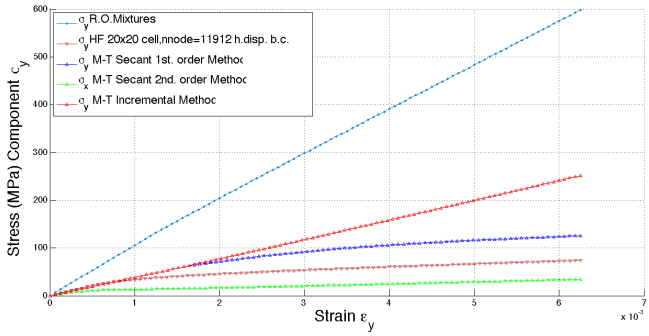

Figure 5.47: Porous material ($\xi = 0.2699$) under biaxial monotonic macro-strain. Comparison of the results obtained for the second component of the macro-stresses ($\varepsilon_x - \sigma_y$).

In order to study such cases, it has been taken a Representative Unit Cell, which has been subjected to five different uniaxial monotonic macroscopic strains. The maximum value for the imposed macroscopic strain has been: $5 \cdot 10^{-3}$, 0.01, 0.05, 0.1 and 0.5. The microgeometry that has been considered corresponds to the second arrangement (see Fig.5.2) from the previous analysis, since its microstructure has a more realistic arrangement than the first arrangement and the computational cost is much lower than for the third microgeometry. The characteristics of the material has been taken equal to the Metal Matrix Composite analyzed in the previous section, due to the fact that for such material the results were quite accurate and thus the divergence of the new results may be seen in a more direct way.

The results that have been obtained to such analysis were not expected at all: the higher accuracy is obtained for the cases, in which the maximum imposed macroscopic strain is larger and thus the accumulated plastic strain are also larger. This has been observed for all three components of the macroscopic stress tensor (the fourth component is negligible for such load case). Figures 5.48 to 5.50 show the results for the macroscopic stresses in the x-direction for three different examples. As it can be observed, the results become more accurate for all three methods when the value of the imposed macrostrain is increased. That occurs for all three methods, since they converge to the results given by the High Fidelity method when the strain increases. Maybe the most remarkable case correspond with the second order secant method, due to the fact that in the previous section it has been observed that tends to provide a too soft response for the composite material, which can be perfectly observed for small values of the imposed strain (see Fig. 5.48). However, when the load is increased, the second order secant method gives a quite accurate response, being very close to the exact solution (as it is observed in Fig. 5.50).

The results obtained for the second component (see Figs. 5.51 to Figs. 5.53) of the macroscopic stress tensor are quite good and follow, in general, the same tendency than for the first component, with some differences that now are commented.

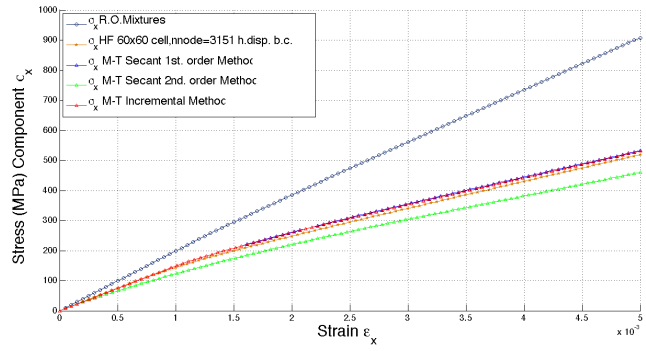

Figure 5.48: MMC ($\xi = 0.2699$) under uniaxial monotonic macro-strain ($\varepsilon_{max} = 5{\cdot}10^{-3}$). Comparison of the results obtained for the first component of the macro-stresses ($\varepsilon_x - \sigma_x$).

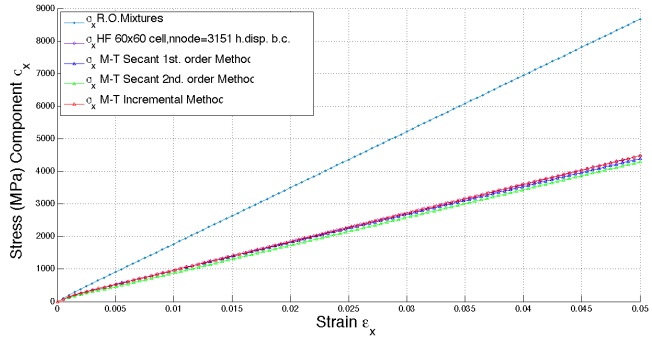

Figure 5.49: MMC ($\xi = 0.2699$) under uniaxial monotonic macro-strain ($\varepsilon_{max} = 0.05$). Comparison of the results obtained for the first component of the macro-stresses ($\varepsilon_x - \sigma_x$).

The results for the minimum value of the imposed macro strain are quite accurate, although both the second order secant method and the incremental method predict a slightly stiffer behavior of the homogenized material, giving values that exceed the exact value in 6% and 15%, respectively. The value corresponding to the error due to the second order approach tends to diminish and it can be neglected when the value of the imposed macroscopic strain is large enough. In this case, the response giving by both secant methods coincide. However, the curve corresponding the results for the incremental strain separates from the exact results when the imposed strain grows and, for the last case studied, the stress at the last step of the analysis is approximately 20% larger than the exact value.

The results regarding the component of the stresses in the z-direction (out-of-plane) are given in the figures 5.54 to 5.54. For this particular case, the differences between the different imposed strain conditions are very similar, although the same tendency for the second order secant method can be observed, coinciding the values for both secant methods when the level of the imposed macro strain is larger. The

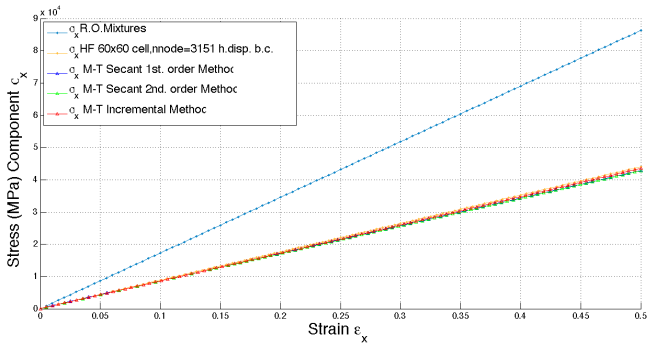

Figure 5.50: MMC ($\xi = 0.2699$) under uniaxial monotonic macro-strain ($\varepsilon_{max} = 0.5$). Comparison of the results obtained for the first component of the macro-stresses ($\varepsilon_x - \sigma_x$).

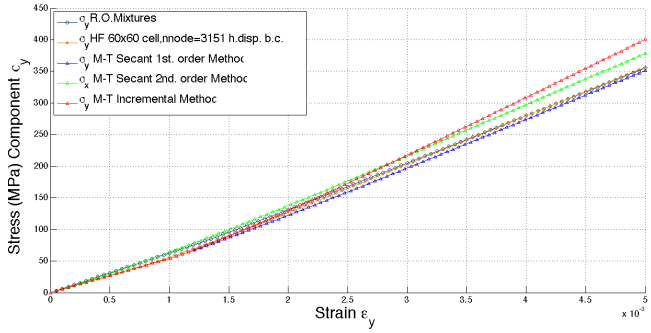

Figure 5.51: MMC ($\xi = 0.2699$) under uniaxial monotonic macro-strain ($\varepsilon_{max} = 5{\cdot}10^{-3}$). Comparison of the results obtained for the second component of the macro-stresses ($\varepsilon_x - \sigma_y$).

incremental method provides also good results, the accuracy of this approach being slightly worse than for the secant methods. Nevertheless the relative error for all the studied cases seems to be constant (around 3%).

5.3.4 Influence of the volume fraction of inclusions

The third (and last) parametrical analysis that has been carried out within the current study corresponds to the numerical simulation of different RCU in order to observe the differences for the different methods when the volume fraction of the inclusions is modified. For this purpose it has been analyzed seven different micro-geometries, in which the material (MMC), the imposed macro strain (monotonic uniaxial load with a maximum value of $6.25 \cdot 10^{-3}$) and the size of the Representative Cell Unit (60x60 mm.) has been kept constant. The volume fraction of the inclusions varies from a minimum nominal value of 0.05 to a maximum nominal

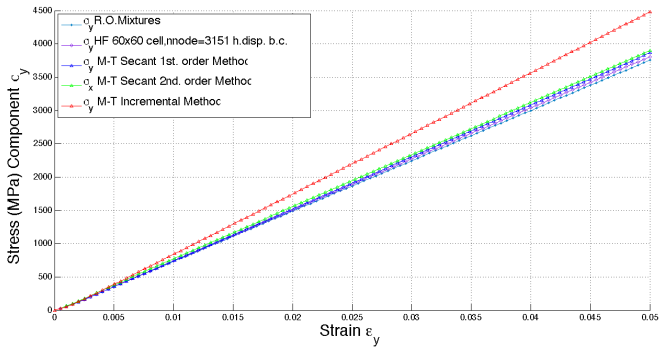

Figure 5.52: MMC ($\xi = 0.2699$) under uniaxial monotonic macro-strain ($\varepsilon_{max} = 0.05$). Comparison of the results obtained for the second component of the macro-stresses ($\varepsilon_x - \sigma_y$).

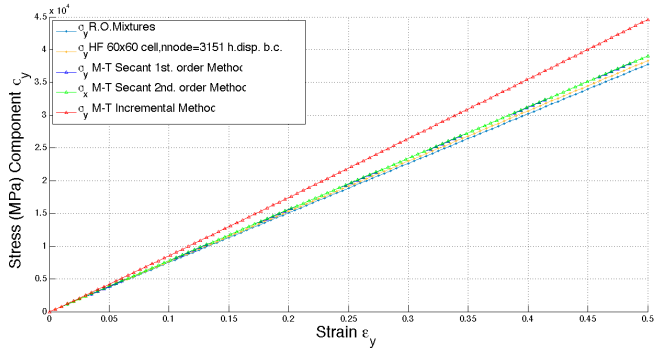

Figure 5.53: MMC ($\xi = 0.2699$) under uniaxial monotonic macro-strain ($\varepsilon_{max} = 0.5$). Comparison of the results obtained for the second component of the macro-stresses ($\varepsilon_x - \sigma_y$).

value of 0.60. The real values for the volume fraction on each RCU vary from the nominal values after the pre-process, in which the distribution of the inclusions has been slightly modified in order to avoid problems during the mesh generation for the Finite Element Approaches. The real values that finally have been considered in the analysis and the arrangement of each microgeometry are summarized on the table 5.7.

In the previous chapters it has been commented the range of validity for the Mean-Field methods according to the literature (see Böhm [10]). According to the experience of different authors, the limit value for the volume fraction of the inclusions in order to obtain a proper accuracy in the results lies around 0.30, i.e., the phase of inclusions represents the 30% of the total volume. From the previous analysis, it has been observed that the exact results are exactly recovered by the analytical methods when only one material is considered (as stated in section 5.3.1).

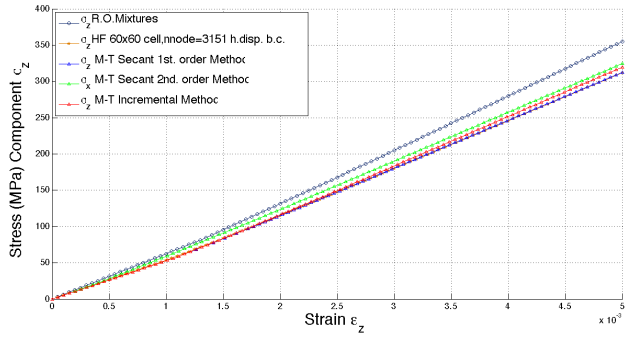

Figure 5.54: MMC ($\xi = 0.2699$) under uniaxial monotonic macro-strain ($\varepsilon_{max} = 5{\cdot}10^{-3}$). Comparison of the results obtained for the third component of the macro-stresses ($\varepsilon_x - \sigma_z$).

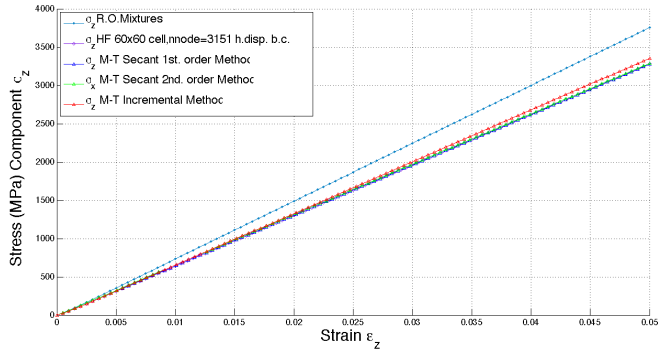

Figure 5.55: MMC ($\xi = 0.2699$) under uniaxial monotonic macro-strain ($\varepsilon_{max} = 0.05$). Comparison of the results obtained for the third component of the macro-stresses ($\varepsilon_x - \sigma_z$).

When both phases are considered, the values tend to show less accuracy, although it has been observed in section 5.3.2 that the main source of inaccuracy is the difference of the mechanical characteristics of materials, since good approximations where observed both for RCU with 15% and 30% of inclusions. In any case, the distribution of the inclusions and the geometry of the cells do not seem to be determining factors for assessing the quality of the results, at least for the volume average response of the homogenized material.

As it was done with the previous parametric study (section 5.3.3), the material and the imposed macroscopic strain have been selected in such a way that the results are known to have a good accuracy for regular values of the volume inclusions, in order to appreciate better the discordances between the results due to exclusively the influence of the volume fraction of the inclusions. The arrangement and size of the inclusions have been selected in order to avoid the appearance of high computational costs.

The first results that will be commented (see figures from Fig. 5.57 to Fig. 5.59)

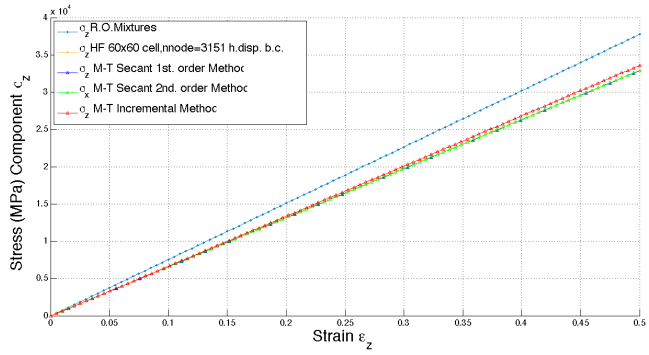

Figure 5.56: MMC ($\xi = 0.2699$) under uniaxial monotonic macro-strain ($\varepsilon_{max} = 0.5$). Comparison of the results obtained for the third component of the macro-stresses ($\varepsilon_x - \sigma_z$).

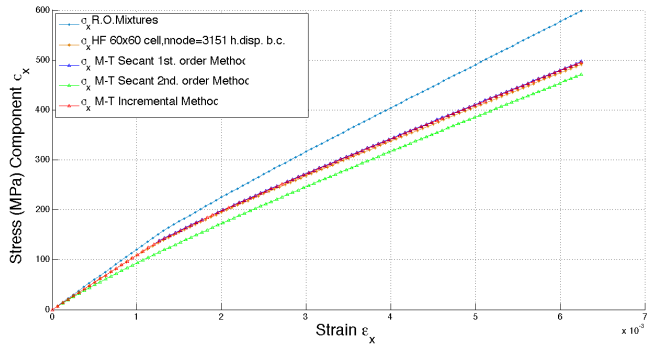

Figure 5.57: MMC ($\xi_1 = 0.0570$) under uniaxial monotonic macro-strain. Comparison of the results obtained for the first component of the macro-stresses ($\varepsilon_x - \sigma_x$).

correspond to the strain-stress diagram for the first component of the macroscopic stress tensor. As it can be observed in the diagrams, there exists no clear influence of the volume fraction of the material and the load case that has been considered. The approximation using both first order methods (secant and incremental) is quite good, while the second order secant method provides a softer response of the homogenized material. In fact, only the second order method seems to get worse when the volume fraction is increased. On the other hand, the Rule of Mixtures shows clearly less accuracy when the volume fraction of the inclusion grows and the predicted results for the macroscopic stress using this method are larger than the exact results predicted by the High Fidelity method.

The results obtained for the second component of the macroscopic stress tensor are shown in figures from Fig. 5.60 to Fig. 5.62. The tendency showed by the different values of the macroscopic strain changes with respect to the component in the x-direction. As it can be appreciated in the results, all the studied methods show a tendency to diverge when the volume fraction of the inclusions is increased.

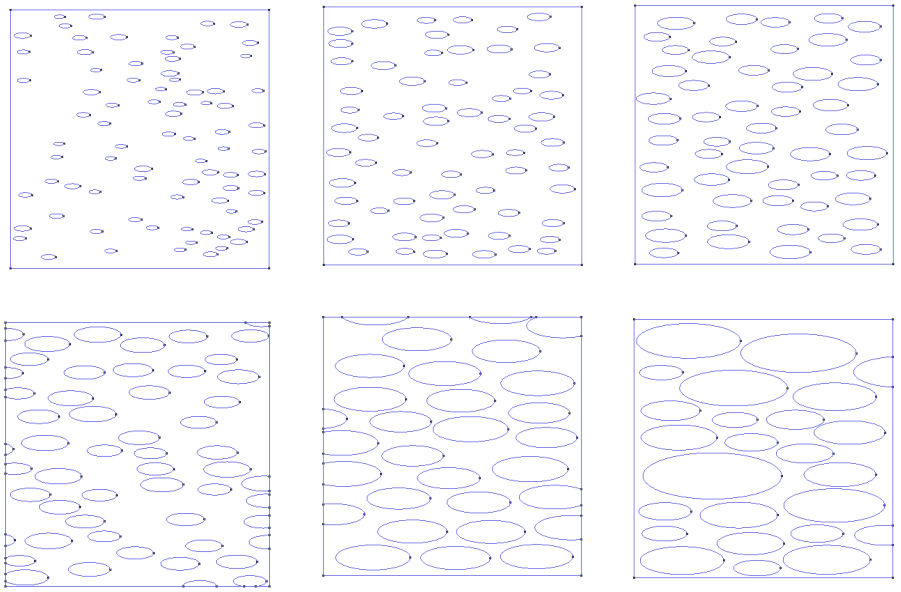

Table 5.7: Different arrangements used to model the different composites. Real values for the volume fraction of inclusions are (beginning from top left and finishing in bottom right): $\xi_1 = 0.0570$; $\xi_2 = 0.1214$; $\xi_3 = 0.2217$; $\xi_4 = 0.2842$; $\xi_5 = 0.4958$; $\xi_6 = 0.5716$.

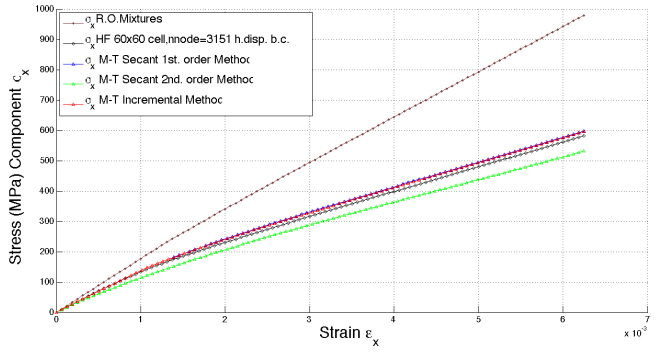

Figure 5.58: MMC ($\xi_3 = 0.2217$) under uniaxial monotonic macro-strain. Comparison of the results obtained for the first component of the macro-stresses ($\varepsilon_x - \sigma_x$).

The greatest discrepancy for the final results are given in the incremental method, which shows a clear tendency to provide much stiffer results for the homogenized material when the influence of the inclusions is more noticeable. However, the results given by the first order secant method tend to become more "stable" in relation with the influence of the inclusions, while the second order secant method

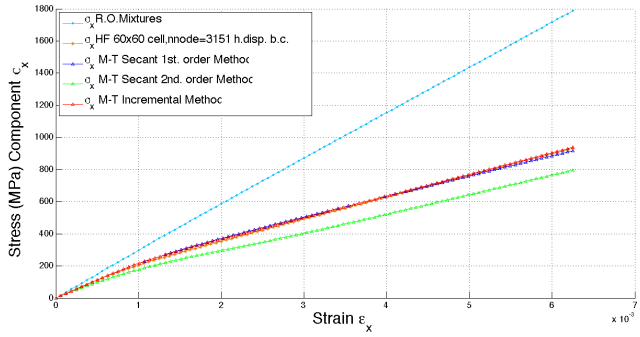

Figure 5.59: MMC ($\xi_6 = 0.5716$) under uniaxial monotonic macro-strain. Comparison of the results obtained for the first component of the macro-stresses ($\varepsilon_x - \sigma_x$).

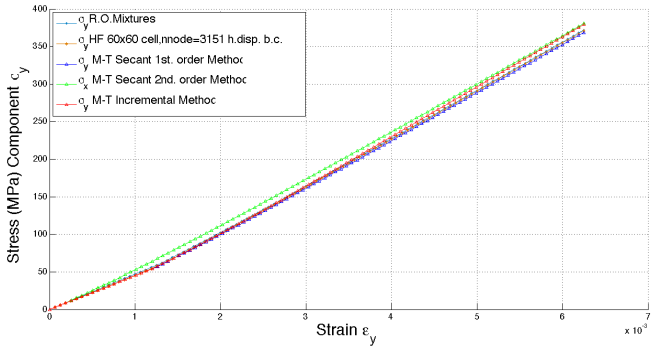

Figure 5.60: MMC ($\xi_1 = 0.0570$) under uniaxial monotonic macro-strain. Comparison of the results obtained for the second component of the macro-stresses ($\varepsilon_x - \sigma_y$).

provides results that behave similar to the incremental method, although the final divergence with respect to the exact results is not so great as the observed for the incremental result. The Rule of Mixtures, whose prediction for the macrostresses shows the best accuracy for low values of ξ, also tends to diverge for increasing values of the volume fraction of the inclusions. As it can be observed in 5.62, the behavior for the material modeled with such method is softer than the real behavior of the material, being the differences in the results for high values of the macroscopic strain quite large.

Similar conclusions can be extracted from the study of the third component of the macroscopic stress tensor, which results for three different values of the volume fraction are shown in the figures 5.63 to 5.65. As it can be observed, the incremental method tends to give a worse description of the out-of-plane stresses when the volume fraction of the inclusions increases, being the predicted results again stiffer in comparison with the exact results. On the other hand, the secant methods provide quite accurate results, independently of the volume fraction considered in

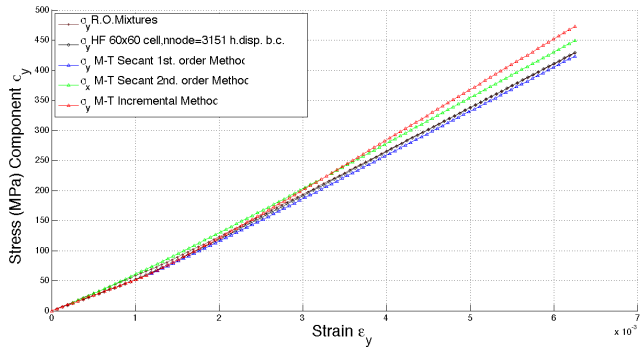

Figure 5.61: MMC ($\xi_3 = 0.2217$) under uniaxial monotonic macro-strain. Comparison of the results obtained for the second component of the macro-stresses ($\varepsilon_x - \sigma_y$).

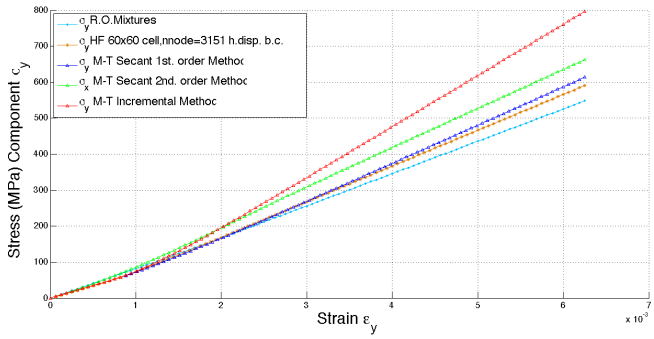

Figure 5.62: MMC ($\xi_6 = 0.5716$) under uniaxial monotonic macro-strain. Comparison of the results obtained for the second component of the macro-stresses ($\varepsilon_x - \sigma_y$).

each case. Such an interesting result has been found for the second order secant method, due to the fact that it tends to provide the same results than the first order secant method when the volume fraction of the inclusions grows.

Some intermediate results have been omitted in this section in order not to overload the text. It has been observed the same tendency in all the different models, so it has been decided to keep in the current work three different representative examples for a lows, an intermediate and a high value of the variable of interest.

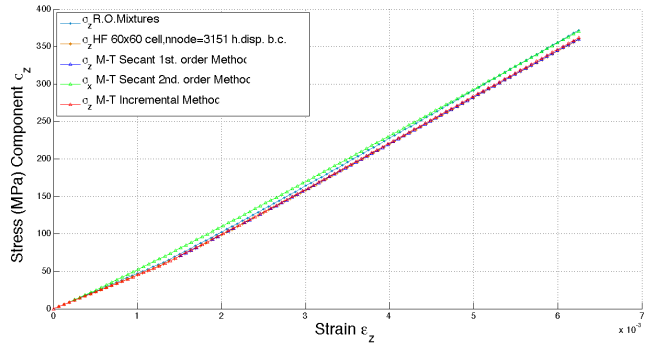

Figure 5.63: MMC ($\xi_1 = 0.0570$) under uniaxial monotonic macro-strain. Comparison of the results obtained for the third component of the macro-stresses ($\varepsilon_x - \sigma_z$).

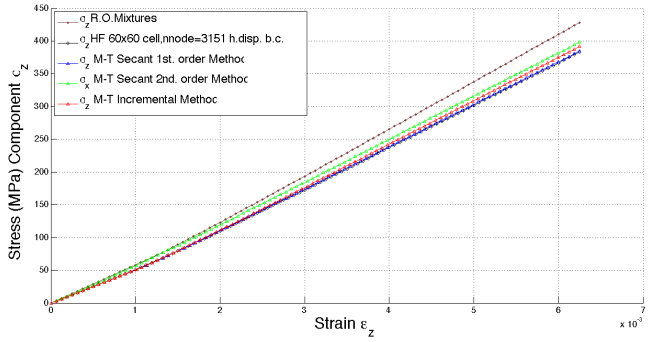

Figure 5.64: MMC ($\xi_3 = 0.2217$) under uniaxial monotonic macro-strain. Comparison of the results obtained for the third component of the macro-stresses ($\varepsilon_x - \sigma_z$).

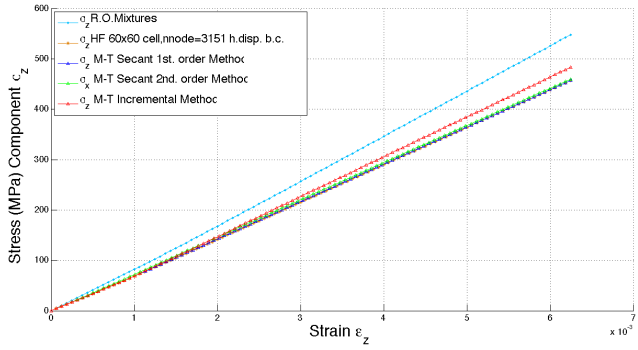

Figure 5.65: MMC ($\xi_6 = 0.5716$) under uniaxial monotonic macro-strain. Comparison of the results obtained for the third component of the macro-stresses ($\varepsilon_x - \sigma_z$).

Chapter 6

Conclusions

Throughout this work, it has been presented the main concepts of the microgeometry as a current tool to deal with the study and design of new materials, in particular with composite materials. The analysis of microheterogeneous materials is not a recent development, since the first studies (under different assumptions) were developed more than 150 years ago. However, a significant progress in this field began to take place from the solution of the so-called *dilute problem*, which was developed by Eshelby in 1957. Nowadays, due to the high development of powerful computers, the number of numerical based methods has grown considerably. The different techniques determine the relationships between the microstructure and the macroscopic response or "structural property" of a material and are based on the concept of *Representative Volume Element* and the assumption of the separation between the different scales that are involved in the problem. Among all the different homogenization techniques that are used to characterize the composite materials, two of them are specially employed by most of authors: the multi-scale method based on a Finite Element Approach (the so-called FE^2 method) and the Mean-Field homogenization techniques.

The so-called Mean-Field homogenization techniques are based on analytical solutions of the boundary value problem defined in the microstructure level of the inhomogeneous material and are an efficient way to predict the behavior of heterogeneous materials. They are based on the Eshelby's solution for the dilute inclusion problem and provide good estimations for the volume average values of the different variables that define the equilibrium of the RVE. In the current work, the most important Mean-Field homogenization techniques and their theoretical aspects and formulation have been discussed. The different procedures show different formulation depending on the different assumptions that are adopted. Many of them have been implemented directly in an algorithm in order to provide a program that can be used to compare the accuracy of the results using such techniques and the results provided by a Finite Element Approach. During the validation of the programs it has been demonstrated that the different methods give different results, which are even more different when the volume fraction of the inclusions is increased. In the comparison analysis done in the current work, only the Mori-Tanaka method has

been considered, since it is the most extended method to simulate the behavior of composites based on a matrix-inclusion microgeometry.

The Mean-Field homogenization techniques were originally developed for elastic materials. In the last decades, however, it has been developed some other methods in order to adapt the formulation for such techniques to the elastoplastic case. Two different group of methods have been developed in this work: one of them (secant approaches), based on a formulation within the context of deformation theory of plasticity, approximating the elastoplastic behavior of materials through a set of nonlinear elastic models; and the other group (incremental or tangent approach), based on a linearization of the local constitutive laws written in rate form. The implementation of both methods (and a variant for the secant method based on the computation of the equivalent stress using a second order approach) have been carried out, using a stress-driven formulation for validating the problem (since most of authors present algorithms based on a stress-driven way) and a strain-driven formulation for analyzing the accuracy for the Mean-Field techniques.

The application of a multi-scale Finite-Element approach has been also described in the current work, giving the main theoretical background. The computational aspects of a Finite Element program (already implemented) has been presented, paying special attention to the main computational aspects related to the definition of a *Representative Volume Element*, which is a very important aspect that has to be well implemented in order to define correctly the micromechanical problem. After defining the main computational aspects of the Finite Element Method adapted to the micromechanical problem, a parametric comparative analysis has been carried out in order to study the accuracy of the Mean-Field homogenization techniques when some variables are modified.

The comparative study has been divided in three different sections, depending on the main variable whose influence in the prediction of the mechanical characteristics of the composite material has been analyzed:

- Firstly, the influence of the characteristics of the materials has been studied, paying special attention to the differences when the stiffness ratio is increased. For each material, three different *Representative Cell Units* and three different loading cases have been addressed. It has been observed that the Mean-Field homogenization techniques provide reasonably accurate results when the values for the stiffness ratio are modest. According to this, quite good results have been obtained for a Metal Matrix Composite reinforced with ceramic inclusions. However, for growing values of the stiffness ratio the accuracy of the results starts decreasing and poor predictions of the behavior of the composite material have been observed in extreme cases, like porous materials. According to each case, it has been observed some differences in the accuracy when the arrangement of the inclusions is modified. However, the differences observed in the results is not as noticeable as for the case of varying the stiffness ratio and only small differences related to the local variation of the main variables have been detected, being the average results very similar. On the other hand, the form of the loading path (materialized through imposed macroscopic strains) plays an important role

in the micromechanical problem. The Mean-Field techniques produce quite good predictions in the case of simple loading cases (like uniaxial and biaxial uniform paths), while the accuracy of the results starts decreasing when more complex loading paths are considered, like was observed for the cyclic case.

- The second analysis that has been carried out corresponds to the comparison of the results when the material and the microgeometry is maintained, but the level of imposed macroscopic strains is modified. The analyzed case corresponds to a uniaxial tensile deformation applied to a material with a low value of the stiffness coefficient. It has not been observed important differences in the quality of the results when the maximum value of the imposed macroscopic strains (and thus the value of the accumulated plastic strain) is increased.

- The same material (MMC) has been analyzed, varying in this case the value of the volume fraction of the inclusions. The accuracy of the prediction provided by the Mean-Field techniques remains constant when the volume fraction of the inclusions is varied and a simple loading path is applied in a material that shows a low value for the stiffness coefficient.

This work showed the general efficiency of mean-field homogenization schemes to capture correctly macroscopic behavior. Although these techniques show some limitations, like the incapability to provide results for the distribution of the different variables over the microgeometry, they represent an efficient way to predict the main general behavior of a composite material spending low computational effort. They are specially indicated to be used in the previous steps of an analysis or as a tool to validate the results with more involved approaches.

The current study has been focused on the main general theoretical aspects and the numerical analysis has been concentrated on the most common problems. Nowadays a large number of authors try to develop more complex procedures to adapt the Mean-Field techniques to more involved problems. Under this perspective it can be proposed the development and implementation of mean-field methods applied to:

- Adapting the Mean-Field methods in order to model the macroscopic behavior of elasto-viscoplastic composites. This is done through an affine formulation based on the Laplace-Carson transform and it has been already developed by some authors (for instance, Pierard [68]).

- Modifying the "traditional" techniques for modeling a two-phase composite to adapt them to more complex materials, consisting of more than two material phases. This can be done through a multi-phase Mean-Field homogenization methods, in which *Orientation Distribution Functions* are used to model the different materials and their distribution over the RVE. This approach has been successfully developed by Doghri *et al.* [19], although the definition of the algorithm (the definition of the ODFs) has not be found in the literature.

- Developing a new approach for the elastoplastic Mean-Field methods in order to improve the quality of the approximation. This can be done, for instance,

by considering other reference states for the phases of the linear comparison composite. Some authors are currently working on developing a new method, which makes use of the second order moment of the stress tensor with the incremental formulation.

- Considering damage mechanisms in the homogenization techniques (inclusion fracture, interface decohesion,...). It has been proposed a statistical method to consider such damage phenomena, since detailed microscopic fields are not available with these methods. However, Mean-Field techniques dealing with damage mechanisms are still an open subject.

- Dealing with the thermal coupling which is especially useful when performing simulations of a complete process of elasto-viscoplastic composites.

Finally, it should be stressed out that some authors consider the multi-scale methods based on a Finite Element Approach to solve the complete mechanical problem for composite materials. This method has been found to be suitable for some mechanical problems but it implies large computational costs, which are far from being acceptable even nowadays. As indicated by some authors (see Pierard [68]), "the use of mean-field homogenization schemes are the only way to solve such problems and guarantees a bright future to these methods". However, some authors (see Hernández *et al.* [34]) are focused on the development of reduction model techniques to reduce considerably the computational costs of the Finite Element method in such cases, which provides opportunity to adapt in the future the use of micromechanical models in order to design materials that are perfectly adapted to the required characteristics.

Appendix A

Eshelby Tensor

A.1 Voigt Notation

During the numerical implementation of the methods used to solve the micromechanical model through analytical expressions, as it is described in section 4.4.5, the symmetric fourth-order tensors have been expressed as matrices using the Voigt form. For this cases, due to the minor symmetries (i.e. $\mathbb{C}_{ijkl} = \mathbb{C}_{jikl}$ and $\mathbb{C}_{ijkl} = \mathbb{C}_{jikl}$), the 81 components associated to a fourth-order tensor is reduced to 36, which can be expressed through a 6x6 matrix. Considering Nye notation, the constitutive tensors, which links stress and strain fields can be written as:

$$\begin{bmatrix} \mathbb{C}_{11} & \mathbb{C}_{12} & \mathbb{C}_{13} & \mathbb{C}_{14} & \mathbb{C}_{15} & \mathbb{C}_{16} \\ \mathbb{C}_{21} & \mathbb{C}_{22} & \mathbb{C}_{23} & \mathbb{C}_{24} & \mathbb{C}_{25} & \mathbb{C}_{26} \\ \mathbb{C}_{31} & \mathbb{C}_{32} & \mathbb{C}_{33} & \mathbb{C}_{34} & \mathbb{C}_{35} & \mathbb{C}_{36} \\ \mathbb{C}_{41} & \mathbb{C}_{42} & \mathbb{C}_{43} & \mathbb{C}_{44} & \mathbb{C}_{45} & \mathbb{C}_{46} \\ \mathbb{C}_{51} & \mathbb{C}_{52} & \mathbb{C}_{53} & \mathbb{C}_{54} & \mathbb{C}_{55} & \mathbb{C}_{56} \\ \mathbb{C}_{61} & \mathbb{C}_{62} & \mathbb{C}_{63} & \mathbb{C}_{64} & \mathbb{C}_{65} & \mathbb{C}_{66} \end{bmatrix} = \begin{bmatrix} \mathbb{C}_{1111} & \mathbb{C}_{1122} & \mathbb{C}_{1133} & \mathbb{C}_{1123} & \mathbb{C}_{1113} & \mathbb{C}_{1112} \\ \mathbb{C}_{2211} & \mathbb{C}_{2222} & \mathbb{C}_{2233} & \mathbb{C}_{2223} & \mathbb{C}_{2213} & \mathbb{C}_{2212} \\ \mathbb{C}_{3311} & \mathbb{C}_{3322} & \mathbb{C}_{3333} & \mathbb{C}_{3323} & \mathbb{C}_{3313} & \mathbb{C}_{3312} \\ \mathbb{C}_{2311} & \mathbb{C}_{2322} & \mathbb{C}_{2333} & \mathbb{C}_{2323} & \mathbb{C}_{2313} & \mathbb{C}_{2312} \\ \mathbb{C}_{1311} & \mathbb{C}_{1322} & \mathbb{C}_{1333} & \mathbb{C}_{1323} & \mathbb{C}_{1313} & \mathbb{C}_{1312} \\ \mathbb{C}_{1211} & \mathbb{C}_{1222} & \mathbb{C}_{1233} & \mathbb{C}_{1223} & \mathbb{C}_{1213} & \mathbb{C}_{1212} \end{bmatrix} \tag{A.1}$$

However, specific care must be taken when contacting the Eshelby tensor for analyzing the micromechanical behavior of a composite. The difficulty arises in contracting the terms of the Eshelby tensor, which links two strain tensors (as defined in 3.2). Therefore, special care should be taken into account since some of the components of the Eshelby tensor will have a different expression (they are

multiplied by a factor of 2):

$$\begin{bmatrix} \mathbb{S}_{11} & \mathbb{S}_{12} & \mathbb{S}_{13} & \mathbb{S}_{14} & \mathbb{S}_{15} & \mathbb{S}_{16} \\ \mathbb{S}_{21} & \mathbb{S}_{22} & \mathbb{S}_{23} & \mathbb{S}_{24} & \mathbb{S}_{25} & \mathbb{S}_{26} \\ \mathbb{S}_{31} & \mathbb{S}_{32} & \mathbb{S}_{33} & \mathbb{S}_{34} & \mathbb{S}_{35} & \mathbb{S}_{36} \\ \mathbb{S}_{41} & \mathbb{S}_{42} & \mathbb{S}_{43} & \mathbb{S}_{44} & \mathbb{S}_{45} & \mathbb{S}_{46} \\ \mathbb{S}_{51} & \mathbb{S}_{52} & \mathbb{S}_{53} & \mathbb{S}_{54} & \mathbb{S}_{55} & \mathbb{S}_{56} \\ \mathbb{S}_{61} & \mathbb{S}_{62} & \mathbb{S}_{63} & \mathbb{S}_{64} & \mathbb{S}_{65} & \mathbb{S}_{66} \end{bmatrix} = \begin{bmatrix} \mathbb{S}_{1111} & \mathbb{S}_{1122} & \mathbb{S}_{1133} & \mathbb{S}_{1123} & \mathbb{S}_{1113} & \mathbb{S}_{1112} \\ \mathbb{S}_{2211} & \mathbb{S}_{2222} & \mathbb{S}_{2233} & \mathbb{S}_{2223} & \mathbb{S}_{2213} & \mathbb{S}_{2212} \\ \mathbb{S}_{3311} & \mathbb{S}_{3322} & \mathbb{S}_{3333} & \mathbb{S}_{3323} & \mathbb{S}_{3313} & \mathbb{S}_{3312} \\ 2\,\mathbb{S}_{2311} & 2\,\mathbb{S}_{2322} & 2\,\mathbb{S}_{2333} & 2\,\mathbb{S}_{2323} & 2\,\mathbb{S}_{2313} & 2\,\mathbb{S}_{2312} \\ 2\,\mathbb{S}_{1311} & 2\,\mathbb{S}_{1322} & 2\,\mathbb{S}_{1333} & 2\,\mathbb{S}_{1323} & 2\,\mathbb{S}_{1313} & 2\,\mathbb{S}_{1312} \\ 2\,\mathbb{S}_{1211} & 2\,\mathbb{S}_{1222} & 2\,\mathbb{S}_{1233} & 2\,\mathbb{S}_{1223} & 2\,\mathbb{S}_{1213} & 2\,\mathbb{S}_{1212} \end{bmatrix} \tag{A.2}$$

A.2 Expressions of the Eshelby's Tensor

Analytical formulae of the Eshelbys tensor were introduced by Eshelby [24] for isotropic materials and spheroidal inclusions. Later, Withers [97] extended the expressions to transversely isotropic medium, although only closed-forms were found for those cases in which the direction of anisotropy coincides with the orientation of the reinforcements. In all other cases (anisotropic material or non-aligned inclusions), a numerical evaluation of the tensor is necessary and was implemented by Gavazzi and Lagoudas [27].

Eshelby's Tensor for Ellipsoids

Hereafter are given the non-nil components of the Eshelbys tensor for an elastic ellipsoidal inclusion of aspect ratio $\alpha = a/b$ embedded in an isotropic elastic matrix (expressions are picked up from Pierard [69]). Reinforcements are aligned along the direction 1.

$$\begin{aligned}
\mathbb{S}_{1111} &= \frac{1}{2(1-\nu)}\left[\frac{4\alpha^2-2}{\alpha^2-1} - 2\nu - g(\alpha)\Big(1-2\nu+\frac{3\alpha^2}{\alpha^2-1}\Big)\right] \\
\mathbb{S}_{2222} = \mathbb{S}_{3333} &= \frac{1}{4(1-\nu)}\left[\frac{3\alpha^2}{2(\alpha^2-1)} + g(\alpha)\Big(1-2\nu-\frac{9}{4(\alpha^2-1)}\Big)\right] \\
\mathbb{S}_{1122} = \mathbb{S}_{1133} &= \frac{1}{2(1-\nu)}\left[-\frac{\alpha^2}{\alpha^2-1} + 2\nu + g(\alpha)\Big(1-2\nu+\frac{3}{2(\alpha^2-1)}\Big)\right] \\
\mathbb{S}_{2211} = \mathbb{S}_{3311} &= \frac{1}{2(1-\nu)}\left[-\frac{\alpha^2}{\alpha^2-1} + \frac{g(\alpha)}{2}\Big(\frac{3\alpha^2}{\alpha^2-1} - (1-2\nu)\Big)\right] \\
\mathbb{S}_{2233} = \mathbb{S}_{3322} &= \frac{1}{4(1-\nu)}\left[\frac{\alpha^2}{2(\alpha^2-1)} - g(\alpha)\Big(1-2\nu+\frac{3}{4(\alpha^2-1)}\Big)\right] \\
\mathbb{S}_{1212} = \mathbb{S}_{1313} &= \frac{1}{4(1-\nu)}\left[-\frac{2}{\alpha^2-1} - 2\nu - \frac{g(\alpha)}{2}\Big(1-2\nu-\frac{3(\alpha^2-1)}{\alpha^2-1}\Big)\right] \\
\mathbb{S}_{2323} &= \frac{\mathbb{S}_{2222}-\mathbb{S}_{2233}}{2}
\end{aligned} \tag{A.3}$$

where $g(\alpha)$ is a function given by:

$$g(\alpha) = \frac{\alpha}{(1-\alpha^2)^{3/2}}[cos^{-1}\alpha - \alpha(1-\alpha^2)^{1/2}] \quad \text{for} \quad 0 < \alpha < 1 \quad \text{(oblate ellips.)}$$
$$g(\alpha) = \frac{\alpha}{(\alpha^2-1)^{3/2}}[\alpha(\alpha^2-1)^{1/2} - cosh^{-1}\alpha] \quad \text{for} \quad 1 < \alpha < \infty \quad \text{(prolate ellips.)} \tag{A.4}$$

The Eshelby's Tensor has the minor symmetries($\mathbb{S}_{ijkl} = \mathbb{S}_{jikl} = \mathbb{S}_{ijlk} = \mathbb{S}_{jilk}$) but not the major ones($\mathbb{S}_{ijkl} \neq \mathbb{S}_{klij}$).

Eshelby's Tensor for Spheres

For the particular case of spherical inclusions, previous equations become invalid and require a study of these functions around $\alpha = 1$. This gives:

$$\mathbb{S}_{1111} = \mathbb{S}_{2222} = \mathbb{S}_{3333} = \frac{7-5\nu}{15(1-\nu)}$$
$$\mathbb{S}_{1122} = \mathbb{S}_{1133} = \mathbb{S}_{2233} = \frac{5\nu-1}{15(1-\nu)}$$
$$\mathbb{S}_{1212} = \mathbb{S}_{1313} = \mathbb{S}_{2323} = \frac{4-5\nu}{15(1-\nu)} \tag{A.5}$$

Eshelby's Tensor for Flat Disks

Flat Disks can be viewed as a particular case that is not covered by the previous expressions for the Eshelby's tensor. It corresponds with ellipsoids whose aspect ratio presents very small values ($\alpha \to 0$). The expressions for the non-nil components of the Eshelby's tensor in case of flat disks embedded in an isotropic elastic matrix (expressions are picked up from Friebel [26]) are:

$$\mathbb{S}_{3333} = 1$$
$$\mathbb{S}_{3311} = \mathbb{S}_{3322} = \frac{\nu}{1-\nu}$$
$$\mathbb{S}_{2323} = \mathbb{S}_{3223} = \mathbb{S}_{2332} = \mathbb{S}_{3232} = \frac{1}{2} \tag{A.6}$$

Eshelby's Tensor for Long Fibers

A third limit case can be deduced from the previous expressions of the Eshelby's tensor in the case of ellipsoidal inclusions. This case corresponds with the upper limit of $g(\alpha)$ and it is produced when the aspect ratio takes high values ($\alpha \to \infty$). This case is given when the inclusions are long bers with circular cross-section. The

non-nil components of the Eshelby's tensor in this case (expressions from [26]) are:

$$
\begin{aligned}
&\mathbb{S}_{1111} = \mathbb{S}_{2222} = \frac{5-4\nu}{8(1-\nu)} \\
&\mathbb{S}_{1122} = \mathbb{S}_{2211} = \frac{4\nu-1}{8(1-\nu)} \\
&\mathbb{S}_{1133} = \mathbb{S}_{2233} = \frac{\nu}{2(1-\nu)} \\
&\mathbb{S}_{1212} = \mathbb{S}_{2112} = \mathbb{S}_{2112} = \mathbb{S}_{2121} = \frac{3-4\nu}{8(1-\nu)} \\
&\mathbb{S}_{2323} = \mathbb{S}_{3223} = \mathbb{S}_{2332} = \mathbb{S}_{3232} = \frac{1}{4} \\
&\mathbb{S}_{3131} = \mathbb{S}_{1331} = \mathbb{S}_{3113} = \mathbb{S}_{1313} = \frac{1}{4}
\end{aligned}
\tag{A.7}
$$

Eshelby's Tensor for Elliptical Inclusion (2D)

Starting from the general expressions for an ellipsoid and taking some assumptions, some various special cases can be derived. For instance, the two-dimensional solution for an infinitely long cylinder of elliptic cross section in plane strain is obtained considering that the axis in direction 3 is much larger than the other two axes ($a_3 \to \infty$). The nonvanishing components of the Eshelby's tensor in case of an isotropic material are (expressions from [31]):

$$
\begin{aligned}
&\mathbb{S}_{1111} = \frac{1}{2(1-\nu)}\left[\frac{a_2^2 + 2a_1a_2}{(a_1+a_2)^2} + (1-2\nu)\frac{a_2}{a_1+a_2}\right] \\
&\mathbb{S}_{2222} = \frac{1}{2(1-\nu)}\left[\frac{a_1^2 + 2a_1a_2}{(a_1+a_2)^2} + (1-2\nu)\frac{a_1}{a_1+a_2}\right] \\
&\mathbb{S}_{1122} = \frac{1}{2(1-\nu)}\left[\frac{a_2^2}{(a_1+a_2)^2} - (1-2\nu)\frac{a_2}{a_1+a_2}\right] \\
&\mathbb{S}_{2211} = \frac{1}{2(1-\nu)}\left[\frac{a_1^2}{(a_1+a_2)^2} - (1-2\nu)\frac{a_1}{a_1+a_2}\right] \\
&\mathbb{S}_{1212} = \frac{1}{2(1-\nu)}\left[\frac{a_1^2 + a_2^2}{2(a_1+a_2)^2} + \frac{1-2\nu}{2}\right] \\
&\mathbb{S}_{1133} = \frac{\nu}{2(1-\nu)}\frac{2a_2}{a_1+a_2}; \qquad \mathbb{S}_{2233} = \frac{\nu}{2(1-\nu)}\frac{2a_1}{a_1+a_2} \\
&\mathbb{S}_{1313} = \frac{a_2}{2(a_1+a_2)}; \qquad \mathbb{S}_{2323} = \frac{a_1}{2(a_1+a_2)}
\end{aligned}
\tag{A.8}
$$

Eshelby's Tensor for Circular Inclusion (2D)

The 2D case can be also consider for a circular inclusion as a particular case from the previous expressions and assuming plane strain state (expresions from [49]):

$$\begin{aligned}
&\mathbb{S}_{1111} = \mathbb{S}_{2222} = \mathbb{S}_{3333} = \frac{5-4\nu}{8(1-\nu)} \\
&\mathbb{S}_{1122} = \mathbb{S}_{2211} = \frac{4\nu-1}{8(1-\nu)} \\
&\mathbb{S}_{1133} = \mathbb{S}_{3311} = \frac{4\nu-1}{8(1-\nu)} \\
&\mathbb{S}_{2233} = \mathbb{S}_{3322} = \frac{4\nu-1}{8(1-\nu)} \\
&\mathbb{S}_{2323} = \mathbb{S}_{1313} = \mathbb{S}_{1212} = \frac{3-4\nu}{8(1-\nu)}
\end{aligned} \tag{A.9}$$

References

[1] J. Aboudi. Micromechanical analysis of composites by the method of cells. *Appl. Mech. Rev.,* 42:193-221, 1989.

[2] J. Aboudi, M.-J. Pindera and S. Arnold. Linear thermo-elastic higher-order theory for periodic multiphase materials. *J. Appl. Mechanics,* 68:697-707, 2001.

[3] J. Aboudi, M.-J. Pindera and S. Arnold. Higher-order theory for periodic multiphase materials with inelastic phases. *Int. J. Plasticity,* 19, 6:805-847, 2003.

[4] L. Bardella. An extension of the Secant Method for the homogenization of the nonlinear behavior of composite materials. *Int. J. of Eng. Sci.,* 41:741768, 2003.

[5] B. Bednarcyk, S. Arnold, J. Aboudi and M.-J. Pindera. Local field effects in titanium matrix composites subject to fiber-matrix debonding. *Int. J. Plasticity,* 20:1707-1737, 2004.

[6] M. Bervellier and A. Zaoui. An extension of the sel-consistent scheme to plastically-flowing polycrystals. *J. Mech. Phys. Sol.,* 26:325-344.

[7] A. Bensoussan, J. Lions and G. Papanicolaou. Asymptotic analysis for periodic structures. *North Holland, Amsterdam*, 1978.

[8] Y. Benveniste. A new approach to the application of Mori-Tanaka's theory in composite materials. *Mech. Mater.,* 6:147-157, 1987.

[9] R. M. Christensen and K. H. Lo. Solutions for effective shear properties in three phase sphere and cylinder models. *J. Mech. Phys. Sol.,* 27:315-330, 1979.

[10] H. J. Böhm. Continuum Micromechanics of Materials. *Institut für Leichtbau und Biomechanik, TU Wien*, 2011.

[11] M. Bornert. Homogénéisation des milieux aléatoires: bornes et estimations, vol. 1. *Hermes Science, Paris,* 5:133-221, 2001.

[12] I. Özdemir, W.A.M. Brekelmans and M.G.D. Geers. FE^2 computational homogenization for the thermo-mechanical analysis of heterogeneous solids. *Comput. Methods Appl. Mech. Engrg.*, 198:602613, 2008.

[13] V. A. Buryachenko. The overall elastoplastic behavior of multiphase materials with isotropic components. *Acta Mechanica,* 119:93-117.

[14] C. R. Chiang. An extended Mori-Tanaka micromechanics model. *16th. International Conference of Composite Materials*, 2007.

[15] P. Chung, K. Tamma and R. Namburu. Asymptotic expansion homogenization for heterogenous media: computational issues and applications. *Composite part A,* 32, 9:1291-1301, 2001.

[16] L.C. Davis. Flow rule for the plastic deformation of particulate metal matrix composites. *Comp. Mater. Sci.,* 6:310-318, 1996.

[17] I. Doghri and A. Ouaar Homogenization of two-phase elasto-plastic composite materials and structures: study of tangent operators, cyclic plasticity and numerical algorithms. *Int. J. Solids Struct.,* 40:1681-1712, 2003.

[18] I. Doghri and C. Friebel. Effective elasto-plastic properties of inclusion-reinforced composites. Study of shape, orientation and cyclic response. *Mech.Mater.,* 37:45-68, 2005.

[19] I. Doghri and L. Tinel. Micromechanical modeling and computation of elasto-plastic materials reinforced with distributed orientation fibers. *Int. J. Plasticity,* 21:1919-1940, 2005.

[20] I. Doghri, A. Ouaar, L. Delannay and J. F. Thimus. Micromechanics of the Deformation and Damage of Steel Fiber-reinforced Concrete. *Int. J. of Damage Mech.,* 16, 2:227-260, 2007.

[21] W. Drugan and J. Willis. A micromechanics-based nonlocal constitutive equations and estimates of representative volume element size for elastic composites. *J. Mech. Phys. Sol.,* 44:497-524, 1996.

[22] G. Dvorak. Transformation field analysis of inelastic composite materials. *Proc. Roy. Soc. Lond.,* A 437:311-327, 1992.

[23] G. Dvorak, Y.A. Bahei-el Din and A. M. Wafa. The modelling of inelastic composite materials with the transformation field analysis. *Modell. Simul. Mater. Sci. Engrg.,* 2:571-586, 1994.

[24] J. Eshelby. The determination of the elastic field of an ellipsoidal inclusion, and related problems. *Proc. Roy. Soc. Lond.,* A 24:376-396, 1957.

[25] F. Feyel. A multilevel finite element method (FE^2) to describe the response of highly non-linear structures using generalized continua. *Comput. Mech. Appl. Mech. Engrg.,* 192:3233-3244, 2003.

[26] C. Friebel. Mechanics and Acoustics of viscoelastic inclusion reinforced composites: micro-macro modeling of effective properties. *PhD thesis, Université Catholique de Louvain,* Belgium, 2007.

[27] A. Gavazzi and D. Lagoudas. On the numerical evaluation of Eshelbys tensor and its application to elastoplastic fibrous composites. *Comput. Mech.,* 7:13-19, 1990.

[28] S. Ghosh, K. Lee and S. Moorthy. Multiple scale analysis of heterogeneous elastic structures using homogenization theory and Voronoi cell finite element method. *Int. J. Solids Struct.,* 32:27-62, 1995.

[29] S. Ghosh, K. Lee and S. Moorthy. Two scale analysis of heterogeneous elastic-plastic materials with asymptotic homogenization and Voronoi cell finite element model. *Comput. Methods Appl. Mech. Engrg.,* 132,1-2:63-116, 1996.

[30] S. Gong, Z. Li, Y.Y. Zhao. An extended MoriTanaka model for the elastic moduli of porous materials of finite size. *Acta Materialia,* 59:68206830, 2011.

[31] D. Gross and T. Seelig. Bruchmechanik, mit einer Einfhrung in die Micromechanik. *Springer, Berlin, Heidelberg*, 2001.

[32] Z. Hashin and S. Shtrikman. Note on a variational approach to the theory of composite elastic materials. *J. Franklin Inst.,* 271:336-341, 1961.

[33] Z. Hashin. The differential scheme and its application to cracked materials. *J. Mech. Phys. Sol.,* 36:719-733, 1988.

[34] J. A. Hernández, J. Oliver, A. E. Huespe and M. Caicedo. High-performance Model Reduction Procedures in Multiscale Simulations. *CIMNE Monograph*, Barcelona 2012.

[35] R. Hill. Elastic properties of reinforced solids: Some theoretical principles. *J. Mech. Phys. Sol.,* 11:357-372, 1963.

[36] R. Hill. Continuum micro-mechanics of composite materials. *J. Mech. Phys. Sol.,* 13, 4:89-101, 1965.

[37] J. W. Hutchinson. Elastic-plastic behavior of polycrystalline metals and composites. *Proceedings of the Royal Society of London,* A319, 247-272, 1970.

[38] M. Jiang, M. Ostoja-Starzewski and I. Jasiuk. Scale-dependent bounds on effective elastoplastic response of random composites. *J. Mech. Phys. Sol.,* 49:655-673, 2001.

[39] M. Jiang, M. Ostoja-Starzewski and I. Jasiuk. Apparent elastic and elastoplastic behavior of periodic composites. *Int. J. Solids Struct.,* 39:199-212, 2002.

[40] T. Kanit, S. Forest, I. Galliet, V. Mounoury and D. Jeulin. Determination of the size of the representative volume element for random composites: statistical and numerical approach. *Int. J. Solids Struct.,* 40, 13-14:3647-3679, 2003.

[41] H. Khatam, M.-J. Pindera. Parametric finite-volume micromechanics of periodic materials with elastoplastic phases. *Int. J. of Plasticity*, 25:1386-1411, 2009.

[42] B. Klusemann and B. Svendsen. Homogenization methods for multi-phase elastic composites: Comparisons and benchmarks. *Technische Mechanik, 30,* 4:274-286, 2009.

[43] V. Kouznetsova, M.G.D. Geers and W.A.M. Brekelmans. Advanced constitutive modeling of heterogeneous materials with a gradient-enhanced computational homogenization scheme. *Int. J. Num. Meth. Engrg.,* 54:1235-1260, 2002.

[44] V. Kouznetsova. Computational homogenization for the multi-scale analysis of multi-phase materials. *PhD thesis, Technische Universiteit Eindhoven,* The Nederlands, 2002.

[45] V. Kouznetsova. Computational homogenization. Micromechanics graduate course lecture notes, Eindhoven, 2004.

[46] W. Kreher. Residual stresses and stored elastic energy of composites and polycrystals. *J. Mech. Phys. Sol.,* 38:115-128, 1990.

[47] E. Kröner. Zur plastischen Verformung des Vielkrystalls. *Acta Metall. 9,* 2:155-161, 1961.

[48] W. P. Kuykendall, W. D. Cash, D. M. Barnett, W. Cai. On the Existence of Eshelby's Equivalent Ellipsoidal Inclusion Solution. *Mathematics and Mechanics of Solids, in press*, 2011.

[49] S. Li, R. Sauer and G. Wang. A circular inclusion in a finite domain I. The Dirichlet-Eshelby problem. *Acta Mechanica,* 179:67-90, 2005.

[50] G. Lielens. Micro-Macro Modeling of Structured Materials. *PhD thesis, Université Catholique de Louvain,* Belgium, 1999.

[51] R. Masson, M. Bornert, P. Suquet and A. Zaoui. An affine formulation for the prediction of the effective properties of nonlinear composites and polycrystals. *J. Mech. Phys. Sol.,* 48:1203-1227, 2000.

[52] J. C. Michel and P. Suquet. Computational analysis of nonlinear composite structures using the nonuniform transformation field analysis. *Comput. Meth. Appl. Mech. Engrg.,* 193:5477-5502, 2004.

[53] C. Miehe. Computational micro-to-macro transitions for discretized microstructures of heterogeneous materials at finite strains based on the minimization of averaged incremental energy. *Comput. Mech. Appl. Mech. Engrg.,* 192:559-591, 2003.

[54] L. Mishnaevsky. Micromechanics of hierarchical materials: a brief overview. *Rev.Adv.Mater. Sci.,* 30:60-72, 2012.

[55] J. Moraleda, J. Segurado and J. Llorca Finite deformation of incompressible fiber-reinforced elastomers: a computational micromechanics approach. *J. of the Mech. and Phys. of Solids,* 57:1596-1613, 2009.

[56] H. Moulinec and P. Suquet. A fast numerical method for computing the linear and nonlinear properties of composites. *C.R. Acad. Sci. Paris II,* 318:1417-1423, 1994.

[57] H. Moulinec and P. Suquet. A FFT-based numerical method for computing the mechanical properties of composites from images of their microstructure. *Kluwer Academic Publ., Dordrecht,* :235-246, 1995.

[58] T. Mura. Micromechanics of defects in solids. *Martinus Nijhoff Publishers*, 1987.

[59] W. H. Müller. Mathematical versus experimental stress analysis of inhomogeneities in solids. *J. Phys. IV,* 6:1-139-C1-148, 1996.

[60] S. Nemat-Nasser. Averaging theorems in finite deformation plasticity. *Mech. Mater.,* 31:493-523, 1999.

[61] S. Nemat-Nasser and M. Hori. *Micromechanics: Overall Properties of Heterogeneous Solids.* North-Holland, Amsterdam, 1993.

[62] S. Nemat-Nasser and M. Hori. *Micromechanics: Overall Properties of Heterogeneous Materials.* 2nd Ed., Elsevier, Amsterdam, 1999.

[63] M. Ortiz and E. P. Popov. Accuracy and stability of integration algorithms for elastoplastic constitutive relations. *Int. J. Numer. Methods,* 21:571-574, 1985.

[64] M. Ostoja-Starzewski. Material spatial randomness: From statistical to representative volume element. *Prob. Eng. Mech.,* 21:112-132, 2006.

[65] M. Paley and J. Aboudi. Micromechanical analyisis of composites by the generalized cells model. *Mech. Materials,* 14,2:127-139, 1992.

[66] H. E. Petterman, A. F. Planskensteiner, H. J. Böhm, F. G. Rammerstorfer. A termo-elasto-plastic constitutive law for inhomogeneous materials based on an incremental Mori-Tanaka approach. *Computers and Structures,* 71:197-214, 2002.

[67] O. Pierard, C. Friebel, I. Doghri. Mean-field homogenization of multi-phase thermo-elastic composites: a general framework and its validation. *Composites Science and Technology,* 64:15871603, 2004.

[68] O. Pierard. Micromechanics of inclusion-reinforced composites in elasto-plasticity and elasto-viscoplasticity: modeling and computation. *PhD thesis, Université Catholique de Louvain,* Belgium, 2006.

[69] O. Pierard, C. González, J. Segurado, J. LLorca, I. Doghri. Micromechanics of elasto-plastic materials reinforced with ellipsoidal inclusions. *J. Mech. Phys. Sol.,* 44:6945-6962, 2007.

[70] M. J. Pindera, H. Khatam, A. Drago and Y. Bansal. Micromechanics of spatially uniform heterogeneous media: A critical review and emerging approaches. *Composites: Part B*, 40:349378, 2009.

[71] P. Ponte Castañeda. The effective mechanical properties of nonlinear isotropic composites. *J. Mech. Phys. Sol.,* 39:45-71, 1991.

[72] P. Ponte Castañeda and J. R. Willis. The effect of spatial distribution on the effective behavior of composite materials and cracked media. *J. Mech. Phys. Sol.,* 43:1919-1951, 1995.

[73] G. Povirk. Incorporation of microstructural information into models of two-phase materials. *Acta Metall. Mater.,* 43, 8:3199-3206, 1995.

[74] Y. P. Qiu and G. J. Weng. On the application of Mori-Tanaka's theory involving transversely isotropic spheroidal inclusions. *Int. J. Engng. Sci.,* 28, 11:1121-1137, 1990.

[75] J. Qu and M. Cherkaoui. Fundamentals of micromechanics of solids. *John Wiley & Sons*, New Jersey, 2006.

[76] R. Roscoe. Isotropic composites with elastic or viscoelastic phases: General bounds for the moduli and solutions for special geometries. *Rheol. Acta,* 12:404-411, 1973.

[77] E. Sánchez-Palencia. Non homogeneous media and vibration theory - lecture notes in physics, 127. *Springer, Berlin*, 1980.

[78] M. Sautter, C. Dietrich, M. H. Poech, S. Schmauder and H. F. Fischmeister. Finite element modeling of a transverse-loaded fibre composite: Effects of section size and net density. *Comput. Mater. Sci.,* 1:225-233, 1993.

[79] J. Segurado, J. Llorca, C. González. On the accuracy of mean-field approaches to simulate the plastic deformation of composites. *Scripta Materialia,* 46:525-529, 2002.

[80] J. Segurado, J. Llorca. A numerical approximation to the elastic properties of sphere-reinforced composites. *J. Mech. Phys. Sol.,* 50:2107-2121, 2002.

[81] J. Segurado. Micromecánica computacional de materiales compuestos reforzados con partículas. *PhD thesis, Universidad Politécnica de Madrid,* Spain, 2004.

[82] J. Segurado, J. Llorca, C. González. Numerical simulation of elastoplastic deformation of composites: evolution of stress microfields and implications for homogenization models.*J. Mech. Phys. Sol.,* 52:1573-1593, 2004.

[83] J. Segurado, J. Llorca. Computational micromechanics of composites: the effect of particle spatial distribution. *Mechanics of Materials,* 38:873-883, 2006.

[84] J. C. Simo and T. J. R. Hughes. Computational Inelasticity. *Springer Verlag*, New York, 1998.

[85] E. S. Perdahcoğlu and H. J. M. Geijselaers. Constitutive modeling of two phase materials using the mean field method for homogenization. *Int. J. Mater. Form.* , 2010.

[86] E. A. de Souza Neto and R. A. Feijóo. Variational Foundations of Multi-Scale Constitutive Models of Solid: Small and Large Strain Kinematical Formulation. *LNCC Research and Development. Report 16.*

[87] P. Suquet. Local and global aspects in the mathematical theory of plasticity. *Plasticity today: modelling, methods and applications, A. Sawczuk G. Bianchi.* London. Elsevier Applied Science Publishers, 1985.

[88] P. Suquet. Overall properties of non-linear composites: a modified secant moduli theory and its link with Ponte Castañeda's non-linear variational procedure. *Comptes rendus de l'Academie des Sciences, Paris, Serie IIb,* 320:563-571.

[89] P. Suquet. Effective properties of nonlinear composites. *Continuum Micromechanics. CISM Course and Lecture Notes*:197-264.

[90] N. Takano, M. Zako and T. Okazaki. Efficient modeling of microscopic heterogeneity and local crack in composite materials by finite element mesh superposition method. *JSME Int. J. Srs. A,* 44:602-609, 2001.

[91] H. Tan, Y. Huang, C. Liu, P.H. Geubelle. The MoriTanaka method for composite materials with nonlinear interface debonding. *Int. J. of Plasticity,* 21:1890-1918, 2005.

[92] G. P. Tandon, G. J. Weng. A theory of particle-reinforced plasticity. *Journal of Applied Mechanics,* 55:126-135, 1988.

[93] M. Tane, T. Ichitsubo, M. Hirao, H. Nakajima. Extended mean-field method for predicting yield behaviors of porous materials. *Mechanics of Materials,* 39:5363, 2007.

[94] S. Torquato. Effective stiffness tensor of composite media: II. Applications to isotropic dispersions. *J. Mech. Phys. Solids,* 35-7:411-440, 1998.

[95] J. Vorel, J. Sýkora and M. Šejnoha. Two Step Homogenization of Effective Thermal Conductivity for Macroscopically Orthotropic C/C composites. *Bulletin of applied mechanics,* 4-14:48-53, 2008.

[96] C. Weinberger, W. Cai and D. Barnett Lecture Notes Elasticity of Microscopic Structures. *ME340B Stanford University Winter 2004.*, 2005.

[97] P. Withers. The determination of the elastic field of an ellipsoidal inclusion in a transversely isotropic medium and its relevance to composite materials. *Philosophical Magazine A 59,* 4:759-781, 1989.

[98] W. Yu and T. Tang. Variational asymptotic method for unit cell homogenization of periodically heterogeneous materials. *Int. J. Sol. Struct.,* 44:3738-3755, 2007.

[99] Q. S. Zheng and D. X. Du. An explicit and universally applicable estimate for the effective properties of multiphase composites which accounts for inclusion distribution. *J. Mech. Phys. Sol.,* 49, 11:2765-2788, 2001.

[100] Q. S. Zheng and D. X. Du. A further exploration of the interaction direct derivative (IDD) estimate for the effective properties of muhiphase composites taking into account inclusion distribution. *Acta Mechanica,* 157:61-80, 2002.

[101] T. Zohdi and P. Wriggers. Introduction to computational micromechanics. *Springer Verlag*, Berlin, 2005.